Development of a Preconditioning Scheme for Real Gases using Asymptotic Expansions

Entwicklung eines Präkonditionieres für reale Gase mit Hilfe asymptotischer Entwicklungen

Vom Fachbereich Mathematik und Naturwissenschaften
der Universität Kassel
zur Verleihung des akademischen Grades
Doktor der Naturwissenschaften (Dr. rer. nat.)
genehmigte

Dissertation

von

Lisa Meyer

Datum der Einreichung: 15.November 2021
Datum der Disputation: 28.März 2022

Erstgutachter: Prof. Dr. Andreas Meister
Zweitgutachter: Prof. Dr.-Ing. Michael Oevermann

Lisa Meyer

Dissertation: “Development of a Preconditioning Scheme for Real Gases using Asymptotic Expansions”.
Mathematical Institute University of Kassel
Institute for Aerodynamics and Flow Technologies, DLR Göttingen
Advisor: Prof. Dr. Andreas Meister
Second Advisor: Prof. Dr.-Ing. Michael Oevermann

Kurzfassung

Bei der Beschreibung von Strömungen wird klassischerweise zwischen inkompressiblen und kompressiblen Bereichen unterschieden. Während inkompressible Strömungen durch ein divergenzfreies Geschwindigkeitsfeld charakterisiert werden, sind kompressible Strömungsfelder durch Expansionsfächer, Kontaktunstetigkeiten und Stoßwellen gekennzeichnet. Die beiden Bereiche werden damit durch stark unterschiedliche Systeme partieller Differentialgleichungen beschrieben.
Diese Unterscheidung zeigt sich auch in der numerischen Strömungsmechanik durch die Entwicklung separater Ansätze für die beiden Bereiche. Dichtebasierte Verfahren eignen sich dabei zur Simulation von kompressiblen Strömungen höherer Mach-Zahlen, während druckbasierte Verfahren für inkompressible Strömungen bei kleinen Mach-Zahlen geeignet sind. Beide Verfahren sind ohne Anpassungen nicht für den jeweils anderen Bereich verwendbar.
In vielen praktischen Anwendungen treten jedoch Strömungen mit einer großen Variation der lokalen Mach-Zahl auf, weshalb seit einigen Jahrzehnten intensiv an numerischen Verfahren für die Strömungssimulation in allen Mach-Zahlbereichen gearbeitet wird. Für dichtebasierte Verfahren wird meist die sogenannte Präkonditionierung angewendet. Die durchgeführten Arbeiten beschränken sich allerdings meist auf Strömungen idealer Gase, womit Realgaseffekte nicht berücksichtigt werden, die jedoch für viele praktische Anwendungen wichtig sind.
Die vorliegende Arbeit beschäftigt sich in diesem Zusammenhang mit der Analyse numerischer Verfahren zur Simulation von Strömungen im Grenzfall einer verschwindenden Mach-Zahl für reale Gase. Als Modell eines realen Gases wird die Van der Waals-Zustandsgleichung verwendet.
Zunächst werden die relevanten Grundgleichungen diskutiert, wobei besonders auf die Herleitung der kalorischen Zustandsgleichung für ein Van der Waals-Gas eingegangen wird. Dabei wird gezeigt, dass die spezifische Wärmekapazität für ein Van der Waals-Gas nur mit der Temperatur variiert. Darauf aufbauend wird eine asymptotische Einskalenanalyse der Euler-Gleichungen durchgeführt. Die Vorgehensweise folgt den aus der Literatur bekannten Arbeiten, allerdings führt der Übergang zu einem Van der Waals-Gas zu einer deutlich komplexeren Analyse. Im Rahmen der Untersuchung wird gezeigt, dass die zeitliche Änderung des thermodynamischen Hintergrunddruckes für ein Van der Waals-Gas nicht nur von den Flüssen über den Rand des betrachteten Gebiets, sondern auch von der Dichteverteilung erster Ordnung abhängt.
Die gewonnenen Erkenntnisse zum Verhalten der Strömungsgrößen im Grenzfall einer verschwindenden Mach-Zahl werden weiter zur Analyse des DLR-TAU-Codes verwen-

det. Die MAPS+-Flussfunktion wird mittels einer diskreten asymptotischen Analyse im Grenzfall einer verschwindenden Mach-Zahl analysiert. Diese Untersuchung führt zu dem Ergebnis, dass sich die beiden verschiedenen Versionen von MAPS+ in der Größenordnung der Druckfluktuationen unterscheiden. Nur für die modifizierte Version von MAPS+ stimmen diese Druckfluktuationen mit den Ergebnissen der kontinuierlichen Analyse überein. Zusätzlich werden Simulationen der Umströmung eines NACA0012-Profils präsentiert, die die analytischen Resultate bestätigen.
Abschließend wird mit einer numerischen Eigenwertberechnung gezeigt, dass ein Idealgas-Präkonditionierer im Limit einer verschwindenden Mach-Zahl für ein Van der Waals-Gas nicht zu einer Reduzierung der Konditionszahl führt und diese sogar verschlechtern kann, während ein angepasster Präkonditionierer für das Van der Waals-Gas zu einer Verringerung der Konditionszahl führt, die vergleichbar mit dem Idealgas-Fall ist. Zusätzlich werden Simulationen mit zwei in den DLR-TAU-Code implementierten Präkonditionierern für ein Van der Waals-Gas präsentiert, die eindrucksvoll zeigen, dass mit Hilfe der Präkonditionierer Strömungen bis zu einer Einströmmachzahl von $M = 10^{-4}$ berechnet werden können. Dabei werden Profilumströmungen verschiedener Van der Waals-Gase im flüssigen, gasförmigen sowie superkritischen Zustand simuliert und es werden glatte Lösungen der Dichte-, Druck- und Geschwindigkeitsverteilung erzielt.

Abstract

Typically, flow fields are distinguished into incompressible and compressible flows. While incompressible flows are characterized by a divergence-free velocity field, compressible flow fields contain expansion fans, contact discontinuities and shock waves. The two fields are thus described by strongly different systems of partial differential equations.
This distinction is also reflected in computational fluid dynamics by the development of separate approaches for the two different types of flows. Density-based methods are suitable for simulating compressible flows at higher Mach numbers, while pressure-based methods are typically used for incompressible flows at low Mach numbers. Both methods cannot be used for the other type of flow without adaptations.
In many practical applications, however, flows with a large variation of the local Mach number occur. Therefore, in the last few decades, intensive research has been done on numerical methods that are applicable to the whole Mach number range. For density-based methods, the so-called preconditioning is usually applied. However, the published work on this topic is mostly limited to flows of ideal gases, not considering real gas effects which are important for many practical applications.
In this context, the present thesis deals with the analysis of numerical methods for the simulation of flows in the limiting case of a vanishing Mach number for real gases. The Van der Waals equation of state is used to model a real gas.
First, the relevant governing equations are discussed, with special emphasis on the derivation of the caloric equation of state for a Van der Waals gas. It is shown that the specific heat capacity for a Van der Waals gas varies only with temperature. Based on this, an asymptotic analysis of the Euler equations is presented. The procedure follows the approach known from the literature, but the transition to a Van der Waals gas leads to a much more complex analysis. As a result, it is shown that the time variation of the thermodynamic background pressure for a Van der Waals gas depends not only on the fluxes over the boundary of the considered domain, but also on the first-order density distribution.
The insights gained concerning the behavior of the flow variables in the limit of a vanishing Mach number are further used to investigate the DLR TAU-code. The MAPS+ flux function is analyzed by means of a discrete asymptotic analysis in the limit of a vanishing Mach number. This analysis leads to the result that the two different versions of MAPS+ differ in the magnitude of the pressure fluctuations. Only for the modified version of MAPS+ do these pressure fluctuations agree with the results of the continuous analysis. In addition, simulations of the flow around a NACA0012 profile are presented, which confirm the analytical results.

Finally, a numerical eigenvalue calculation is used to show that in the limit of a vanishing Mach number, an ideal gas preconditioning scheme does not lead to a reduction of the condition number for a Van der Waals gas and may even worsen it, while an adapted preconditioner leads to a reduction of the condition number for the Van der Waals gas comparable to the ideal gas case. In addition, simulations with two preconditioning schemes for a Van der Waals gas that are implemented in the DLR TAU-code are presented, which impressively show that flows down to an inflow Mach number of $M = 10^{-4}$ can be calculated using a preconditioning scheme. Flows of different Van der Waals gases in liquid, gaseous and supercritical states are simulated and smooth solutions of the density, pressure and velocity distribution are obtained.

Contents

List of Symbols

Physical Quantities

a	intermolecular forces-constant
b	co-volume
c	speed of sound
c_p	mass-specific heat at constant pressure
c_v	mass-specific heat at constant volume
e	mass-specific internal energy
e_m	molar internal energy
E	mass-specific total energy
γ	isentropic exponent
H	specific total enthalpy
M_w	molecular weight
p	pressure
q	total directional velocity
ρ	density
R	specific gas constant
$\mathcal{R}$	universal gas constant
s	mass-specific entropy
t	time
$\boldsymbol{v} = (v_1, \ldots, v_d)^T$	velocity vector
V_m	molar volume
T	temperature

Nondimensional Numbers

M	Mach number
Ma	local Mach number
Ma_{in}	inflow Mach number

Sequences, Sets and Spaces

$\mathcal{B}$	set of control volumes
$\mathcal{C}^m(\mathcal{A};\mathcal{Z})$	space of m-times continuously differentiable mapping from set $\mathcal{A}$ to set $\mathcal{Z}$
$\mathcal{G}$	spatial domain in $\mathbb{R}^d$
$\partial\mathcal{G}$	boundary of the spatial domain $\mathcal{G}$
$\lvert\mathcal{G}\rvert$	volume of the spatial domain $\mathcal{G}$
$\mathcal{I}$	subset of $\mathbb{R}\cup\{+\infty,-\infty\}$
$L^1(\mathcal{A};\mathcal{Z})$	space of absolutely integrable functions from set $\mathcal{A}$ to set $\mathcal{Z}$
$L^\infty(\mathcal{A};\mathcal{Z})$	space of measurable and regarding the maximum norm finite functions from set $\mathcal{A}$ to set $\mathcal{Z}$
$\mathcal{N}(i)$	set of the grid points of neighbors with regard to $\boldsymbol{x}_i$
$\mathcal{N}_h$	set of all grid points
$\{\phi_n\}_{n\in\mathbb{N}_0}$	asymptotic sequence
σ	control volume in $\mathbb{R}^d$
$\mathcal{T}$	triangle
$\mathcal{T}_h$	triangular grid
$\partial\mathcal{T}_h$	boundary of the triangular grid $\mathcal{T}_h$
$\mathcal{U}$	set of single scale expansions
$\mathcal{S}_h$	structured grid
$\mathcal{Z}$	state space of the conservative variables

Scalars, Vectors and Matrices

$\boldsymbol{A}_{\boldsymbol{u}}^{(j)}$	Jacobi matrix
β	preconditioning parameter
δ_{ij}	Kronecker delta
$\boldsymbol{f}_j(\boldsymbol{u})$	flux function in the direction of j
$\boldsymbol{\Gamma}(\boldsymbol{u})$	preconditioning matrix in conservative variables
$\boldsymbol{n}$	outer normal vector
$\boldsymbol{P}(\boldsymbol{q})$	preconditioning matrix in primitive variables
$\boldsymbol{q}$	vector of primitive variables
$\triangle t^n$	size of time step $n+1$
$\boldsymbol{T}(\boldsymbol{n})$	rotational matrix
$\boldsymbol{u}$	vector of conservative variables
$\widetilde{\boldsymbol{u}}_i^n$	cell mean values of σ_i at time t^n
$\boldsymbol{x}=(x_1,\ldots,x_d)^T$	vector of spatial coordinates

Operators

$\mathcal{H}$	numerical flux function
$\mathcal{O}_S, \mathcal{O}, o$	Landau symbols
$\mathcal{L}$	flux operator regarding σ
$\mathcal{M}_\sigma$	averaging operator
∂	partial differential
Φ	function
$\triangle_{ij}$	difference operator
$\nabla_{\boldsymbol{x}}$	gradient operator
$\nabla_{\boldsymbol{x}}\cdot$	divergence operator

1. Introduction

Computational fluid dynamics (CFD) is a well-established approach to analyze and solve fluid flow problems using numerical analysis. Modern CFD methods are applied within a wide range of industrial and research problems. Over the last decades, these schemes were thoroughly enhanced and today's sophisticated CFD methods can be used to model problems in different fields including aerodynamics and aerospace, environmental and biological engineering or weather simulations. The possible applications range from low subsonic to hypersonic flows, including both inviscid and viscous calculations as well as turbulence and a variety of thermodynamic effects. In addition, numerous boundary conditions are available. But computational fluid dynamics still remain a field of active research since there are many problems left to be solved.

The early CFD methods were only applicable to fluids that can be described by a simple thermodynamic relation. For gases, the ideal gas law was used. Therefore, the methods were limited by the assumption that the molecules within the gas move randomly, interact only by elastic collisions and are of equal mass and negligible volume. These ideal gas assumptions are only true when the density is very low, which is for example for air the case at ambient temperature and pressure.

The earliest description of real gas thermodynamics dates back as early as 1873 where Van der Waals proposed his famous equation of state. About one century later, other more detailed equations of state were developed and introduced into CFD methods. Within the last decades an increasing amount of research was put into the accurate description of real gas thermodynamic behavior.

At the present, real gas effects are important to many practical applications. Examples are the modeling of combustion processes, flows through cooling channels or at high temperatures or pressures. They all have in common that they require the ability to accurately model the behavior of a real fluid.

Both ideal and real gas flows can be classified by the Mach number. It is defined as the ratio of flow velocity to speed of sound and it is one of the dimensionless quantities describing the flow. Depending on the Mach number, a flow can have very different properties.

In the region of low Mach numbers, flows can be characterized by an almost constant background pressure with low frequency acoustic pressure waves of a small magnitude. In many cases flows in this region can be regarded as incompressible since the effect of pressure changes on the density is in general negligible. Both the acoustic pressure waves and high frequency pressure fluctuations with a very low amplitude have an essential impact on the velocity field. Due to this importance of changes in pressure, flow solvers developed for the low Mach number, incompressible region are typically pressure based. In the region of medium to high Mach numbers, the compressible flow field shows effects like expansion fans and shock waves. The conservative nature of a numerical scheme becomes important. Hence, flow solvers for compressible flows at higher Mach numbers are typically density based.

In general, flow solvers can only be used within the region of the Mach number for which they are developed. While pressure based flow solvers designed for an incompressible flow cannot simulate compressible effects, density based flow solvers designed for a compressible flow tend to decrease considerably in both accuracy and efficiency when used at small Mach numbers. Hence, the simulation of a flow reaching from high to very low Mach numbers cannot be performed by either type of flow solver without further adaptions.

Many modern applications, however, require a CFD method that is applicable to both compressible and incompressible flows. In the simulation of an aircraft moving at transsonic or hypersonic velocities, there are regions close to the stagnation point or the surface of the vehicle, where the local Mach number approaches zero while it is close to or even higher than one in the major part of the flow domain. In the simulation of combustion processes at the transition between deflagration and detonation, the local Mach number can change from 10^{-3} to values between 5 and 10 within a small spatial distance. And even for the simulation of flows within the low subsonic region, the consideration of compressible effects can be important since they can also be introduced by large changes in pressure or temperature. All these examples require a flow solver that is capable of simulating both flows at low Mach numbers and compressible effects, typically at high Mach numbers.

In order to attain a flow solver suitable for all Mach numbers, two different approaches are possible. The first option is to expand a density based compressible solver towards the incompressible limit. The second option is to introduce compressibility effects to a pressure based incompressible solver and thereby expand it into the compressible region. For the applications motivating this work the first approach is the more attractive one. The considered applications can be summarized in two categories, the first one being flows

with only locally low Mach numbers which require a full compressible flow description in all other parts of the domain. The second category contains flows with low Mach numbers in parts or the whole domain with distinct real gas effects such as supercritical fluids, liquids or fluids in the two-phase region. These flows require the implementation of a thermodynamic model that covers the whole range of thermodynamic states from liquid to supercritical. Such models are widely available in compressible solvers. Hence, for all applications considered in the frame of this work, expanding a compressible flow solver towards the incompressible limit is the better choice.

A common approach for the expansion of a density based compressible flow solver towards the incompressible limit is the use of a preconditioning scheme. Different versions of a preconditioner for an ideal gas have been proposed by many authors (see for example the work by Turkel [68], Briley et al. [9], Choi and Merkle [12] and Weiss and Smith [77]) and many studies are concerned with their effects. A preconditioning scheme scales the acoustic velocities in order to reduce the stiffness of the equations. This enables a compressible flow solver to simulate flows in the region of low Mach numbers without the inherent loss of accuracy and efficiency.

However, these preconditioning schemes are only developed for ideal gases and fail for flow solvers that include the modeling of real gas effects. The mathematical properties of real gas equations of state differ from the ideal gas one. Hence a system of equations describing a real fluid has properties that differ from the ideal gas case. So, for simulations that are not limited to ideal gas assumptions the preconditioning schemes available in the literature cannot be used.

As a result, many relevant applications cannot be solved in an efficient way with the flow solvers currently available. For example, the flow of a refrigerant through cooling channels requires the modeling of real gas thermodynamics at very low Mach numbers. In addition, compressible effects become important if the refrigerant undergoes phase change. The same applies to the investigation of cryogenic fluids, which need to be modeled by real gas thermodynamics, in the tank of a rocket in orbit. The corresponding flows occur at very low Mach numbers while compressible effects are important due to the massive changes in pressure and the possibility of a phase change. Another example is the combustion of liquid fuel. In all cases, the availability of a compressible scheme for real gases that is applicable to low Mach numbers is crucial for the successful simulation. Therefore, the objective of this thesis is to develop a low Mach preconditioning scheme applicable to real gases. For the analytical analysis of the equations a Van der Waals gas is chosen as the simplest representative of a real gas.

To transfer the concept of a preconditioning scheme to a real gas, the two objectives of a preconditioner – increase of accuracy and of efficiency as the Mach number decreases – are approached separately. The first step is to maintain a high accuracy of the flow solver as the Mach number approaches zero. This is accomplished by choosing a flux function that has a numerical error independent of the Mach number in this regime for both ideal and real gases. In the second step a preconditioning scheme suitable for a Van der Waals gas is constructed that increases the efficiency of the flow solver at low Mach numbers.

To investigate the behavior of the flux function in the limit of a vanishing Mach number, an asymptotic analysis is chosen. In the next chapters this method is explained, the mathematical formulation of the problem is given and the flow solver meeting the objectives is described.

In the first chapter, the governing equations of fluid dynamics are given. After a short description of the conservation equations for mass, momentum and energy, more emphasis is put on the definition and derivation of the thermal and caloric equations of state. Another focus of the chapter lies on the nondimensionalization of the physical quantities which is an important step for the asymptotic analysis.

This method is described in detail in the second chapter where an overall introduction to asymptotic analyses is given. An asymptotic sequence is defined and its fundamental properties are stated. Then the analysis of the governing equations is conducted and the results are discussed.

In the third chapter, a numerical scheme meeting the objectives stated above is described. After a brief overview of the DLR TAU-code which is the baseline code, the numerical flux function and the preconditioning scheme are discussed in more detail. The chosen flux function, MAPS+, is described and the favorable behavior for small Mach numbers is shown by the use of a discrete asymptotic analysis. In addition, some numerical results are presented that confirm the outcome of the analysis. In the next section, a preconditioning scheme applicable to a Van der Waals gas is presented. First a summary of the existing preconditioners for ideal gases as well as some approaches for real gases are given. Second the different requirements on a preconditioning scheme in a real gas environment are explained and a preconditioning scheme applicable to a Van der Waals gas is constructed. Finally, two different preconditioners are applied using the thermodynamics implemented in the TAU-code. A comparison of the results of these schemes is shown and their capability is demonstrated.

2. Governing Equations

A mathematical formulation of the physical phenomena under consideration is a requirement for the numerical simulation. There are many such physical phenomena that are relevant for practical applications and hence are described by some kind of mathematical equation. In many cases, conservation equations are used, since this type of formulation is favorable for the numerical implementation. In this study, we investigate the low Mach number asymptotic limit of the set of partial differential equations that represent a mathematical formulation of a flow field in the continuous regime.

The Navier Stokes equations of gas dynamics govern the time-dependent viscous flow. They are a hyperbolic-parabolic system of partial differential equations and result from natural laws expressed by the conservation of mass, momentum and energy; closed by an equation of state. If viscous effects are neglected, the Navier Stokes equations can be simplified to the Euler equations which govern an inviscid flow. For simplicity, we only consider the Euler equations.

In this chapter, we introduce the governing equations relevant for the subsequent chapters. First, we define conservation equations and describe the fundamental conservation laws on an open domain $\mathcal{G} \subset \mathbb{R}^d$. We also discuss the assumptions made as well as different ways to express the Euler equations.

Since a special emphasis is put on the description of thermodynamics, the next section is dedicated to the Van der Waals equation of state. We discuss the assumptions made for the usage of the ideal gas law and which assumptions can be lifted due to the extension to the Van der Waals equation of state. Then we describe the thermal equation of state, followed by the derivation of a caloric state equation. In the end, we briefly discuss the changes in the caloric equation of state that need to be made if the assumptions about the considered fluid are changed.

In the last section, we introduce the nondimensionalization of physical quantities which plays an important role in an asymptotic analysis. By inserting these nondimensional variables into the governing equations, we present the nondimensional forms of both the conservation and the state equations. We also introduce the Mach number as a nondimensional characteristic quantity.

2.1. Euler Equations

Physical processes are often described by conservation equations. The Euler equations, which are a system of partial differential equations, are part of this class. We define conservation equations in the following.

Definition 2.1.1.
Assume $\mathcal{G} \subset \mathbb{R}^d$ is an open domain and $\boldsymbol{f}_j \in \mathcal{C}^1(\mathcal{G}; \mathbb{R}^{d+2}),\ j = 1, ..., d$ is given, then

$$\partial_t \boldsymbol{u} + \sum_{j=1}^{d} \partial_{x_j} \boldsymbol{f}_j(\boldsymbol{u}) = \boldsymbol{0} \text{ in } \mathcal{G} \times \mathbb{R}_0^+$$

is a system of conservation equations in d spatial dimensions for the function vector of the conservative variables

$$\mathcal{G} \times \mathbb{R}_0^+ \ni (\boldsymbol{x}, t) \overset{\boldsymbol{u}}{\mapsto} \boldsymbol{u}(\boldsymbol{x}, t) \in \mathcal{Z}.$$

The set $\mathcal{Z}$ is called a state space and the mapping $\boldsymbol{f}_j$ with $j = 1, ..., d$ a flux function. Time is represented by t and x_j with $j = 1, \ldots, d$ stands for the Cartesian coordinate in j-direction.

In the next paragraphs we present a short description of the Euler equations. A detailed derivation can be found in standard textbooks such as Anderson [1]. We write the Euler equations in dimensional form where the superscript $\hat{}$ indicates the dimensional quantities. The equations are written in a general d-dimensional form where $d = 1, 2, 3$ are the spatial dimensions.
For the Euler equations, the effects of the viscosity of the fluid are neglected. Hence, the viscous terms that are present in the full Navier Stokes equations are not considered in the following description. Here, we only focus on the inviscid terms.
The conservation of mass is represented by the continuity equation

$$\partial_{\hat{t}} \hat{\rho} + \sum_{j=1}^{d} \partial_{\hat{x}_j} \left(\hat{\rho} \hat{v}_j \right) = \hat{0},$$

where $\hat{\rho}$ is the density and $\hat{v}_j$ are the Cartesian velocity components.
The conservation of momentum describes the second Newtonian law and can be written as

$$\partial_{\hat{t}} \left(\hat{\rho} \hat{v}_i \right) + \sum_{j=1}^{d} \partial_{\hat{x}_j} \left(\hat{\rho} \hat{v}_i \hat{v}_j \right) = \sum_{j=1}^{d} \partial_{\hat{x}_j} \left(-\hat{p} \delta_{ij} \right) \text{ for } i = 1, \ldots, d,$$

where $\hat{p}$ is pressure and δ_{ij} the Kronecker delta.
The first law of thermodynamics is expressed by the energy equation which we write as

$$\partial_{\hat{t}} \left(\hat{\rho} \hat{E} \right) + \sum_{j=1}^{d} \partial_{\hat{x}_j} \left(\hat{\rho} \hat{E} \hat{v}_j \right) = \hat{0}.$$

Here $\hat{E}$ represents the mass-specific total energy which consists of the mass-specific internal energy $\hat{e}$ and the mass-specific kinetic energy. So $\hat{E}$ is given by

$$\hat{E} = \hat{e} + \frac{1}{2} \sum_{j=1}^{d} \hat{v}_j^2.$$

In d spatial dimensions, this set of conservation equations contains $d+2$ equations with $d+3$ different variables. Hence, we need another equation to close the system. This additional equation is typically provided by the law governing the thermodynamic behavior of the fluid, in other words by the equation of state. In the next section, we describe the state equation used in this work in detail.

Remark.
In the presented description of the governing equations, we neglect viscous terms which leads to the Euler equations. In addition, continuum assumptions are applied. This means that the length scales considered in this work are several orders of magnitude higher than the mean free path. This assumption is valid for most practical applications excluding only flows like entry problems of spacecrafts, where the mean free path in high altitudes increases greatly, and flows with very small length scales e.g. the internal structure of shock waves or micro channel flows. Further, external forces are not considered.

If we write the conservative variables in form of the vector

$$\hat{\boldsymbol{u}} = \begin{pmatrix} \hat{\rho} \\ \hat{\rho} \hat{v}_1 \\ \vdots \\ \hat{\rho} \hat{v}_d \\ \hat{\rho} \hat{E} \end{pmatrix},$$

we can express the Euler equations as the system of conservation equations

$$\partial_{\hat{t}}\hat{\boldsymbol{u}} + \sum_{j=1}^{d} \partial_{\hat{x}_j} \hat{\boldsymbol{f}}_j(\hat{\boldsymbol{u}}) = \hat{\mathbf{0}}. \tag{2.1}$$

Here the vector $\hat{\boldsymbol{f}}_j(\hat{\boldsymbol{u}})$ represents the convective flux functions and is defined by

$$\hat{\boldsymbol{f}}_j(\hat{\boldsymbol{u}}) = \begin{pmatrix} \hat{\rho}\hat{v}_j \\ \hat{\rho}\hat{v}_1\hat{v}_j + \delta_{1j}\hat{p} \\ \vdots \\ \hat{\rho}\hat{v}_d\hat{v}_j + \delta_{dj}\hat{p} \\ \hat{\rho}\hat{H}\hat{v}_j \end{pmatrix} \text{ for } j = 1, \ldots, d, \tag{2.2}$$

where $\hat{H}$ stands for the specific total enthalpy of the fluid which is defined by

$$\hat{H} = \hat{E} + \frac{\hat{p}}{\hat{\rho}}.$$

The system of equations (2.1) can be replaced by the notation

$$\partial_{\hat{t}}\hat{\boldsymbol{u}} + \sum_{j=1}^{d} \hat{\boldsymbol{A}}_{\hat{\boldsymbol{u}}}^{(j)} \partial_{\hat{x}_j} \hat{\boldsymbol{u}} = \hat{\mathbf{0}} \tag{2.3}$$

with the flux Jacobi matrix

$$\hat{\boldsymbol{A}}_{\hat{\boldsymbol{u}}}^{(j)} = \frac{\partial \hat{\boldsymbol{f}}_j(\hat{\boldsymbol{u}})}{\partial \hat{\boldsymbol{u}}}. \tag{2.4}$$

The eigenvalues of this matrix represent the propagation of information in the flow. They are the convective and acoustic velocities. If the convective velocities become very small compared to the acoustic velocities, the difference between these eigenvalues becomes important for the ability of the numerical algorithm to solve the system of equations simultaneously. We discuss this in more detail in section 4.3 about low Mach preconditioning.

2.2. Van der Waals Equation of State

The simplest form of an equation of state can be formulated for an ideal gas. If a fluid is considered to be an ideal gas, four assumptions are made: First, the volume of the gas particles can be neglected. Second, all gas particles have equal mass and there is no interaction force between the particles. This means attraction or repulsion is not

considered. In addition, the gas particles are assumed to move randomly. And last, collisions between particles are assumed as being perfect elastic collisions without energy loss.
Given these assumptions, the thermal ideal gas equation is

$$\hat{p} = \hat{\rho}\hat{R}\hat{T},$$

with the specific gas constant $\hat{R}$ and the temperature $\hat{T}$. The caloric equation of state for an ideal gas is given as

$$\hat{p} = (\gamma - 1)\,\hat{\rho}\left(\hat{E} - \frac{1}{2}\hat{\boldsymbol{v}}^2\right), \tag{2.5}$$

where γ is the isentropic exponent. A caloric state equation represents the relationship between pressure and energy.
However, the state space within which the ideal gas law is a good approximation is limited by the stated assumptions. Air at ambient temperature and pressure is a good example for an application where the ideal gas assumptions are fulfilled in a sufficient manner for the usage of the ideal gas law. For low temperatures or high pressures, this is no longer the case and the ideal gas law does not model the behavior of the fluid in an adequate way. In addition, many fluids cannot be modeled by the ideal gas law even at ambient conditions, for example if the fluid is in a liquid state. Hence, many interesting problems cannot be modeled solely by the ideal gas equation of state and it is necessary to extend it.
To increase the state space, we need to take effects into account that contradict the ideal gas assumptions. An example for a real gas effect that is comparably simple to model is the effect of the forces between molecules. In addition, the volume of the molecules in the fluid can be considered with a simple extension of the equation of state. With these changes, the resulting state law leads to a better approximation of the physical behavior of fluids at low temperature and high pressure compared to the ideal gas law.
With these changes, we can apply the resulting state law to lower temperatures and higher pressures than it would be possible using the ideal gas law.
To reproduce real gas effects there are two main classes of simple equations of state available: cubic and virial equations. The representation of a fluid by virial equations of state usually does not have a high enough accuracy over a sufficient range of states to be used in engineering applications, see for example Pfenning [55]. Hence, we only consider cubic equations of state. Their name stems from the fact that these equations are cubic in terms of the molecular volume.

The Van der Waals equation of state is the simplest representative of a cubic state equation. It is an extension of the ideal gas law and was proposed by Van der Waals [75] in 1873. Historically, it was the first equation of state that could be used to predict real gas effects. Compared to the ideal gas equation of state, it reduces the assumptions necessary for the application by correcting for both the excluded volume of gas particles and the attractive forces between molecules in the gas.
At moderately high pressures, the Van der Waals equation is a reasonable approximation for real gases. In addition, it qualitatively exhibits key characteristics of the fluid, such as liquid vapor coexistence and it correctly describes the critical point. For fluids at temperatures above the critical value it is an improvement to the ideal gas law. However, in this region the values predicted by the Van der Waals equation differ from experimental values. Hence, at temperatures above the critical point, it is more of qualitative then of quantitative use. A thorough discussion of the state space within which the Van der Waals equation of state can be applied is given in Hill [28].
At thermodynamic states that greatly deviate from an ideal gas or if a more precise description of real gas effects is required, more sophisticated cubic equation of state can be used. Examples are the relations presented by Peng and Robinson [54], Redlich and Kwong [56] or Soave [65]. These equations can be considered to be modifications and extensions of the Van der Waals equation of state. They add properties such as additional dependencies on temperature. To accomplish this, functions of temperature that vary in complexity depending on the specific equation of state are used instead of the constants in the Van der Waals equation of state. However, the basic structure of the equation is kept, which is the one of a cubic state equation. Therefore, insight from the analysis of the Van der Waals equation is also useful for the application of other cubic equations of state.

2.2.1. Thermal Equation of State

The dimensional thermal Van der Waals equation of state is given as

$$\hat{p} = \frac{\hat{\mathcal{R}}\hat{T}}{\hat{V}_m - \hat{b}} - \frac{\hat{a}}{\hat{V}_m^2}, \tag{2.6}$$

where $\hat{V}_m$ is the molar volume defined as

$$\hat{V}_m = \frac{\hat{M}_w}{\hat{\rho}} \tag{2.7}$$

with the molecular weight $\hat{M}_w$. The constant $\hat{\mathcal{R}}$ represents the universal gas constant which has a value of $\hat{\mathcal{R}} = 8.314 \frac{J}{mol \cdot K}$. The universal gas constant and the molecular weight have the following relationship with the specific gas constant, which is used in the ideal gas equation of state (2.2):

$$\hat{\mathcal{R}} = \hat{M}_w \hat{R} \tag{2.8}$$

The two constants $\hat{a}$ and $\hat{b}$ represent the extension of the ideal gas law made by Van der Waals. The constant $\hat{a}$ introduces an attractive potential between the particles in the gas, where a higher value of $\hat{a}$ stands for a higher compression of the gas due to greater attraction. This effect is subtracted from the acting pressure. The volume occupied by gas particles is represented by the constant $\hat{b}$. The available volume is reduced by this molecular volume. Both $\hat{a}$ and $\hat{b}$ depend on the specific fluid and can be calculated if the critical values are known. For many common fluids these values are listed in standard textbooks such as Weigand [76]. If both values approach zero, the Van der Waals equation of state turns into the ideal gas law (see also equations (2.7) and (2.8)).
Since the Euler equations are in terms of density, it is helpful for the analysis to rewrite the state equation. By substituting the molecular volume (2.7) into equation (2.6) we get

$$\hat{p} = \frac{\hat{\rho}\hat{\mathcal{R}}\hat{T}}{\hat{M}_w - \hat{b}\hat{\rho}} - \frac{\hat{a}\hat{\rho}^2}{\hat{M}_w{}^2}. \tag{2.9}$$

2.2.2. Derivation of Caloric Equation of State

Unlike for an ideal gas, for a Van der Waals gas the caloric equation of state is not given by a simple, generally valid relation. However, it can be derived using simple thermodynamic principles. We derive the caloric equation of state in the following.
The total differential of the molar internal energy is defined as

$$d\hat{e}_m = \left(\frac{\partial \hat{e}_m}{\partial \hat{T}}\right)_{\hat{V}_m} d\hat{T} + \left(\frac{\partial \hat{e}_m}{\partial \hat{V}_m}\right)_{\hat{T}} d\hat{V}_m.$$

Note that we consider the molar internal energy $\hat{e}_m$ and the molar volume $\hat{V}_m$ for this derivation. The relationship between $\hat{e}_m$ and the specific internal energy $\hat{e}$ is

$$\hat{e}_m = \hat{e}\hat{M}_w.$$

After inserting the specific heat at constant volume $\hat{c}_{\hat{v},m} = \left(\frac{\partial \hat{e}_m}{\partial \hat{T}}\right)_{\hat{V}_m}$ and applying an

integral, we arrive at

$$\hat{e}_m = \int_{\hat{T}_0}^{\hat{T}} \hat{c}_{\hat{v},m} d\hat{T} + \int_{\hat{V}_{m,0}}^{\hat{V}_m} \left(\frac{\partial \hat{e}_m}{\partial \hat{V}_m}\right)_{\hat{T}} d\hat{V}_m + \hat{e}_m(\hat{V}_{m,0}, \hat{T}_0). \tag{2.10}$$

A combination of the first and second law of thermodynamics can be used to derive the partial derivative of the internal energy. It is given by

$$d\hat{e}_m = \hat{T} d\hat{s}_m - \hat{p} d\hat{V}_m$$

with the molar entropy $\hat{s}_m$. We rewrite this equation to get the necessary derivative as

$$\left(\frac{\partial \hat{e}_m}{\partial \hat{V}_m}\right)_{\hat{T}} = \hat{T} \left(\frac{\partial \hat{s}_m}{\partial \hat{V}_m}\right)_{\hat{T}} - \hat{p}.$$

In the next step we insert the Maxwell relation

$$\left(\frac{\partial \hat{s}_m}{\partial \hat{V}_m}\right)_{\hat{T}} = \left(\frac{\partial \hat{p}}{\partial \hat{T}}\right)_{\hat{V}_m}$$

which leads to

$$\left(\frac{\partial \hat{e}_m}{\partial \hat{V}_m}\right)_{\hat{T}} = \hat{T} \left(\frac{\partial \hat{p}}{\partial \hat{T}}\right)_{\hat{V}_m} - \hat{p}. \tag{2.11}$$

Now we evaluate this expression using the thermal Van der Waals equation of state (2.6). This results in

$$\left(\frac{\partial \hat{e}_m}{\partial \hat{V}_m}\right)_{\hat{T}} = \hat{T} \left(\frac{\hat{\mathcal{R}}}{\hat{V}_m - \hat{b}}\right) - \left(\frac{\hat{\mathcal{R}}\hat{T}}{\hat{V}_m - \hat{b}} - \frac{\hat{a}}{\hat{V}_m^2}\right) = \frac{\hat{a}}{\hat{V}_m^2}. \tag{2.12}$$

Now, to solve the integral in equation (2.10), a representation of the specific heat at constant volume $\hat{c}_{\hat{v},m}$ is necessary. Since $\hat{c}_{\hat{v},m} = \left(\frac{\partial \hat{e}_m}{\partial \hat{T}}\right)_{\hat{V}_m}$, in general, $\hat{c}_{\hat{v},m}$ is a function of both temperature and molar volume. However, in the following Lemma we show that $\hat{c}_{\hat{v},m}$ is independent of the molar volume for a Van der Waals gas.

Lemma 1.
For a Van der Waals gas, the specific heat at constant volume only depends on temperature.

Proof.
With $\hat{c}_{\hat{v},m} = \left(\frac{\partial \hat{e}_m}{\partial \hat{T}}\right)_{\hat{V}_m}$ we get the following expression for the change of $\hat{c}_{\hat{v},m}$ with molar volume:

$$\left(\frac{\partial \hat{c}_{\hat{v},m}}{\partial \hat{V}_m}\right)_{\hat{T}} = \frac{\partial}{\partial \hat{V}_m} \left(\frac{\partial \hat{e}_m}{\partial \hat{T}}\right)_{\hat{T}} = \frac{\partial}{\partial \hat{T}} \left(\frac{\partial \hat{e}_m}{\partial \hat{V}_m}\right)_{\hat{T}}$$

Next, we combine this relation with the derivative in equation (2.11) which leads to

$$\left(\frac{\partial \hat{c}_{\hat{v},m}}{\partial \hat{V}_m}\right)_{\hat{T}} = \frac{\partial}{\partial \hat{T}}\left(\hat{T}\left(\frac{\partial \hat{p}}{\partial \hat{T}}\right)_{\hat{V}_m} - \hat{p}\right)_{\hat{T}} = \hat{T}\left(\frac{\partial^2 \hat{p}}{\partial \hat{T}^2}\right)_{\hat{V}_m}. \tag{2.13}$$

We use the thermal Van der Waals equation (2.9) to evaluate the derivative. In a first step we get

$$\left(\frac{\partial \hat{p}}{\partial \hat{T}}\right)_{\hat{V}_m} = \left(\frac{\hat{\rho}\hat{\mathcal{R}}}{\hat{M}_w - \hat{b}\hat{\rho}}\right).$$

If we insert this result into the derivative in equation (2.13), we arrive at

$$\hat{T}\left(\frac{\partial^2 \hat{p}}{\partial \hat{T}^2}\right)_{\hat{V}_m} = \hat{T}\frac{\partial}{\partial \hat{T}}\left(\frac{\hat{\rho}\hat{\mathcal{R}}}{\hat{M}_w - \hat{b}\hat{\rho}}\right) = 0$$

which is equal to

$$\left(\frac{\partial \hat{c}_{\hat{v},m}}{\partial \hat{V}_m}\right)_{\hat{T}} = 0.$$

So, for a Van der Waals gas, the specific heat at constant volume is independent of the molar volume and hence only dependent on temperature. □

Inserting the results from equation (2.12) and Lemma 1 into equation (2.10), we can write the integral of the molar internal energy as

$$\hat{e}_m = \int_{\hat{T}_0}^{\hat{T}} \hat{c}_{\hat{v},m}(\hat{T})d\hat{T} + \int_{\hat{V}_{m,0}}^{\hat{V}_m} \frac{\hat{a}}{\hat{V}_m^2} d\hat{V}_m + \hat{e}_m(\hat{V}_{m,0}, \hat{T}_0).$$

To arrive at an expression for $\hat{c}_{\hat{v},m}(\hat{T})$, we need to make some assumptions about the fluid under consideration. Here we assume that the fluid is a monoatomic gas at a temperature where electronic excitation has no influence on the value of the specific heats. Under these conditions, we can assume $\hat{c}_{\hat{v},m}$ to be a constant with the value of $\hat{c}_{\hat{v},m} = \frac{3}{2}\hat{\mathcal{R}}$. This is also true for a non-monoatomic gas at a temperature where it has no change in the excitation of internal degrees of freedom. A detailed description of the behavior of $\hat{c}_{\hat{v},m}$ with temperature can be found in textbooks such as Vincenti and Kruger [73] and is beyond the scope of this work.
Now we integrate from $\hat{T}_0 = \hat{0}$, $\hat{V}_{m,0} = \hat{0}$ to $\hat{T} = \hat{T}$, $\hat{V}_m = \hat{V}_m$ to arrive at a form of the caloric equation of state. This leads to

$$\hat{e}_m = \frac{3}{2}\hat{\mathcal{R}}\hat{T} - \frac{\hat{a}}{\hat{V}_m}.$$

Next, we replace the molar internal energy $\hat{e}_m$ by the expression

$$\hat{E} = \frac{1}{2}|\hat{\boldsymbol{v}}|^2 + \frac{\hat{e}_m}{\hat{M}_w}$$

and insert the thermal equation of state (2.6) for the product $\hat{\mathcal{R}}\hat{T}$. After rearranging the expression, we arrive at the final form

$$\hat{p} = \frac{\hat{M}_w\hat{E} - \frac{1}{2}\hat{M}_w|\hat{\boldsymbol{v}}|^2 + \frac{\hat{a}}{\hat{V}_m}}{\frac{3}{2}\left(\hat{V}_m - \hat{b}\right)} - \frac{\hat{a}}{\hat{V}_m^2} \tag{2.14}$$

of the caloric equation of state for a Van der Waals gas with constant specific heat. Again, we reformulated the equation in terms of density to get the final result

$$\hat{p} = \frac{\hat{M}_w\hat{\rho}\hat{E} - \frac{1}{2}\hat{\rho}\hat{M}_w|\hat{\boldsymbol{v}}|^2 + \frac{\hat{a}\hat{\rho}^2}{\hat{M}_w}}{\frac{3}{2}\left(\hat{M}_w - \hat{b}\hat{\rho}\right)} - \frac{\hat{a}\hat{\rho}^2}{\hat{M}_w^2}. \tag{2.15}$$

Remark.
We show in Lemma 1 that the specific heat at constant volume only depends on temperature. The assumptions we make about the fluid limit the validity of the caloric equation of state to a specific temperature range. To apply the state equation to gases outside these assumptions, we can insert other expressions for $\hat{c}_{\hat{v},m}$. For example, a diatomic gas at moderate temperatures has a specific heat at constant volume of $\hat{c}_{\hat{v},m} = \frac{5}{2}\hat{\mathcal{R}}$. Hence, in the final caloric equation of state (2.15), only some factors need to be adjusted while the structure of the equation remains identical to the one analyzed in the following chapters.

2.3. Nondimensionalization

Every physical quantity is the product of a value and the corresponding unit. In this work, we use the SI-system as the set of fundamental units. This means that every unit is based on one of the SI units or a combination of them. For the quantities considered here, the basic units of length ($[m]$), time ($[s]$), mass ($[kg]$), temperature ($[K]$) and amount of substance ($[mol]$) are necessary. In Table 2.1 all physical quantities appearing within this work are listed. We can see that all units can be expressed as a combination of these five base units.
We can match all physical quantities with a dimensional reference value within a defined region in space and time. These reference values are indicated by the subscript $_{\text{ref}}$. The reference values are taken from the underlying flow. For the velocity, the reference value

Table 2.1.: Names, units and reference values of physical quantities

Physical Quantity		Unit	Reference Value
Cartesian coordinate	$\hat{\boldsymbol{x}}$	[m]	$\hat{l}_{\text{ref}}$
time	$\hat{t}$	[s]	$\hat{t}_{\text{ref}} = \frac{\hat{l}_{\text{ref}}}{\hat{v}_{\text{ref}}}$
velocity vector	$\hat{\boldsymbol{v}}$	[m/s]	$\hat{v}_{\text{ref}}$
density	$\hat{\rho}$	$[\text{kg/m}^3]$	$\hat{\rho}_{\text{ref}}$
temperature	$\hat{T}$	[K]	$\hat{T}_{\text{ref}}$
pressure	$\hat{p}$	$[\text{Pa}] = [\text{kg}/(\text{m} \cdot \text{s}^2)]$	$\hat{p}_{\text{ref}}$
specific internal energy	$\hat{e}$	$[\text{J/kg}] = [\text{m}^2/\text{s}^2]$	$\frac{\hat{p}_{\text{ref}}}{\hat{\rho}_{\text{ref}}}$
specific total energy	$\hat{E}$	$[\text{J/kg}] = [\text{m}^2/\text{s}^2]$	$\frac{\hat{p}_{\text{ref}}}{\hat{\rho}_{\text{ref}}}$
specific total enthalpy	$\hat{H}$	$[\text{J/kg}] = [\text{m}^2/\text{s}^2]$	$\frac{\hat{p}_{\text{ref}}}{\hat{\rho}_{\text{ref}}}$
speed of sound	$\hat{c}$	[m/s]	$\hat{c}_{\text{ref}} = \sqrt{\frac{\hat{p}_{\text{ref}}}{\hat{\rho}_{\text{ref}}}}$
molecular weight	$\hat{M}_w$	[kg/mol]	$\hat{M}_{w,\text{ref}}$
specific heat at constant volume	$\hat{c}_{\hat{v}}$	$[(\text{kg} \cdot \text{m}^2)/(\text{K} \cdot \text{mol} \cdot \text{s}^2)]$	$\frac{\hat{p}_{\text{ref}}\hat{M}_{w,\text{ref}}}{\hat{\rho}_{\text{ref}}\hat{T}_{\text{ref}}}$
universal gas constant	$\hat{\mathcal{R}}$	$[(\text{kg} \cdot \text{m}^2)/(\text{K} \cdot \text{mol} \cdot \text{s}^2)]$	$\frac{\hat{p}_{\text{ref}}\hat{M}_{w,\text{ref}}}{\hat{\rho}_{\text{ref}}\hat{T}_{\text{ref}}}$
intermolecular forces-constant	$\hat{a}$	$[(\text{kg} \cdot \text{m}^5)/(\text{mol}^2 \cdot \text{s}^2)]$	$\frac{\hat{p}_{\text{ref}}\hat{M}^2_{w,\text{ref}}}{\hat{\rho}^2_{\text{ref}}}$
co-volume	$\hat{b}$	$[\text{m}^3/\text{mol}]$	$\frac{\hat{M}_{w,\text{ref}}}{\hat{\rho}_{\text{ref}}}$

$\hat{v}_{\text{ref}}$ is the absolute value of the velocity vector. Each dimensional physical quantity $\hat{\Phi}$ can be expressed by the product

$$\hat{\Phi} = \Phi \cdot \hat{\Phi}_{\text{ref}}, \tag{2.16}$$

where Φ is nondimensional. If the reference value and the variable show the same behavior for a vanishing Mach number, the resulting nondimensional variable is of $\mathcal{O}(1)$ as $M \to 0$. To ensure this similarity in orders of magnitude, we choose the values of the surrounding flow field as references. The process of turning a variable nondimensional is called nondimensionalization.

By replacing the dimensional variables in the governing equations by products of the form (2.16), we can write the equations in a nondimensional form. The advantage of such equations is that one solution is valid for multiple sets of conditions, as long as they have the same nondimensional form. A possible application is the transfer of experimental results from measurements on a smaller model to the size of the actual configuration by scaling the nondimensional values in an appropriate way. The results of the nondimensional equations do not depend on the chosen system of units, they can be transferred to any given system and hence be compared to measurements of actual physical values. On the basis of the reference values listed in Table 2.1, we transform the Euler equations given in equation (2.1) on page 8 with the fluxes given by equation (2.2) into

$$\partial_t \boldsymbol{u} + \sum_{j=1}^{d} \partial_{x_j} \boldsymbol{f}_j(\boldsymbol{u}) = \boldsymbol{0} \tag{2.17}$$

with

$$\boldsymbol{f}_j(\boldsymbol{u}) = \begin{pmatrix} \rho v_j \\ \rho v_1 v_j + \delta_{1j} \frac{p}{M^2} \\ \vdots \\ \rho v_d v_j + \delta_{dj} \frac{p}{M^2} \\ \rho H v_j \end{pmatrix} \text{ for } j = 1, \ldots, d.$$

In this nondimensional form of the equations, the Mach number M appears as a nondimensional characteristic number. It is defined as

$$M = \frac{\hat{v}_{\text{ref}}}{\hat{c}_{\text{ref}}}, \tag{2.18}$$

where $\hat{c}_{\text{ref}}$ is the reference value for the speed of sound. This allows us to investigate the behavior of the physical quantities in the Euler equations as the Mach number approaches zero by means of a formal asymptotic analysis.

The set of reference values contains separate references for pressure, density and the velocity vector, see Table 2.1. Another common approach is to use only two of these reference values. This can be realized by either replacing the pressure reference by $\hat{\rho}_{\text{ref}} \hat{v}_{\text{ref}}^2$ or using $\sqrt{\frac{\hat{p}_{\text{ref}}}{\hat{\rho}_{\text{ref}}}}$ as a velocity reference. Both alternative approaches lead to nondimensional equations that have a similar form as the dimensional system formulated in equation (2.1) with the fluxes in equation (2.2), i.e. the Mach number does not appear in the nondimensional equations. This form of nondimensionalization is typically used in numerical codes and we come back to it in chapter 4 where we describe and analyze a numerical scheme.

However, these choices of reference values are not favorable for an asymptotic analysis as $M \to 0$. The nondimensional values for pressure and velocity, which result from these two choices of reference values, are not of $\mathcal{O}(1)$ as the local velocity approaches zero. Hence, we choose the presented set of references values. It is advantageous due to both the Mach number appearing in the nondimensional Euler equations and the nondimensional quantities being of $\mathcal{O}(1)$ as $M \to 0$.

Remark.
Note that $\hat{c}_{\text{ref}} = \sqrt{\frac{\hat{p}_{\text{ref}}}{\hat{\rho}_{\text{ref}}}}$ differs from the local speed of sound of the gas, especially when a Van der Waals gas is considered. Hence, the Mach number M that appears in the momentum equations is not equal to the local Mach number Ma. However, both $\hat{c}_{\text{ref}}$ and the local speed of sound have the same asymptotic behavior for a vanishing Mach number. Due to the definition of the Mach number (2.18), the same is true for M and Ma. Using the order symbols we define in chapter 3 on page 24, we can say that $M = \mathcal{O}_S(Ma)$ as $M \to 0$.
Hence, in the context of the asymptotic analysis within this work, the usage of M and Ma can be considered to be equivalent.

The thermal equation of state (2.9) on page 11 can be nondimensionalized in a similar way to the Euler equations, leading to

$$p = \frac{\rho \mathcal{R} T}{M_w - b\rho} - \frac{a\rho^2}{M_w^2}.$$

The nondimensionalization of the caloric equation of state (2.15) gives us

$$p = \frac{2M_w \rho E - M^2 M_w \rho |\boldsymbol{v}|^2 + 2\frac{a\rho^2}{M_w}}{3M_w - 3b\rho} - \frac{a\rho^2}{M_w^2}. \tag{2.19}$$

Remark.
We choose reference values depending on the underlying physical flow field for the nondimensionalization of the thermodynamic quantities instead of the critical values as it is done in many other works. Here, the goal are nondimensional quantities of a similar order of magnitude for a better understanding of their behavior by means of an asymptotic analysis. By choosing the critical values as a reference, the constants a and b can be eliminated from the nondimensional equations, resulting in one single thermal equation of state for all fluids, in terms of their critical values. This concept is known as the corresponding states principle (see for example Emanuel [21]). However, in this case the order of magnitude of the thermodynamic quantities can differ greatly, since they are

in terms of their critical values. Therefore, this form of nondimensionalization is not suitable for the purpose of this work.

2.4. Initial and boundary conditions

The boundary conditions influence the fluxes over the boundary of the flow domain. Here we consider two different boundary conditions that require the specification of distinct boundary values. Hence, we separate the boundary of the triangular grid $\mathcal{T}_h$ into two separate parts

$$\partial\mathcal{T}_h = \partial\mathcal{T}_{h,\mathrm{w}} \cup \partial\mathcal{T}_{h,\mathrm{ff}},$$

where $\partial\mathcal{T}_{h,\mathrm{w}}$ describes a solid wall and $\partial\mathcal{T}_{h,\mathrm{ff}}$ stands for the farfield boundary condition which covers the remaining boundaries. The reference frame is chosen such that the body is at rest and there are no moving walls. Hence, the flow is moving through the farfield boundary. The condition at the farfield is defined in the farfield state $\boldsymbol{u}_{\mathrm{ff}}$.

2.4.1. Solid Wall

The surface of the body is modeled as a solid wall through which the fluid cannot flow. So, the velocity perpendicular to the wall has to follow

$$v_{\boldsymbol{n}} = 0, \tag{2.20}$$

where the subscript $\boldsymbol{n}$ indicates the component normal to a face, in this case normal to the wall.
With this boundary condition, an exact calculation of the integral at the boundary is possible. Hence, for a solid wall, the calculation of a numerical flux function is not necessary.
For an inviscid flow, nonzero velocity components tangential to the wall are permitted. In the viscous case, however, the no-slip condition is applied. So the tangential velocity is set to zero as well. Hence, at the wall,

$$\boldsymbol{v} = \boldsymbol{0}$$

has to be true. In the viscous case, an additional boundary condition for the energy equation is required at a solid wall, e.g. an isothermal wall.

2.4.2. Farfield Boundary

The outer boundary of the flow domain is modeled using a farfield boundary condition based on the theory of Whitfield [78]. A Riemann problem is defined with the left state located on the boundary face, representing the flow condition within the computational domain and the right state being external to the computational domain. The treatment of the boundary face depends on the sign and magnitude of the Mach number in the direction of $\boldsymbol{n}$

$$Ma_{\boldsymbol{n}} = \frac{v_{\boldsymbol{n}}}{c}.$$

The magnitude of $Ma_{\boldsymbol{n}}$ at the left state is used to decide whether the boundary is super- or subsonic. The direction of the flow decides over the usage of an inflow or outflow boundary condition.

Supersonic Inflow/Outflow

If the absolute value of $Ma_{\boldsymbol{n}}$ at the left state is greater than or equal to one, the face is assumed to be a supersonic boundary. If $(Ma_{\boldsymbol{n}})_L$ is positive, the boundary is recognized as a supersonic outflow. Hence, the outer state is set equal to the left hand state. In case of a negative sign of the left state Mach number $Ma_{\boldsymbol{n}}$, the flow conditions at the outer state, which represents the approaching flow, are set to the farfield state to gain a supersonic inflow.

Subsonic Outflow

If the left state Mach number $Ma_{\boldsymbol{n}}$ is positive and smaller than one, the face lies on a subsonic outflow boundary. In this case, the MAPS+ flux function, that is described in section 4.2.2, is used to calculate the flow over the boundary face. Here, the left states are given by the flow state within the computational domain and represent the flow approaching the boundary. The pressure on the boundary p_{bdry} equals the pressure of the leaving flow which is the farfield pressure. Hence, it is

$$p_{\text{bdry}} = p_R = p_{\text{ff}}$$

For the right state, which represents the flow leaving the boundary, the remaining quantities are calculated using the pressure difference over the boundary. The density of the right state results in

$$\rho_R = \rho_L + \frac{p_{\text{bdry}} - p_L}{c_L^2},$$

where c_L is the speed of sound calculated for the left state. The subscript L and R

indicate the left and right state, respectively.
The velocity components are calculated as

$$(v_i)_R = (v_i)_L + n_i \frac{p_{\text{bdry}} - p_L}{\rho_L c_L}, \text{ for } i \in \{1, \ldots, d\}$$

where n_i, $i \in \{1, \ldots d\}$ are the components of the outer unit normal vector of the boundary face in the Cartesian directions. The remaining quantities of the right state are calculated with the thermodynamic modules implemented in the TAU-code using the values for density and pressure estimated above.

Subsonic Inflow

If the left state Mach number $Ma_{\boldsymbol{n}}$ lies between negative one and zero, the face lies on a subsonic inflow boundary. As for the subsonic outflow, the MAPS+ flux function is used to calculate the flow over the boundary face. Again, the left states are the states within the computational domain but in this case they represent the flow leaving the boundary. The right states represent the flow approaching the boundary. In a general d-dimensional system, the pressure on the boundary face p_{bdry} can be calculated with

$$p_{\text{bdry}} = \frac{1}{2} \left[p_L + p_R + \rho_L c_L \begin{pmatrix} n_1 \\ \vdots \\ n_d \end{pmatrix} \cdot \left[\begin{pmatrix} v_1 \\ \vdots \\ v_d \end{pmatrix}_L - \begin{pmatrix} v_1 \\ \vdots \\ v_d \end{pmatrix}_R \right] \right].$$

Again, the right states are calculated using the pressure difference over the boundary. The density of the right state results in

$$\rho_R = \rho_{\text{ff}} + \frac{p_{\text{bdry}} - p_{\text{ff}}}{c_L^2},$$

where the subscript $_{\text{ff}}$ indicates the farfield value of the given quantity.
The velocity components are calculated as

$$(v_i)_R = (v_i)_{\text{ff}} + n_i \frac{p_{\text{ff}} - p_{\text{bdry}}}{\rho_L c_L}, \text{ for } i \in \{1, \ldots, d\}.$$

Again, the remaining quantities of the right state are calculated using the thermodynamic modules.

2.4.3. Initial Conditions

The initial conditions for the numerical simulation are given by the reference values

$$(\rho_{\text{ref}}, v_{1,\text{ref}}, \ldots, v_{d,\text{ref}}, p_{\text{ref}})^T .$$

All other quantities can be calculated from this set using the implemented thermodynamic relations.

3. Asymptotic Analysis

Asymptotic analyses are used to investigate central properties of the solution without solving the entire problem. They can be applied to analyze both ordinary and partial differential equations or explicitly stated functions. There are many applications for asymptotic analyses in science and industry, see for example Schneider [63] or Kevorkian and Cole [30].

The right choice of the asymptotic sequence is important for the success of the analysis since it defines the function space within which the solution has to exist. This means that the choice of the asymptotic sequence can decide whether the analysis is successful. However, the asymptotic analysis does not guarantee the existence of a solution within the chosen function space, regardless of the chosen sequence.

In addition, the success of the analysis depends on the choice of suitable spatial and time scales. The results only contain phenomena that happen on the chosen scales. If a given problem encloses several scales, for example due to a convective and an acoustic component, the result of the asymptotic analysis can give an incomplete picture of the actual solution even if a suitable asymptotic sequence is chosen. So, in order to gain the best results, both the choice of the asymptotic sequence and the investigated scales are important.

In this chapter, we introduce asymptotic functions and conduct an asymptotic analysis of the Euler equations. We begin with a brief overview of the work this thesis builds on. We summarize the published work on asymptotic analyses of the Navier Stokes and Euler equations as well as asymptotic analyses of numerical schemes.

Next, we introduce some properties of asymptotic functions that are important for the following analysis. We define order functions and an asymptotic sequence. In addition, we state a property which helps us solve the asymptotic equations.

In the third section, we introduce single scale asymptotic expansions. We explain the difference between a single scale and a multiple scale expansion and give the definition of the former. Finally, we describe the typical procedure of an asymptotic analysis of a homogeneous differential equation.

We conclude this chapter by conducting an asymptotic analysis of the Euler equations for a Van der Waals gas. We repeat some conclusions of other authors concerning the

behavior of the pressure distribution that result from the momentum equations. Finally, we present the first asymptotic analysis of the Van der Waals equation of state. This also leads to constraints on the behavior of pressure. At the end, we compare the results to the ones of an ideal gas and discuss the differences.

3.1. State of the Art

In 1981, Klainerman and Majda [33], [34] used a single scale asymptotic analysis to investigate the inviscid flow of an ideal gas as the Mach number approaches zero. Choosing the proper initial conditions, they show the convergence of the compressible solution of the Euler equations towards the incompressible one where density is independent of pressure. Klainerman and Majda investigate both open domains and domains bounded by periodic boundary conditions. Ebin [18] arrives at similar results using more general boundary conditions.
These investigations were repeated and extended by Ukai [70] and Asano [2]. They broaden the validness of the results by the usage of more general initial conditions that no longer require the leading order velocity distribution to be divergence free. However, all these analyses were limited by the considerations of only one spatial scale and more detailed insight about the behavior of the flow at low Mach numbers could not be gained.
A decade later, Klein [35] analyzed the compressible Euler equations in the limit of small Mach numbers using a multiple scale asymptotic analysis. By considering two different spatial scales, they investigate both convective and acoustic effects. Klein uses the results of this analysis to propose an extension of a compressible numerical scheme towards the incompressible limit that is based on physics. Meister [46] gives a mathematical justification for the approach by Klein and presents a single scale asymptotic analysis of a bounded domain and a multiple scale analysis of an open domain. In addition, they further develop the numerical method proposed by Klein to cover simulations in two spatial dimensions. A detailed summary of the improvement of numerical schemes for the Navier-Stokes and Euler equations and the extension towards the incompressible limit is given in the review article of Klein et al. [36]. There the application of single and multiple scale asymptotic analyses is described precisely.
The asymptotic analysis of a numerical scheme is described by Meister [48] for an ideal gas inviscid flow solver. A similar investigation is published by Guillard and Nkonga [27]. In both publications it is shown that the solution of the discrete scheme contains pressure fluctuations on a different scale than the continuous pressure. This explains the failure of a compressible numerical scheme as the Mach number approaches zero. In addition, it is

shown that a correct scaling of the discrete pressure can be gained by preconditioning the numerical dissipation tensor. This investigation is extended by Meister [49] to viscous simulations.
In this work, we apply the analysis presented by Meister to a flow with a more general thermodynamic description. We extend the continuous single scale analysis described in Meister [46] to the Euler equations for a Van der Waals gas. In addition, we apply the discrete analysis of a numerical scheme described in Meister [48] to a flux function that can also be used to simulate real gases.

3.2. Properties of Asymptotic Functions

Order functions play an important role in asymptotic analyses. Since they were first used by Landau, they are commonly referred to as Landau symbols. They describe the relationship between the behavior of two functions as an additional parameter approaches a limit. We define order functions in the following as shorthand notations for these relative properties of the respective functions, following the description by Kimmerle and Stroppel [32] and Malham [45].

Definition 3.2.1.
Suppose $f(\boldsymbol{x};\epsilon)$ and $g(\boldsymbol{x};\epsilon)$ are functions of the real variable $\boldsymbol{x}$ and an additional variable ϵ. If $\epsilon_0 \in \mathcal{I}$, we write for $f, g : \mathcal{G} \times \mathcal{I}\backslash\{\epsilon_0\} \to \mathbb{R}$:

(a) Asymptotically bounded:

$$f(\boldsymbol{x};\epsilon) = \mathcal{O}(g(\boldsymbol{x};\epsilon)) \text{ for } \epsilon \to \epsilon_0,$$

if there exists a function $h : \mathcal{G} \to \mathbb{R}$, such that

$$\lim_{\epsilon\to\epsilon_0} \frac{f(\boldsymbol{x};\epsilon)}{g(\boldsymbol{x};\epsilon)} = h(\boldsymbol{x})$$

holds for each $\boldsymbol{x} \in \mathcal{G}$.
This means that $f(\boldsymbol{x};\epsilon)$ is asymptotically bounded in magnitude by $g(\boldsymbol{x};\epsilon)$ as $\epsilon \to \epsilon_0$. We say $f(\boldsymbol{x};\epsilon)$ is of "order big O" of $g(\boldsymbol{x};\epsilon)$.

(b) Asymptotically smaller:

$$f(\boldsymbol{x};\epsilon) = o(g(\boldsymbol{x};\epsilon)) \text{ for } \epsilon \to \epsilon_0,$$

if

$$\lim_{\epsilon \to \epsilon_0} \frac{f(\boldsymbol{x};\epsilon)}{g(\boldsymbol{x};\epsilon)} = 0$$

holds for each $\boldsymbol{x} \in \mathcal{G}$. This means that $f(\boldsymbol{x};\epsilon)$ is asymptotically smaller than $g(\boldsymbol{x};\epsilon)$. We say $f(\boldsymbol{x};\epsilon)$ is of "order little o" of $g(\boldsymbol{x};\epsilon)$.

(c) Asymptotically equal:

$$f(\boldsymbol{x};\epsilon) = \mathcal{O}_S(g(\boldsymbol{x};\epsilon)) \text{ for } \epsilon \to \epsilon_0,$$

if $f(\boldsymbol{x};\epsilon) = \mathcal{O}(g(\boldsymbol{x};\epsilon))$ and $g(\boldsymbol{x};\epsilon) = \mathcal{O}(f(\boldsymbol{x};\epsilon))$ for $\epsilon \to \epsilon_0$.

An asymptotic sequence is the base of asymptotic expansions. We specify such sequences with the help of the o-order relation in the following Definition.

Definition 3.2.2.
A sequence of functions $\{\phi_n\}_{n\in\mathbb{N}_0}$ with $\phi_n : \mathcal{I}\backslash\{\epsilon_0\} \to \mathbb{R}$ is said to form an asymptotic sequence with regard to $\epsilon_0 \in \mathcal{I}$ if, for all n,

$$\phi_{n+1}(\epsilon) = o(\phi_n(\epsilon)),$$

as $\epsilon \to \epsilon_0$.

As an extension to this property of an asymptotic sequence, the following Lemma allows us to identify terms multiplied by the same function ϕ_n.

Lemma 2.
If $\{\phi_n\}_{n\in\mathbb{N}_0}$ is an asymptotic sequence and L_n for $n = 0, \ldots, N$ are arbitrary terms independent of ϵ, then the two statements

$$\sum_{n=0}^{N} \phi_n(\epsilon) L_n = o(\phi_N(\epsilon)) \text{ for } \epsilon \to \epsilon_0$$

and

$$L_n = 0 \text{ for } n = 0, ..., N$$

are equivalent.

The proof of this Lemma is given by Meister [46].

3.3. Single Scale Asymptotic Expansions

Single scale asymptotic expansions are the simplest form of asymptotic expansions. They are a subset of multiple scale asymptotic expansions which are out of the scope of this work but are explained in detail by Meister [46]. If a single scale asymptotic expansion is used to analyze a function, only phenomena on the chosen spatial or time scale are represented in the solution.
For problems with characteristics on several scales this often leads to a limited area of validity. In these cases, another single scale asymptotic expansion can be conducted using a different scale which corresponds to a scaling of the initial problem. The two locally valid solutions can then be combined within a common area of validity to gain a single solution, see Kevorkian and Cole [30] and Schneider [63].
However, since the final expansion includes different scales it belongs to the multiple scale asymptotic expansions. Hence, for some problems, it can be useful to start the analysis with a multiple scale asymptotic expansion. For the analysis we present here, a single scale expansion is sufficient.

Definition 3.3.1.
If $\{\phi_n\}_{n\in\mathbb{N}_0}$ is an asymptotic sequence of functions $f : \mathcal{G} \times \mathcal{I}\backslash\{\epsilon_0\} \to \mathbb{R}, (\boldsymbol{x};\epsilon) \overset{f}{\mapsto} f(\boldsymbol{x};\epsilon)$, where $\{f_n\}_{n\in\mathbb{N}_0}$ is a function sequence with $f_n : \mathcal{G} \to \mathbb{R}$, we say that

$$\sum_{n=0}^{N} \phi_n(\epsilon) f_n(\boldsymbol{x})$$

is an asymptotic (N + 1)-term single scale expansion of f, if for each N

$$f(\boldsymbol{x};\epsilon) - \sum_{n=0}^{N} \phi_n(\epsilon) f_n(\boldsymbol{x}) = o(\phi_N(\epsilon)),$$

as $\epsilon \to \epsilon_0$. This means the error is asymptotically smaller than the last term of the expansion.

The typical procedure of an asymptotic analysis of a homogeneous differential equation is as follows. First, we choose an asymptotic sequence $\{\phi_n\}_{n\in\mathbb{N}_0}$, giving an ansatz of the form

$$f(\boldsymbol{x};\epsilon) = \sum_{n=0}^{N} \phi_n(\epsilon) f_n(\boldsymbol{x}) + o(\phi_N(\epsilon)) \text{ for } \epsilon \to \epsilon_0$$

for the solution f of the differential equation. Then we insert this ansatz into the differ-

ential equation, which is then written in the form

$$\sum_{k=0}^{M} \psi_k(\epsilon) L_k(f_0, ..., f_N) = o(\psi_M(\epsilon)) \text{ for } \epsilon \to \epsilon_0$$

with $M \in \mathbb{N}_0$ and the asymptotic sequence $\{\psi_k\}$ for $k = 0, ..., M$. The terms L_k are independent of ϵ for $k = 0, ..., M$. Hence, due to Lemma 2, we can find the functions f_n for $n = 0, ..., N$ by solving the differential equations

$$L_k(f_0, ..., f_N) = 0 \text{ for } k = 0, ..., M.$$

3.4. Asymptotic Analysis of the Governing Equations

In this section, we present a single scale asymptotic analysis of the nondimensional Euler equations in the limit of a vanishing Mach number. The Mach number itself acts as an additional variable, next to the spatial coordinates and time. We indicate this by writing $\boldsymbol{u}(\boldsymbol{x}, t; M)$ for the vector of the solution.
The success of an asymptotic analysis greatly depends on the definition of a proper asymptotic sequence and the choice of suitable spatial and time scales. Both parts need to match the properties of the considered equations. For the definition of the asymptotic sequence, we follow the proposal of Meister [48] and choose the sequence

$$\phi_n(M) = M^n \text{ for } n \in \mathbb{N}_0$$

for the asymptotic analyses presented here.
We consider the Euler equations in $\mathcal{G} \times \mathbb{R}_0^+$ with the bounded region $\mathcal{G}$. The set of state vectors $\boldsymbol{u} : \mathcal{G} \times \mathbb{R}_0^+ \times (0, M) \to \mathbb{R}^d$ that fulfill the Euler equations (2.17) is called U_s. In this set every physical quantity ψ can be expressed through an asymptotic single scale expansion

$$\psi(\boldsymbol{x}, t; M) = \sum_{i=0}^{j} \phi_i(M) \psi^{(i)}(\boldsymbol{x}, t) + o(M^j) \text{ for } j = 0, 1, 2 \text{ and } M \to 0$$

valid on $\mathcal{G} \times \mathbb{R}_0^+$ with the asymptotic functions $\phi^{(i)} : \mathcal{G} \times \mathbb{R}_0^+ \to \mathbb{R}$.
To conduct an asymptotic analysis, we insert the asymptotic expansion of the physical quantities into the conservation equations. For the continuity equation, this leads to

$$\sum_{i=0}^{2} M^i \left[\partial_t \rho^{(i)} + \nabla_{\boldsymbol{x}} \cdot (\rho \boldsymbol{v})^{(i)}\right] = o(M^2) \text{ for } M \to 0 \text{ in } \mathcal{G} \times \mathbb{R}_0^+. \tag{3.1}$$

In a similar way we can write the momentum equations as

$$\sum_{i=0}^{2} M^i \left[\partial_t \left(\rho \boldsymbol{v}\right)^{(i)} + \nabla_{\boldsymbol{x}} \cdot [(\rho \boldsymbol{v}) \otimes \boldsymbol{v}]^{(i)} + \frac{1}{M^2} \nabla_{\boldsymbol{x}} p^{(i)}\right] = o(M^2) \quad \text{for } M \to 0 \text{ in } \mathcal{G} \times \mathbb{R}_0^+ \tag{3.2}$$

and the energy equation becomes

$$\sum_{i=0}^{2} M^i \left[\partial_t \left(\rho E\right)^{(i)} + \nabla_{\boldsymbol{x}} \cdot (\rho \boldsymbol{v} H)^{(i)}\right] = o(M^2) \text{ for } M \to 0 \text{ in } \mathcal{G} \times \mathbb{R}_0^+. \tag{3.3}$$

Considering Lemma 2, we get the following equation that is identical to the $\mathcal{O}(1)$-formulation of the continuity equation (3.1):

$$\partial_t \rho^{(0)} + \nabla_{\boldsymbol{x}} \cdot (\rho \boldsymbol{v})^{(0)} = 0 \tag{3.4}$$

in $\mathcal{G} \times \mathbb{R}_0^+$. The terms associated with the $\mathcal{O}(M)$ and $\mathcal{O}(M^2)$-formulations can be written as

$$\partial_t \rho^{(1)} + \nabla_{\boldsymbol{x}} \cdot (\rho \boldsymbol{v})^{(1)} = 0$$

and

$$\partial_t \rho^{(2)} + \nabla_{\boldsymbol{x}} \cdot (\rho \boldsymbol{v})^{(2)} = 0$$

in $\mathcal{G} \times \mathbb{R}_0^+$, respectively. In the same way, the momentum equation (3.2) leads to

$$\nabla_{\boldsymbol{x}} p^{(0)} = 0, \tag{3.5}$$

$$\nabla_{\boldsymbol{x}} p^{(1)} = 0 \tag{3.6}$$

and

$$\partial_t \left(\rho \boldsymbol{v}\right)^{(0)} + \nabla_{\boldsymbol{x}} \cdot [(\rho \boldsymbol{v}) \otimes \boldsymbol{v}]^{(0)} + \nabla_{\boldsymbol{x}} p^{(2)} = 0 \tag{3.7}$$

in $\mathcal{G} \times \mathbb{R}_0^+$. Finally, the energy equation (3.3) leads to

$$\partial_t \left(\rho E\right)^{(i)} + \nabla_{\boldsymbol{x}} \cdot (\rho \boldsymbol{v} H)^{(i)} = 0 \text{ for } i = 0, 1, 2 \text{ in } \mathcal{G} \times \mathbb{R}_0^+.$$

From these asymptotic equations, several conclusions can be drawn concerning the behavior of the different physical quantities. A direct conclusion from equations (3.5) and (3.6) is the following Theorem.

Theorem 3.
For $\boldsymbol{u} \in U_s$,

$$p^{(0)} = p^{(0)}(t)$$

and

$$p^{(1)} = p^{(1)}(t).$$

The proof for this Theorem is given by Meister [46].
One implication of Theorem 3 is that the pressure fluctuations in $\boldsymbol{u} \in \mathcal{U}_s$ can at most have an influence of $o(M)$ on the pressure distribution. In addition, changes of the order of $\mathcal{O}(1)$ or $\mathcal{O}(M)$ can only appear simultaneous in the whole flow domain, changing only with time. In the limit of a vanishing Mach number, there is a spatially constant pressure distribution.
It should be noted, however, that the second order pressure fluctuations with a small amplitude have an influence of $\mathcal{O}(1)$ on the leading order momentum distribution. We can see this from the last term on the left-hand side of equation (3.7). Hence, these fluctuations have a great importance for the whole flow field. For more detail see the work published by Meister [46].

Theorem 4.
For $\boldsymbol{u} \in U_s$,

$$\frac{1}{|\mathcal{G}|}\int_{\mathcal{G}} \frac{-3M_w^2 b\rho^{(0)} + 3M_w^3}{6ab[\rho^{(0)}]^3 - M_w a[\rho^{(0)}]^2 + 5M_w^3 p^{(0)}} dx \frac{dp^{(0)}}{dt} = -\frac{1}{|\mathcal{G}|}\int_{\partial\mathcal{G}} \boldsymbol{v}^{(0)} \cdot \boldsymbol{n} ds, \tag{3.8}$$

where $|\mathcal{G}|$ *is the volume of the spatial domain* $\mathcal{G}$, $\partial\mathcal{G}$ *is its boundary and* $\boldsymbol{n}$ *represents the outer unit normal vector on* $\partial\mathcal{G}$.

Proof.
Inserting the asymptotic sequence into the caloric equation of state (2.19) on page 17 gives us the relation between the leading orders of pressure and total energy density as

$$p^{(0)} = \frac{2M_w \left(\rho E\right)^{(0)} + \frac{2a}{M_w}[\rho^{(0)}]^2}{3M_w - 3b\rho^{(0)}} - \frac{a[\rho^{(0)}]^2}{M_w^2}.$$

This relation is the $\mathcal{O}(1)$ part of the expression we get by inserting the asymptotic sequence. To separate this part, we need to expand the expression into a Taylor series

which we describe in section A.4. The above equation is the result presented in equation A.15.
We can reformulate this equation to get the leading order of total energy density:

$$(\rho E)^{(0)} = \frac{3M_w^3 p^{(0)} - 3M_w^2 b\,(\rho p)^{(0)} + M_w a[\rho^{(0)}]^2 - 3ab[\rho^{(0)}]^3}{2M_w^3}$$

Hence, the leading order of the total enthalpy density can be written as

$$\begin{aligned}(\rho H)^{(0)} = (\rho E)^{(0)} + p^{(0)} =& \frac{3M_w^3 p^{(0)} - 3M_w^2 b\,(\rho p)^{(0)} + M_w a[\rho^{(0)}]^2 - 3ab[\rho^{(0)}]^3}{2M_w^3} + p^{(0)} \\ =& \frac{5M_w^3 p^{(0)} - 3M_w^2 b\,(\rho p)^{(0)} + M_w a[\rho^{(0)}]^2 - 3ab[\rho^{(0)}]^3}{2M_w^3}.\end{aligned}$$

Now we insert these two relations into the leading order energy conservation equation

$$\partial_t\,(\rho E)^{(0)} + \nabla_x \cdot (\rho H \boldsymbol{v})^{(0)} = 0.$$

This leads to

$$\begin{aligned}&\partial_t \left(\frac{3M_w^3 p^{(0)} - 3M_w^2 b\,(\rho p)^{(0)} + M_w a[\rho^{(0)}]^2 - 3ab[\rho^{(0)}]^3}{2M_w^3} \right) \\ &+\nabla_x \cdot \left(\left[\frac{5M_w^3 p^{(0)} - 3M_w^2 b\,(\rho p)^{(0)} + M_w a[\rho^{(0)}]^2 - 3ab[\rho^{(0)}]^3}{2M_w^3} \right] \boldsymbol{v}^{(0)} \right) = 0.\end{aligned}$$

After some transformation we get

$$\begin{aligned}&\left(\frac{3}{2} - \frac{3b\rho^{(0)}}{2M_w} \right) \partial_t p^{(0)} + \left(-\frac{3bp^{(0)}}{2M_w} + \frac{a\rho^{(0)}}{M_w^2} - \frac{9ab[\rho^{(0)}]^2}{2M_w^3} \right) \partial_t \rho^{(0)} \\ &\qquad + \boldsymbol{v}^{(0)} \left(-\frac{3bp^{(0)}}{2M_w} + \frac{a\rho^{(0)}}{M_w^2} - \frac{9ab[\rho^{(0)}]^2}{2M_w^3} \right) \nabla_x \rho^{(0)} \\ &\qquad + \boldsymbol{v}^{(0)} \left(\frac{5}{2} - \frac{3b\rho^{(0)}}{2M_w} \right) \nabla_x p^{(0)} \\ &\qquad + \left(\frac{5p^{(0)}}{2} - \frac{3b\,(\rho p)^{(0)}}{2M_w} + \frac{a[\rho^{(0)}]^2}{2M_w^2} - \frac{3ab[\rho^{(0)}]^3}{2M_w^3} \right) \nabla_x \cdot \boldsymbol{v}^{(0)} = 0.\end{aligned}$$

With the relation $\nabla_x p^{(0)} = 0$ that results from Theorem 3 we can simplify this equation

to

$$\left(\frac{3}{2}-\frac{3b\rho^{(0)}}{2M_w}\right)\partial_t p^{(0)}+\left(-\frac{3bp^{(0)}}{2M_w}+\frac{a\rho^{(0)}}{M_w^2}-\frac{9ab[\rho^{(0)}]^2}{2M_w^3}\right)\partial_t\rho^{(0)}$$
$$+\boldsymbol{v}^{(0)}\left(-\frac{3bp^{(0)}}{2M_w}+\frac{a\rho^{(0)}}{M_w^2}-\frac{9ab[\rho^{(0)}]^2}{2M_w^3}\right)\nabla_x\rho^{(0)}$$
$$+\left(\frac{5p^{(0)}}{2}-\frac{3b\,(\rho p)^{(0)}}{2M_w}+\frac{a[\rho^{(0)}]^2}{2M_w^2}-\frac{3ab[\rho^{(0)}]^3}{2M_w^3}\right)\nabla_x\cdot\boldsymbol{v}^{(0)}=0.$$

Now we rearrange the expression to get

$$\left(\frac{3}{2}-\frac{3b\rho^{(0)}}{2M_w}\right)\partial_t p^{(0)}+\left(-\frac{3bp^{(0)}}{2M_w}+\frac{a\rho^{(0)}}{M_w^2}-\frac{9ab[\rho^{(0)}]^2}{2M_w^3}\right)\partial_t\rho^{(0)}$$
$$+\boldsymbol{v}^{(0)}\left(-\frac{3bp^{(0)}}{2M_w}+\frac{a\rho^{(0)}}{M_w^2}-\frac{9ab[\rho^{(0)}]^2}{2M_w^3}\right)\nabla_x\rho^{(0)}$$
$$+\rho^{(0)}\left(-\frac{3bp^{(0)}}{2M_w}+\frac{a\rho^{(0)}}{M_w^2}-\frac{9ab[\rho^{(0)}]^2}{2M_w^3}\right)\nabla_x\cdot\boldsymbol{v}^{(0)}$$
$$+\left(\frac{5p^{(0)}}{2}-\frac{a[\rho^{(0)}]^2}{2M_w^2}+\frac{6ab[\rho^{(0)}]^3}{2M_w^3}\right)\nabla_x\cdot\boldsymbol{v}^{(0)}=0,$$

which we can also write as

$$\left(\frac{3}{2}-\frac{3b\rho^{(0)}}{2M_w}\right)\partial_t p^{(0)}+\left(-\frac{3bp^{(0)}}{2M_w}+\frac{a\rho^{(0)}}{M_w^2}-\frac{9ab[\rho^{(0)}]^2}{2M_w^3}\right)\partial_t\rho^{(0)}$$
$$+\left(-\frac{3bp^{(0)}}{2M_w}+\frac{a\rho^{(0)}}{M_w^2}-\frac{9ab[\rho^{(0)}]^2}{2M_w^3}\right)\nabla_x\cdot(\rho\boldsymbol{v})^{(0)}\qquad(3.9)$$
$$+\left(\frac{5p^{(0)}}{2}-\frac{a[\rho^{(0)}]^2}{2M_w^2}+\frac{6ab[\rho^{(0)}]^3}{2M_w^3}\right)\nabla_x\cdot\boldsymbol{v}^{(0)}=0.$$

From the leading order of the continuity equation (3.4), we get the relation

$$\partial_t\rho^{(0)}=-\nabla_x\cdot(\rho\boldsymbol{v})^{(0)}.$$

When we insert this into equation (3.9), we can simplify it to

$$\left(-\frac{3b\rho^{(0)}}{M_w}+3\right)\partial_t p^{(0)}+\left(\frac{6ab[\rho^{(0)}]^3}{M_w^3}-\frac{a[\rho^{(0)}]^2}{M_w^2}+5p^{(0)}\right)\nabla_x\cdot\boldsymbol{v}^{(0)}=0.$$

After integrating this equation over $\mathcal{G}$, we finally arrive at

$$\frac{1}{|\mathcal{G}|}\int_{\mathcal{G}} \frac{-3M_w^2 b\rho^{(0)} + 3M_w^3}{6ab[\rho^{(0)}]^3 - M_w a[\rho^{(0)}]^2 + 5M_w^3 p^{(0)}} dx \frac{dp^{(0)}}{dt} = -\frac{1}{|\mathcal{G}|}\int_{\partial\mathcal{G}} \boldsymbol{v}^{(0)} \cdot \boldsymbol{n} ds.$$

□

Next, we consider this equation in the limit of an ideal gas. To transform the Van der Waals equation of state into the ideal gas law, we set $a = 0$ and $b = 0$. Then, equation (3.8) becomes

$$\frac{3}{5p^{(0)}}\frac{dp^{(0)}}{dt} = -\frac{1}{|\mathcal{G}|}\int_{\partial\mathcal{G}} \boldsymbol{v}^{(0)} \cdot \boldsymbol{n} ds, \tag{3.10}$$

which equals the result of the ideal gas analysis conducted by Meister [46] for a ratio of specific heats of $\gamma = \frac{5}{3}$. This is the value for γ we expect due to our choice for the specific heat at constant volume of $\hat{c}_{\hat{v}} = \frac{3}{2}\hat{\mathcal{R}}$.

Equation (3.10) describes the correlation between the leading orders of the pressure and the velocity distribution for an inviscid, ideal gas. The conclusion drawn by Meister is that the global temporal evolution of the spatial constant pressure term $p^{(0)}$ is governed by compression of the gas over the boundary of the flow domain or expansion of the gas due to chemical reactions. This is important for the construction of a numerical scheme for low Mach number flows. Following this conclusion one can define the leading order pressure to be the same in the whole computational domain.

The additional terms present in the case of a Van der Waals gas that can be seen in equation (3.8) on page 29 are products of the leading order of the density distribution, the molecular weight and the constants a and b. These quantities are always of $\mathcal{O}(1)$ as the Mach number approaches zero. Hence, the conclusions drawn in the ideal gas analysis are still valid for a Van der Waals gas in general.

However, the influence of expansion or compression of the gas over the boundary of the flow domain on pressure is not as simple for a Van der Waals gas as it is in the formulation of the ideal gas law. In the case of a Van der Waals gas, the acting pressure is reduced by the two terms depending on the constants a and b that are introduced in section 2.2.1. The two terms that are shown in equation (2.9) on page 11 do not only depend on a and b but also on the density. Since the effects that alter pressure also influence the density distribution, these correctional terms can lead to either an increase or a decrease of the change in pressure, depending on the specific fluid. Hence, the influence of expansion or compression of the gas over the boundary of the flow domain that can be found for an ideal gas still applies for a Van der Waals gas in general, but the real gas effects present in the Van der Waals equation of state can alter this influence.

In this analysis, no acoustic effects are observed. This is due to the choice of the spatial scale which only shows the convective velocities. To analyze the acoustic effects, a spatial scale of $M \cdot x$ could be chosen instead. To obtain both acoustic and convective influences at once, a multiple scale analysis needs to be conducted that includes both a spatial scale of $M \cdot x$ and the x-scale used in this work.
A multiple scale analysis for both viscous and inviscid flows using a spatial $M \cdot x$ and a x-scale is conducted by Meister [46]. In their work, the governing equations are thoroughly analyzed for an ideal gas. Here we are concerned with the enhancement of a numerical scheme for a Van der Waals gas. The insight necessary for this purpose can be gained by conducting only a single scale asymptotic analysis. Hence, a multiple scale analysis is out of the scope of this work.

4. Numerical Scheme

The formulation of governing equations is helpful to understand and analyze a problem. However, to gain a detailed spatial solution or even the temporal development of this solution, the use of a numerical scheme is necessary. Especially when there is no analytical solution to a problem, solving it with the help of a numerical scheme is the best way to obtain results. In this chapter we cover the numerical approximation of the governing equations we discuss in chapter 2. We limit our discussion to two-dimensional schemes.
We begin this chapter with giving a brief overview of the code used in this work. We describe finite volume methods in general and define both weak solutions and the operators necessary to formulate the balance equation which is the foundation of finite volume methods. We also describe the discretization of both the computational domain and the convective fluxes in detail. Then we introduce the estimation of thermodynamic quantities within the code. We also briefly cover the nondimensionalization applied in the numerical scheme.
In the second part of the chapter we consider flux functions. We summarize the challenges in applying a flux function to the region of small Mach numbers and give an overview over functions adapted for flows under these conditions. We identify two numerical schemes that are suitable for the objectives of this work.
Then we choose the MAPS (Mach number-based Advection Pressure Splitting) flux function for the further analysis. We describe both MAPS and the extension to MAPS+ in detail. We also distinguish between the general version of MAPS+ and special adaptations for low Mach number flows.
In the next step we investigate whether MAPS+ can also be used to calculate the flux of a Van der Waals gas. To do this, we first analyze the differences in the continuous flux Jacobi matrix depending on the equation of state since these differences need to be present in MAPS+ as well. Then we transform MAPS+ into a sum of discrete flux Jacobi matrices in terms of the conservative variables. This way we are able to compare the discrete flux function to the results of the analysis of the continuous flux Jacobi matrix of the Euler equations. We conduct this comparison both for a high Mach number and for $M \to 0$. In the latter case, we analyze the $\mathcal{O}$-behavior of the different terms of both matrices as the Mach number approaches zero. By this means we demonstrate that the

MAPS+ scheme is defined in a way suitable for a Van der Waals gas.
In the last part of the section concerning flux functions, we perform a discrete asymptotic analysis of both the general and the altered MAPS+ scheme. The results for the general MAPS+ scheme contradict the results of the continuous asymptotic analysis while both agree for the altered MAPS+ scheme. This difference is also present in the numerical results we show to conclude the section.
In the last part of the chapter, we focus on preconditioning schemes for the low Mach number region. First we present some general reasons for the usage of a preconditioner in addition to a description of its effects. We also generally define a preconditioning scheme and cover the transformation from primitive to conservative variables.
Then we give an overview of preconditioners currently available for an ideal gas. We briefly cover the evolution of preconditioning schemes and the different ways to construct a preconditioning matrix. We also describe the approaches of other authors to use preconditioning schemes for real gases.
Next, we explain the different requirements of a numerical scheme for a Van der Waals gas concerning a preconditioning scheme compared to one for an ideal gas and deduce the overall form a preconditioning matrix must have. The mentioned differences are then demonstrated by calculating the eigenvalues and condition numbers of the preconditioning of both the ideal gas and the Van der Waals gas continuous flux Jacobi matrix. By doing this we show that it is possible to alter the eigenvalues in the Van der Waals gas case in a favorable way.
In the next section, we describe the preconditioning schemes we use for the simulations. Finally, we present the results of numerical simulations. We compare two different preconditioning schemes for a Van der Waals gas and show that their convergence rates are independent of the Mach number for $M \to 0$. Then we show the capability of one of the schemes for different characteristic thermodynamic conditions.

4.1. Overview

The CFD (computational fluid dynamics) platform used in the following is the DLR TAU-code. It can be applied for the simulation of both viscous and inviscid flows from the low subsonic to the hypersonic flow regime. TAU is a compressible flow solver that can be used to model a variety of steady and unsteady flows. It contains a wide range of models and adaptations for different requirements. Here, we only give a brief overview of the code and only cover the models used in the subsequent sections; a detailed description of the DLR TAU-code can be found in Schwamborn et al. [64], Gerhold [24] and Mack

and Hannemann [44].
TAU can be used with structured and unstructured grids. They are transferred into a dual grid during the preprocessing, making the solver independent of the specific grid elements used in the primary grids. All terms within the solver are computed on the nodes or at the faces of this dual grid.
In TAU, a Godunov-type finite volume method is used to solve the system of governing equations. For the calculation of the inviscid terms, either a second-order central scheme or one of many different upwind schemes is available. The viscous terms are computed with a second-order central scheme. If an upwind scheme is used, a second-order spatial accuracy can be achieved by using linear reconstruction which is applied on the left and right states of the dual grid faces. In the following, we focus on upwind schemes.
Both implicit and explicit methods can be used for time integration. As an implicit scheme, the Lower-Upper Symmetric Gauss-Seidel scheme is available, which is an approximate factorization scheme. For explicit schemes one of many Runge-Kutta schemes can be chosen. A dual time stepping approach following the work of Jameson [29] is available for time-accurate computations. There, within every physical time step a steady state problem is solved.
To improve the performance of the code in the region of low Mach numbers, several ideal gas preconditioning schemes are available. The implemented preconditioners are to be used together with an explicit Runge-Kutta method.

4.1.1. Finite Volume Method

Finite volume methods can be used to discretize the conservation equations. Based on the integral formulation, weak solutions are determined. The computational domain is separated into many control volumes within which the governing equations are solved. We describe the properties of control volumes in subsection 4.1.2.

Definition 4.1.1.
Let $\mathbb{R}_0^+ \ni t \overset{\boldsymbol{u}}{\mapsto} \boldsymbol{u}(.,t)$ be of limited variation and $\boldsymbol{u}(.,t) \in \left[L^\infty \cap L^1\right](\mathcal{G} \cup \partial\mathcal{G}; \mathcal{Z})$ for every fixed $t \in \mathbb{R}_0^+$. Then the mapping $\boldsymbol{u}$ is called a weak solution of system (2.17) on page 16 if

$$\frac{d}{dt}\int_\sigma \boldsymbol{u} d\boldsymbol{x} + \sum_{j=1}^{d}\int_{\partial\sigma} \boldsymbol{f}_j(\boldsymbol{u})\, n_j ds = 0 \tag{4.1}$$

for every control volume $\sigma \subset \mathcal{G}$, where $\boldsymbol{n} = (n_1, \ldots, n_d)^T$ is the outer unit normal vector of $\partial\sigma$.

For conservation equations like the Euler equations, a weak solution describes the property that the temporal variation of the mean values of the physical quantities within a control volume are defined by the fluxes over the boundaries of said control volume. However, the introduction of weak solutions leads to a loss of the uniqueness of the solution for the Euler equations. So multiple solutions that fulfill the governing equations are possible.
Next, we introduce the cell averaging operator $\mathcal{M}_\sigma$. This is motivated by the integral form presented in equation (4.1).

Definition 4.1.2.
Let $|\sigma|$ be the volume of the control volume $\sigma \subset \mathcal{G}$. Then

$$\left[L^\infty \cap L^1\right](\sigma;\mathcal{Z}) \ni \boldsymbol{u}(.,t) \xmapsto{\mathcal{M}_\sigma} (\mathcal{M}_\sigma \boldsymbol{u})(t) \coloneqq \frac{1}{|\sigma|}\int_\sigma \boldsymbol{u}(\boldsymbol{x},t)\,d\boldsymbol{x} \in \mathbb{R}^{d+2}$$

is called the cell averaging operator on σ.

We take $\mathcal{B}$ to be the set of control volumes $\sigma_i \subset \mathcal{G}, i = 1,\dots,\#\mathcal{B}$, which represents a disjoint covering of the limited domain $\mathcal{G}$. With the use of the operator $\mathcal{L}_{\sigma_i}$ which is given by

$$(\mathcal{L}_{\sigma_i}\boldsymbol{u})(t) = \frac{1}{|\sigma_i|}\sum_{j=1}^{d}\int_{\partial\sigma_i} \boldsymbol{f}_j(\boldsymbol{u}(\boldsymbol{x},t))\,n_j(\boldsymbol{x})\,ds \text{ for all } \sigma_i \in \mathcal{B},$$

we arrive at the integral form of the balance equation

$$\frac{d}{dt}(\mathcal{M}_{\sigma_i}\boldsymbol{u})(t) + (\mathcal{L}_{\sigma_i}\boldsymbol{u})(t) = \mathbf{0} \text{ for all } \sigma_i \in \mathcal{B} \tag{4.2}$$

by introducing the cell averaging operator into the representation of the weak solution.
This form of the balance equation represents the foundation of any finite volume method. Within these methods, the temporal evolution of values averaged on the cells is calculated. With the help of equation (4.2), a separation of the temporal and spatial discretization is possible. This leads to a great flexibility of the numerical schemes. In many cases, the approximation of equation (4.2) is accomplished in two subsequent steps. First, the discretization of the contour integrals in applied, which leads to a semi discrete system. In the second step this system is approximated with the help of a time integration scheme. In the following subsections, we describe the discretization of the computational domain and the convective fluxes.

4.1.2. Discretization of the computational domain

To simulate a flow with the help of a numerical scheme, we need to discretize both the spatial part $\mathcal{G}$ and the temporal part $\mathbb{R}_0^+$. In the following, we describe the spatial discretization of $\mathcal{G}$ in two dimensions. We also introduce the necessary notation.
To generate the triangulation, we define a set of boundary node points both on the surface of the profile and at the farfield boundary. The number of boundary points and hence the distance between two adjacent points defines the size of the resulting triangles. A higher amount of boundary points leads to smaller triangles.
In the following step a Delaunay triangulation is applied using this set of boundary points. A characteristic of this method is that no additional node point lies within the circumcircle of any triangle. The Delaunay triangulation maximizes the minimum angle of all the triangles which is favorable for the numerical scheme. Then inner node points of the grid are calculated with the algorithm developed by Friedrich [23]. These points are then linked with the existing triangulation using the algorithm by Bowyer [7] which ensures that the grid fulfills the Delaunay criteria. The resulting triangulation represents the primary grid.
In the final step, the secondary grid is constructed from the primary one. For this purpose, the inner points $\boldsymbol{x}_s = (x_{s1}, x_{s2})^T$ are defined as follows.

$$\boldsymbol{x}_s = \sum_{m \in \mathcal{C}(\mathcal{T})} \alpha_m^s \boldsymbol{x}_m$$

with

$$\mathcal{C}(\mathcal{T}) = \{i \in \{1. \ldots, \#\mathcal{N}_h\} \mid \text{point } \boldsymbol{x}_i \text{ is vertex of } \mathcal{T}\},$$

where $\mathcal{T}$ is a triangle, and

$$\alpha_m^s = \frac{1}{2\sum_{m \in \mathcal{C}(\mathcal{T})} |l_m|} \sum_{\substack{\overline{m} \in \mathcal{C}(\mathcal{T}) \\ \overline{m} \neq m}} |l_{\overline{m}}|$$

and

$$|l_i| = \|\boldsymbol{x}_j - \boldsymbol{x}_k\|_2 \text{ for } i, j, k \in \mathcal{C}(\mathcal{T}).$$

To create the secondary grid, these inner points are connected to the center points of the edges of all triangles. This concept is also illustrated in Figure 4.1 (left).
Now we introduce the necessary notation to specify a control volume. Let $\mathcal{T}_h$ be an arbitrary triangulation of the region $\mathcal{G}$, where we indicate the separate triangles as $\mathcal{T}$. In addition, $\mathcal{N}_h$ is the index set of all node points of the triangulation $\mathcal{T}_h$. We separate

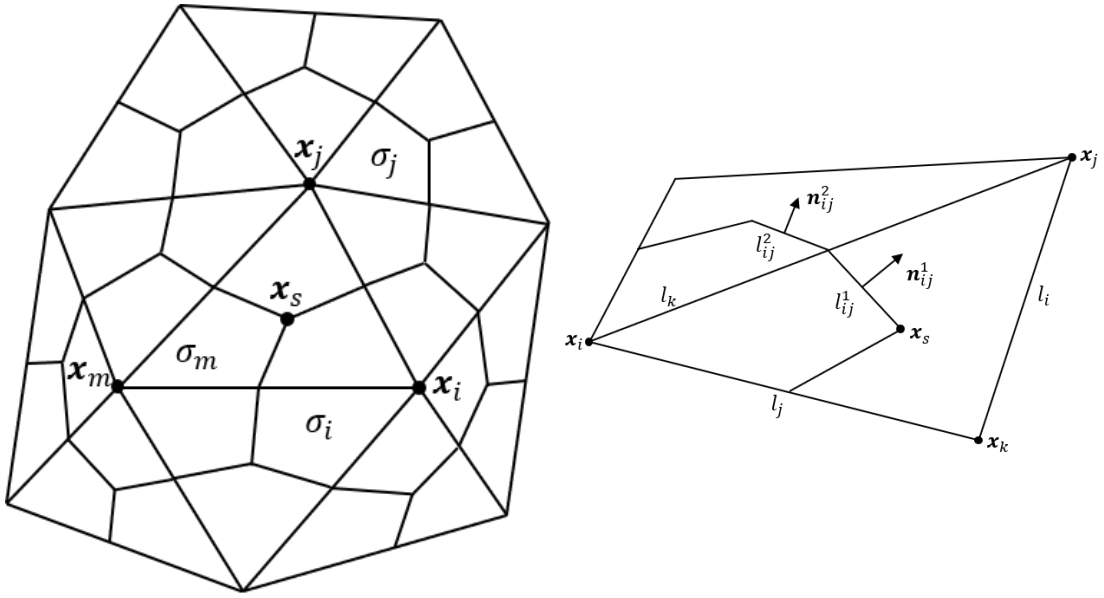

Figure 4.1.: General form of a control volume (left) and representation of the boundaries between control volumes σ_i and σ_j (right)

this set into the indices of the internal node points $\mathcal{N}_{h,\mathcal{G}}$ and the indices of the boundary node points $\mathcal{N}_{h,\partial\mathcal{G}}$. So, it is $\mathcal{N}_h = \mathcal{N}_{h,\mathcal{G}} \cup \mathcal{N}_{h,\partial\mathcal{G}}$.
We call the open subset of $\mathbb{R}^2$ that contains the node point $\boldsymbol{x}_i = (x_{i1}, x_{i2})^T$ control volume σ_i. This control volume is bounded by the connecting lines between the inner points $\boldsymbol{x}_s$ and the center points of the edges of the respective triangles. This is illustrated in Figure 4.1 (left). If the node point $\boldsymbol{x}_i$ is a boundary point, the connecting line between $\boldsymbol{x}_i$ and the center point of the boundary edge is part of the boundary of the control volume.
With $\mathcal{N}(i)$ we describe the set of all indices j, for which $\int_{\partial\sigma_i \cap \partial\sigma_j} 1 \, ds \neq 0$ is true.
The two straight sections that separate control volume σ_i from control volume σ_j for $j \in \mathcal{N}(i)$ are called $l_{ij}^k, k = 1, 2$. The respective unit normal vectors on l_{ij}^k are called $\boldsymbol{n}_{ij}^k$, see Figure 4.1 (right).

4.1.3. Discretization of the convective fluxes

Based on the spatial discretization of the two-dimensional computational domain $\mathcal{G}$ which we introduce in the preceding subsection 4.1.2, we can write the convective fluxes of the balance equation (4.2) as

$$\left(\widetilde{\mathcal{L}}_{\sigma_i}\widetilde{\boldsymbol{u}}\right)(t) = \frac{1}{|\sigma_i|}\Bigg\{ \sum_{j\in\mathcal{N}(i)}\sum_{k=1}^{2}\int_{l_{ij}^k} \boldsymbol{T}(\boldsymbol{n})^{-1}\,\widetilde{\boldsymbol{f}_1}\left(\boldsymbol{T}(\boldsymbol{n})\,\widetilde{\boldsymbol{u}}\right)\,ds + \int_{\partial\sigma_i\cap\partial\mathcal{T}_h} \boldsymbol{T}(\boldsymbol{n})^{-1}\,\widetilde{\boldsymbol{f}_1}\left(\boldsymbol{T}(\boldsymbol{n})\,\widetilde{\boldsymbol{u}}\right)\Bigg\} \tag{4.3}$$

with the rotational matrix $\boldsymbol{T}$.
Within the finite volume method, average values on each grid cell are calculated which we indicate by the notation $\widetilde{u}$. If we view these values as constant distributions within each control volume, there are in general jump discontinuities of the physical values at the boundary pieces l_{ij}^k. To approximate this Riemann problem, we introduce the term numerical flux function.

Definition 4.1.3.
A mapping

$$\mathcal{H} : \mathbb{R}^4 \times \mathbb{R}^4 \times \mathbb{R}^2 \to \mathbb{R}^4$$

is called numerical flux function.

To ensure that this arbitrary numerical flux function has a reasonable physical and mathematical relationship with the considered differential equation, we define the allowed set of numerical flux functions by the following consistency constraint.

Definition 4.1.4.
The numerical flux function $\mathcal{H}$ is called consistent to the operator $\widetilde{\mathcal{L}}$, if

$$\mathcal{H}\left(\widetilde{\boldsymbol{u}},\widetilde{\boldsymbol{u}};\boldsymbol{n}\right) = \boldsymbol{T}(\boldsymbol{n})^{-1}\,\widetilde{\boldsymbol{f}}_1\left(\boldsymbol{T}(\boldsymbol{n})\,\widetilde{\boldsymbol{u}}\right)$$

for all $\widetilde{\boldsymbol{u}} \in \mathcal{Z}$ and $\boldsymbol{n} \in \mathbb{R}^2$ with $\|\boldsymbol{n}\|_2 = 1$ is true.

Godunov realized the discontinuous jump at the interface to be the Riemann problem which has an exact solution for the Euler equations. Hence, the numerical flux functions which are introduced by this definition are often referred to as Riemann solvers.
In modern CFD codes, the Riemann problem is no longer solved exactly. Instead, approximate Riemann solvers are used. The approach presented by Godunov and Bohachevsky [25], using the exact solution of the Riemann problem, requires iterative computations within every time step which are numerically expensive. The approximate Riemann solvers only produce a fraction of the computational costs while still providing a sufficient accuracy.

The choice of an appropriate Riemann solver for a specific problem is an important part of building a stable and sufficiently precise numerical scheme. We discuss flux functions in more detail in section 4.2 and describe the MAPS+ flux function $\mathcal{H}_{MAPS+}$ in subsection 4.2.2. With the help of this numerical flux function we can discretize the inner contour integrals by

$$\int_{l_{ij}^k} \boldsymbol{T}(\boldsymbol{n})^{-1} \widetilde{\boldsymbol{f}}_1(\boldsymbol{T}(\boldsymbol{n}) \widetilde{\boldsymbol{u}}) \; ds \cong |l_{ij}^k| \mathcal{H}_{MAPS+}\left(\widetilde{\boldsymbol{u}}_i, \widetilde{\boldsymbol{u}}_j; \boldsymbol{n}_{ij}^k\right).$$

To approximate the integrals over the boundary pieces we use the boundary conditions described in subsection 2.4 on page 18. The solid wall boundary condition (2.20) allows for an exact calculation of the contour integral in equation (4.3). Hence, the application of a numerical flux function is not necessary at a solid wall and the contour integral takes the form

$$\int_{\partial\sigma_i \cap \partial\mathcal{T}_{h,w}} \boldsymbol{T}(\boldsymbol{n})^{-1} \widetilde{\boldsymbol{f}}_1(\boldsymbol{T}(\boldsymbol{n}) \widetilde{\boldsymbol{u}}) \; ds \cong \sum_{l_{\sigma_i} \subset \partial\mathcal{T}_{h,w}} |l_{\sigma_i}| \begin{pmatrix} 0 \\ \widetilde{p}(\boldsymbol{x}_i^m, t)\, n_1 \\ \widetilde{p}(\boldsymbol{x}_i^m, t)\, n_2 \\ 0 \end{pmatrix},$$

where $\boldsymbol{x}_i^m$ is the center point of an arbitrary line segment l_{σ_i} which is part of the boundary $\partial\sigma_i$.

For the farfield boundary condition, the usage of the numerical flux function $\mathcal{H}_{MAPS+}$ is required. For the following description, we separate the farfield boundary condition into $\mathcal{T}_{h,\mathrm{ff}} = \mathcal{T}_{h,\mathrm{in}} + \mathcal{T}_{h,\mathrm{out,sub}} + \mathcal{T}_{h,\mathrm{out,sup}}$, where $\mathcal{T}_{h,\mathrm{in}}$ stands for the inflow boundary conditions while $\mathcal{T}_{h,\mathrm{out,sub}}$ and $\mathcal{T}_{h,\mathrm{out,sup}}$ represents the subsonic and supersonic outflow conditions, respectively. At the inflow boundaries, we take $\widetilde{\boldsymbol{u}}_{\mathrm{in}}(\boldsymbol{x}_i^m)$ to be the vector of conservative variables that is defined in subsection 2.4.2 for the flow approaching the boundary. Then we get

$$\int_{\partial\sigma_i \cap \partial\mathcal{T}_{h,\mathrm{in}}} \boldsymbol{T}(\boldsymbol{n})^{-1} \widetilde{\boldsymbol{f}}_1(\boldsymbol{T}(\boldsymbol{n}) \widetilde{\boldsymbol{u}}) \; ds \cong \sum_{\partial\sigma_i \subset \partial\mathcal{T}_{h,\mathrm{in}}} |l_{\sigma_i}| \mathcal{H}_{MAPS+}(\widetilde{\boldsymbol{u}}_i, \widetilde{\boldsymbol{u}}_{\mathrm{in}}(\boldsymbol{x}_i^m); \boldsymbol{n})$$

with $i \in \mathcal{C}(\mathcal{T}_{h,\mathrm{in}})$.

For the subsonic outflow boundary condition, we write $\widetilde{\boldsymbol{u}}_{out}(\boldsymbol{x}_i^m)$ for the vector of conservative variables defined in subsection 2.4.2 for the flow leaving the boundary. With this we get

$$\int_{\partial\sigma_i \cap \partial\mathcal{T}_{h,\text{out,sub}}} \boldsymbol{T}(\boldsymbol{n})^{-1} \widetilde{\boldsymbol{f}}_1(\boldsymbol{T}(\boldsymbol{n})\widetilde{\boldsymbol{u}})\ ds \cong \sum_{\partial\sigma_i \subset \partial\mathcal{T}_{h,\text{out,sub}}} |l_{\sigma_i}| \mathcal{H}_{MAPS+}(\widetilde{\boldsymbol{u}}_i, \widetilde{\boldsymbol{u}}_{out}(\boldsymbol{x}_i^m); \boldsymbol{n})$$

with $i \in \mathcal{C}(\mathcal{T}_{h,\text{out,sub}})$.
For the supersonic outflow boundary condition, the left- and right-hand side values of the conservative variables at the boundary are identical. Hence, we get the convective boundary fluxes

$$\int_{\partial\sigma_i \cap \partial\mathcal{T}_{h,\text{out,sup}}} \boldsymbol{T}(\boldsymbol{n})^{-1} \widetilde{\boldsymbol{f}}_1(\boldsymbol{T}(\boldsymbol{n})\widetilde{\boldsymbol{u}})\ ds \cong \sum_{\partial\sigma_i \subset \partial\mathcal{T}_{h,\text{out,sup}}} |l_{\sigma_i}| \boldsymbol{T}(\boldsymbol{n})^{-1} \widetilde{\boldsymbol{f}}_1(\boldsymbol{T}(\boldsymbol{n})\widetilde{\boldsymbol{u}}_i)$$

with $i \in \mathcal{C}(\mathcal{T}_{h,\text{out,sup}})$.

4.1.4. Implementation of Thermodynamics

In TAU, real gases represented by cubic equations of state are implemented as an extension to the ideal gas modeling. This way gases that follow another state equation than the ideal gas law can be modeled. The approach follows the Multi-Fluid Mixing method as proposed by Banuti et al. [5].
In addition, caloric imperfect gases can be considered. This means that the specific heat at constant pressure is not a constant but depends on temperature. The available states for the fluids range from liquid to supercritical condition. The evaluation of the thermodynamic properties is an important part of the flow solver since a precise estimation of pressure and temperature or enthalpy in every grid cell is needed for the calculation of the fluxes during each time step.
In general, the thermodynamic model in TAU requires two state variables as an input. The different modules then calculate all remaining variables. The specific input variables depend on the problem within the solver and consist of the set density, temperature, pressure, enthalpy, internal energy and entropy. In addition to these variables, the output of the specific thermodynamic module can contain the speed of sound, the specific heats at constant volume and pressure and a variety of transport coefficients.
We consider the description of the thermodynamics, represented by a cubic equation of state in two parts. This agrees with the implementation in TAU. This way, any quantity ψ can be written as

$$\psi = \psi^{\text{id}} + \psi^{\text{res}}.$$

The first part ψ^{id} represents the ideal gas component while the second part ψ^{res} describes

the deviation from the ideal gas behavior. This second part is called the residual component. Note that ψ^{res} increases as the real gas deviates from an ideal gas. If the fluid can be described by the ideal gas law, ψ^{res} equals zero.
With a given thermal equation of state, the deviations can be calculated. The specific relations for ψ^{res} are derived in standard textbooks such as Baehr and Kabalac [3] and a summary is given in Banuti [4].
In TAU, several cubic equations of state (EOS) are implemented following this approach. The available equations include the Van der Waals EOS [75], the Soave-Redlich-Kwong EOS as proposed by Soave [65], the Peng-Robinson EOS [54] and the RK-PR EOS proposed by Cismondi and Mollerup [14]. The equations are implemented in the form presented by Kim et al. [31].

4.1.5. Nondimensionalization

The nondimensionalization used for the analysis within this chapter differs from the one introduced in chapter 2.3 on page 14. Since we want to analyze the behavior of the flux function as it is implemented in the numerical scheme, we apply the same reference values for the nondimensionalization as they are used in the code. Most numerical schemes do not use a separate reference velocity but a combination of thermodynamic reference values to nondimensionalize the velocity.
In the DLR TAU-code, the expression chosen for the reference velocity is $v_{\text{ref}} = \sqrt{\frac{p_{\text{ref}}}{\rho_{\text{ref}}}}$. This is not a reference value in the sense that we introduce in chapter 2.3 as it is generally not of the same order of magnitude as the local velocity. Hence, it shows a different behavior for $M \to 0$ than $\boldsymbol{v}$ does.
For the nondimensionalization, some basic reference values are defined by the user of the code. The thermodynamic references $\hat{p}_{\text{ref}}$ and $\hat{T}_{\text{ref}}$ are given by the freestream values and the lenght-reference $\hat{l}_{\text{ref}}$ is defined using the specific grid. In addition, the reference value of the co-volume $\hat{b}_{\text{ref}}$ is defined for the Van der Waals thermodynamics. The density reference $\hat{\rho}_{\text{ref}}$ is calculated within the code using the implemented thermal equation of state and the given reference values for pressure and temperature. All other reference values are calculated using these given values.
The full set of reference values used in the TAU-code is listed in Table 4.1. These are the expressions used for the nondimensionalization, the analysis of the numerical scheme within this chapter is based on.
The usage of the set of reference values presented in chapter 2.3 leads to dimensionless quantities of $\mathcal{O}(1)$ as the Mach number approaches zero. However, this is not achieved for the nondimensionalization used in numerical codes. The choice of reference values for

Table 4.1.: Names, units and reference values of physical quantities as used in the DLR TAU-code

Physical Quantity		Unit	Reference Value
Cartesian coordinate	$\hat{\boldsymbol{x}}$	[m]	$\hat{l}_{\text{ref}}$
pressure	$\hat{p}$	$[\text{Pa}] = [\text{kg}/(\text{m} \cdot \text{s}^2)]$	$\hat{p}_{\text{ref}}$
temperature	$\hat{T}$	[K]	$\hat{T}_{\text{ref}}$
density	$\hat{\rho}$	$[\text{kg}/\text{m}^3]$	$\hat{\rho}_{\text{ref}}$
co-volume	$\hat{b}$	$[\text{m}^3/\text{mol}]$	$\hat{b}_{\text{ref}}$
velocity vector	$\hat{\boldsymbol{v}}$	[m/s]	$\hat{v}_{\text{ref}} = \sqrt{\frac{p_{\text{ref}}}{\rho_{\text{ref}}}}$
time	$\hat{t}$	[s]	$\frac{\hat{l}_{\text{ref}}}{\hat{v}_{\text{ref}}}$
speed of sound	$\hat{c}$	[m/s]	$\sqrt{\frac{\hat{p}_{\text{ref}}}{\hat{\rho}_{\text{ref}}}}$
specific internal energy	$\hat{e}$	$[\text{J}/\text{kg}] = [\text{m}^2/\text{s}^2]$	$\frac{\hat{p}_{\text{ref}}}{\hat{\rho}_{\text{ref}}}$
specific total energy	$\hat{E}$	$[\text{J}/\text{kg}] = [\text{m}^2/\text{s}^2]$	$\frac{\hat{p}_{\text{ref}}}{\hat{\rho}_{\text{ref}}}$
specific total enthalpy	$\hat{H}$	$[\text{J}/\text{kg}] = [\text{m}^2/\text{s}^2]$	$\frac{\hat{p}_{\text{ref}}}{\hat{\rho}_{\text{ref}}}$
molar mass	$\hat{M}_w$	$[\text{kg}/\text{mol}]$	$\hat{b}_{\text{ref}}\hat{\rho}_{\text{ref}}$
specific gas constant	$\hat{R}$	$[\text{m}^2/(\text{K} \cdot \text{s}^2)]$	$\frac{\hat{v}_{\text{ref}}^2}{\hat{T}_{\text{ref}}}$
intermolecular forces-constant	$\hat{a}$	$[(\text{kg} \cdot \text{m}^5)/(\text{mol}^2 \cdot \text{s}^2)]$	$\hat{\rho}_{\text{ref}}\hat{v}_{\text{ref}}^2\hat{b}_{\text{ref}}^2$

the DLR TAU-code as listed in Table 4.1 results in dimensionless convective velocities of $\mathcal{O}(M)$.

The nondimensionalization with this set of reference values leads to the following form of the Euler equations:

$$\partial_t \boldsymbol{u} + \sum_{j=1}^{d} \partial_{x_j} \boldsymbol{f}_j(\boldsymbol{u}) = 0$$

with

$$\boldsymbol{f}_j(\boldsymbol{u}) = \begin{pmatrix} \rho v_j \\ \rho v_1 v_j + \delta_{1j} p \\ \vdots \\ \rho v_d v_j + \delta_{dj} p \\ \rho H v_j \end{pmatrix} \text{ for } j = 1, \ldots, d.$$

The caloric Van der Waals equation of state has the dimensionless form

$$p = \frac{2M_w \rho E - M_w \rho |\boldsymbol{v}|^2 + 2\frac{a\rho^2}{M_w}}{3M_w - 3b\rho} - \frac{a\rho^2}{M_w^2}. \tag{4.4}$$

Here, the Mach number does not appear in the dimensionless equations, other than in the ones that result from the nondimensionalization in chapter 2.3.

4.2. Flux Function

In this section we are concerned with numerical flux functions that are consistent in the sense of Definition 4.1.4 on page 40.

4.2.1. Flux Functions for low Mach numbers

For flows that encounter both high and low Mach numbers, special schemes can be developed. Many well-known flux functions have been adapted in an attempt to improve the properties of the scheme within the region of low Mach numbers. Ideally, in this region the convergence becomes independent of the Mach number.
The compressible equations tend towards the incompressible ones where the density is independent of pressure, as the Mach number approaches zero (see for example Klainerman and Majda [34]). The flux functions have to represent the behavior of the compressible equations in the entire flow regime. Hence, at low Mach numbers, the flux functions should represent the incompressible equations as well.
However, there are two major challenges for a compressible scheme at low Mach numbers that are thoroughly investigated by Guillard and Nkonga [27] and Volpe [74]. First, the time step size needs to be very small compared to the characteristic times of the flow since the acoustic velocities are very high compared to the convective ones. The relationship between time step size and the characteristic velocities is expressed in the CFL-constraint. Second, the numerical diffusion negatively impairs the solution.
There are many attempts to modify the flux function of a finite volume scheme with the goal to obtain better results for a flow at low Mach numbers. This idea was first

proposed by Turkel [68]. Examples of this approach are the works of Dellacherie [16] or Rieper [58], where the authors attempt to only modify the part of the flux function that describes the numerical diffusion. Another, more detailed approach is published by Klein [35]. Their method is based on an asymptotic expansion and considers different orders in terms of the Mach number in the composition of the pressure term. It is applied for example in the works of Cordier et al. [15] and Noelle et al. [53]. The algorithm proposed by Schneider et al. [62] is also based on the work of Klein. They develop a method to construct numerical fluxes in an upwind scheme in a way that the divergence constraint in the asymptotic limit is met.

A group of popular upwind methods are AUSM (Advection Upstream Splitting Method)-family schemes. This is due to their simple structure and robust as well as accurate behavior at high Mach numbers. The AUSM scheme was initially developed by Liou and Steffen [43], [41]. There are different modifications for flows at low Mach numbers. The AUSM$^+$-up scheme proposed by Liou [42] is based on a special design of the dissipation terms, while Edwards and Liou [20] introduce a pressure-velocity coupling. The method by Edwards and Liou also depends on the usage of a time-derivative preconditioning. Sachdev et al. [61] further develop the AUSM$^+$-up scheme into a more generalized form that is better suitable for unsteady flows.

Rossow [60] follows a similar approach in expanding the MAPS (Mach number-based Advection Pressure Splitting) scheme towards the incompressible limit. They compare the MAPS flux function to the Roe flux-difference splitting (see Roe [59]). By expanding both schemes in terms of the Mach number and analyzing them in the limit of $M \to 0$, certain dissipation terms are identified that are only present in the Roe scheme and play an important part in the modeling of crossflow diffusion. These terms are then included into the basic MAPS scheme, extending it to MAPS+. Like most flux functions that are extended towards the incompressible limit, MAPS+ is intended to be used together with a time-derivative preconditioning.

Both the AUSM$^+$-up and the MAPS+ scheme prove to be robust and accurate at all Mach numbers. However, in their development only ideal gases are considered. Since the MAPS+ scheme also shows good results for simulations of supercritical fluids, we decide to use MAPS+ for the investigations in this work.

4.2.2. MAPS+

MAPS+ is an extension of the MAPS flux function which consists of momentum fluxes based on the central velocity component q_{cd} and the upwind velocity component q_{up} as well as the pressure term p_{12}. In the following, we use q to refer to the total directional

velocity, hence, it is $q = v_1 n_1 + v_2 n_2$.
MAPS+ is formulated in the conservative variables $(\rho, \rho v_1, \rho v_2, \rho h)$, where h is the specific internal enthalpy. So here the energy equation is not represented by the internal energy but by the enthalpy. For the presentation of MAPS+ we use $\boldsymbol{u}_L$ and $\boldsymbol{u}_R$ for the left- and right-hand side variable at the interface between two cells, respectively. They are the mean values of the respective grid cells.
The two velocity components of the MAPS scheme are defined as

$$q_{\mathrm{cd}} = \frac{c^{av}}{2}\left(\frac{Ma_L + Ma_R}{2} - \beta^M \frac{|Ma_R| - |Ma_L|}{2}\right)$$

and

$$q_{\mathrm{up}} = \frac{c^{av}}{2} Ma_m$$

with the average speed of sound

$$c^{av} = \frac{(c_L + c_R)}{2}$$

and the left- and right-hand Mach numbers given by

$$Ma_L = \frac{q_L}{c^{av}} \quad \text{and} \quad Ma_R = \frac{q_R}{c^{av}}.$$

The maximum Mach number Ma_m is defined as

$$Ma_m = \max\left(|Ma_L|, |Ma_R|\right),$$

while the function β^M is given by

$$\beta^M = \max\left(0, 2Ma_{\max 1} - 1\right) \tag{4.5}$$

with

$$Ma_{\max,1} = \min\left(Ma_m, 1\right).$$

The contribution of pressure is defined as

$$p_{12} = p_{av} - \beta^p p_d$$

with the average pressure

$$p_{av} = \frac{p_L + p_R}{2}$$

and the pressure difference

$$p_d = \frac{1}{2}\left(p_R \frac{Ma_R}{|Ma_R|} - p_L \frac{Ma_L}{|Ma_L|}\right).$$

The scaling function β^p is defined as

$$\beta^p = \max(0, 2Ma_{\min,1} - 1) \tag{4.6}$$

with the Mach number

$$Ma_{\min,1} = \min\left[\min\left(|Ma_L|, |Ma_R|\right), 1\right].$$

The two momentum fluxes $(\rho v)_L$ and $(\rho v)_R$ of MAPS are defined as

$$(\rho v)_L = (q_{\text{cd}} + q_{\text{up}})\,\rho_L$$

and

$$(\rho v)_R = (q_{\text{cd}} - q_{\text{up}})\,\rho_R.$$

Finally, the flux function is given by

$$\mathcal{H}^{\rho\Phi}_{MAPS}\left(\widetilde{\boldsymbol{u}}_i, \widetilde{\boldsymbol{u}}_j; \boldsymbol{n}\right) = (\rho v)_L\,\Phi_L + (\rho v)_R\,\Phi_R + p_{12}\Psi,$$

with $\Phi = (1, v_1, v_2, h)^T$ and $\Psi = (0, n_1, n_2, 0)^T$.
For the extension to MAPS+, dissipation terms are added to improve the behavior of the compressible scheme in the incompressible limit. The extended MAPS+ flux function is given by

$$\mathcal{H}^{\rho\Phi}_{MAPS+}\left(\widetilde{\boldsymbol{u}}_i, \widetilde{\boldsymbol{u}}_j; \boldsymbol{n}\right) = \mathcal{H}^{\rho\Phi}_{MAPS}\left(\widetilde{\boldsymbol{u}}_i, \widetilde{\boldsymbol{u}}_j; \boldsymbol{n}\right) - (\Phi_L + \Phi_R)\,p_{\text{scal}} - \Psi q_{\text{scal}}.$$

The terms of extension are the pressure scaling

$$p_{\text{scal}} = \frac{\max\left(1 - Ma_0, 0\right)}{2c_{\max}} \frac{p_R - p_L}{2}$$

and the velocity scaling

$$q_{\text{scal}} = \frac{\rho_L + \rho_R}{4} \max\left(1 - Ma_0, 0\right) c_{\min}\left(q_R - q_L\right)$$

with the Mach number

$$Ma_0 = \min\left(\frac{q_{\max}}{c_{\min}}, 1\right). \tag{4.7}$$

The remaining terms are defined as:

$$c_{\max} = \max\left(c_L, c_R\right),$$

$$c_{\min} = \min\left(c_L, c_R\right)$$

and

$$q_{\max} = Ma_m c_{\max}. \tag{4.8}$$

In the case of a low Mach number, MAPS+ is adapted by changing these additional terms to

$$c_{\max,\mathrm{mod}} = \sqrt{q_{\max}^2 \left[\frac{1}{2}\left(1 - \frac{q_{\mathrm{ref}^2}}{c_{\max}^2}\right)\right]^2 + q_{\mathrm{ref}^2}}, \tag{4.9}$$

$$c_{\min,\mathrm{mod}} = c_{\max,\mathrm{mod}}$$

and

$$q_{\max,\mathrm{mod}} = q_{\max}\left[1 - \frac{1}{2}\left(1 - \frac{q_{\mathrm{ref}}^2}{c_{\max}^2}\right)\right],$$

with the reference velocity

$$q_{\mathrm{ref}}^2 = \min\left[\max\left(|q|^2, K^2 c_{\max}^2\right), c_{\max}^2\right],$$

where K is the product of a constant K_c and the reference Mach number. Usually, K_c is set to be one.
In this case, the Mach number Ma_0 is calculated using the modified expressions. It gets changed to

$$Ma_0 = \min\left(\frac{q_{\max,\mathrm{mod}}}{c_{\min,\mathrm{mod}}}, 1\right). \tag{4.10}$$

In the following, we refer to the MAPS+ scheme using terms (4.7) to (4.8) as the general MAPS+ scheme while we call the one using terms (4.9) to (4.10) the altered MAPS+ scheme.

4.2.3. Approximation of the continuous flux function

The continuous flux function of the Euler equations can be expressed by a Jacobi matrix as defined in equation (2.4) on page 8. We want to analyze the differences in this matrix caused by the use of an ideal and a Van der Waals gas equation of state. To do this,

we examine the $\mathcal{O}$-formulation of the entries of the matrix for both cases as the Mach number approaches zero.

In a first step, it is helpful to look at the transformation matrix between the primitive variables $\boldsymbol{q}_1 = (\rho, v_1, v_2, p)^T$ and the conservative variables $\boldsymbol{u} = (u_1, u_2, u_3, u_4)^T = (\rho, \rho v_1, \rho v_2, \rho E)^T$. To arrive at this matrix, we first write the primitive variables in terms of the conservative ones. For an ideal gas we get

$$\boldsymbol{q}_{1,id} = \left(u_1, \frac{u_2}{u_1}, \frac{u_3}{u_1}, (\gamma - 1) \left[u_4 - \frac{1}{2} \frac{u_2^2 + u_3^2}{u_1} \right] \right)^T, \tag{4.11}$$

where the first three entries can be gained directly from the vector of conservative variables. To get the fourth entry we first rearrange the dimensionless version of the caloric ideal gas equation (2.5) to

$$p = (\gamma - 1) \left(\rho E - \frac{1}{2} \rho \boldsymbol{v}^2 \right)$$

which then leads us to the fourth entry of the vector in equation (4.11).

In the next step we calculate the transformation matrix $\left(\frac{\partial \boldsymbol{q}_1}{\partial \boldsymbol{u}} \right)_{id}$ using the representation of the primitive variables given in equation (4.11). This leads to

$$\left(\frac{\partial \boldsymbol{q}_1}{\partial \boldsymbol{u}} \right)_{id} = \begin{bmatrix} 1 & 0 & 0 & 0 \\ -\frac{u_2}{u_1^2} & \frac{1}{u_1} & 0 & 0 \\ -\frac{u_3}{u_1^2} & 0 & \frac{1}{u_1} & 0 \\ \frac{1}{2}(\gamma - 1) \frac{u_2^2 + u_3^2}{u_1^2} & -(\gamma - 1) \frac{u_2}{u_1} & -(\gamma - 1) \frac{u_3}{u_1} & \gamma - 1 \end{bmatrix}. \tag{4.12}$$

If we replace the conservative variables, we can also write this matrix as

$$\left(\frac{\partial \boldsymbol{q}_1}{\partial \boldsymbol{u}} \right)_{id} = \begin{bmatrix} 1 & 0 & 0 & 0 \\ -\frac{v_1}{\rho} & \frac{1}{\rho} & 0 & 0 \\ -\frac{v_2}{\rho} & 0 & \frac{1}{\rho} & 0 \\ \frac{1}{2}(\gamma - 1) |\boldsymbol{v}|^2 & -v_1 (\gamma - 1) & -v_2 (\gamma - 1) & \gamma - 1 \end{bmatrix}.$$

To calculate the transformation matrix for a Van der Waals gas, we first write the vector of primitive variables in terms of the conservative ones applying the nondimensional caloric equation of state for a Van der Waals gas (4.4) on page 45. The first three entries

are identical to the vector in equation (4.11). For the fourth entry we write the right-hand side of equation (4.4) in terms of the conservative variables and arrive at

$$p = \frac{2M_w u_4 - M_w \frac{u_2^2+u_3^2}{u_1} + 2\frac{au_1^2}{M_w}}{3M_w - 3bu_1} - \frac{au_1^2}{M_w^2}.$$

Hence, we get the following form of the vector of primitive variables:

$$\boldsymbol{q}_{1,VdW} = \left(u_1, \frac{u_2}{u_1}, \frac{u_3}{u_1}, \frac{2M_w u_4 - M_w \frac{u_2^2+u_3^2}{u_1} + 2\frac{au_1^2}{M_w}}{3M_w - 3bu_1} - \frac{au_1^2}{M_w^2} \right)^T \tag{4.13}$$

Now we calculate the transformation matrix $\left(\frac{\partial \boldsymbol{q}_1}{\partial \boldsymbol{u}}\right)_{VdW}$ using this vector. The first three rows are identical to the ones in matrix (4.12). For the first entry in the last row we get

$$\begin{aligned}
\left(\frac{\partial (q_1)_4}{\partial u_1}\right)_{VdW} &= \frac{(3M_w - 3bu_1)\left(M_w \frac{u_2^2+u_3^2}{u_1^2} + 4\frac{au_1}{M_w}\right) + 3b\left(2M_w u_4 - M_w \frac{u_2^2+u_3^2}{u_1} + 2\frac{au_1^2}{M_w}\right)}{(3M_w - 3bu_1)^2} \\
&\quad -2\frac{au_1}{M_w^2} \\
&= \frac{3M_w^2 \frac{u_2^2+u_3^2}{u_1^2} + 12au_1 - 3bM_w \frac{u_2^2+u_3^2}{u_1} - 12\frac{ab}{M_w}u_1^2}{(3M_w - 3bu_1)^2} \\
&\quad + \frac{6bM_w u_4 - 3bM_w \frac{u_2^2+u_3^2}{u_1} + 6\frac{ab}{M_w}u_1^2}{(3M_w - 3bu_1)^2} - 2\frac{au_1}{M_w^2}
\end{aligned}$$

We can further simplify this equation to

$$\begin{aligned}
\left(\frac{\partial (q_1)_4}{\partial u_1}\right)_{VdW} &= \frac{6bM_w u_4 + 3M_w^2 \frac{u_2^2+u_3^2}{u_1^2} - 6bM_w \frac{u_2^2+u_3^2}{u_1} - 6\frac{ab}{M_w}u_1^2 + 12au_1}{(3M_w - 3bu_1)^2} - 2\frac{au_1}{M_w^2} \\
&= \frac{2bM_w^3 u_4 + M_w^4 \frac{u_2^2+u_3^2}{u_1^2} - 2bM_w^3 \frac{u_2^2+u_3^2}{u_1} - 2abM_w u_1^2 + 4aM_w^2 u_1}{3M_w^2 (M_w - bu_1)^2} \\
&\quad + \frac{-6ab^2 u_1^3 + 12abM_w u_1^2 - 6aM_w^2 u_1}{3M_w^2 (M_w - bu_1)^2} \\
&= \frac{2bM_w^3 u_4 + M_w^4 \frac{u_2^2+u_3^2}{u_1^2} - 2bM_w^3 \frac{u_2^2+u_3^2}{u_1} - 6ab^2 u_1^3 + 10abM_w u_1^2 - 2aM_w^2 u_1}{3M_w^2 (M_w - bu_1)^2}.
\end{aligned}$$

If we replace the conservative variables we can rewrite this as

$$\begin{aligned}\left(\frac{\partial(q_1)_4}{\partial u_1}\right)_{VdW} &= \frac{2bM_w^3\rho E + M_w^4|\boldsymbol{v}|^2 - 2bM_w^3\rho|\boldsymbol{v}|^2 - 6ab^2\rho^3 + 10abM_w\rho^2 - 2aM_w^2\rho}{3M_w^2\left(M_w - b\rho\right)^2} \\ &= \frac{2bM_w\rho\left(E - |\boldsymbol{v}|^2\right) + M_w^2|\boldsymbol{v}|^2 - 6\frac{ab^2}{M_w^2}\rho^3 + 10\frac{ab}{M_w}\rho^2 - 2a\rho}{3\left(M_w - b\rho\right)^2}\end{aligned}$$

The second entry in the last row becomes

$$\left(\frac{\partial(q_1)_4}{\partial u_2}\right)_{VdW} = \frac{-2M_w\frac{u_2}{u_1}}{3M_w - 3bu_1}.$$

If we replace the conservative variables we get

$$\left(\frac{\partial(q_1)_4}{\partial u_2}\right)_{VdW} = \frac{-2M_w v_1}{3M_w - 3b\rho}.$$

In a similar manner, we get

$$\left(\frac{\partial(q_1)_4}{\partial u_3}\right)_{VdW} = \frac{-2M_w v_2}{3M_w - 3b\rho}$$

for the third entry of the last row. Finally, we calculate the last entry which becomes

$$\left(\frac{\partial(q_1)_4}{\partial u_4}\right)_{VdW} = \frac{2M_w}{3M_w - 3bu_1}.$$

Again, we replace the conservative variables and arrive at

$$\left(\frac{\partial(q_1)_4}{\partial u_4}\right)_{VdW} = \frac{2M_w}{3M_w - 3b\rho}.$$

Hence, for a Van der Waals gas with the caloric equation of state (4.4) we get the following form of the transformation matrix:

$$\left(\frac{\partial \boldsymbol{q}_1}{\partial \boldsymbol{u}}\right)_{VdW} =$$

$$\begin{bmatrix} 1 & 0 & 0 & 0 \\ -\frac{v_1}{\rho} & \frac{1}{\rho} & 0 & 0 \\ -\frac{v_2}{\rho} & 0 & \frac{1}{\rho} & 0 \\ \frac{2bM_w\rho\left(E-|\boldsymbol{v}|^2\right)+M_w^2|\boldsymbol{v}|^2-6\frac{ab^2}{M_w^2}\rho^3+10\frac{ab}{M_w}\rho^2-2a\rho}{3(M_w-b\rho)^2} & \frac{-2M_wv_1}{3M_w-3b\rho} & \frac{-2M_wv_2}{3M_w-3b\rho} & \frac{2M_w}{3M_w-3b\rho} \end{bmatrix}. \tag{4.14}$$

Clearly, only the last row of the transformation matrix differs depending on which equation of state is used. The last row contains the changes of pressure with the different conservative variables. In the first row, the changes of density are listed. Since density is both a primitive variable in $\boldsymbol{q}_1$ and a conservative variable, this row does not change depending on the choice of the state equation as density is solely described by itself. Therefore, pressure is the only primitive variable out of $\boldsymbol{q}_1$ that depends on the specific equation of state and hence we only see a change in the last row of the two matrices.
For $M \to 0$, we get the following behavior of the different terms of the transformation matrix for an ideal gas

$$\left(\frac{\partial \boldsymbol{q}_1}{\partial \boldsymbol{u}}\right)_{id} = \begin{bmatrix} 1 & 0 & 0 & 0 \\ \mathcal{O}(M) & \mathcal{O}(1) & 0 & 0 \\ \mathcal{O}(M) & 0 & \mathcal{O}(1) & 0 \\ \mathcal{O}(M^2) & \mathcal{O}(M) & \mathcal{O}(M) & \mathcal{O}(1) \end{bmatrix}. \tag{4.15}$$

For a Van der Waals gas we get

$$\left(\frac{\partial \boldsymbol{q}_1}{\partial \boldsymbol{u}}\right)_{VdW} = \begin{bmatrix} 1 & 0 & 0 & 0 \\ \mathcal{O}(M) & \mathcal{O}(1) & 0 & 0 \\ \mathcal{O}(M) & 0 & \mathcal{O}(1) & 0 \\ \mathcal{O}(1) & \mathcal{O}(M) & \mathcal{O}(M) & \mathcal{O}(1) \end{bmatrix}. \tag{4.16}$$

Since $|\boldsymbol{v}|$ is of $\mathcal{O}(M)$ as $M \to 0$ while all thermodynamic quantities are of $\mathcal{O}(1)$, the only difference in the behavior of the terms of these matrices is the first term in the last row $\frac{(\partial \boldsymbol{q}_1)_4}{\partial \boldsymbol{u}_1} = \frac{\partial p}{\partial \rho}$. For an ideal gas, it is $\mathcal{O}(M^2)$ but for a Van der Waals gas it is of $\mathcal{O}(1)$.
In a similar way, we can look at the behavior of the terms of the continuous Jacobi matrix

in x_1-direction $\boldsymbol{A}_{\boldsymbol{u}}^{(1)} = \frac{\partial f_1(\boldsymbol{u})}{\partial \boldsymbol{u}}$. For the detailed derivation see Appendix (A.1). For an ideal gas, we get

$$\boldsymbol{A}_{\boldsymbol{u}}^{(1)} = \begin{bmatrix} 0 & 1 & 0 & 0 \\ \mathcal{O}(M^2) & \mathcal{O}(M) & \mathcal{O}(M) & \mathcal{O}(1) \\ \mathcal{O}(M^2) & \mathcal{O}(M) & \mathcal{O}(M) & 0 \\ \mathcal{O}(M) & \mathcal{O}(1) & \mathcal{O}(M^2) & \mathcal{O}(M) \end{bmatrix}, \tag{4.17}$$

see equation (A.4), while the usage of a Van der Waals gas leads to

$$\boldsymbol{A}_{\boldsymbol{u}}^{(1)} = \begin{bmatrix} 0 & 1 & 0 & 0 \\ \mathcal{O}(1) & \mathcal{O}(M) & \mathcal{O}(M) & \mathcal{O}(1) \\ \mathcal{O}(M^2) & \mathcal{O}(M) & \mathcal{O}(M) & 0 \\ \mathcal{O}(M) & \mathcal{O}(1) & \mathcal{O}(M^2) & \mathcal{O}(M) \end{bmatrix}, \tag{4.18}$$

see equation (A.7).

As for the transformation matrices, only one term shows a different behavior as $M \to 0$. This is the first term in the second row $\frac{\partial (f_1(\boldsymbol{u}))_2}{\partial u_1} = \frac{\partial (\rho v_1^2 + p)}{\partial \rho}$. For an ideal gas it is of $\mathcal{O}(M^2)$ as $M \to 0$ while for a Van der Waals gas it is of $\mathcal{O}(1)$. This difference is expected due to the different behaviors of $\frac{\partial p}{\partial \rho}$ depending on the chosen equation of state, which is dominant over the behavior of $\frac{\partial (\rho v_1^2)}{\partial \rho}$ in the case of a Van der Waals gas. Of course, if we consider the continuous Jacobi matrix in x_2-direction, the term showing a different behavior depending on the state equation is the first term in the third row $\frac{\partial (f_2(\boldsymbol{u}))_3}{\partial u_1} = \frac{\partial (\rho v_2^2 + p)}{\partial \rho}$.

This analysis shows that there is a great difference in the behavior of some terms in the Jacobi matrices as the Mach number approaches zero. Hence, a numerical flux function designed for an ideal gas can only be expected to show good results for a Van der Waals gas if these differences introduced due to the different state equations are also present in the definition of the numerical flux function. Therefore, we need to analyze the MAPS+ function in this regard.

To compare the numerical MAPS+ flux function to the continuous Jacobi matrix of the Euler equations, we have to transfer the dissipation terms of MAPS+ into the form of a Jacobi Matrix. Following Rossow [60], we write the dissipation terms of the MAPS+ scheme as

$$
\begin{aligned}
\mathcal{H}^{\rho}_{MAPS+}\left(\widetilde{\boldsymbol{u}}_i, \widetilde{\boldsymbol{u}}_j; \boldsymbol{n}\right) &= \frac{1}{2c_{\max}}\left(1 - |Ma_0|\right) \triangle p + \rho\beta^M \triangle q + |q| \triangle \rho \\
\mathcal{H}^{\rho v_1}_{MAPS+}\left(\widetilde{\boldsymbol{u}}_i, \widetilde{\boldsymbol{u}}_j; \boldsymbol{n}\right) &= n_1\beta^p \triangle p + \frac{1}{2c_{\max}} v_1 \left(1 - |Ma_0|\right) \triangle p + \frac{1}{2} n_1 \rho c_{\max} \left(1 - |Ma_0|\right) \triangle q \\
&\quad + \rho v_1 \beta^M \triangle q + |q| \triangle \left(\rho v_1\right) \\
\mathcal{H}^{\rho v_2}_{MAPS+}\left(\widetilde{\boldsymbol{u}}_i, \widetilde{\boldsymbol{u}}_j; \boldsymbol{n}\right) &= n_2\beta^p \triangle p + \frac{1}{2c_{\max}} v_2 \left(1 - |Ma_0|\right) \triangle p + \frac{1}{2} n_2 \rho c_{\max} \left(1 - |Ma_0|\right) \triangle q \\
&\quad + \rho v_2 \beta^M \triangle q + |q| \triangle \left(\rho v_2\right) \\
\mathcal{H}^{\rho h}_{MAPS+}\left(\widetilde{\boldsymbol{u}}_i, \widetilde{\boldsymbol{u}}_j; \boldsymbol{n}\right) &= \frac{1}{2c_{\max}} h \left(1 - |Ma_0|\right) \triangle p + \rho h \beta^M \triangle q + |q| \triangle \left(\rho h\right).
\end{aligned}
$$

The notation $\triangle\phi$ is an abbreviation for the numerical difference $\phi_L - \phi_R$.
We can express these equations as the sum of two Jacobi matrices. The first one being in terms of the primitive variables $\boldsymbol{q}_1$, the second in terms of the conservative ones. Using the transformation matrix $\frac{\partial \boldsymbol{q}_1}{\partial \boldsymbol{u}}$ from primitive variables $\boldsymbol{q}_1$ to conservative variables $\boldsymbol{u}$, we can rewrite this sum in terms of conservative variables. This is necessary to compare it to the continuous Jacobi matrix of the Euler equations which is formulated in conservative variables as well. For simplicity, in the flowing we consider a flow-aligned coordinate system. This gives us $q = v_1$. With this, we can write the Jacobi matrix of the diffusive part of the general MAPS+ scheme as

$$
\begin{aligned}
A_{\boldsymbol{u},MAPS+} = &\begin{bmatrix}
0 & \rho\beta^M & 0 & \frac{1}{2c_{\max}}\left(1 - |Ma_0|\right) \\
0 & \rho v_1 \beta^M + \frac{\rho c_{\min}}{2}\left(1 - |Ma_0|\right) & 0 & \frac{v_1}{2c_{\max}}\left(1 - |Ma_0|\right) + \beta^p \\
0 & \rho v_2 \beta^M + \frac{\rho c_{\min}}{2}\left(1 - |Ma_0|\right) & 0 & \frac{v_2}{2c_{\max}}\left(1 - |Ma_0|\right) + \beta^p \\
0 & \rho(E + \frac{p}{\rho})\beta^M & 0 & \frac{E+\frac{p}{\rho}}{2c_{\max}}\left(1 - |Ma_0|\right) + v_1
\end{bmatrix} \cdot \frac{\partial \boldsymbol{q}_1}{\partial \boldsymbol{u}} \\
&+ \begin{bmatrix}
v_1 & 0 & 0 & 0 \\
0 & v_1 & 0 & 0 \\
0 & 0 & v_1 & 0 \\
0 & 0 & 0 & v_1
\end{bmatrix}.
\end{aligned}
\tag{4.19}
$$

To compare this representation of MAPS+ to the Jacobi matrix of the Euler equations, we transform the latter into a similar form. Since we consider a flow-aligned coordinate system with $q = v_1$, we can compare matrix (4.19) to the continuous Jacobi matrix in x_1-direction $\boldsymbol{A}^{(1)}_{\boldsymbol{u}} = \frac{\partial \boldsymbol{f}_1(\boldsymbol{u})}{\partial \boldsymbol{u}}$. We separate a matrix in terms of the conservative variables similar to the last term in equation (4.19) as it is done for the MAPS+ scheme and

write the remaining terms as functions of the primitive variables $\boldsymbol{q}_1$. The detailed derivation is presented in Appendix A.2. This leads us to the following representation of the continuous Jacobi matrix in x_1-direction, written as the sum of two matrices

$$\boldsymbol{A}_{\boldsymbol{u}}^{(1)} = \begin{bmatrix} 0 & \rho & 0 & 0 \\ 0 & \rho v_1 & 0 & 1 \\ 0 & \rho v_2 & 0 & 0 \\ 0 & \rho(E + \frac{p}{\rho}) & 0 & v_1 \end{bmatrix} \frac{\partial \boldsymbol{q}_1}{\partial \boldsymbol{u}} + \begin{bmatrix} v_1 & 0 & 0 & 0 \\ 0 & v_1 & 0 & 0 \\ 0 & 0 & v_1 & 0 \\ 0 & 0 & 0 & v_1 \end{bmatrix}. \tag{4.20}$$

This matrix is valid for both an ideal and a Van der Waals gas, as it is shown in Appendices A.2.1 and A.2.2. Comparing equations (4.19) and (4.20), it stands out that we only consider the pressure component in the momentum equation in x_1-direction in the continuous Jacobi matrix while it is present in both momentum equations in the flow-aligned MAPS+ scheme. However, the momentum equation in x_2-direction including the pressure component is of course included in the continuous Jacobi matrix in x_2-direction. Apart from this difference, MAPS+ is a close approximation of the continuous flux function represented by equation (4.20) for Mach numbers close to or above one. Note that the terms multiplied by $(1 - |Ma_0|)$ only have a small influence as the Mach number approaches unity from below. For supersonic flows, these terms are not considered, since $Ma_0 = 1$ in this flow region, see the definition of Ma_0 in equation (4.7) on page 49. In addition, for supersonic flows it is $\beta^M = \beta^p = 1$, see the definitions of β^M and β^p in equations (4.5) and (4.6), respectively. Hence, in this flow region, the MAPS+ Jacobi matrix is an exact representation of the continuous flux function of the Euler equation. Due to the separation in primitive and conservative variables, this holds for any thermodynamic state equation. The multiplication with $\frac{\partial \boldsymbol{q}_1}{\partial \boldsymbol{u}}$ introduces the different behaviors of the equations of state into the MAPS+ scheme. Hence, the numerical algorithm given by equation (4.19) represents the flux of a Van der Waals gas as well as the one of an ideal gas.

However, this is only the case for a Mach number above 0.5. For smaller Mach numbers, and hence in the case of $M \to 0$, the functions β^M and β^p become zero, see their definition in equations (4.5) and (4.6), respectively. At the same time, the influence of the terms multiplied by $(1 - |Ma_0|)$ increases. These differences are introduced to MAPS+ to ensure the correct calculation of diffusion at small Mach numbers, both in and across the direction of the flow, see Rossow [60].

Since we are interested in the application of MAPS+ to small Mach numbers, we look at the flow aligned Jacobi matrix of the MAPS+ scheme for a Mach number below 0.5:

$$\boldsymbol{A}_{\boldsymbol{u},MAPS+} = \begin{bmatrix} 0 & 0 & 0 & \frac{1}{2c_{\max,\mathrm{mod}}}\left(1-|Ma_0|\right) \\ 0 & \frac{\rho c_{\min,\mathrm{mod}}}{2}\left(1-|Ma_0|\right) & 0 & \frac{v_1}{2c_{\max,\mathrm{mod}}}\left(1-|Ma_0|\right) \\ 0 & \frac{\rho c_{\min,\mathrm{mod}}}{2}\left(1-|Ma_0|\right) & 0 & \frac{v_2}{2c_{\max,\mathrm{mod}}}\left(1-|Ma_0|\right) \\ 0 & 0 & 0 & \frac{E+\frac{p}{\rho}}{2c_{\max,\mathrm{mod}}}\left(1-|Ma_0|\right)+v_1 \end{bmatrix} \frac{\partial \boldsymbol{q}_1}{\partial \boldsymbol{u}} + \begin{bmatrix} v_1 & 0 & 0 & 0 \\ 0 & v_1 & 0 & 0 \\ 0 & 0 & v_1 & 0 \\ 0 & 0 & 0 & v_1 \end{bmatrix}. \tag{4.21}$$

Here, we use $c_{\max,\mathrm{mod}}$ and $c_{\min,\mathrm{mod}}$ instead of $c_{\max}$ and $c_{\min}$ since we are concerned with flows at a low Mach number and hence want to analyze the altered MAPS+ scheme.
It is clear that this matrix is not as easily compared to the continuous Jacobi matrix as the one given in equation (4.19). The additional terms introduced to MAPS+ that are shown in equation (4.21) are thoroughly investigated by Rossow [60]. In their work, they show that these terms have the expected effect for an ideal gas. Hence, we can deduce that the matrix representing MAPS+ for a Mach number below 0.5 closely resembles the matrix (4.19) for an ideal gas. Therefore, our goal is to show that the differences in the behavior of the terms of the matrix between an ideal gas and a Van der Waals gas are correctly reproduced by the MAPS+ scheme.
As for the continuous flux Jacobi matrix of the Euler equations, we investigate the behavior of the terms of the MAPS+ flux Jacobi matrix as the Mach number approaches zero. Again, we look at a flow-aligned coordinate system. For an ideal gas we get

$$\boldsymbol{A}_{\boldsymbol{u},MAPS+} = \begin{bmatrix} \mathcal{O}(M) & \mathcal{O}(1) & \mathcal{O}(1) & O(M^{-1}) \\ \mathcal{O}(M^2) & \mathcal{O}(M) & \mathcal{O}(M) & \mathcal{O}(1) \\ \mathcal{O}(M^2) & \mathcal{O}(M) & \mathcal{O}(M) & \mathcal{O}(1) \\ \mathcal{O}(M) & \mathcal{O}(1) & \mathcal{O}(1) & O(M^{-1}) \end{bmatrix},$$

as $M \to 0$ while for a Van der Waals gas we get the following behavior:

$$\boldsymbol{A}_{\boldsymbol{u},MAPS+} = \begin{bmatrix} O(M^{-1}) & \mathcal{O}(1) & \mathcal{O}(1) & O(M^{-1}) \\ \mathcal{O}(1) & \mathcal{O}(M) & \mathcal{O}(M) & \mathcal{O}(1) \\ \mathcal{O}(1) & \mathcal{O}(M) & \mathcal{O}(M) & \mathcal{O}(1) \\ O(M^{-1}) & \mathcal{O}(1) & \mathcal{O}(1) & O(M^{-1}) \end{bmatrix}. \tag{4.22}$$

The derivation of the behavior of the different terms is shown in Appendix A.3. The

obvious difference of the Jacobi matrix for a Van der Waals gas is the increase of all terms in the first column by two orders of magnitude with respect to the Mach number compared to the Jacobi matrix for an ideal gas. These terms are the ones that are multiplied by $\triangle\rho$. The analysis of the continuous Jacobi matrices shows this difference in the momentum equations, see the matrices (4.17) and (4.18). Hence, the influence of the different equation of state on the flux Jacobi matrix that we found by analyzing the continuous Jacobi matrices is also present in the MAPS+ scheme.
The additional differences concerning the increased influence of the terms multiplied by $\triangle\rho$ on the continuity and energy equations, so the changes in behavior of the first terms in the first and last row, do not alter the performance of MAPS+. For a Van der Waals gas, the terms multiplied by the density difference show the same behavior for a vanishing Mach number as the terms multiplied by the energy density differences do. So, in matrix (4.22), the first and the forth column contain identical entries. However, in the density and energy density equations, the terms multiplied by $\triangle\rho E$ are higher than the terms multiplied by $\triangle\rho$ by a factor over 1000, where the exact value depends on the fluid. So even though for a Van der Waals gas the terms multiplied by $\triangle\rho$ show the same behavior for $M \to 0$ as the terms multiplied by $\triangle\rho E$ do, the latter are dominant independent of the Mach number. Hence, the energy density differences are still the main components in these two equations.
Therefore, the adjustments made for small Mach numbers work as well for a Van der Waals gas as they do for an ideal gas.

4.2.4. Asymptotic Analysis

Since we want to analyze the flux function the way it is implemented in the numerical scheme, it is favorable to nondimensionalize the equations by applying the reference values used in the scheme instead of using the nondimensionalization that is suitable for an asymptotic analysis. We also discuss this in section 4.1.5 and the used reference values are listed in Table 4.1 on page 44. This leads to nondimensional parameters that are not all of $\mathcal{O}(1)$ as $M \to 0$. To overcome this issue and arrive at parameters of $\mathcal{O}(1)$, we introduce the following auxiliary parameters into all equations of the flux functions:

$$\widetilde{c} = c, \quad \widetilde{p} = p, \ \widetilde{h} = h \ \widetilde{\rho} = \rho, \ \widetilde{q} = Mq, \text{ and } \widetilde{\boldsymbol{v}} = M\boldsymbol{v}$$

As in chapter 3, we use the Mach number M instead of the local Mach number Ma for the investigation.
Using the auxiliary variables, we get the following form of the integral balance equation

presented in equation (4.2) on page 37:

$$\frac{d}{dt}\left(\mathcal{M}_{\sigma_i}\widetilde{\boldsymbol{u}}\right)(t) + \left(\widetilde{\mathcal{L}}_{\sigma_i}\widetilde{\boldsymbol{u}}\right)(t) = 0 \text{ for all } \sigma_i \in \mathcal{B}$$

We conduct this analysis for both the general and the altered MAPS+ scheme. Since both are an extension of MAPS, we start with an analysis of the MAPS scheme.
In the following, we use the discretization described in subsection 4.1.2 on page 38. The subscript $_i$ indicates the cell mean value of the respective quantity in a grid cell $\sigma_i \in \mathcal{B}$. The subscript $_j$ refers to a grid cell σ_j with $j \in \mathcal{N}(i)$. The maximum and minimum functions that are indicated by the subscripts $_{\max,ij}$ and $_{\min,ij}$, respectively, indicate the maximum and minimum of the respective quantities in the grid cells σ_i and σ_j.

4.2.4.1. MAPS scheme

For the average speed of sound, the introduction of the auxiliary parameters leads to

$$\widetilde{c}^{av} = \frac{\widetilde{c}_i + \widetilde{c}_j}{2} = \frac{c_i + c_j}{2},$$

while the Mach number of each grid cell becomes

$$\widetilde{Ma}_i = \frac{\widetilde{q}_i}{\widetilde{c}^{av}} = M\frac{2q_i}{c_i + c_j} \quad \text{and} \quad \widetilde{Ma}_j = M\frac{2q_j}{c_i + c_j}.$$

With $\Phi_{\max,ij} = \max(\Phi_i, \Phi_j)$ the maximum Mach number becomes

$$\begin{aligned}\widetilde{Ma}_m &= \max\left(|\widetilde{Ma}_i|, |\widetilde{Ma}_j|\right) = \max\left(|M\frac{2q_i}{c_i + c_j}|, |M\frac{2q_j}{c_i + c_j}|\right) \\ &= M\frac{2|q|_{\max,ij}}{c_i + c_j},\end{aligned}$$

while for the Mach number $\widetilde{Ma}_{\max,1}$, the following is true:

$$\widetilde{Ma}_{\max,1} = \min\left[\max\left(|\widetilde{Ma}_i|, |\widetilde{Ma}_j|\right), 1\right] = \min\left(M\frac{2|q|_{\max,ij}}{c_i + c_j}, 1\right)$$

For $M \to 0$ the first term of the minimum function is dominant and we get

$$\widetilde{Ma}_{\max,1} = M\frac{2|q|_{\max,ij}}{c_i + c_j}.$$

With this, we can evaluate the function $\widetilde{\beta}^M$:

$$\widetilde{\beta}^M = \max\left(0, 2 \cdot \widetilde{Ma}_{\max,1} - 1\right) = \max\left(0, M\frac{4|q|_{\max,ij}}{c_i + c_j} - 1\right)$$

for $M \to 0$ we get:

$$\widetilde{\beta}^M = 0.$$

Given these intermediate results, we can write the velocity components as

$$\begin{aligned}\widetilde{q}_{\mathrm{cd}} &= \frac{\widetilde{c}_{av}}{2}\left(\frac{\widetilde{Ma}_i + \widetilde{Ma}_j}{2} - \widetilde{\beta}^M \frac{|\widetilde{Ma}_j| - |\widetilde{Ma}_i|}{2}\right) \\ &= \frac{c_i + c_j}{4}\left(\frac{M}{2}\frac{2q_i}{c_i + c_j} + \frac{M}{2}\frac{2q_j}{c_i + c_j}\right) = \frac{c_i + c_j}{4}\left(M\frac{q_i + q_j}{c_i + c_j}\right) = M\frac{q_i + q_j}{4}\end{aligned}$$

and

$$\widetilde{q}_{\mathrm{up}} = \frac{\widetilde{c}_{av}}{2}\widetilde{Ma}_m = \frac{c_i + c_j}{4} \cdot M\frac{2|q|_{\max,ij}}{c_i + c_j} = M\frac{|q|_{\max,ij}}{2},$$

which leads to the momentum fluxes

$$(\widetilde{\rho v})_i = (\widetilde{q}_{\mathrm{cd}} + \widetilde{q}_{\mathrm{up}})\,\rho_i = M\left(\frac{q_i + q_j}{4} + \frac{|q|_{\max,ij}}{2}\right)\rho_i$$

and

$$(\widetilde{\rho v})_j = (\widetilde{q}_{\mathrm{cd}} - \widetilde{q}_{\mathrm{up}})\,\rho_j = M\left(\frac{q_i + q_j}{4} - \frac{|q|_{\max,ij}}{2}\right)\rho_j.$$

In the next step, we evaluate the components of the pressure contribution. For the average pressure we get

$$\widetilde{p}_{av} = \frac{\widetilde{p}_i + \widetilde{p}_j}{2} = \frac{p_i + p_j}{2},$$

while the pressure difference becomes

$$\begin{aligned}\widetilde{p}_d &= \frac{1}{2}\left(\widetilde{p}_j\frac{\widetilde{Ma}_j}{|\widetilde{Ma}_j|} - \widetilde{p}_i\frac{\widetilde{Ma}_i}{|\widetilde{Ma}_i|}\right) = \frac{1}{2}\left(p_j\frac{M\frac{2q_j}{c_i+c_j}}{|M\frac{2q_j}{c_i+c_j}|} - p_i\frac{M\frac{2q_i}{c_i+c_j}}{|M\frac{2q_i}{c_i+c_j}|}\right) \\ &= \frac{1}{2}\left(p_j\frac{q_j}{|q_j|} - p_i\frac{q_i}{|q_i|}\right).\end{aligned}$$

With $\Phi_{\min,ij} = \min(\Phi_i, \Phi_j)$ the Mach number $\widetilde{Ma}_{\min,1}$ is

$$\widetilde{Ma}_{\min,1} = \min\left[\min\left(|\widetilde{Ma}_i|, |\widetilde{Ma}_j|\right), 1\right] = \min\left(M\frac{2|q|_{\min,ij}}{c_i + c_j}, 1\right).$$

For $M \to 0$ we get:

$$\widetilde{Ma}_{\min,1} = M\frac{2|q|_{\min,ij}}{c_i + c_j}.$$

Hence, we can evaluate $\widetilde{\beta}^p$:

$$\widetilde{\beta}^p = \max(0, 2 \cdot \widetilde{Ma}_{\min,1} - 1) = \max\left(0, 2 \cdot M\frac{2|q|_{\min,ij}}{c_i + c_j} - 1\right)$$

For $M \to 0$ we get

$$\widetilde{\beta}^p = 0.$$

With these results, the pressure contribution $\widetilde{p}_{12}$ simplifies to

$$\widetilde{p}_{12} = \widetilde{p}_{av} - \widetilde{\beta}^p\widetilde{p}_d = \frac{p_i + p_j}{2}.$$

For the extension to MAPS+ we distinguish between the general MAPS+ scheme for all Mach numbers and the altered MAPS+ scheme with modified terms for low Mach numbers.

4.2.4.2. General MAPS+ scheme

In the general case, we can write the remaining terms as

$$\widetilde{c}_{\max,ij} = \max\left(\widetilde{c}_i, \widetilde{c}_j\right) = c_{\max,ij},$$

$$\widetilde{c}_{\min,ij} = \min\left(\widetilde{c}_i, \widetilde{c}_j\right) = c_{\min,ij}$$

and

$$\widetilde{q}_{\max,ij} = \widetilde{Ma}_m\widetilde{c}_{\max,ij} = M\frac{2|q|_{\max,ij}c_{\max,ij}}{c_i + c_j}.$$

And the Mach number $\widetilde{Ma}_0$ becomes:

$$\widetilde{Ma}_0 = \min\left(\frac{\widetilde{q}_{\max,ij}}{\widetilde{c}_{\min,ij}}, 1\right) = \min\left(\frac{M\frac{2|q|_{\max,ij}c_{\max,ij}}{c_i+c_j}}{c_{\min,ij}}, 1\right) = \min\left(M\frac{2|q|_{\max,ij}}{c_i + c_j}\frac{c_{\max,ij}}{c_{\min,ij}}, 1\right)$$

For $M \to 0$ again the first term of the minimum function is the dominant one. Hence, we get:

$$\widetilde{Ma}_0 = M\frac{2|q|_{\max,ij}}{c_i + c_j}\frac{c_{\max,ij}}{c_{\min,ij}} \tag{4.23}$$

For the pressure scaling we get

$$\widetilde{p}_{\text{scal}} = \frac{\max\left(1 - \widetilde{Ma}_0, 0\right)}{2 \cdot \widetilde{c}_{\max,ij}} \cdot \frac{\widetilde{p}_j - \widetilde{p}_i}{2} \tag{4.24}$$

In equation (4.23) we see that $\widetilde{Ma}_0$ is smaller than 1 as $M \to 0$. Hence, we can further simplify equation (4.24) to

$$\begin{aligned}\widetilde{p}_{\text{scal}} &= \frac{1 - \widetilde{Ma}_0}{2 \cdot \widetilde{c}_{\max,ij}} \cdot \frac{\widetilde{p}_j - \widetilde{p}_i}{2} = \frac{\left(1 - M \frac{2|q|_{\max,ij}}{c_i + c_j} \frac{c_{\max,ij}}{c_{\min,ij}}\right)(p_j - p_i)}{4 c_{\max,ij}} \\ &= \frac{p_j - p_i}{4 c_{\max,ij}} - M \frac{|q|_{\max,ij}\,(p_j - p_i)}{2 c_{\min,ij}\,(c_i + c_j)}.\end{aligned}$$

The velocity scaling becomes

$$\widetilde{q}_{\text{scal}} = \frac{\widetilde{\rho}_i + \widetilde{\rho}_j}{4} \cdot \max\left(1 - \widetilde{Ma}_0, 0\right) \widetilde{c}_{\min,ij}\,(\widetilde{q}_j - \widetilde{q}_i)\,.$$

Again, we use the fact that $\widetilde{Ma}_0 < 1$ for $M \to 0$ to simplify the maximum function. This leads us to

$$\begin{aligned}\widetilde{q}_{\text{scal}} &= \frac{\widetilde{\rho}_i + \widetilde{\rho}_j}{4} \cdot \left(1 - \widetilde{Ma}_0\right) \widetilde{c}_{\min,ij}\,(\widetilde{q}_j - \widetilde{q}_i) \\ &= \frac{\rho_i + \rho_j}{4} \left(1 - M \frac{2|q|_{\max,ij}}{c_i + c_j} \frac{c_{\max,ij}}{c_{\min,ij}}\right) c_{\min,ij} \cdot M\,(q_j - q_i) \\ &= \frac{M}{4}\,(\rho_i + \rho_j)\, c_{\min,ij}\,(q_j - q_i) - M^2 \frac{|q|_{\max,ij} c_{\max,ij}\,(\rho_i + \rho_j)}{2\,(c_i + c_j)}\,(q_j - q_i)\,.\end{aligned}$$

Finally, we can combine all intermediate results and arrive at the expression for the flux functions. With the shorthand notation $\triangle_{ij}\Phi = \Phi_i - \Phi_j$ we get for the density flux:

$$\begin{aligned}\mathcal{H}^{\rho}_{MAPS+}\left(\widetilde{\boldsymbol{u}}_i, \widetilde{\boldsymbol{u}}_j; \boldsymbol{n}\right) &= \left(\widetilde{\rho v}\right)_i + \left(\widetilde{\rho v}\right)_j - 2\widetilde{p}_{\text{scal}} \\ &= M\left(\frac{q_i + q_j}{4} + \frac{|q|_{\max,ij}}{2}\right)\rho_i + M\left(\frac{q_i + q_j}{4} - \frac{|q|_{\max,ij}}{2}\right)\rho_j \\ &\quad -2\left(\frac{p_j - p_i}{4 c_{\max,ij}} - M \frac{|q|_{\max,ij}\,(p_j - p_i)}{2 c_{\min,ij}\,(c_i + c_j)}\right) \\ &= \frac{\triangle_{ij} p}{2 c_{\max,ij}} - M \frac{|q|_{\max,ij}}{c_{\min,ij}} \frac{\triangle_{ij} p}{c_i + c_j} + M \frac{|q|_{\max,ij}}{2} \triangle_{ij}\rho \\ &\quad + M \frac{(q_i + q_j)\,(\rho_i + \rho_j)}{4}\end{aligned} \tag{4.25}$$

The two momentum fluxes $\mathcal{H}^{\rho v_\zeta}_{MAPS+}\left(\widetilde{\boldsymbol{u}}_i, \widetilde{\boldsymbol{u}}_j; \boldsymbol{n}\right)$ with $\zeta = 1, 2$ can be written as

$$\begin{aligned}
\mathcal{H}^{\rho v_\zeta}_{MAPS+}\left(\widetilde{\boldsymbol{u}}_i, \widetilde{\boldsymbol{u}}_j; \boldsymbol{n}\right) &= \left(\widetilde{\rho v}\right)_i \left(\widetilde{v}_\zeta\right)_i + \left(\widetilde{\rho v}\right)_j \left(\widetilde{v}_\zeta\right)_j + n_\zeta \widetilde{p}_{12} - \left[\left(\widetilde{v}_\zeta\right)_i + \left(\widetilde{v}_\zeta\right)_j\right] \widetilde{p}_{\text{scal}} - n_\zeta \widetilde{q}_{\text{scal}} \\
&= M\left(\frac{q_i + q_j}{4} + \frac{|q|_{\max,ij}}{2}\right) \rho_i \cdot M \left(v_\zeta\right)_i \\
&\quad + M\left(\frac{q_i + q_j}{4} - \frac{|q|_{\max,ij}}{2}\right) \rho_j \cdot M \left(v_\zeta\right)_j + n_\zeta \frac{p_i + p_j}{2} \\
&\quad - M\left[\left(v_\zeta\right)_i + \left(v_\zeta\right)_j\right] \left(\frac{p_j - p_i}{4 c_{\max,ij}} - M \frac{|q|_{\max,ij} \left(p_j - p_i\right)}{2 c_{\min,ij} \left(c_i + c_j\right)}\right) \\
&\quad - n_\zeta \left(\frac{M}{4} \left(\rho_i + \rho_j\right) c_{\min,ij} \left(q_j - q_i\right)\right. \\
&\qquad \left. - M^2 \frac{|q|_{\max,ij} c_{\max,ij} \left(\rho_i + \rho_j\right)}{2 \left(c_i + c_j\right)} \left(q_j - q_i\right)\right) \\
&= n_\zeta \frac{p_i + p_j}{2} + M \frac{\left(v_\zeta\right)_i + \left(v_\zeta\right)_j}{4 c_{\max,ij}} \triangle_{ij} p + n_\zeta M \frac{\rho_i + \rho_j}{4} c_{\min,ij} \triangle_{ij} q \\
&\quad - M^2 \frac{|q|_{\max,ij}}{2 c_{\min,ij}} \frac{\left(v_\zeta\right)_i + \left(v_\zeta\right)_j}{c_i + c_j} \triangle_{ij} p \\
&\quad - n_\zeta M^2 \frac{|q|_{\max,ij} c_{\max,ij}}{2} \frac{\rho_i + \rho_j}{c_i + c_j} \triangle_{ij} q \\
&\quad + M^2 \frac{|q|_{\max,ij}}{2} \triangle_{ij} \left(\rho v_\zeta\right) + M^2 \frac{q_i + q_j}{4} \left[\left(\rho v_\zeta\right)_i + \left(\rho v_\zeta\right)_j\right].
\end{aligned} \tag{4.26}$$

The enthalpy flux becomes

$$\begin{aligned}
\mathcal{H}^{\rho h}_{MAPS+}\left(\widetilde{\boldsymbol{u}}_i, \widetilde{\boldsymbol{u}}_j; \boldsymbol{n}\right) &= \left(\widetilde{\rho v}\right)_i \widetilde{h}_i + \left(\widetilde{\rho v}\right)_j \widetilde{h}_j - \left(\widetilde{h}_i + \widetilde{h}_j\right) \widetilde{p}_{\text{scal}} \\
&= M\left(\frac{q_i + q_j}{4} + \frac{|q|_{\max,ij}}{2}\right) \left(\rho h\right)_i + M\left(\frac{q_i + q_j}{4} - \frac{|q|_{\max,ij}}{2}\right) \left(\rho h\right)_j \\
&\quad - \left(h_i + h_j\right) \left(\frac{p_j - p_i}{4 c_{\max,ij}} - M \frac{|q|_{\max,ij} \left(p_j - p_i\right)}{2 c_{\min,ij} \left(c_i + c_j\right)}\right) \\
&= \frac{h_i + h_j}{4 c_{\max,ij}} \triangle_{ij} p - M \frac{|q|_{\max,ij}}{2 c_{\min,ij}} \frac{h_i + h_j}{c_i + c_j} \triangle_{ij} p + M \frac{|q|_{\max,ij}}{2} \triangle_{ij} \left(\rho h\right) \\
&\quad + M \frac{q_i + q_j}{4} \left[\left(\rho h\right)_i + \left(\rho h\right)_j\right].
\end{aligned} \tag{4.27}$$

To conduct an asymptotic analysis, we insert an asymptotic series of the form

$$\psi_j = \psi_j^{(0)} + M \psi_j^{(1)} + M^2 \psi_j^{(2)} + o\left(M^2\right)$$

for every physical quantity in the numerical flux functions (4.25), (4.26) and (4.27). Due to Lemma 2 this results in the following asymptotic difference equations:

$$\frac{d}{dt}\rho_i^{(0)} = \sum_{j\in\mathcal{N}(i)}\sum_{k=1}^{2}\frac{\triangle_{ij}p^{(0)}}{2c_{\max,ij}^{(0)}}|l_{ij}^k|, \tag{4.28}$$

$$0 = \sum_{j\in\mathcal{N}(i)}\sum_{k=1}^{2}\frac{p_i^{(0)}+p_j^{(0)}}{2}n_{ij,\zeta}^k|l_{ij}^k| \text{ for } \zeta = 1,2$$

and

$$\frac{d}{dt}(\rho E)_i^{(0)} = \sum_{j\in\mathcal{N}(i)}\sum_{k=1}^{2}\frac{h_i^{(0)}+h_j^{(0)}}{4c_{\max,ij}^{(0)}}\triangle_{ij}p^{(0)}|l_{ij}^k| \tag{4.29}$$

for every $i \in \mathcal{N}_{h,\mathcal{G}}$. Again, we need to expand the relations into Taylor series to gain equations (4.28) and (4.29) which are given by equations (A.17) and (A.24).
A direct result of equations (4.28) and (4.29) is the following Theorem.

Theorem 5.
For $\partial\mathcal{T}_h = \partial\mathcal{T}_{h,w} \cup \partial\mathcal{T}_{h,ff}$ with the boundary condition

$$p(\boldsymbol{x},t) = const + Mp^{(1)}(\boldsymbol{x},t) + M^2p^{(2)}(\boldsymbol{x},t)$$

for all $(\boldsymbol{x},t) \in \partial\mathcal{T}_{h,ff} \times \mathbb{R}_0^+$ and $const \in \mathbb{R}^+$, the following is true for the leading order pressure distribution calculated by the general MAPS+ scheme:

$$p_i^{(0)} = p_j^{(0)} \textit{for all } i,j \in \mathcal{N}_h.$$

The proof is given by Meister [47].
Now, we analyze the function $\mathcal{H}_{MAPS+}^{\rho}(\widetilde{\boldsymbol{u}}_i, \widetilde{\boldsymbol{u}}_j; \boldsymbol{n})$ in equation (4.25) in more detail. We get for the mass balance

$$\frac{d}{dt}(\rho) = \sum_{j\in\mathcal{N}(i)}\sum_{k=1}^{2}\left(\frac{\triangle_{ij}p^{(0)}}{2c^{(0)}_{\max,ij}}\right)|l^k_{ij}|$$
$$+M\sum_{j\in\mathcal{N}(i)}\sum_{k=1}^{2}\left(\frac{\triangle_{ij}p^{(1)}}{2c^{(0)}_{\max,ij}} - \frac{c^{(1)}_{\max,ij}\triangle_{ij}p^{(0)}}{2\left(c^{(0)}_{\max,ij}\right)^2} - \frac{|q|^{(0)}_{\max,ij}}{c^{(0)}_{\min,ij}}\frac{\triangle_{ij}p^{(0)}}{c^{(0)}_i + c^{(0)}_j}\right.$$
$$\left. + \frac{|q|^{(0)}_{\max,ij}}{2}\triangle_{ij}\rho^{(0)} + \frac{\left(q^{(0)}_i + q^{(0)}_j\right)\left(\rho^{(0)}_i + \rho^{(0)}_j\right)}{4}\right)|l^k_{ij}|$$
$$+\mathcal{O}(M^2), \tag{4.30}$$

where the different terms are given by equations (A.17) and (A.18).
In the following we consider the special case of a structured, equidistant, Cartesian grid to which we refer as $\mathcal{S}_h$.

Theorem 6.
If $\mathcal{S}_h$ is a structured discretization of the flow domain $\mathcal{G}$ with $\partial\mathcal{S}_h = \partial\mathcal{S}_{h,w} \cup \partial\mathcal{S}_{h,ff}$ and with the boundary condition

$$p(\boldsymbol{x}, t) = const + M^2 p^{(2)}(\boldsymbol{x}, t)$$

for all $(\boldsymbol{x}, t) \in \partial\mathcal{S}_{h,\mathit{ff}} \times \mathbb{R}^+_0$ and $const \in \mathbb{R}^+$, and for all $i \in \mathcal{N}_{h,\mathcal{G}}$ the statement

$$\rho^{(0)}_i = \rho^{(0)}_j \text{ for all } j \in N(i) \tag{4.31}$$

with

$$\boldsymbol{n}_{il} = -\boldsymbol{n}_{ik} = \begin{pmatrix} 1 \\ 0 \end{pmatrix} \text{ for } l, k \in \mathcal{N}(i)$$

is true, then there exists a velocity field such that the following statement holds for the pressure terms evaluated by the general MAPS+ scheme:

$$p^{(1)}_i \neq p^{(1)}_k$$

Proof.
Due to Theorem 5, the leading order pressure is constant everywhere. Considering the discretization S_h, we can simplify the asymptotic mass equation (4.30) to

$$\frac{d}{dt}\rho_i = M \sum_{j\in(l,k)} \left(\frac{\triangle_{ij} p^{(1)}}{2c^{(0)}_{\max,ij}} + \frac{|q|^{(0)}_{\max,ij}}{2} \triangle_{ij}\rho^{(0)} + \frac{\left(q_i^{(0)} + q_j^{(0)}\right)\left(\rho_i^{(0)} + \rho_j^{(0)}\right)}{4} \right) + \mathcal{O}(M^2).$$

We arrive at the following mass equation of order $\mathcal{O}(M)$:

$$\frac{p_i^{(1)} - p_l^{(1)}}{2c^{(0)}_{\max,il}} + \frac{p_i^{(1)} - p_k^{(1)}}{2c^{(0)}_{\max,ik}} = -\frac{|q|^{(0)}_{\max,il}}{2}\left(\rho_i^{(0)} - \rho_l^{(0)}\right) - \frac{|q|^{(0)}_{\max,ik}}{2}\left(\rho_i^{(0)} - \rho_k^{(0)}\right) - \frac{\left(q_i^{(0)} + q_l^{(0)}\right)\left(\rho_i^{(0)} + \rho_l^{(0)}\right)}{4} - \frac{\left(q_i^{(0)} + q_k^{(0)}\right)\left(\rho_i^{(0)} + \rho_k^{(0)}\right)}{4}.$$

Using condition (4.31) we can simplify this to

$$\frac{p_i^{(1)} - p_l^{(1)}}{2c^{(0)}_{\max,il}} + \frac{p_i^{(1)} - p_k^{(1)}}{2c^{(0)}_{\max,ik}} = \frac{\rho^{(0)}}{2}\left(-2q_i^{(0)} - q_l^{(0)} - q_k^{(0)}\right). \tag{4.32}$$

From this relation, it is obvious that $p^{(1)}$ cannot be spatially constant for an arbitrary velocity field. □

If we do not consider the special case of a constant density field, the relationship between velocity and pressure is more complicated than the one stated in equation (4.32) since it also includes the density field. So, for $p^{(1)}$ to be spatially constant, the velocity field needs to be a certain function of the density field. If the density field is arbitrary, there exists a velocity field such that the first order of pressure cannot be spatially constant. This Theorem shows that there can be fluctuations of the first order pressure term independent of both the fineness of the discretization and the Mach number. This leads to the following corollary:

Corollary 6.1.
There is a discretization of the domain $\mathcal{G}$ so that with the existence of an $i \in \mathcal{N}_{h,\partial\mathcal{G}}$ with

$$\rho_i^{(0)} = \rho_j^{(0)} \text{ for all } j \in \mathcal{N}(i),$$

the first order pressure terms as calculated by the general MAPS+ scheme have variations on a length scale independent of M.

This clearly contradicts the results of the continuous asymptotic analysis. This analysis of the numerical scheme is based on one spatial and one temporal scale. Hence, it should result in a first order pressure term that is spatially constant.
We can repeat the proof of Theorem 6 using the asymptotic balance equations for the momentum and energy equations. This is redundant to proof the existence of pressure waves on a length scale independent of M since the evidence that one relation causes these fluctuations is sufficient. However, in the next step we want to show that these pressure waves are not caused with the altered MAPS+ scheme, hence we need to detect all mechanisms that result in these fluctuations.
Now, we analyze the momentum flux functions with $\mathcal{H}^{\rho v_\zeta}_{MAPS+}\left(\widetilde{\boldsymbol{u}}_i, \widetilde{\boldsymbol{u}}_j; \boldsymbol{n}\right)$ given in equation (4.26) in more detail. To arrive at the final form, we expand the equation into a Taylor series. We get the momentum balance as shown in equation (A.22) as

$$
\begin{aligned}
\frac{d}{dt}\left(\rho v_\zeta\right)_i = & \sum_{j\in\mathcal{N}(i)}\sum_{k=1}^{2}\left(\frac{p_i^{(0)}+p_j^{(0)}}{2}\right)n_{ij,\zeta}^k|l_{ij}^k| \\
& +M\sum_{j\in\mathcal{N}(i)}\sum_{k=1}^{2}\Bigg(\frac{p_i^{(1)}+p_j^{(1)}}{2}n_{ij,\zeta}^k+\frac{(v_\zeta)_i^{(0)}+(v_\zeta)_j^{(0)}}{4c_{\max,ij}^{(0)}}\triangle_{ij}p^{(0)} \\
& \qquad\qquad +\frac{\rho_i^{(0)}+\rho_j^{(0)}}{4}c_{\min,ij}^{(0)}\triangle_{ij}q^{(0)}n_{ij,\zeta}^k\Bigg)|l_{ij}^k| \\
& +M^2\sum_{j\in\mathcal{N}(i)}\sum_{k=1}^{2}\Bigg(\frac{p_i^{(2)}+p_j^{(2)}}{2}n_{ij,\zeta}^k+\frac{(v_\zeta)_i^{(0)}+(v_\zeta)_j^{(0)}}{4c_{\max,ij}^{(0)}}\triangle_{ij}p^{(1)} \\
& \qquad +\frac{(v_\zeta)_i^{(1)}+(v_\zeta)_j^{(1)}}{4c_{\max,ij}^{(0)}}\triangle_{ij}p^{(0)}+\frac{(v_\zeta)_i^{(0)}+(v_\zeta)_j^{(0)}}{4\left(c_{\max,ij}^{(0)}\right)^2}c_{\max,ij}^{(1)}\triangle_{ij}p^{(0)} \\
& \qquad +\frac{\rho_i^{(1)}+\rho_j^{(1)}}{4}c_{\min,ij}^{(0)}\triangle_{ij}q^{(0)}n_{ij,\zeta}^k \\
& \qquad +\frac{\rho_i^{(0)}+\rho_j^{(0)}}{4}c_{\min,ij}^{(1)}\triangle_{ij}q^{(0)}n_{ij,\zeta}^k \\
& \qquad +\frac{\rho_i^{(0)}+\rho_j^{(0)}}{4}c_{\min,ij}^{(0)}\triangle_{ij}q^{(1)}n_{ij,\zeta}^k \\
& \qquad -\frac{|q^{(0)}|_{\max,ij}}{2c_{\min,ij}^{(0)}}\frac{(v_\zeta)_i^{(0)}+(v_\zeta)_j^{(0)}}{c_i^{(0)}+c_j^{(0)}}\triangle_{ij}p^{(0)} \\
& \qquad -\frac{|q^{(0)}|_{\max,ij}c_{\max,ij}^{(0)}}{2}\frac{\rho_i^{(0)}+\rho_j^{(0)}}{c_i^{(0)}+c_j^{(0)}}\triangle_{ij}q^{(0)}n_{ij,\zeta}^k \\
& \qquad +\frac{|q^{(0)}|_{\max,ij}}{2}\triangle_{ij}\left(\rho v_\zeta\right)^{(0)} \\
& \qquad +\frac{q_i^{(0)}+q_j^{(0)}}{4}\left[(\rho v_\zeta)_i^{(0)}+(\rho v_\zeta)_j^{(0)}\right]\Bigg)|l_{ij}^k| \\
& +\mathcal{O}(M^3) \text{ for } \zeta=1,2.
\end{aligned}
$$

Again, we consider the special case of a structured, equidistant, Cartesian grid $\mathcal{S}_h$. The leading order pressure is constant in the vicinity of control volume σ_i, see Theorem 5.

Hence, we can simplify the momentum balance to

$$
\begin{aligned}
\frac{d}{dt}\left(\rho v_\zeta\right)_i = & \sum_{j\in(l,k)} p^{(0)} n_{ij,\zeta} \\
& + M \sum_{j\in(l,k)} \left(\frac{p_i^{(1)} + p_j^{(1)}}{2} + \frac{\rho_i^{(0)} + \rho_j^{(0)}}{4} c_{\min,ij}^{(0)} \triangle_{ij} q^{(0)} \right) n_{ij,\zeta} \\
& + M^2 \sum_{j\in(l,k)} \Bigg(\frac{p_i^{(2)} + p_j^{(2)}}{2} n_{ij,\zeta} + \frac{(v_\zeta)_i^{(0)} + (v_\zeta)_j^{(0)}}{4 c_{\max,ij}^{(0)}} \triangle_{ij} p^{(1)} \\
& \qquad + \frac{\rho_i^{(1)} + \rho_j^{(1)}}{4} c_{\min,ij}^{(0)} \triangle_{ij} q^{(0)} n_{ij,\zeta} \\
& \qquad + \frac{\rho_i^{(0)} + \rho_j^{(0)}}{4} c_{\min,ij}^{(1)} \triangle_{ij} q^{(0)} n_{ij,\zeta} \\
& \qquad + \frac{\rho_i^{(0)} + \rho_j^{(0)}}{4} c_{\min,ij}^{(0)} \triangle_{ij} q^{(1)} n_{ij,\zeta} \\
& \qquad - \frac{|q^{(0)}|_{\max,ij} c_{\max,ij}^{(0)}}{2} \frac{\rho_i^{(0)} + \rho_j^{(0)}}{c_i^{(0)} + c_j^{(0)}} \triangle_{ij} q^{(0)} n_{ij,\zeta} \\
& \qquad + \frac{|q^{(0)}|_{\max,ij}}{2} \triangle_{ij} \left(\rho v_\zeta\right)^{(0)} \\
& \qquad + \frac{q_i^{(0)} + q_j^{(0)}}{4} \left[(\rho v_\zeta)_i^{(0)} + (\rho v_\zeta)_j^{(0)} \right] \Bigg) \\
& + \mathcal{O}(M^3) \text{ for } \zeta = 1, 2.
\end{aligned}
$$

We can rewrite the momentum balance of $\mathcal{O}(M^2)$ as

$$\begin{aligned}
&\left(p_i^{(1)} - p_l^{(1)}\right) \frac{(v_\zeta)_i^{(0)} + (v_\zeta)_l^{(0)}}{4c_{\max,il}^{(0)}} + \left(p_i^{(1)} - p_k^{(1)}\right) \frac{(v_\zeta)_i^{(0)} + (v_\zeta)_k^{(0)}}{4c_{\max,ik}^{(0)}} = \\
&\quad - \frac{p_i^{(2)} + p_l^{(2)}}{2} + \frac{p_i^{(2)} + p_k^{(2)}}{2} - \frac{\rho_i^{(1)} + \rho_l^{(1)}}{4} c_{\min,il}^{(0)} \left(q_i^{(0)} - q_l^{(0)}\right) \\
&\quad + \frac{\rho_i^{(1)} + \rho_k^{(1)}}{4} c_{\min,ik}^{(0)} \left(q_i^{(0)} - q_k^{(0)}\right) - \frac{\rho_i^{(0)} + \rho_l^{(0)}}{4} c_{\min,il}^{(1)} \left(q_i^{(0)} - q_l^{(0)}\right) \\
&\quad + \frac{\rho_i^{(0)} + \rho_k^{(0)}}{4} c_{\min,ik}^{(1)} \left(q_i^{(0)} - q_k^{(0)}\right) - \frac{\rho_i^{(0)} + \rho_l^{(0)}}{4} c_{\min,il}^{(0)} \left(q_i^{(1)} - q_l^{(1)}\right) \\
&\quad + \frac{\rho_i^{(0)} + \rho_k^{(0)}}{4} c_{\min,ik}^{(0)} \left(q_i^{(1)} - q_k^{(1)}\right) \\
&\quad + \frac{|q^{(0)}|_{\max,il} c_{\max,il}^{(0)}}{2} \frac{\rho_i^{(0)} + \rho_l^{(0)}}{c_i^{(0)} + c_l^{(0)}} \left(q_i^{(0)} - q_l^{(0)}\right) \\
&\quad - \frac{|q^{(0)}|_{\max,ik} c_{\max,ik}^{(0)}}{2} \frac{\rho_i^{(0)} + \rho_k^{(0)}}{c_i^{(0)} + c_k^{(0)}} \left(q_i^{(0)} - q_k^{(0)}\right) \\
&\quad - \frac{|q^{(0)}|_{\max,il}}{2} \left[(\rho v_\zeta)_i^{(0)} - (\rho v_\zeta)_l^{(0)}\right] - \frac{|q^{(0)}|_{\max,ik}}{2} \left[(\rho v_\zeta)_i^{(0)} - (\rho v_\zeta)_k^{(0)}\right] \\
&\quad - \frac{q_i^{(0)} + q_l^{(0)}}{4} \left[(\rho v_\zeta)_i^{(0)} + (\rho v_\zeta)_l^{(0)}\right] - \frac{q_i^{(0)} + q_k^{(0)}}{4} \left[(\rho v_\zeta)_i^{(0)} + (\rho v_\zeta)_k^{(0)}\right]
\end{aligned}$$

for $\zeta = 1, 2$.

Using condition (4.31),we can simplify this equation to

$$\begin{aligned}
\left(p_i^{(1)}-p_l^{(1)}\right)\frac{(v_\zeta)_i^{(0)}+(v_\zeta)_l^{(0)}}{4c_{\max,il}^{(0)}}+\left(p_i^{(1)}-p_k^{(1)}\right)\frac{(v_\zeta)_i^{(0)}+(v_\zeta)_k^{(0)}}{4c_{\max,ik}^{(0)}}= \\
-\frac{p_i^{(2)}+p_l^{(2)}}{2}+\frac{p_i^{(2)}+p_k^{(2)}}{2}-\frac{\rho^{(1)}}{2}c_{\min,il}^{(0)}\left(q_i^{(0)}-q_l^{(0)}\right) \\
+\frac{\rho^{(1)}}{2}c_{\min,ik}^{(0)}\left(q_i^{(0)}-q_k^{(0)}\right)-\frac{\rho^{(0)}}{2}c_{\min,il}^{(1)}\left(q_i^{(0)}-q_l^{(0)}\right) \\
+\frac{\rho^{(0)}}{2}c_{\min,ik}^{(1)}\left(q_i^{(0)}-q_k^{(0)}\right)-\frac{\rho^{(0)}}{2}c_{\min,il}^{(0)}\left(q_i^{(1)}-q_l^{(1)}\right) \\
+\frac{\rho^{(0)}}{2}c_{\min,ik}^{(0)}\left(q_i^{(1)}-q_k^{(1)}\right)+\frac{|q^{(0)}|_{\max,il}c_{\max,il}^{(0)}\rho^{(0)}}{c_i^{(0)}+c_l^{(0)}}\left(q_i^{(0)}-q_l^{(0)}\right) \\
-\frac{|q^{(0)}|_{\max,ik}c_{\max,ik}^{(0)}\rho^{(0)}}{c_i^{(0)}+c_k^{(0)}}\left(q_i^{(0)}-q_k^{(0)}\right)-\frac{|q^{(0)}|_{\max,il}}{2}\left[(\rho v_\zeta)_i^{(0)}-(\rho v_\zeta)_l^{(0)}\right] \\
-\frac{|q^{(0)}|_{\max,ik}}{2}\left[(\rho v_\zeta)_i^{(0)}-(\rho v_\zeta)_k^{(0)}\right]-\frac{q_i^{(0)}+q_l^{(0)}}{4}\left[(\rho v_\zeta)_i^{(0)}+(\rho v_\zeta)_l^{(0)}\right] \\
-\frac{q_i^{(0)}+q_k^{(0)}}{4}\left[(\rho v_\zeta)_i^{(0)}+(\rho v_\zeta)_k^{(0)}\right]
\end{aligned}$$

for $\zeta=1,2$.

(4.33)

Without further simplification, this relation shows that the first order pressure distribution cannot be always spatially constant for arbitrary velocity and momentum fields.

Finally, we look at the function $\mathcal{H}^{\rho h}_{MAPS+}\left(\widetilde{\boldsymbol{u}}_i, \widetilde{\boldsymbol{u}}_j; \boldsymbol{n}\right)$ in equation (4.27). We get

$$\begin{aligned}
\frac{d}{dt}\left(\rho h\right)_i = & \sum_{j\in\mathcal{N}(i)}\sum_{k=1}^{2}\left(\frac{h_i^{(0)}+h_j^{(0)}}{4c^{(0)}_{\max,ij}}\triangle_{ij}p^{(0)}\right)|l_{ij}^k| \\
& +M\sum_{j\in\mathcal{N}(i)}\sum_{k=1}^{2}\Bigg(\frac{h_i^{(0)}+h_j^{(0)}}{4c^{(0)}_{\max,ij}}\triangle_{ij}p^{(1)}+\frac{h_i^{(1)}+h_j^{(1)}}{4c^{(0)}_{\max,ij}}\triangle_{ij}p^{(0)} \\
& \qquad -\frac{\left(h_i^{(0)}+h_j^{(0)}\right)c^{(1)}_{\max,ij}}{4\left(c^{(0)}_{\max,ij}\right)^2}\triangle_{ij}p^{(1)} \\
& \qquad -\frac{|q|^{(0)}_{\max,ij}}{2c^{(0)}_{\min,ij}}\frac{h_i^{(0)}+h_j^{(0)}}{c_i^{(0)}+c_j^{(0)}}\triangle_{ij}p^{(0)} \\
& \qquad +\frac{|q|^{(0)}_{\max,ij}}{2}\triangle_{ij}\left(\rho h\right)^{(0)} \\
& \qquad +\frac{q_i^{(0)}+q_j^{(0)}}{4}\left[(\rho h)_i^{(0)}+(\rho h)_j^{(0)}\right]\Bigg)|l_{ij}^k| \\
& +\mathcal{O}(M^2).
\end{aligned}$$

With the leading order pressure being constant in the vicinity of control volume σ_i, see Theorem 5, and the structured, equidistant, Cartesian grid $\mathcal{S}_h$, we can simplify this equation to

$$\begin{aligned}
\frac{d}{dt}\left(\rho h\right)_i = M\sum_{j\in(l,k)}\Bigg(&\frac{h_i^{(0)}+h_j^{(0)}}{4c^{(0)}_{\max,ij}}\triangle_{ij}p^{(1)}-\frac{\left(h_i^{(0)}+h_j^{(0)}\right)c^{(1)}_{\max,ij}}{4\left(c^{(0)}_{\max,ij}\right)^2}\triangle_{ij}p^{(1)} \\
&+\frac{|q|^{(0)}_{\max,ij}}{2}\triangle_{ij}\left(\rho h\right)^{(0)} \\
&+\frac{q_i^{(0)}+q_j^{(0)}}{4}\left[(\rho h)_i^{(0)}+(\rho h)_j^{(0)}\right]\Bigg)+\mathcal{O}(M^2).
\end{aligned}$$

We arrive at the following equation of order $\mathcal{O}(M)$ for the stationary case:

$$\begin{aligned}\left(p_i^{(1)}-p_l^{(1)}\right)\frac{h_i^{(0)}+h_l^{(0)}}{2c_{\max,il}^{(0)}}+\left(p_i^{(1)}-p_k^{(1)}\right)\frac{h_i^{(0)}+h_k^{(0)}}{2c_{\max,ik}^{(0)}}-\left(p_i^{(1)}-p_l^{(1)}\right)\frac{\left(h_i^{(0)}+h_l^{(0)}\right)c_{\max,il}^{(1)}}{4\left(c_{\max,il}^{(0)}\right)^2}\\ -\left(p_i^{(1)}-p_k^{(1)}\right)\frac{\left(h_i^{(0)}+h_k^{(0)}\right)c_{\max,ik}^{(1)}}{4\left(c_{\max,ik}^{(0)}\right)^2}=-\frac{|q|_{\max,il}^{(0)}}{2}\left[(\rho h)_i^{(0)}-(\rho h)_l^{(0)}\right]\\ -\frac{|q|_{\max,jk}^{(0)}}{2}\left[(\rho h)_i^{(0)}-(\rho h)_k^{(0)}\right]\\ -\frac{q_i^{(0)}+q_l^{(0)}}{4}\left[(\rho h)_i^{(0)}+(\rho h)_l^{(0)}\right]\\ -\frac{q_i^{(0)}+q_k^{(0)}}{4}\left[(\rho h)_i^{(0)}+(\rho h)_k^{(0)}\right]\end{aligned} \tag{4.34}$$

If we extend condition (4.31) of a constant density field to a constant enthalpy-density field

$$(\rho h)_i^{(0)}=(\rho h)_j^{(0)}\ \text{ for all } j\in N(i),$$

we can simplify equation (4.34) to

$$\begin{aligned}\left(p_i^{(1)}-p_l^{(1)}\right)\frac{h_i^{(0)}+h_l^{(0)}}{2c_{\max,il}^{(0)}}\left(1-\frac{c_{\max,il}^{(1)}}{2c_{\max,il}^{(0)}}\right)+\left(p_i^{(1)}-p_k^{(1)}\right)\frac{h_i^{(0)}+h_k^{(0)}}{2c_{\max,ik}^{(0)}}\left(1-\frac{c_{\max,ik}^{(1)}}{2c_{\max,ik}^{(0)}}\right)\\ =\frac{(\rho h)^{(0)}}{2}\left(-2q_i^{(0)}-q_l^{(0)}-q_k^{(0)}\right).\end{aligned} \tag{4.35}$$

For an arbitrary velocity field and without special requirements on the first and second order speed of sound this relation also leads to a first order pressure term $p^{(1)}$ that cannot be spatially constant.

Now, we repeat this analysis for the altered MAPS+ scheme.

4.2.4.3. Altered MAPS+ scheme

In the case of the altered MAPS+ scheme, we need to consider the reference velocity $\widetilde{q}_{\mathrm{ref},ij}^2$. For a small Mach number, it becomes

$$\begin{aligned}\widetilde{q}_{\mathrm{ref},ij}^2&=\min\left[\max\left(|\widetilde{q}|^2,M^2K_c^2\widetilde{c}_{\max,ij}^2\right),\widetilde{c}_{\max,ij}^2\right]\\ &=\min\left[\max\left(M^2|q|^2,M^2c_{\max,ij}^2\right),c_{\max,ij}^2\right].\end{aligned}$$

For $M \to 0$ we can simplify this expression to

$$\widetilde{q}^2_{\mathrm{ref},ij} = M^2 \max\left(|q|^2, c^2_{\mathrm{max},ij}\right) = M^2 q^2_{\mathrm{ref},ij}.$$

Hence, we use the dimensionless quantity $q^2_{\mathrm{ref},ij}$ to refer to the maximum of $|q|^2$ and $c^2_{\mathrm{max},ij}$.
With this, we can write the remaining modified terms as

$$\begin{aligned}
\widetilde{c}_{\mathrm{max,mod}} &= \sqrt{\widetilde{q}^2_{\mathrm{max},ij}\left[\frac{1}{2}\left(1 - \frac{\widetilde{q}^2_{\mathrm{ref},ij}}{\widetilde{c}^2_{\mathrm{max},ij}}\right)\right]^2 + \widetilde{q}^2_{\mathrm{ref},ij}} \\
&= \sqrt{\left(M\frac{2|q|_{\mathrm{max},ij}c_{\mathrm{max},ij}}{c_i + c_j}\right)^2\left[\frac{1}{2}\left(1 - M^2\frac{q^2_{\mathrm{ref},ij}}{c^2_{\mathrm{max},ij}}\right)\right]^2 + M^2 q^2_{\mathrm{ref},ij}} \\
&= M\sqrt{\left(\frac{4|q|^2_{\mathrm{max},ij}c^2_{\mathrm{max},ij}}{(c_i + c_j)^2}\right)\left(\frac{c^4_{\mathrm{max},ij} - 2M^2 c^2_{\mathrm{max},ij}q^2_{\mathrm{ref},ij} + M^4 q^4_{\mathrm{ref},ij}}{4 \cdot c^4_{\mathrm{max},ij}}\right) + q^2_{\mathrm{ref},ij}} \\
&= M\sqrt{\frac{|q|^2_{\mathrm{max},ij}\left(M^2 q^2_{\mathrm{ref},ij} - c^2_{\mathrm{max},ij}\right)^2}{c^2_{\mathrm{max},ij}(c_i + c_j)^2} + q^2_{\mathrm{ref},ij}},
\end{aligned}$$

$$\widetilde{c}_{\mathrm{min,mod}} = \widetilde{c}_{\mathrm{max,mod}}$$

and

$$\begin{aligned}
\widetilde{q}_{\mathrm{max,mod}} &= \widetilde{q}_{\mathrm{max},ij}\left[1 - \frac{1}{2}\left(1 - \frac{\widetilde{q}^2_{\mathrm{ref},ij}}{\widetilde{c}^2_{\mathrm{max},ij}}\right)\right] \\
&= M\frac{2|q|_{\mathrm{max},ij}c_{\mathrm{max},ij}}{c_i + c_j}\left[1 - \frac{1}{2}\left(1 - M^2\frac{q^2_{\mathrm{ref},ij}}{c^2_{\mathrm{max},ij}}\right)\right] \\
&= M\frac{2|q|_{\mathrm{max},ij}c_{\mathrm{max},ij}}{c_i + c_j} - M\frac{|q|_{\mathrm{max},ij}c_{\mathrm{max},ij}}{c_i + c_j}\left(1 - M^2\frac{q^2_{\mathrm{ref},ij}}{c^2_{\mathrm{max},ij}}\right) \\
&= M\frac{2|q|_{\mathrm{max},ij}c_{\mathrm{max},ij}}{c_i + c_j} - M\frac{|q|_{\mathrm{max},ij}c_{\mathrm{max},ij}}{c_i + c_j} + M^3\frac{q^2_{\mathrm{ref},ij}}{c_{\mathrm{max},ij}}\frac{|q|_{\mathrm{max},ij}}{c_i + c_j} \\
&= M\frac{|q|_{\mathrm{max},ij}c_{\mathrm{max},ij}}{c_i + c_j} + M^3\frac{q^2_{\mathrm{ref},ij}}{c_{\mathrm{max},ij}}\frac{|q|_{\mathrm{max},ij}}{c_i + c_j}.
\end{aligned}$$

The modified terms are also used to calculate the Mach number $\widetilde{Ma}_0$. Hence, we get

$$\begin{aligned}\widetilde{Ma}_0 = \min\left(\frac{\widetilde{q}_{\max,\mathrm{mod}}}{\widetilde{c}_{\min,\mathrm{mod}}}, 1\right) &= \min\left(\frac{M\frac{|q|_{\max,ij}c_{\max,ij}}{c_i+c_j} + M^3\frac{q_{\mathrm{ref},ij}^2}{c_{\max,ij}}\frac{|q|_{\max,ij}}{c_i+c_j}}{M\sqrt{\frac{|q|_{\max,ij}^2\left(M^2q_{\mathrm{ref},ij}^2-c_{\max,ij}^2\right)^2}{c_{\max,ij}^2(c_i+c_j)^2}+q_{\mathrm{ref},ij}^2}}, 1\right) \\ &= \min\left(\frac{\frac{|q|_{\max,ij}c_{\max,ij}}{c_i+c_j} + M^2\frac{q_{\mathrm{ref},ij}^2}{c_{\max,ij}}\frac{|q|_{\max,ij}}{c_i+c_j}}{\sqrt{\frac{|q|_{\max,ij}^2\left(M^2q_{\mathrm{ref},ij}^2-c_{\max,ij}^2\right)^2}{c_{\max,ij}^2(c_i+c_j)^2}+q_{\mathrm{ref},ij}^2}}, 1\right).\end{aligned} \tag{4.36}$$

To be able to use this Mach number for the asymptotic analysis, we expand the first term of the minimum condition as a Taylor series, see equation (A.32) in appendix A.4. This results in

$$\begin{aligned}\widetilde{Ma}_0 = \min\Bigg(\Bigg[&\frac{c_{\max,ij}|q|_{\max,ij}}{\sqrt{c_{\max,ij}^2|q|_{\max,ij}^2+q_{\mathrm{ref},ij}^2\left(c_i+c_j\right)^2}} \\ &+ M^2\frac{|q|_{\max,ij}q_{\mathrm{ref},ij}^2\left(2c_{\max,ij}^2|q|_{\max,ij}^2+q_{\mathrm{ref},ij}^2\left(c_i+c_j\right)^2\right)}{c_{\max,ij}\left(c_{\max,ij}^2|q|_{\max,ij}^2+q_{\mathrm{ref},ij}^2\left(c_i+c_j\right)^2\right)^{\frac{3}{2}}}+\mathcal{O}(M^4)\Bigg], 1\Bigg).\end{aligned}$$

If we look at the first term, we can see that it is smaller than one. Hence, for $M \to 0$ we can simplify this expression to

$$\begin{aligned}\widetilde{Ma}_0 = &\frac{c_{\max,ij}|q|_{\max,ij}}{\sqrt{c_{\max,ij}^2|q|_{\max,ij}^2+q_{\mathrm{ref},ij}^2\left(c_i+c_j\right)^2}} \\ &+M^2\frac{|q|_{\max,ij}q_{\mathrm{ref},ij}^2\left(2c_{\max,ij}^2|q|_{\max,ij}^2+q_{\mathrm{ref},ij}^2\left(c_i+c_j\right)^2\right)}{c_{\max,ij}\left(c_{\max,ij}^2|q|_{\max,ij}^2+q_{\mathrm{ref},ij}^2\left(c_i+c_j\right)^2\right)^{\frac{3}{2}}}+\mathcal{O}(M^4).\end{aligned}$$

The pressure scaling using the modified expressions is defined as

$$\widetilde{p}_{\mathrm{scal}} = \frac{\max\left(1-\widetilde{Ma}_0, 0\right)}{2\widetilde{c}_{\max,\mathrm{mod}}}\cdot\frac{\widetilde{p}_j-\widetilde{p}_i}{2}.$$

Since the Mach number $\widetilde{Ma}_0$ is smaller than one as $M \to 0$, we can simplify this to

$$\begin{aligned}
\widetilde{p}_{\text{scal}} &= \frac{1 - \widetilde{Ma}_0}{2\widetilde{c}_{\text{max,mod}}} \cdot \frac{\widetilde{p}_j - \widetilde{p}_i}{2} \\
&= \frac{1}{2M} \frac{1}{\sqrt{\frac{|q|^2_{\text{max},ij}\left(M^2 q^2_{\text{ref},ij} - c^2_{\text{max},ij}\right)^2}{c^2_{\text{max},ij}(c_i+c_j)^2} + q^2_{\text{ref},ij}}} \\
&\quad \cdot \left(1 - \frac{c_{\text{max},ij}|q|_{\text{max},ij}}{\sqrt{c^2_{\text{max},ij}|q|^2_{\text{max},ij} + q^2_{\text{ref},ij}\left(c_i + c_j\right)^2}} \right. \\
&\qquad \left. -M^2 \frac{|q|_{\text{max},ij} q^2_{\text{ref},ij}\left(2c^2_{\text{max},ij}|q|^2_{\text{max},ij} + q^2_{\text{ref},ij}\left(c_i + c_j\right)^2\right)}{c_{\text{max},ij}\left(c^2_{\text{max},ij}|q|^2_{\text{max},ij} + q^2_{\text{ref},ij}\left(c_i + c_j\right)^2\right)^{\frac{3}{2}}} + \mathcal{O}(M^4) \right) \cdot \frac{p_j - p_i}{2}.
\end{aligned} \tag{4.37}$$

For the asymptotic analysis, we expand the second factor into a Taylor series, see equation (A.33) in appendix A.4. This leads to

$$\begin{aligned}
&\widetilde{p}_{\text{scal}} \\
&= \frac{1}{2M} \left(\frac{c_i + c_j}{\sqrt{c^2_{\text{max},ij}|q|^2_{\text{max},ij} + q^2_{\text{ref},ij}\left(c_i + c_j\right)^2}} \right. \\
&\qquad \left. + M^2 \frac{|q|^2_{\text{max},ij} q^2_{\text{ref},ij}\left(c_i + c_j\right)}{\left(c^2_{\text{max},ij}|q|^2_{\text{max},ij} + q^2_{\text{ref},ij}\left(c_i + c_j\right)^2\right)^{\frac{3}{2}}} + \mathcal{O}(M^4) \right) \\
&\quad \cdot \left(1 - \frac{c_{\text{max},ij}|q|_{\text{max},ij}}{\sqrt{c^2_{\text{max},ij}|q|^2_{\text{max},ij} + q^2_{\text{ref},ij}\left(c_i + c_j\right)^2}} \right. \\
&\qquad \left. -M^2 \frac{|q|_{\text{max},ij} q^2_{\text{ref},ij}\left(2c^2_{\text{max},ij}|q|^2_{\text{max},ij} + q^2_{\text{ref},ij}\left(c_i + c_j\right)^2\right)}{c_{\text{max},ij}\left(c^2_{\text{max},ij}|q|^2_{\text{max},ij} + q^2_{\text{ref},ij}\left(c_i + c_j\right)^2\right)^{\frac{3}{2}}} + \mathcal{O}(M^4) \right) \cdot \frac{p_j - p_i}{2}
\end{aligned}$$

We can simplify this to

$$
\begin{aligned}
&\widetilde{p}_{\mathrm{scal}} \\
&= \frac{1}{4M}\left(\frac{c_i + c_j}{\sqrt{c_{\mathrm{max},ij}^2 |q|_{\mathrm{max},ij}^2 + q_{\mathrm{ref},ij}^2 (c_i + c_j)^2}}\right. \\
&\quad \left. - \frac{c_{\mathrm{max},ij} |q|_{\mathrm{max},ij} (c_i + c_j)}{c_{\mathrm{max},ij}^2 |q|_{\mathrm{max},ij}^2 + q_{\mathrm{ref},ij}^2 (c_i + c_j)^2}\right)(p_j - p_i) \\
&\quad + \frac{M}{4}\left(\frac{|q|_{\mathrm{max},ij}^2 q_{\mathrm{ref},ij}^2 (c_i + c_j)}{\left(c_{\mathrm{max},ij}^2 |q|_{\mathrm{max},ij}^2 + q_{\mathrm{ref},ij}^2 (c_i + c_j)^2\right)^{\frac{3}{2}}} + \frac{c_{\mathrm{max},ij} |q|_{\mathrm{max},ij}^3 q_{\mathrm{ref},ij}^2 (c_i + c_j)}{\left(c_{\mathrm{max},ij}^2 |q|_{\mathrm{max},ij}^2 + q_{\mathrm{ref},ij}^2 (c_i + c_j)^2\right)^2}\right. \\
&\qquad \left. - \frac{|q|_{\mathrm{max},ij} q_{\mathrm{ref},ij}^2 \left(2c_{\mathrm{max},ij}^2 |q|_{\mathrm{max},ij}^2 + q_{\mathrm{ref},ij}^2 (c_i + c_j)^2\right)(c_i + c_j)}{c_{\mathrm{max},ij}\left(c_{\mathrm{max},ij}^2 |q|_{\mathrm{max},ij}^2 + q_{\mathrm{ref},ij}^2 (c_i + c_j)^2\right)^2}\right)(p_j - p_i) \\
&\quad + \mathcal{O}(M^3).
\end{aligned}
$$

The velocity scaling can be written as

$$
\widetilde{q}_{\mathrm{scal}} = \frac{\widetilde{\rho}_i + \widetilde{\rho}_j}{4} \cdot \max\left(1 - \widetilde{Ma}_0, 0\right) \cdot \widetilde{c}_{\mathrm{min,mod}} \left(\widetilde{q}_j - \widetilde{q}_i\right)
$$

which we can simplify to

$$
\begin{aligned}
\widetilde{q}_{\mathrm{scal}} &= \frac{\widetilde{\rho}_i + \widetilde{\rho}_j}{4}\left(1 - \widetilde{Ma}_0\right) \cdot \widetilde{c}_{\mathrm{min,mod}} \left(\widetilde{q}_j - \widetilde{q}_i\right) \\
&= \frac{\rho_i + \rho_j}{4}\left(1 - \frac{c_{\mathrm{max},ij} |q|_{\mathrm{max},ij}}{\sqrt{c_{\mathrm{max},ij}^2 |q|_{\mathrm{max},ij}^2 + q_{\mathrm{ref},ij}^2 (c_i + c_j)^2}}\right. \\
&\qquad \left. - M^2 \frac{|q|_{\mathrm{max},ij} q_{\mathrm{ref},ij}^2 \left(2c_{\mathrm{max},ij}^2 |q|_{\mathrm{max},ij}^2 + q_{\mathrm{ref},ij}^2 (c_i + c_j)^2\right)}{c_{\mathrm{max},ij}\left(c_{\mathrm{max},ij}^2 |q|_{\mathrm{max},ij}^2 + q_{\mathrm{ref},ij}^2 (c_i + c_j)^2\right)^{\frac{3}{2}}} + \mathcal{O}(M^4)\right) \\
&\qquad \cdot M \sqrt{\frac{|q|_{\mathrm{max},ij}^2 \left(M^2 q_{\mathrm{ref},ij}^2 - c_{\mathrm{max},ij}^2\right)^2}{c_{\mathrm{max},ij}^2 (c_i + c_j)^2} + q_{\mathrm{ref},ij}^2} \cdot M \left(q_j - q_i\right).
\end{aligned}
\tag{4.38}
$$

Here, we expand the last square root into a Taylor series. See equation (A.34) in Appendix A.4 for the detailed derivation. This leads to the following expression, which is suitable for an asymptotic analysis:

$$
\begin{aligned}
\widetilde{q}_{\mathrm{scal}} = \frac{\rho_i+\rho_j}{4}\Bigg(1 &- \frac{c_{\mathrm{max},ij}|q|_{\mathrm{max},ij}}{\sqrt{c_{\mathrm{max},ij}^2|q|_{\mathrm{max},ij}^2 + q_{\mathrm{ref},ij}^2\left(c_i+c_j\right)^2}} \\
&- M^2\frac{|q|_{\mathrm{max},ij}q_{\mathrm{ref},ij}^2\left(2\left(c_{\mathrm{max},ij}|q|_{\mathrm{max},ij}\right)^2 + q_{\mathrm{ref},ij}^2\left(c_i+c_j\right)^2\right)}{c_{\mathrm{max},ij}\left[\left(c_{\mathrm{max},ij}|q|_{\mathrm{max},ij}\right)^2 + q_{\mathrm{ref},ij}^2\left(c_i+c_j\right)^2\right]^{\frac{3}{2}}} + \mathcal{O}(M^4)\Bigg) \\
&\cdot M\Bigg(\sqrt{\frac{c_{\mathrm{max},ij}^2|q|_{\mathrm{max},ij}^2}{\left(c_i+c_j\right)^2} + q_{\mathrm{ref},ij}^2} \\
&- M^2\frac{q_{\mathrm{ref},ij}^2|q|_{\mathrm{max},ij}^2}{\left(c_i+c_j\right)^2\sqrt{\frac{|q|_{\mathrm{max},ij}^2c_{\mathrm{max},ij}^2}{\left(c_i+c_j\right)^2} + q_{\mathrm{ref},ij}^2}} + \mathcal{O}(M^4)\Bigg)\cdot M\left(q_j-q_i\right) \\
= M^2\frac{\rho_i+\rho_j}{4}&\Bigg(\sqrt{\frac{c_{\mathrm{max},ij}^2|q|_{\mathrm{max},ij}^2}{\left(c_i+c_j\right)^2} + q_{\mathrm{ref},ij}^2} \\
&- \frac{c_{\mathrm{max},ij}|q|_{\mathrm{max},ij}\sqrt{c_{\mathrm{max},ij}^2|q|_{\mathrm{max},ij}^2 + q_{\mathrm{ref},ij}^2\left(c_i+c_j\right)^2}}{\sqrt{c_{\mathrm{max},ij}^2|q|_{\mathrm{max},ij}^2 + q_{\mathrm{ref},ij}^2\left(c_i+c_j\right)^2}\left(c_i+c_j\right)}\Bigg)\left(q_j-q_i\right) \\
-M^4\frac{\rho_i+\rho_j}{4}&\Bigg(\frac{|q|_{\mathrm{max},ij}q_{\mathrm{ref},ij}^2\left(2\left(c_{\mathrm{max},ij}|q|_{\mathrm{max},ij}\right)^2 + q_{\mathrm{ref},ij}^2\left(c_i+c_j\right)^2\right)}{c_{\mathrm{max},ij}\left[\left(c_{\mathrm{max},ij}|q|_{\mathrm{max},ij}\right)^2 + q_{\mathrm{ref},ij}^2\left(c_i+c_j\right)^2\right]^{\frac{3}{2}}} \\
&\cdot\sqrt{\frac{c_{\mathrm{max},ij}^2|q|_{\mathrm{max},ij}^2}{\left(c_i+c_j\right)^2} + q_{\mathrm{ref},ij}^2} - \frac{q_{\mathrm{ref},ij}^2|q|_{\mathrm{max},ij}^2}{\left(c_i+c_j\right)^2\sqrt{\frac{c_{\mathrm{max},ij}^2|q|_{\mathrm{max},ij}^2}{\left(c_i+c_j\right)^2} + q_{\mathrm{ref},ij}^2}} \\
&+ \frac{c_{\mathrm{max},ij}|q|_{\mathrm{max},ij}}{\sqrt{c_{\mathrm{max},ij}^2|q|_{\mathrm{max},ij}^2 + q_{\mathrm{ref},ij}^2\left(c_i+c_j\right)^2}} \\
&\cdot\frac{q_{\mathrm{ref},ij}^2|q|_{\mathrm{max},ij}^2}{\left(c_i+c_j\right)^2\sqrt{\frac{c_{\mathrm{max},ij}^2|q|_{\mathrm{max},ij}^2}{\left(c_i+c_j\right)^2} + q_{\mathrm{ref},ij}^2}}\Bigg) \\
&+\mathcal{O}(M^6)
\end{aligned}
$$

We can further simplify this equation to get

$$\begin{aligned}\widetilde{q}_{\text{scal}} = M^2 \frac{\rho_i + \rho_j}{4} &\left(\sqrt{\frac{c_{\max,ij}^2 |q|_{\max,ij}^2}{(c_i + c_j)^2} + q_{\text{ref},ij}^2} - \frac{c_{\max,ij}|q|_{\max,ij}}{(c_i + c_j)} \right) (q_j - q_i) \\ -M^4 \frac{\rho_i + \rho_j}{4} &\left(\frac{|q|_{\max,ij} q_{\text{ref},ij}^2 \left[2 \left(c_{\max,ij}|q|_{\max,ij} \right)^2 + q_{\text{ref},ij}^2 \left(c_i + c_j \right)^2 \right]}{c_{\max,ij} \left[\left(c_{\max,ij}|q|_{\max,ij} \right)^2 + q_{\text{ref},ij}^2 \left(c_i + c_j \right)^2 \right] (c_i + c_j)} \right. \\ &\qquad - \frac{q_{\text{ref},ij}^2 |q|_{\max,ij}^2}{(c_i + c_j)^2 \sqrt{\frac{c_{\max,ij}^2 |q|_{\max,ij}^2}{(c_i + c_j)^2} + q_{\text{ref},ij}^2}} \\ &\qquad \left. + \frac{c_{\max,ij} q_{\text{ref},ij}^2 |q|_{\max,ij}^3}{\left(c_{\max,ij}^2 |q|_{\max,ij}^2 + q_{\text{ref},ij}^2 \left(c_i + c_j \right)^2 \right) (c_i + c_j)} \right) + \mathcal{O}(M^6).\end{aligned}$$

As for the general MAPS+ scheme, we combine the intermediate results to arrive at the flux functions. The density flux becomes

$$\begin{aligned}&\mathcal{H}_{MAPS+}^{\rho} \left(\widetilde{\boldsymbol{u}}_i, \widetilde{\boldsymbol{u}}_j; \boldsymbol{n} \right) \\ &= \left(\widetilde{\rho v} \right)_i + \left(\widetilde{\rho v} \right)_j - 2 \widetilde{p}_{\text{scal}} \\ &= M \left(\frac{q_i + q_j}{4} + \frac{|q|_{\max,ij}}{2} \right) \rho_i + M \left(\frac{q_i + q_j}{4} - \frac{|q|_{\max,ij}}{2} \right) \rho_j \\ &\quad - \frac{1}{2M} \left(\frac{c_i + c_j}{\sqrt{c_{\max,ij}^2 |q|_{\max,ij}^2 + q_{\text{ref},ij}^2 \left(c_i + c_j \right)^2}} \right. \\ &\qquad \left. - \frac{c_{\max,ij}|q|_{\max,ij} \left(c_i + c_j \right)}{c_{\max,ij}^2 |q|_{\max,ij}^2 + q_{\text{ref},ij}^2 \left(c_i + c_j \right)^2} \right) (p_j - p_i) \\ &\quad - \frac{M}{2} \left(\frac{|q|_{\max,ij}^2 q_{\text{ref},ij}^2 \left(c_i + c_j \right)}{\left(c_{\max,ij}^2 |q|_{\max,ij}^2 + q_{\text{ref},ij}^2 \left(c_i + c_j \right)^2 \right)^{\frac{3}{2}}} + \frac{c_{\max,ij}|q|_{\max,ij}^3 q_{\text{ref},ij}^2 \left(c_i + c_j \right)}{\left(c_{\max,ij}^2 |q|_{\max,ij}^2 + q_{\text{ref},ij}^2 \left(c_i + c_j \right)^2 \right)^2} \right. \\ &\qquad \left. - \frac{|q|_{\max,ij} q_{\text{ref},ij}^2 \left(2 c_{\max,ij}^2 |q|_{\max,ij}^2 + q_{\text{ref},ij}^2 \left(c_i + c_j \right)^2 \right) \left(c_i + c_j \right)}{c_{\max,ij} \left(c_{\max,ij}^2 |q|_{\max,ij}^2 + q_{\text{ref},ij}^2 \left(c_i + c_j \right)^2 \right)^2} \right) (p_j - p_i) \\ &\quad + \mathcal{O}(M^3).\end{aligned} \tag{4.39}$$

We can simplify this to

$$
\begin{aligned}
&\mathcal{H}^{\rho}_{MAPS+}\left(\widetilde{\boldsymbol{u}}_i, \widetilde{\boldsymbol{u}}_j; \boldsymbol{n}\right) \\
&= \frac{1}{2M}\left(\frac{c_i + c_j}{\sqrt{c^2_{\max,ij}|q|^2_{\max,ij} + q^2_{\mathrm{ref},ij}\left(c_i + c_j\right)^2}} - \frac{c_{\max,ij}|q|_{\max,ij}\left(c_i + c_j\right)}{c^2_{\max,ij}|q|^2_{\max,ij} + q^2_{\mathrm{ref},ij}\left(c_i + c_j\right)^2}\right) \triangle_{ij} p \\
&\quad + \frac{M}{2}\left(\frac{|q|^2_{\max,ij} q^2_{\mathrm{ref},ij}\left(c_i + c_j\right)}{\left(c^2_{\max,ij}|q|^2_{\max,ij} + q^2_{\mathrm{ref},ij}\left(c_i + c_j\right)^2\right)^{\frac{3}{2}}} + \frac{c_{\max,ij}|q|^3_{\max,ij} q^2_{\mathrm{ref},ij}\left(c_i + c_j\right)}{\left(c^2_{\max,ij}|q|^2_{\max,ij} + q^2_{\mathrm{ref},ij}\left(c_i + c_j\right)^2\right)^2}\right. \\
&\qquad \left. - \frac{|q|_{\max,ij} q^2_{\mathrm{ref},ij}\left(2c^2_{\max,ij}|q|^2_{\max,ij} + q^2_{\mathrm{ref},ij}\left(c_i + c_j\right)^2\right)\left(c_i + c_j\right)}{c_{\max,ij}\left(c^2_{\max,ij}|q|^2_{\max,ij} + q^2_{\mathrm{ref},ij}\left(c_i + c_j\right)^2\right)^2}\right) \triangle_{ij} p \\
&\quad + M\frac{|q|_{\max,ij}}{2}\triangle\rho + M\frac{\left(q_i + q_j\right)\left(\rho_i + \rho_j\right)}{4} + \mathcal{O}(M^3).
\end{aligned}
\tag{4.40}
$$

The momentum flux $\mathcal{H}^{\rho v_\zeta}_{MAPS+}\left(\widetilde{\boldsymbol{u}}_i, \widetilde{\boldsymbol{u}}_j; \boldsymbol{n}\right)$ results in

$$
\begin{aligned}
&\mathcal{H}^{\rho v_\zeta}_{MAPS+}\left(\widetilde{\boldsymbol{u}}_i, \widetilde{\boldsymbol{u}}_j; \boldsymbol{n}\right) \\
&= \left(\widetilde{\rho v}\right)_i \left(\widetilde{v}_\zeta\right)_i + \left(\widetilde{\rho v}\right)_j \left(\widetilde{v}_\zeta\right)_j + n_\zeta \widetilde{p}_{12} - \left[\left(\widetilde{v}_\zeta\right)_i + \left(\widetilde{v}_\zeta\right)_j\right] \widetilde{p}_{\mathrm{scal}} - n_\zeta \widetilde{q}_{\mathrm{scal}} \\
&= M \left(\frac{q_i + q_j}{4} + \frac{|q|_{\max,ij}}{2}\right) \rho_i \cdot M \left(v_\zeta\right)_+ M \left(\frac{q_i + q_j}{4} - \frac{|q|_{\max,ij}}{2}\right) \rho_j \cdot M \left(v_\zeta\right)_j \\
&\quad + n_\zeta \frac{p_i + p_j}{2} - M \left[\left(v_\zeta\right)_i + \left(v_\zeta\right)_j\right] \\
&\quad \cdot \Bigg[\frac{1}{4M} \Bigg(\frac{c_i + c_j}{\sqrt{c^2_{\max,ij} |q|^2_{\max,ij} + q^2_{\mathrm{ref},ij} \left(c_i + c_j\right)^2}} \\
&\qquad\qquad - \frac{c_{\max,ij} |q|_{\max,ij} \left(c_i + c_j\right)}{c^2_{\max,ij} |q|^2_{\max,ij} + q^2_{\mathrm{ref},ij} \left(c_i + c_j\right)^2} \Bigg) \left(p_j - p_i\right) \\
&\qquad + \frac{M}{4} \Bigg(\frac{|q|^2_{\max,ij} q^2_{\mathrm{ref},ij} \left(c_i + c_j\right)}{\left(c^2_{\max,ij} |q|^2_{\max,ij} + q^2_{\mathrm{ref},ij} \left(c_i + c_j\right)^2\right)^{\frac{3}{2}}} \\
&\qquad\qquad + \frac{c_{\max,ij} |q|^3_{\max,ij} q^2_{\mathrm{ref},ij} \left(c_i + c_j\right)}{\left(c^2_{\max,ij} |q|^2_{\max,ij} + q^2_{\mathrm{ref},ij} \left(c_i + c_j\right)^2\right)^2} \\
&\qquad\qquad - \frac{|q|_{\max,ij} q^2_{\mathrm{ref},ij} \left(2 c^2_{\max,ij} |q|^2_{\max,ij} + q^2_{\mathrm{ref},ij} \left(c_i + c_j\right)^2\right) \left(c_i + c_j\right)}{c_{\max,ij} \left(c^2_{\max,ij} |q|^2_{\max,ij} + q^2_{\mathrm{ref},ij} \left(c_i + c_j\right)^2\right)^2} \Bigg) \\
&\qquad \cdot \left(p_j - p_i\right) + \mathcal{O}(M^3) \Bigg] \\
&- n_\zeta \Bigg[M^2 \frac{\rho_i + \rho_j}{4} \left(\sqrt{\frac{c^2_{\max,ij} |q|^2_{\max,ij}}{\left(c_i + c_j\right)^2} + q^2_{\mathrm{ref},ij}} - \frac{c_{\max,ij} |q|_{\max,ij}}{\left(c_i + c_j\right)} \right) \left(q_j - q_i\right) \\
&\quad - M^4 \frac{\rho_i + \rho_j}{4} \Bigg(\frac{|q|_{\max,ij} q^2_{\mathrm{ref},ij} \left[2 \left(c_{\max,ij} |q|_{\max,ij}\right)^2 + q^2_{\mathrm{ref},ij} \left(c_i + c_j\right)^2\right]}{c_{\max,ij} \left[\left(c_{\max,ij} |q|_{\max,ij}\right)^2 + q^2_{\mathrm{ref},ij} \left(c_i + c_j\right)^2\right] \left(c_i + c_j\right)} \\
&\qquad\qquad - \frac{q^2_{\mathrm{ref},ij} |q|^2_{\max,ij}}{\left(c_i + c_j\right)^2 \sqrt{\frac{c^2_{\max,ij} |q|^2_{\max,ij}}{\left(c_i + c_j\right)^2} + q^2_{\mathrm{ref},ij}}} \\
&\qquad\qquad + \frac{c_{\max,ij} q^2_{\mathrm{ref},ij} |q|^3_{\max,ij}}{\left(c^2_{\max,ij} |q|^2_{\max,ij} + q^2_{\mathrm{ref},ij} \left(c_i + c_j\right)^2\right) \left(c_i + c_j\right)} \Bigg) \Bigg] \\
&\qquad\qquad + \mathcal{O}(M^6) \text{ for } \zeta = 1, 2.
\end{aligned}
$$

We rearrange this equation to

$$
\begin{aligned}
&\mathcal{H}^{\rho v_\zeta}_{MAPS+}\left(\widetilde{\boldsymbol{u}}_i, \widetilde{\boldsymbol{u}}_j; \boldsymbol{n}\right) \\
&= -n_\zeta \frac{p_i + p_j}{2} + \left(\frac{c_i + c_j}{\sqrt{c^2_{\max,ij}|q|^2_{\max,ij} + q^2_{\mathrm{ref},ij}\left(c_i + c_j\right)^2}} \right. \\
&\qquad \left. - \frac{c_{\max,ij}|q|_{\max,ij}\left(c_i + c_j\right)}{c^2_{\max,ij}|q|^2_{\max,ij} + q^2_{\mathrm{ref},ij}\left(c_i + c_j\right)^2} \right) \frac{\left[\left(v_\zeta\right)_i + \left(v_\zeta\right)_j\right]}{4} \triangle_{ij} p \\
&\quad + \frac{M}{16}\left(\frac{|q|^2_{\max,ij} q^2_{\mathrm{ref},ij}\left(c_i + c_j\right)}{\left(c^2_{\max,ij}|q|^2_{\max,ij} + q^2_{\mathrm{ref},ij}\left(c_i + c_j\right)^2\right)^{\frac{3}{2}}} + \frac{c_{\max,ij}|q|^3_{\max,ij} q^2_{\mathrm{ref},ij}\left(c_i + c_j\right)}{\left(c^2_{\max,ij}|q|^2_{\max,ij} + q^2_{\mathrm{ref},ij}\left(c_i + c_j\right)^2\right)^2} \right. \\
&\qquad \left. - \frac{|q|_{\max,ij} q^2_{\mathrm{ref},ij}\left(2c^2_{\max,ij}|q|^2_{\max,ij} + q^2_{\mathrm{ref},ij}\left(c_i + c_j\right)^2\right)\left(c_i + c_j\right)}{c_{\max,ij}\left(c^2_{\max,ij}|q|^2_{\max,ij} + q^2_{\mathrm{ref},ij}\left(c_i + c_j\right)^2\right)^2} \right) \\
&\qquad \cdot \left[\left(v_\zeta\right)_i + \left(v_\zeta\right)_j\right] \triangle_{ij} p \\
&\quad + n_\zeta M^2 \frac{\rho_i + \rho_j}{4}\left(\sqrt{\frac{c^2_{\max,ij}|q|^2_{\max,ij}}{\left(c_i + c_j\right)^2} + q^2_{\mathrm{ref},ij}} - \frac{c_{\max,ij}|q|_{\max,ij}}{\left(c_i + c_j\right)} \right) \triangle_{ij} q \\
&\quad + M^2 \frac{|q|_{\max,ij}}{2} \triangle_{ij}\left(\rho v_\zeta\right) + M^2 \frac{q_i + q_j}{4}\left[\left(\rho v_\zeta\right)_i + \left(\rho v_\zeta\right)_j\right] + \mathcal{O}(M^3)
\end{aligned}
\tag{4.41}
$$

with $\zeta = 1, 2$.

Finally, we can write the ρh-flux as

$$
\begin{aligned}
&\mathcal{H}^{\rho h}_{MAPS+}\left(\widetilde{\boldsymbol{u}}_i, \widetilde{\boldsymbol{u}}_j; \boldsymbol{n}\right) \\
&= \left(\widetilde{\rho v}\right)_i \cdot \widetilde{h}_i + \left(\widetilde{\rho v}\right)_j \cdot \widetilde{h}_j - \left(\widetilde{h}_i + \widetilde{h}_j\right) \cdot \widetilde{p}_{\mathrm{scal}} \\
&= M \left(\frac{q_i + q_j}{4} + \frac{|q|_{\max,ij}}{2} \right) (\rho h)_i + M \left(\frac{q_i + q_j}{4} - \frac{|q|_{\max,ij}}{2} \right) (\rho h)_j \\
&\quad - \left(h_i + h_j\right) \frac{1}{4M} \left(\frac{c_i + c_j}{\sqrt{c^2_{\max,ij} |q|^2_{\max,ij} + q^2_{\mathrm{ref},ij} \left(c_i + c_j\right)^2}} \right. \\
&\qquad\qquad \left. - \frac{c_{\max,ij} |q|_{\max,ij} \left(c_i + c_j\right)}{c^2_{\max,ij} |q|^2_{\max,ij} + q^2_{\mathrm{ref},ij} \left(c_i + c_j\right)^2} \right) \left(p_j - p_i\right) \\
&\quad + \left(h_i + h_j\right) \frac{M}{4} \left(\frac{|q|^2_{\max,ij} q^2_{\mathrm{ref},ij} \left(c_i + c_j\right)}{\left(c^2_{\max,ij} |q|^2_{\max,ij} + q^2_{\mathrm{ref},ij} \left(c_i + c_j\right)^2 \right)^{\frac{3}{2}}} \right. \\
&\qquad\qquad + \frac{c_{\max,ij} |q|^3_{\max,ij} q^2_{\mathrm{ref},ij} \left(c_i + c_j\right)}{\left(c^2_{\max,ij} |q|^2_{\max,ij} + q^2_{\mathrm{ref},ij} \left(c_i + c_j\right)^2 \right)^2} \\
&\qquad\qquad \left. - \frac{|q|_{\max,ij} q^2_{\mathrm{ref},ij} \left(2c^2_{\max,ij} |q|^2_{\max,ij} + q^2_{\mathrm{ref},ij} \left(c_i + c_j\right)^2 \right)}{c_{\max,ij} \left(c^2_{\max,ij} |q|^2_{\max,ij} + q^2_{\mathrm{ref},ij} \left(c_i + c_j\right)^2 \right)^2} \left(c_i + c_j\right) \right) \\
&\qquad\qquad \cdot \left(p_j - p_i\right) + \mathcal{O}(M^3).
\end{aligned}
$$

We rearrange this equation to

$$
\begin{aligned}
&\mathcal{H}^{\rho h}_{MAPS+}\left(\widetilde{\boldsymbol{u}}_i, \widetilde{\boldsymbol{u}}_j; \boldsymbol{n}\right) \\
&= \frac{1}{M}\frac{h_i + h_j}{4}\left(\frac{c_i + c_j}{\sqrt{c^2_{\max,ij}|q|^2_{\max,ij} + q^2_{\mathrm{ref},ij}\left(c_i + c_j\right)^2}}\right. \\
&\qquad\qquad \left. - \frac{c_{\max,ij}|q|_{\max,ij}\left(c_i + c_j\right)}{c^2_{\max,ij}|q|^2_{\max,ij} + q^2_{\mathrm{ref},ij}\left(c_i + c_j\right)^2}\right) \triangle_{ij} p \\
&\quad - M\frac{(h_i + h_j)}{4}\left(\frac{|q|^2_{\max,ij} q^2_{\mathrm{ref},ij}\left(c_i + c_j\right)}{\left(c^2_{\max,ij}|q|^2_{\max,ij} + q^2_{\mathrm{ref},ij}\left(c_i + c_j\right)^2\right)^{\frac{3}{2}}}\right. \\
&\qquad\qquad + \frac{c_{\max,ij}|q|^3_{\max,ij} q^2_{\mathrm{ref},ij}\left(c_i + c_j\right)}{\left(c^2_{\max,ij}|q|^2_{\max,ij} + q^2_{\mathrm{ref},ij}\left(c_i + c_j\right)^2\right)^2} \\
&\qquad\qquad \left. - \frac{|q|_{\max,ij} q^2_{\mathrm{ref},ij}\left(2c^2_{\max,ij}|q|^2_{\max,ij} + q^2_{\mathrm{ref},ij}\left(c_i + c_j\right)^2\right)}{c_{\max,ij}\left(c^2_{\max,ij}|q|^2_{\max,ij} + q^2_{\mathrm{ref},ij}\left(c_i + c_j\right)^2\right)^2}\left(c_i + c_j\right)\right) \triangle_{ij} p \\
&\quad + M\frac{|q|_{\max,ij}}{2}\triangle_{ij}\left(\rho h\right) + M\frac{q_i + q_j}{4}\left[\left(\rho h\right)_i + \left(\rho h\right)_j\right] + \mathcal{O}(M^3).
\end{aligned}
\tag{4.42}
$$

In the next step, we insert the asymptotic sequence into the equations. To arrive at a final result, we expand each equation into a Taylor series. The mass balance is given by equation (A.27) as

$$
\begin{aligned}
\frac{d}{dt}\rho_i = \frac{1}{M} \sum_{j\in\mathcal{N}(i)} \sum_{k=1}^{2} \Bigg[\frac{1}{2} \Bigg(& \frac{\xi_2}{\sqrt{\xi_1^2 + \left(q_{\text{ref}}^{(0)}\right)^2 \xi_2^2}} - \frac{\xi_1\xi_2}{\xi_1^2 + \left(q_{\text{ref}}^{(0)}\right)^2 \xi_2^2} \Bigg) \triangle_{ij} p^{(0)} \Bigg] |l_{ij}^k| \\
& + \sum_{j\in\mathcal{N}(i)} \sum_{k=1}^{2} \Bigg[\frac{1}{2} \Bigg(\frac{\xi_2}{\sqrt{\xi_1^2 + \left(q_{\text{ref}}^{(0)}\right)^2 \xi_2^2}} - \frac{\xi_1\xi_2}{\xi_1^2 + \left(q_{\text{ref}}^{(0)}\right)^2 \xi_2^2} \Bigg) \triangle_{ij} p^{(1)} \\
& \quad + \frac{1}{2} \Bigg(\frac{\left(c_i^{(1)} + c_j^{(1)}\right)}{\sqrt{\xi_1^2 + \left(q_{\text{ref}}^{(0)}\right)^2 \xi_2^2}} - \frac{\xi_2}{2\left[\xi_1^2 + \left(q_{\text{ref}}^{(0)}\right)^2 \xi_2^2\right]^{\frac{3}{2}}} \\
& \qquad \cdot \Big[2c_{\max,ij}^{(0)} \xi_1 |q^{(1)}|_{\max,ij} + 2c_{\max,ij}^{(1)} |q^{(0)}|_{\max,ij} \xi_1 \\
& \qquad\quad + 2\left(q_{\text{ref}}^{(0)}\right)^2 \xi_2 \left(c_i^{(1)} + c_j^{(1)}\right) + 2q_{\text{ref}}^{(0)} q_{\text{ref}}^{(1)} \xi_2 \Big] \\
& \qquad - \frac{\xi_1 \left(c_i^{(1)} + c_j^{(1)}\right)}{\xi_1^2 + \left(q_{\text{ref}}^{(0)}\right)^2 \xi_2^2} - \frac{c_{\max,ij}^{(0)} |q^{(1)}|_{\max,ij} \xi_2}{\xi_1^2 + \left(q_{\text{ref}}^{(0)}\right)^2 \xi_2^2} \\
& \qquad - \frac{c_{\max,ij}^{(1)} |q^{(0)}|_{\max,ij} \xi_2}{\xi_1^2 + \left(q_{\text{ref}}^{(0)}\right)^2 \xi_2^2} + \frac{\xi_1\xi_2}{\left[\xi_1^2 + \left(q_{\text{ref}}^{(0)}\right)^2 \xi_2^2\right]^2} \\
& \qquad \cdot \Big[2c_{\max,ij}^{(0)} |q^{(1)}|_{\max,ij} \xi_1 + 2c_{\max,ij}^{(1)} |q^{(0)}|_{\max,ij} \xi_1 \\
& \qquad\quad + 2\left(q_{\text{ref}}^{(0)}\right)^2 \xi_2 \left(c_i^{(1)} + c_j^{(1)}\right) + 2q_{\text{ref}}^{(0)} q_{\text{ref}}^{(1)} \xi_2 \Big] \Bigg) \triangle_{ij} p^{(0)} \Bigg] |l_{ij}^k| \\
& + \mathcal{O}(M)
\end{aligned}
\tag{4.43}
$$

with

$$
\xi_1 = c_{\max,ij}^{(0)} |q^{(0)}|_{\max,ij} \tag{4.44}
$$

and

$$
\xi_2 = c_i^{(0)} + c_j^{(0)}. \tag{4.45}
$$

From this equation, it is clear that Theorem 5 is also true for the altered MAPS+ scheme. Next, we deduce the following Theorem from the mass equation of $\mathcal{O}(1)$:

Theorem 7.
If $\mathcal{S}_h$ is a structured discretization of the flow domain $\mathcal{G}$ with $\partial\mathcal{S}_h = \partial\mathcal{S}_{h,w} \cup \partial\mathcal{S}_{h,ff}$, then the following statement holds for the pressure terms evaluated by the altered MAPS+ scheme:

$$p_i^{(1)} = p_j^{(1)} \text{ for all } i, j \in N_h.$$

Proof.
Due to Theorem 5, the leading order pressure is constant everywhere. Considering the discretization $\mathcal{S}_h$, we can simplify the asymptotic mass equation (4.43) to

$$\frac{d}{dt}\rho_i = \sum_{j\in\mathcal{N}(i)} \sum_{k=1}^{2} \left[\frac{1}{2} \left(\frac{\xi_2}{\sqrt{\xi_1^2 + \left(q_{\text{ref}}^{(0)}\right)^2 \xi_2^2}} - \frac{\xi_1\xi_2}{\xi_1^2 + \left(q_{\text{ref}}^{(0)}\right)^2 \xi_2^2} \right) \triangle_{ij} p^{(1)} \right] |l_{ij}^k| + \mathcal{O}(M).$$

We arrive at the following mass equation of order $\mathcal{O}(1)$:

$$\begin{aligned}
&\left(p_i^{(1)} - p_l^{(1)}\right) \left(\frac{c_i^{(0)} + c_l^{(0)}}{2\sqrt{\left(c_{\text{max},il}^{(0)} |q^{(0)}|_{\text{max},il}\right)^2 + \left(q_{\text{ref,il}}^{(0)}\right)^2 \left(c_i^{(0)} + c_l^{(0)}\right)^2}} \right. \\
&\qquad \left. - \frac{c_{\text{max},il}^{(0)} |q^{(0)}|_{\text{max},il} \left(c_i^{(0)} + c_l^{(0)}\right)}{2\left(c_{\text{max},il}^{(0)} |q^{(0)}|_{\text{max},il}\right)^2 + 2\left(q_{\text{ref,il}}^{(0)}\right)^2 \left(c_i^{(0)} + c_l^{(0)}\right)^2} \right) \\
&+ \left(p_i^{(1)} - p_k^{(1)}\right) \left(\frac{c_i^{(0)} + c_k^{(0)}}{2\sqrt{\left(c_{\text{max},ik}^{(0)} |q^{(0)}|_{\text{max},ik}\right)^2 + \left(q_{\text{ref,ik}}^{(0)}\right)^2 \left(c_i^{(0)} + c_k^{(0)}\right)^2}} \right. \\
&\qquad \left. - \frac{c_{\text{max},ik}^{(0)} |q^{(0)}|_{\text{max},ik} \left(c_i^{(0)} + c_k^{(0)}\right)}{2\left(c_{\text{max},ik}^{(0)} |q^{(0)}|_{\text{max},ik}\right)^2 + 2\left(q_{\text{ref,ik}}^{(0)}\right)^2 \left(c_i^{(0)} + c_k^{(0)}\right)^2} \right) = 0
\end{aligned}$$

From this relation, it is obvious that $p^{(1)}$ is spatially constant regardless of the velocity distribution.
However, so far, we only show that fluctuations in $p^{(1)}$ are not caused by the mass balance. But for the general MAPS+ scheme we show that these fluctuations can also originate in

the balances of momentum and enthalpy density, see equations (4.33) and (4.35) on page 71. Hence, in the following we show that both the momentum and the density enthalpy flux functions lead to a spatially constant $p^{(1)}$-field as well.
First, we analyze the functions $\mathcal{H}^{\rho v_\zeta}_{MAPS+}\left(\widetilde{\boldsymbol{u}}_i, \widetilde{\boldsymbol{u}}_j; \boldsymbol{n}\right)$ for $\zeta = 1, 2$ in equation (4.41) in more detail. The result of the expansion into a Taylor series is presented in equation (A.29). Hence, we get the momentum balance

$$
\begin{aligned}
\frac{d}{dt}\left(\rho v_\zeta\right)_i = & \sum_{j\in\mathcal{N}(i)}\sum_{k=1}^{2}\left(-n_\zeta\frac{p_i^{(0)}+p_j^{(0)}}{2}\right)|l_{ij}^k| \\
& + \sum_{j\in\mathcal{N}(i)}\sum_{k=1}^{2}\left[\left(\frac{\xi_2}{\sqrt{\xi_1^2+\xi_3\xi_2^2}}-\frac{\xi_1\xi_2}{\xi_1^2+\xi_3\xi_2^2}\right)\frac{(v_\zeta)_i^{(0)}+(v_\zeta)_j^{(0)}}{4}\triangle_{ij}p^{(0)}\right]|l_{ij}^k| \\
& + M\sum_{j\in\mathcal{N}(i)}\sum_{k=1}^{2}\left[-n_\zeta\frac{p_i^{(1)}+p_j^{(1)}}{2}+\left(\frac{\xi_2}{\sqrt{\xi_1^2+\xi_3\xi_2^2}}-\frac{\xi_1\xi_2}{\xi_1^2+\xi_3\xi_2^2}\right)\right. \\
& \qquad \left.\cdot\frac{(v_\zeta)_i^{(0)}+(v_\zeta)_j^{(0)}}{4}\triangle_{ij}p^{(1)}\right]|l_{ij}^k| \\
& + M\sum_{j\in\mathcal{N}(i)}\sum_{k=1}^{2}\left[\left(\frac{\xi_2}{\sqrt{\xi_1^2+\xi_3\xi_2^2}}-\frac{\xi_1\xi_2}{\xi_1^2+\xi_3\xi_2^2}\right)\frac{(v_\zeta)_i^{(1)}+(v_\zeta)_j^{(1)}}{4}\triangle_{ij}p^{(0)}\right]|l_{ij}^k| \\
& + M\sum_{j\in\mathcal{N}(i)}\sum_{k=1}^{2}\left[\frac{1}{2}\left(\frac{c_i^{(1)}+c_j^{(1)}}{\sqrt{\xi_1^2+\xi_3\xi_2^2}}-\frac{\xi_2}{2\left(\xi_1^2+\xi_3\xi_2^2\right)^{\frac{3}{2}}}\left[2c_{\max,ij}^{(0)}\xi_1|q^{(1)}|_{\max,ij}\right.\right.\right. \\
& \qquad \left.+2c_{\max,ij}^{(1)}|q^{(0)}|_{\max,ij}\xi_1+2\xi_3\xi_2\left(c_i^{(1)}+c_j^{(1)}\right)+2\sqrt{\xi_3}q_{\mathrm{ref}}^{(1)}\xi_2\right] \\
& \qquad -\frac{\xi_1\left(c_i^{(1)}+c_j^{(1)}\right)}{\xi_1^2+\xi_3\xi_2^2}-\frac{c_{\max,ij}^{(0)}|q^{(1)}|_{\max,ij}\xi_2}{\xi_1^2+\xi_3\xi_2^2} \\
& \qquad -\frac{+c_{\max,ij}^{(1)}|q^{(0)}|_{\max,ij}\xi_2}{\xi_1^2+\xi_3\xi_2^2}+\frac{\xi_1\xi_2}{\left(\xi_1^2+\xi_3\xi_2^2\right)^2}\left[2c_{\max,ij}^{(0)}|q^{(1)}|_{\max,ij}\xi_1\right. \\
& \qquad \left.\left.+2c_{\max,ij}^{(1)}|q^{(0)}|_{\max,ij}\xi_1+2\xi_3\xi_2\left(c_i^{(1)}+c_j^{(1)}\right)+2\sqrt{\xi_3}q_{\mathrm{ref}}^{(1)}\xi_2\right]\right) \\
& \qquad \left.\cdot\frac{(v_\zeta)_i^{(0)}+(v_\zeta)_j^{(0)}}{4}\triangle_{ij}p^{(0)}\right]|l_{ij}^k| \\
& + M\sum_{j\in\mathcal{N}(i)}\sum_{k=1}^{2}\left[\frac{1}{16}\left(\frac{|q^{(0)}|_{\max,ij}^2\xi_3\xi_2}{\left(\xi_1^2+\xi_3\xi_2^2\right)^{\frac{3}{2}}}+\frac{\xi_1|q^{(0)}|_{\max,ij}^2\xi_3\xi_2}{\left(\xi_1^2+\xi_3\xi_2^2\right)^2}\right.\right. \\
& \qquad \left.-\frac{|q^{(0)}|_{\max,ij}\xi_3\xi_2}{c_{\max,ij}^{(0)}\left(\xi_1^2+\xi_3\xi_2^2\right)^2}\left[2\xi_1^2+\xi_3\xi_2^2\right]\right) \\
& \qquad \left.\cdot\left[(v_\zeta)_i^{(0)}+(v_\zeta)_j^{(0)}\right]\triangle_{ij}p^{(0)}\right]|l_{ij}^k|+\mathcal{O}(M^2) \quad \text{for} \quad \zeta=1,2.
\end{aligned}
$$

where ξ_1 and ξ_2 are given by equations (4.44) and (4.45), respectively and ξ_3 represents

$$\xi_3 = \left(q^{(0)}_{\text{ref},ij}\right)^2.$$

Again, we consider the special case of a structured, equidistant, Cartesian grid $\mathcal{S}_h$. With the leading order pressure being constant in the vicinity of control volume σ_i, see Theorem 5, we can simplify the momentum balance to

$$\begin{aligned}\frac{d}{dt}\left(\rho v_\zeta\right)_i = &\sum_{j\in\mathcal{N}(i)}\sum_{k=1}^{2} -p^{(0)} n^k_{ij,\zeta}|l^k_{ij}| \\ &+M\sum_{j\in\mathcal{N}(i)}\sum_{k=1}^{2}\left[-n_\zeta\frac{p^{(1)}_i+p^{(1)}_j}{2}+\left(\frac{\xi_2}{\sqrt{\xi_1^2+\xi_3\xi_2^2}}-\frac{\xi_1\xi_2}{\xi_1^2+\xi_3\xi_2^2}\right)\right. \\ &\left.\cdot\frac{(v_\zeta)^{(0)}_i+(v_\zeta)^{(0)}_j}{4}\triangle_{ij}p^{(1)}\right]|l^k_{ij}| \\ &+\mathcal{O}(M^2) \text{ for } \zeta = 1,2.\end{aligned}$$

With the given discretization, we can write the momentum balance of $\mathcal{O}(M)$ as

$$\begin{aligned}&\frac{p^{(1)}_i-p^{(1)}_l}{4}\left(\frac{c^{(0)}_i+c^{(0)}_l}{\sqrt{\left(c^{(0)}_{\max,il}\right)^2\left(|q^{(0)}|_{\max,il}\right)^2+\left(q^{(0)}_{\text{ref},il}\right)^2\left(c^{(0)}_i+c^{(0)}_l\right)^2}}\right. \\ &\left.-\frac{c^{(0)}_{\max,il}|q^{(0)}|_{\max,il}\left(c^{(0)}_i+c^{(0)}_l\right)}{\left(c^{(0)}_{\max,il}\right)^2\left(|q^{(0)}|_{\max,il}\right)^2+\left(q^{(0)}_{\text{ref},il}\right)^2\left(c^{(0)}_i+c^{(0)}_l\right)^2}\right)\left[(v_\zeta)^{(0)}_i+(v_\zeta)^{(0)}_l\right]+ \\ &\frac{p^{(1)}_i-p^{(1)}_k}{4}\left(\frac{c^{(0)}_i+c^{(0)}_k}{\sqrt{\left(c^{(0)}_{\max,ik}\right)^2\left(|q^{(0)}|_{\max,ik}\right)^2+\left(q^{(0)}_{\text{ref},ik}\right)^2\left(c^{(0)}_i+c^{(0)}_k\right)^2}}\right. \\ &\left.-\frac{c^{(0)}_{\max,ik}|q^{(0)}|_{\max,ik}\left(c^{(0)}_i+c^{(0)}_k\right)}{\left(c^{(0)}_{\max,ik}\right)^2\left(|q^{(0)}|_{\max,ik}\right)^2+\left(q^{(0)}_{\text{ref},ik}\right)^2\left(c^{(0)}_i+c^{(0)}_k\right)^2}\right)\left[(v_\zeta)^{(0)}_i+(v_\zeta)^{(0)}_k\right] \\ &=\frac{p^{(1)}_l-p^{(1)}_k}{2} \text{ for } \zeta = 1,2\end{aligned}$$

Again the $p^{(1)}$-distribution is spatially constant regardless of the velocity field.
Finally, we analyze the function $\mathcal{H}^{\rho h}_{MAPS+}(\widetilde{\boldsymbol{u}}_i, \widetilde{\boldsymbol{u}}_j; \boldsymbol{n})$ in equation (4.42). The result of

the expansion into a Taylor series is shown in equation (A.31). With this, we can write the balance

$$
\begin{aligned}
&\frac{d}{dt}\left(\rho h\right)_i = \\
&\frac{1}{M}\sum_{j\in\mathcal{N}(i)}\sum_{k=1}^{2}\left[\left(\frac{\xi_2}{\sqrt{\xi_1^2+\left(q_{\mathrm{ref},ij}^{(0)}\right)^2\xi_2^2}}-\frac{\xi_1\xi_2}{\xi_1^2+\left(q_{\mathrm{ref},ij}^{(0)}\right)^2\xi_2^2}\right)\frac{h_i^{(0)}+h_j^{(0)}}{4}\triangle_{ij}p^{(0)}\right]|l_{ij}^k| \\
&+\sum_{j\in\mathcal{N}(i)}\sum_{k=1}^{2}\left[\left(\frac{\xi_2}{\sqrt{\xi_1^2+\left(q_{\mathrm{ref},ij}^{(0)}\right)^2\xi_2^2}}-\frac{\xi_1\xi_2}{\xi_1^2+\left(q_{\mathrm{ref},ij}^{(0)}\right)^2\xi_2^2}\right)\frac{h_i^{(0)}+h_j^{(0)}}{4}\triangle_{ij}p^{(1)}\right. \\
&\qquad+\left(\frac{\xi_2}{\sqrt{\xi_1^2+\left(q_{\mathrm{ref},ij}^{(0)}\right)^2\xi_2^2}}-\frac{\xi_1\xi_2}{\xi_1^2+\left(q_{\mathrm{ref},ij}^{(0)}\right)^2\xi_2^2}\right)\frac{h_i^{(1)}+h_j^{(1)}}{4}\triangle_{ij}p^{(0)} \\
&\qquad+\frac{1}{2}\left(\frac{\left(c_i^{(1)}+c_j^{(1)}\right)}{\sqrt{\xi_1^2+\left(q_{\mathrm{ref},ij}^{(0)}\right)^2\xi_2^2}}-\frac{\xi_2}{2\left[\xi_1^2+\left(q_{\mathrm{ref},ij}^{(0)}\right)^2\xi_2^2\right]^{\frac{3}{2}}}\left[2c_{\mathrm{max},ij}^{(0)}\xi_1|q^{(1)}|_{\mathrm{max},ij}\right.\right. \\
&\qquad\left.+2c_{\mathrm{max},ij}^{(1)}|q^{(0)}|_{\mathrm{max},ij}\xi_1+2\left(q_{\mathrm{ref},ij}^{(0)}\right)^2\xi_2\left(c_i^{(1)}+c_j^{(1)}\right)+2\sqrt{\left(q_{\mathrm{ref},ij}^{(0)}\right)^2}q_{\mathrm{ref}}^{(1)}\xi_2\right] \\
&\qquad-\frac{\xi_1\left(c_i^{(1)}+c_j^{(1)}\right)}{\xi_1^2+\left(q_{\mathrm{ref},ij}^{(0)}\right)^2\xi_2^2}-\frac{c_{\mathrm{max},ij}^{(0)}|q^{(1)}|_{\mathrm{max},ij}\xi_2}{\xi_1^2+\left(q_{\mathrm{ref},ij}^{(0)}\right)^2\xi_2^2}-\frac{+c_{\mathrm{max},ij}^{(1)}|q^{(0)}|_{\mathrm{max},ij}\xi_2}{\xi_1^2+\left(q_{\mathrm{ref},ij}^{(0)}\right)^2\xi_2^2} \\
&\qquad+\frac{\xi_1\xi_2}{\left[\xi_1^2+\left(q_{\mathrm{ref},ij}^{(0)}\right)^2\xi_2^2\right]^2}\left[2c_{\mathrm{max},ij}^{(0)}|q^{(1)}|_{\mathrm{max},ij}\xi_1+2c_{\mathrm{max},ij}^{(1)}|q^{(0)}|_{\mathrm{max},ij}\xi_1\right. \\
&\qquad\left.\left.\left.+2\left(q_{\mathrm{ref},ij}^{(0)}\right)^2\xi_2\left(c_i^{(1)}+c_j^{(1)}\right)+2\sqrt{\left(q_{\mathrm{ref},ij}^{(0)}\right)^2}q_{\mathrm{ref}}^{(1)}\xi_2\right]\right)\frac{h_i^{(0)}+h_j^{(0)}}{4}\triangle_{ij}p^{(0)}\right]|l_{ij}^k|
\end{aligned}
$$

where ξ_1 and ξ_2 are given by equations (4.44) and (4.45), respectively.
Again, we consider the special case of a structured, equidistant, Cartesian grid $\mathcal{S}_h$. The leading order pressure is constant in the vicinity of control volume σ_i, see Theorem 5.

Hence, we can simplify the balance equation to

$$\frac{d}{dt}\left(\rho h\right)_i = \sum_{j\in\mathcal{N}(i)}\sum_{k=1}^{2}\left[\left(\frac{\xi_2}{\sqrt{\xi_1^2+\left(q^{(0)}_{\mathrm{ref},ij}\right)^2\xi_2^2}}-\frac{\xi_1\xi_2}{\xi_1^2+\left(q^{(0)}_{\mathrm{ref},ij}\right)^2\xi_2^2}\right)\frac{h_i^{(0)}+h_j^{(0)}}{4}\triangle_{ij}p^{(1)}\right]|l_{ij}^k| + \mathcal{O}(M).$$

We write the balance of $\mathcal{O}(1)$ as

$$\begin{aligned}
&\frac{p_i^{(1)}-p_l^{(1)}}{4}\left(\frac{c_i^{(0)}+c_l^{(0)}}{\sqrt{\left(c^{(0)}_{\max,il}\right)^2\left(|q^{(0)}|_{\max,il}\right)^2+\left(q^{(0)}_{\mathrm{ref},il}\right)^2\left(c_i^{(0)}+c_l^{(0)}\right)^2}}\right.\\
&\qquad\left.-\frac{c^{(0)}_{\max,il}|q^{(0)}|_{\max,il}\left(c_i^{(0)}+c_l^{(0)}\right)}{\left(c^{(0)}_{\max,il}\right)^2\left(|q^{(0)}|_{\max,il}\right)^2+\left(q^{(0)}_{\mathrm{ref},il}\right)^2\left(c_i^{(0)}+c_l^{(0)}\right)^2}\right)\left(h_i^{(0)}+h_l^{(0)}\right)+\\
&\frac{p_i^{(1)}-p_k^{(1)}}{4}\left(\frac{c_i^{(0)}+c_k^{(0)}}{\sqrt{\left(c^{(0)}_{\max,ik}\right)^2\left(|q^{(0)}|_{\max,ik}\right)^2+\left(q^{(0)}_{\mathrm{ref},ik}\right)^2\left(c_i^{(0)}+c_k^{(0)}\right)^2}}\right.\\
&\qquad\left.-\frac{c^{(0)}_{\max,ik}|q^{(0)}|_{\max,ik}\left(c_i^{(0)}+c_k^{(0)}\right)}{\left(c^{(0)}_{\max,ik}\right)^2\left(|q^{(0)}|_{\max,ik}\right)^2+\left(q^{(0)}_{\mathrm{ref},ik}\right)^2\left(c_i^{(0)}+c_k^{(0)}\right)^2}\right)\left(h_i^{(0)}+h_k^{(0)}\right)=0.
\end{aligned}$$

From this relation we can see that $p^{(1)}$ is spatially constant.
Hence, for the altered MAPS+ scheme, all flux functions lead to a spatially constant field of the first order pressure. □

4.2.5. Numerical Results

To fortify the results of the asymptotic analysis of the MAPS+ scheme in numerical simulations, we choose the inviscid flow around the NACA0012-profile. We vary the inflow Mach number in the region from 0.1 to 10^{-4}. For all calculations a two step Runge-Kutta scheme is used. The grid is built following the description in subsection 4.1.2 on page 38.
The initial conditions are a spatially constant distribution of all thermodynamic variables. We define the inflow pressure $p_{\mathrm{in}} = p_{\mathrm{ref}}$ and the inflow temperature $T_{\mathrm{in}} = T_{\mathrm{ref}}$, all other variables are calculated by the thermodynamic modules in the solver. In addition, a

spatially constant velocity field is given by initiating a spatially constant field of the Mach number of $Ma_{\text{in}} = Ma_{\text{ref}}$. These values are also taken for the farfield state that is needed to define the farfield boundary condition.
The pressure distributions of the results for inflow Mach numbers 10^{-1}, 10^{-2} and 10^{-3} are shown in Figure 4.2. On the left-hand side, we show the calculations using the general MAPS+ scheme while on the right-hand side the calculations using the altered MAPS+ scheme are presented. From top to bottom, the inflow Mach number is altered from 10^{-1} over 10^{-2} to 10^{-3}. For these calculations, nitrogen modeled as a Van der Waals gas is used with the inflow conditions of a pressure of $p_{\text{in}} = 10^5 Pa$ and a temperature of $T_{\text{in}} = 300K$. This is condition 1 as listed in Table 4.4 on page 115.
The variations in pressure which are present in the flow field are small compared to the inflow and background pressure. Hence, in Figure 4.2, we show the distribution of the local deviation from this background pressure of $10^5 Pa$. We call this difference the pressure offset.
In the figure, we see that the general MAPS+ scheme only produces a reasonable result for the Mach numbers of $Ma_{\text{in}} = 10^{-1}$ and 10^{-2} which are shown in Subfigures 4.2a and 4.2c, respectively. For lower Mach numbers, the numerical error increases and the results deteriorate, see Subfigure 4.2e. The altered MAPS+ scheme, on the other hand, leads to reasonable results for all investigated Mach numbers.
Now we compare the results obtained for an inflow Mach number of 10^{-1} using the general and altered MAPS+ scheme that are shown in Subfigures 4.2a and 4.2b, respectively. Both results are qualitatively similar, which supports the observation that the general MAPS+ scheme correctly calculates the flow at an inflow Mach number of 10^{-1}. Next, we compare the results for the general and the altered MAPS+ scheme for an inflow Mach number of 10^{-2} shown in Subfigures 4.2c and 4.2d, respectively. At this Mach number, we see a distinct difference between the results obtained with the two schemes. While the result obtained with the altered MAPS+ scheme contains smooth transitions between the different pressure levels, we see disrupted transitions in Subfigure 4.2c which is obtained using the general MAPS+ scheme. Hence, at an inflow Mach number of 10^{-2}, we can already see an influence of the numerical error in the results obtained with the general MAPS+ scheme.
Comparing the plots for the different calculations done with the altered MAPS+ scheme, we first notice that the three plots in Subfigures 4.2b, 4.2d and 4.2f are qualitatively similar. They only differ by the general magnitude of the pressure offset which is of $\mathcal{O}(M^2)$ as the Mach number decreases.

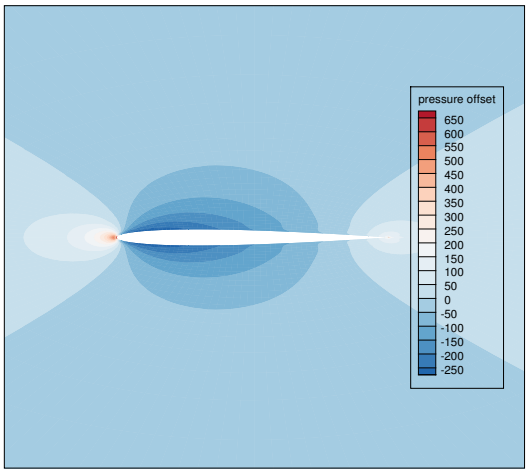

(a) general MAPS+, $Ma_{\text{in}} = 10^{-1}$

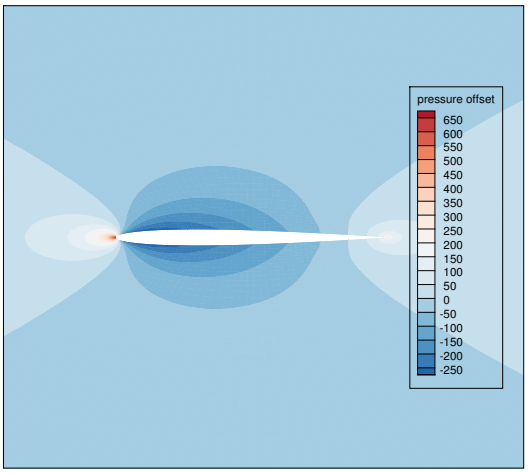

(b) altered MAPS+, $Ma_{\text{in}} = 10^{-1}$

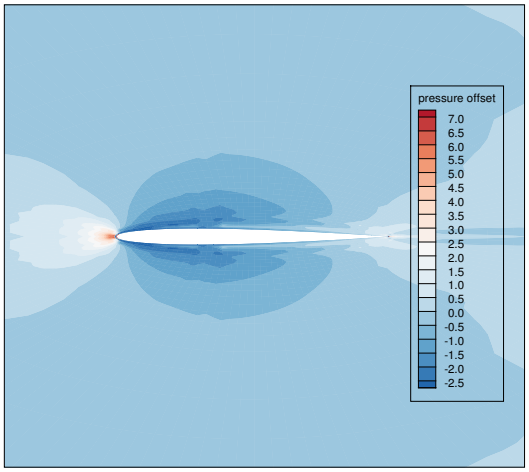

(c) general MAPS+, $Ma_{\text{in}} = 10^{-2}$

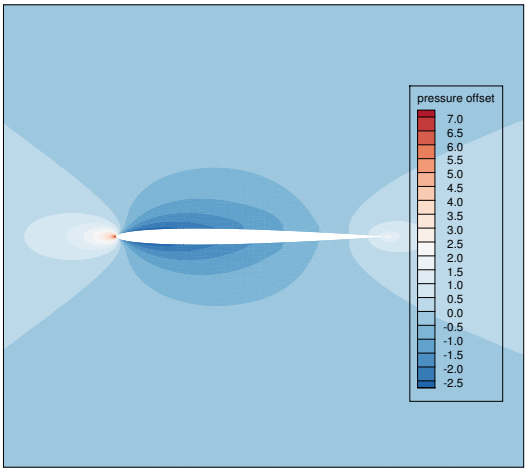

(d) altered MAPS+, $Ma_{\text{in}} = 10^{-2}$

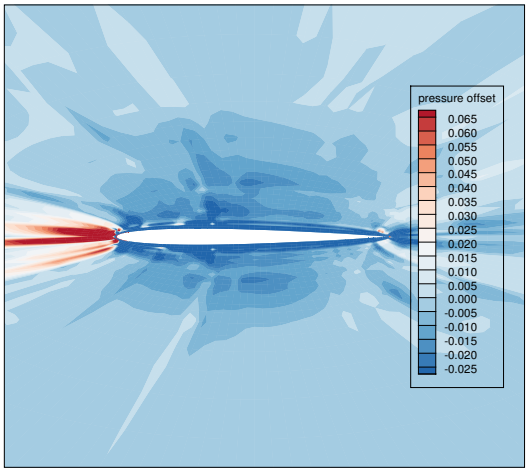

(e) general MAPS+, $Ma_{\text{in}} = 10^{-3}$

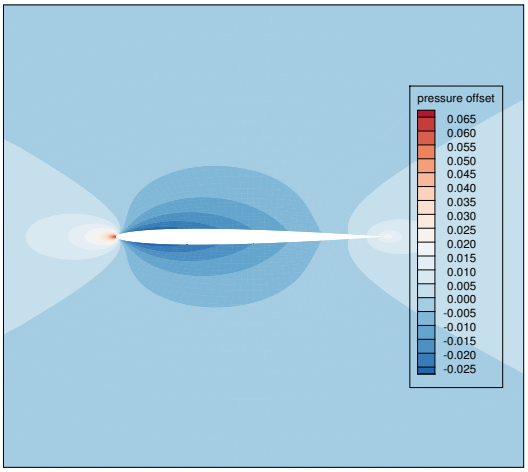

(f) altered MAPS+, $Ma_{\text{in}} = 10^{-3}$

Figure 4.2.: Pressure distributions in Pa (offset to background pressure of $10^5 Pa$) calculated with the general and altered MAPS+ scheme at different inflow Mach numbers

Clearly, we do not see this similarity in the plots for the calculations done with the general MAPS+ scheme. The cause of the deterioration of the general MAPS+ scheme are the fluctuations of the first order pressure term on a length scale independent of the Mach number shown in Corollary 6.1. To prove the existence of these fluctuations in the numerical results, we consider the behavior of the pressure quotient

$$p_{\text{ind}} = \frac{\widetilde{p}_{\max} - \widetilde{p}_{\min}}{\widetilde{p}_{\max}},$$

with

$$\widetilde{p}_{\max} = \max\left(\widetilde{p}_i\right) \text{ for } i \text{ in } N_h$$

and

$$\widetilde{p}_{\min} = \min\left(\widetilde{p}_i\right) \text{ for } i \text{ in } N_h$$

as a function of the Mach number analogous to the work of Meister [48]. For stationary numerical results the behavior

$$p_{\text{ind}} = \frac{\widetilde{p}_{\max} - \widetilde{p}_{\min}}{\widetilde{p}_{\max}} = \mathcal{O}(M^2) \text{ for } M \to 0$$

reflects the behavior of the Euler equations as can be deducted from the single scale asymptotic analysis.
In Figure 4.3, p_{ind} is shown for the general MAPS+ scheme as a function of the Mach number. The plot follows the relation

$$p_{\text{ind}} = \frac{\widetilde{p}_{\max} - \widetilde{p}_{\min}}{\widetilde{p}_{\max}} = \mathcal{O}(M) \text{ for } M \to 0,$$

as it can be expected from the results of the analytical analysis presented in Corollary 6.1. So, we can show the existence of fluctuations in the first order pressure term in the numerical experiment. This agrees with the results of the asymptotic analysis and shows why the general MAPS+ scheme leads to unphysical results in the limit of small Mach numbers. Note that p_{ind} is of order $\mathcal{O}(M^2)$ down to a Mach number of 10^{-2}. This agrees with our observation that the result obtained with the general MAPS+ scheme for a Mach number of 10^{-2} is qualitatively reasonable.
Next, we consider the behavior of the pressure quotient for calculations with the altered MAPS+ scheme. From the asymptotic analysis, we expect the first order pressure term to be spatially constant in these calculations. The plot of the pressure quotient shown in Figure 4.4 satisfies this expectation. For the altered MAPS+ scheme, the pressure quotient shows the behavior

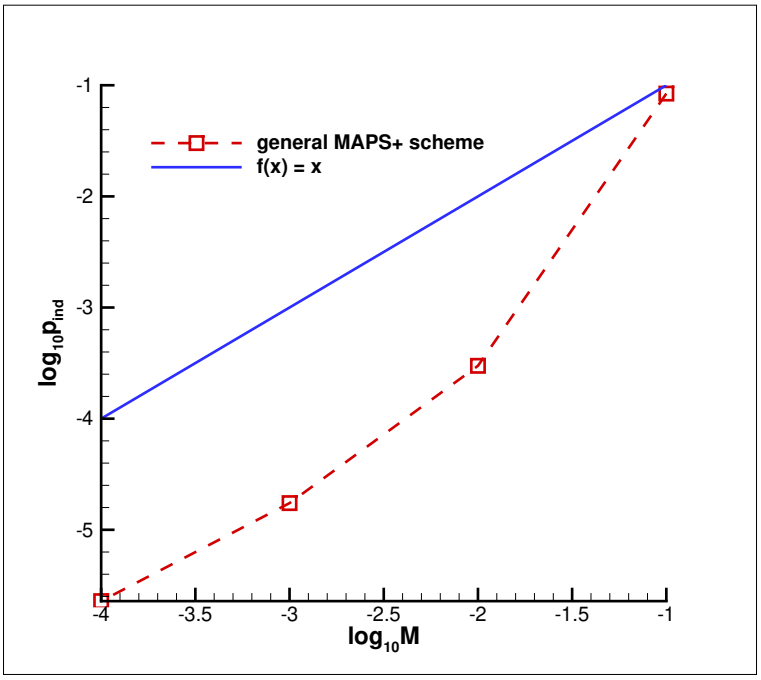

Figure 4.3.: Plot of the pressure quotient for the general MAPS+ scheme

$$p_{\text{ind}} = \frac{\widetilde{p}_{\max} - \widetilde{p}_{\min}}{\widetilde{p}_{\max}} = \mathcal{O}(M^2) \text{ for } M \to 0,$$

which indicates that there are no fluctuations of the first order pressure term. This as well agrees with the results of the asymptotic analysis.

Remark.

In this section, we show that the altered MAPS+ scheme correctly models the Euler equations to an inflow Mach number as low as 10^{-4}. However, to gain these numerical results very small CFL numbers have to be used for the numerical scheme to be stable. Birken and Meister [6] notice that a scheme becomes unstable unless the time step size is of $\mathcal{O}(M^2)$ as $M \to 0$, hence we choose the CFL number to be of $\mathcal{O}(M^2)$. To gain results using this method is numerically very expensive and not suitable for practical applications. A solution to this problem is the use of a preconditioning scheme which allows for a time step size and hence a CFL number of $\mathcal{O}(1)$ as the Mach number approaches zero. Therefore, we cover preconditioning schemes in the next section.

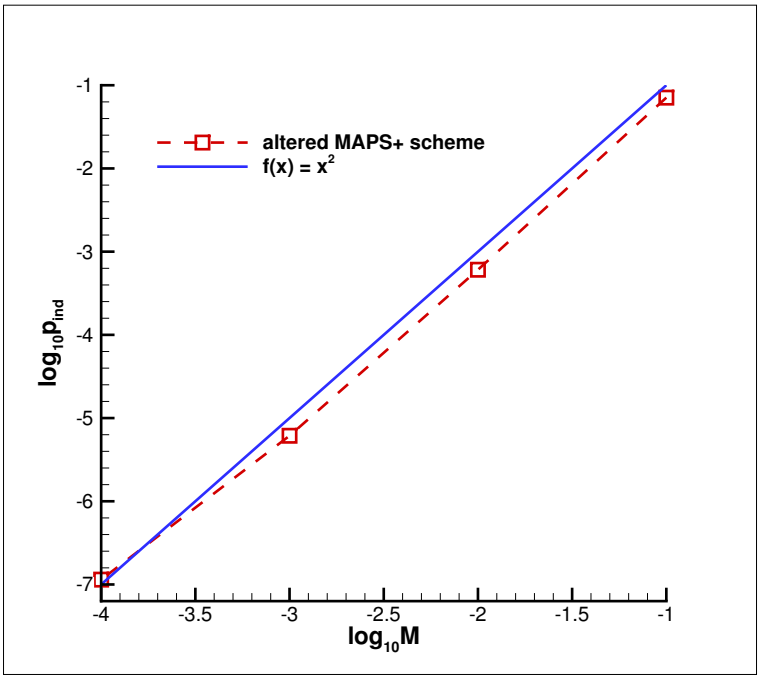

Figure 4.4.: Plot of the pressure quotient for the altered MAPS+ scheme

4.3. Preconditioning Scheme

Flows relevant for practical applications can often cover a range of Mach numbers from low subsonic to hypersonic. An example is the flow around an airfoil at transonic Mach numbers. In the region of the stagnation point, the Mach number approaches zero while it can reach values above one in other parts of the domain. Ground test cases of rockets also cover a wide range of Mach numbers as the supersonic plume is in close proximity to the surrounding air that moves at very low Mach numbers, if at all. A third example are combustion processes, where a subsonic deflagration can turn into a supersonic detonation within a small spatial distance. If we want to simulate these flows with a numerical flow solver, a scheme covering the whole range of Mach numbers is necessary.

However, the unmodified flow solvers available in the literature are only applicable to a part of the Mach number regime. Solvers based on the incompressible equations are not built to model compressible effects and hence cannot be used to simulate flows at high Mach numbers. Flow solvers that originate from the compressible equations, on the other hand, cannot be applied to incompressible flows in general. A thorough discussion of this issue is given by Langer [38].

To obtain a flow solver suitable for the whole range of Mach numbers, two different

approaches are common. On the one hand, it is possible to take an incompressible scheme and add compressible effects to cover flows at a higher Mach number. On the other hand, a compressible scheme can be extended towards the incompressible limit. Here, we choose to follow the second approach since the flows we are interested in show strong compressible effects in a big part of the flow domain.
If a compressible scheme is used to calculate flows at low Mach numbers, different problems occur. Typically, the numerical error grows as the Mach number decreases. At the same time the computational costs increase. These issues with both accuracy and efficiency have been reported by many different authors, see for example the work of Briley et al. [8], Merkle and Choi [51] and Volpe [74].
This is due to the growing difference between the eigenvalues of the problem which are the characteristic velocities. The influence of this difference in the eigenvalues at low Mach numbers on numerical schemes is shown by Guillard and Nkonga [27]. The convective velocities are of order $\mathcal{O}(M)$ as the Mach number decreases while the acoustic velocities are of order $\mathcal{O}(1)$.

Remark.
Note that this is only true for the chosen nondimensionalization. With a different set of reference values, the convective velocities v_1 and v_2 and the total velocity q can be of $\mathcal{O}(1)$ and the speed of sound c of $O\left(\frac{1}{M}\right)$. However, there is still a difference of $\mathcal{O}(M)$ between q and c. So, they are of different orders as the Mach number approaches zero.

The increasing difference of the eigenvalues can better be described by their ratio. This is closely related to the condition number of the flux Jacobi matrix.

Definition 4.3.1.
The property

$$\kappa(\boldsymbol{A}) = \frac{|\lambda_{\max}(\boldsymbol{A})|}{|\lambda_{\min}(\boldsymbol{A})|},$$

where $\lambda_{\max}(\boldsymbol{A})$ and $\lambda_{\min}(\boldsymbol{A})$ are the largest and smallest eigenvalue of $\boldsymbol{A}$, respectively, is called the condition number of the matrix $\boldsymbol{A}$.

A problem with a low condition number is said to be well-conditioned while a problem with a high condition number is said to be ill-conditioned. Since $\lambda_{\max}(\boldsymbol{A}_{\boldsymbol{u}}^{(i)})$ and $\lambda_{\min}(\boldsymbol{A}_{\boldsymbol{u}}^{(i)})$ are of different orders as the Mach number approaches zero, the flux Jacobi matrix of the Euler equations $\boldsymbol{A}_{\boldsymbol{u}}^{(i)}$ is ill-conditioned for small Mach numbers. This eigenvalue stiffness has negative effects on the convergence of both explicit and implicit schemes.

A preconditioning scheme is a common remedy for these issues. The goal of a preconditioner is to decrease the condition number by altering the eigenvalues so that they are of the same order of magnitude. This allows for a numerical error independent of the Mach number as well as a bigger time step size and hence a reduction in costs. An ideal preconditioning scheme would lead to a condition number of one.
In general, a preconditioning scheme is used to premultiply the time derivative by a matrix suitable for scaling the eigenvalues of the system. This method is not consistent in time and can only be used to find a steady state solution. The steady state solution of the preconditioned system is the same as the solution of the original system.
As stated in section 4.1 on page 35, a dual time-stepping approach is used for time accurate computation in the DLR TAU-code. This means that a steady state problem is solved within every physical time step. Hence, this limitation to steady state solutions does not prevent us from using a preconditioning scheme for time accurate computations within TAU.
A preconditioner can be built following different approaches and using different sets of variables. Hence, there is not just one preconditioner, but several families of preconditioning matrices. Premultiplying the time derivative by a preconditioning matrix means equation (2.3) on page 8 is replaced by

$$\boldsymbol{\Gamma}(\boldsymbol{u})\frac{\partial \boldsymbol{u}}{\partial t} + \sum_{i=1}^{d} \boldsymbol{A}_{\boldsymbol{u}}^{(i)} \frac{\partial \boldsymbol{u}}{\partial \boldsymbol{x}_i} = \boldsymbol{0}, \tag{4.46}$$

where $\boldsymbol{\Gamma}(\boldsymbol{u})$ is the preconditioning matrix formulated in the conservative variables $\boldsymbol{u}$. Equation (4.46) is equivalent to the following expression:

$$\frac{\partial \boldsymbol{u}}{\partial t} + \boldsymbol{\Gamma}^{-1}(\boldsymbol{u}) \sum_{i=1}^{d} \boldsymbol{A}_{\boldsymbol{u}}^{(i)} \frac{\partial \boldsymbol{u}}{\partial \boldsymbol{x}_i} = \boldsymbol{0},$$

with the inverse of the preconditioning matrix $\boldsymbol{\Gamma}^{-1}(\boldsymbol{u})$.
Preconditioning schemes are usually derived using a set of primitive variables that contains pressure, the Cartesian velocities and one additional variable. The choice of pressure as a primitive variable is preferable since it plays an important role in the incompressible limit and allows for a direct treatment of pressure waves. To distinguish a preconditioning matrix formulated in the primitive variables $\boldsymbol{q}$ from the preconditioner $\boldsymbol{\Gamma}(\boldsymbol{u})$ that is formulated in conservative variables, we call the former $\boldsymbol{P}(\boldsymbol{q})$.
Since the preconditioning matrix $\boldsymbol{P}(\boldsymbol{q})$ is in terms of some set of primitive variables $\boldsymbol{q}$ and the system (4.46), where the preconditioner is applied, is in terms of the conservative

variables, the preconditioning matrix needs to be transformed to conservative variables. This leads to the following form of the preconditioning matrix in terms of the conservative variables $\boldsymbol{u}$:

$$\boldsymbol{\Gamma}(\boldsymbol{u}) = \frac{\partial \boldsymbol{u}}{\partial \boldsymbol{q}} \boldsymbol{P}(\boldsymbol{q}) \frac{\partial \boldsymbol{q}}{\partial \boldsymbol{u}}, \tag{4.47}$$

where $\frac{\partial \boldsymbol{u}}{\partial \boldsymbol{q}}$ and $\frac{\partial \boldsymbol{q}}{\partial \boldsymbol{u}}$ are the transformation matrices from conservative to primitive variables and vice versa, respectively.
Here, we consider the following sets of primitive variables:

- $\boldsymbol{q}_1 = (\rho, v_1, v_2, p)$
- $\boldsymbol{q}_2 = (p, v_1, v_2, T)$
- $\boldsymbol{q}_3 = (p, v_1, v_2, h)$
- $\boldsymbol{q}_4 = (p, v_1, v_2, s)$
- $\boldsymbol{q}_5 = (p, v_1, v_2, \rho)$

Different authors mean either $\boldsymbol{\Gamma}(\boldsymbol{u})$ and $\boldsymbol{P}(\boldsymbol{q})$ or $\boldsymbol{\Gamma}^{-1}(\boldsymbol{u})$ and $\boldsymbol{P}^{-1}(\boldsymbol{q})$ when they refer to the preconditioning matrix. Within this work, we call $\boldsymbol{\Gamma}(\boldsymbol{u})$ and $\boldsymbol{P}(\boldsymbol{q})$ preconditioner.

4.3.1. Preconditioning schemes for an ideal gas

In this section, we briefly discuss the evolution of preconditioning schemes and the currently available preconditioners. A detailed review is given by Turkel [67]. For simplicity, we formulate all schemes in two spatial dimensions.
In 1967, Chorin [13] proposed the method of artificial compressibility to solve the steady state incompressible Euler equations. The idea of this method is to add a density time derivative to the continuity equation to regain the hyperbolic type of the equation. This converts a mixed system of elliptic-hyperbolic type to a fully hyperbolic system. The continuity equation

$$\frac{\partial v_1}{\partial x_1} + \frac{\partial v_2}{\partial x_2} = 0,$$

is replaced by

$$\frac{\partial \rho}{\partial t} + \frac{\partial v_1}{\partial x_1} + \frac{\partial v_2}{\partial x_2} = 0$$

with

$$\rho = \delta p, \tag{4.48}$$

where the relation (4.48) plays the role of the state equation. The parameter δ is called artificial compressibility. Inserting the state equation, this can also be written as

$$\frac{\partial(\delta p)}{\partial t} + \frac{\partial v_1}{\partial x_1} + \frac{\partial v_2}{\partial x_2} = 0.$$

In other words, the time derivative is multiplied by the preconditioning matrix

$$\boldsymbol{P} = \begin{bmatrix} \delta & 0 & 0 \\ 0 & 1 & 0 \\ 0 & 0 & 1 \end{bmatrix}.$$

Chorin chooses the parameter δ and the time step size in a way such that the scheme is stable and the convergence towards steady state is as fast as possible.
The idea to multiply the time derivative by an artificial term with the goal to accelerate the convergence to steady state has since been studied by several authors. It cannot only be applied to the incompressible equations, but also to the compressible ones.
Turkel [66] presents a generalization of the artificial compressibility method. In a first step, they develop a preconditioning matrix for the incompressible Euler equations following the same approach as Chorin but with the difference that the pressure time derivative is added to all equations. So,

$$\begin{bmatrix} \frac{1}{\beta^2} & 0 & 0 \\ \frac{\alpha v_1}{\beta^2} & 1 & 0 \\ \frac{\alpha v_2}{\beta^2} & 0 & 1 \end{bmatrix} \cdot \frac{\partial}{\partial t} \begin{bmatrix} p \\ v_1 \\ v_2 \end{bmatrix}, \tag{4.49}$$

with functions α and β is added to the system of equations

$$\begin{bmatrix} 0 & 0 & 0 \\ 0 & 1 & 0 \\ 0 & 0 & 1 \end{bmatrix} \cdot \frac{\partial}{\partial t} \begin{bmatrix} p \\ v_1 \\ v_2 \end{bmatrix} + \begin{bmatrix} 0 & 1 & 0 \\ 1 & v_1 & 0 \\ 0 & 0 & v_1 \end{bmatrix} \cdot \frac{\partial}{\partial x_1} \begin{bmatrix} p \\ v_1 \\ v_2 \end{bmatrix} + \begin{bmatrix} 0 & 0 & 1 \\ 0 & v_2 & 0 \\ 1 & 0 & v_2 \end{bmatrix} \cdot \frac{\partial}{\partial x_2} \begin{bmatrix} p \\ v_1 \\ v_2 \end{bmatrix} = 0.$$

Here, α is evaluated using

$$\alpha = \begin{cases} 1 + Ma_g^2, & Ma_{\text{ref}} < 1 \\ 2\left(1 - \sqrt{1 + \frac{1}{Ma_g^2}}\right), & Ma_{\text{ref}} \geq 1, \end{cases}$$

with the global Mach number Ma_g and a reference Mach number Ma_{ref}, while β is a

function of $(v_1^2 + v_2^2)$. Turkel chooses β in a way that ensures it to have a nonzero value at the stagnation point. They define

$$\beta \begin{cases} \max\left[(2-\alpha)\left(v_1^2+v_2^2\right),\epsilon\right], & \alpha < 1 \\ K\max\left[\alpha\left(v_1^2+v_2^2\right),\epsilon\right], & \alpha \geq 1, \end{cases}$$

where K is a constant slightly larger than one and ϵ is chosen to be a fraction of the maximum value of $\left(v_1^2 + v_2^2\right)$.
In the next step, the compressible system

$$\frac{\partial}{\partial t}\begin{bmatrix} p \\ v_1 \\ v_2 \\ s \end{bmatrix} + \begin{bmatrix} v_1 & \rho c^2 & 0 & 0 \\ \rho^{-1} & v_1 & 0 & 0 \\ 0 & 0 & v_1 & 0 \\ 0 & 0 & 0 & v_1 \end{bmatrix} \cdot \frac{\partial}{\partial x_1}\begin{bmatrix} p \\ v_1 \\ v_2 \\ s \end{bmatrix} + \begin{bmatrix} v_2 & 0 & \rho c^2 & 0 \\ 0 & v & 0 & 0 \\ \rho^{-1} & 0 & v_2 & 0 \\ 0 & 0 & 0 & v_2 \end{bmatrix} \cdot \frac{\partial}{\partial x_2}\begin{bmatrix} p \\ v_1 \\ v_2 \\ s \end{bmatrix} = 0$$

is considered.
In a generalization of the preconditioning matrix for the incompressible equations that is shown in equation (4.49), the compressible system is preconditioned with

$$\boldsymbol{P}(\boldsymbol{q}_4) = \begin{bmatrix} \frac{1}{\rho\beta^2} & 0 & 0 & 0 \\ \frac{\alpha v_1}{\rho\beta^2} & 1 & 0 & 0 \\ \frac{\alpha v_2}{\rho\beta^2} & 0 & 1 & 0 \\ 0 & 0 & 0 & 1 \end{bmatrix}. \tag{4.50}$$

This has the effect that the equations are decoupled and the entropy equation is not preconditioned. Therefore, the compressible system is similar to the incompressible one. Usually, this preconditioner is applied in $\boldsymbol{q}_2$ variables where it takes the form

$$\boldsymbol{P}(\boldsymbol{q}_2) = \begin{bmatrix} \frac{1}{\beta^2} & 0 & 0 & 0 \\ \frac{\alpha v_1}{\rho\beta^2 c^2} & 1 & 0 & 0 \\ \frac{\alpha v_2}{\rho\beta^2 c^2} & 0 & 1 & 0 \\ \frac{1-\beta^2}{\rho c_p \beta^2} & 0 & 0 & 1 \end{bmatrix}. \tag{4.51}$$

For the transformation, ideal gas assumptions are applied.
This preconditioning scheme is further modified by Turkel [66] to also include precondi-

tioners by other authors. The modified scheme can be written as

$$\boldsymbol{P}(\boldsymbol{q}_2) = \begin{bmatrix} \frac{1}{\beta^2} - (\gamma-1)\delta & 0 & 0 & \frac{\gamma p}{T}\delta \\ \frac{\alpha v_1}{\rho\beta^2 c^2} & 1 & 0 & 0 \\ \frac{\alpha v_2}{\rho\beta^2 c^2} & 0 & 1 & 0 \\ \frac{1}{\rho c_p}\left(\frac{1}{\beta^2} - g\right) & 0 & 0 & g \end{bmatrix}, \tag{4.52}$$

with $g = 1 + (\gamma - 1)\,\delta$. The parameter δ is needed for the transformation to a not preconditioned system. It is set to $\delta = 1$ if the preconditioning is required and to $\delta = 0$ to switch the preconditioning off. This is the most commonly used preconditioning scheme by Turkel.

Turkel also applies the approach used in (4.50) to $\boldsymbol{q}_5$ variables. Again, a generalization of the incompressible preconditioning matrix is applied which leads to the compressible preconditioner

$$\boldsymbol{P}(\boldsymbol{q}_5) = \begin{bmatrix} \frac{1}{\rho\beta^2} & 0 & 0 & 0 \\ \frac{\alpha v_1}{\rho\beta^2} & 1 & 0 & 0 \\ \frac{\alpha v_2}{\rho\beta^2} & 0 & 1 & 0 \\ 0 & 0 & 0 & 1 \end{bmatrix} \tag{4.53}$$

If this matrix is transferred to $\boldsymbol{q}_4$ variables, assuming an ideal gas, it takes the following form:

$$\boldsymbol{P}(\boldsymbol{q}_4) = \begin{bmatrix} \frac{1}{\rho\beta^2} & 0 & 0 & 0 \\ \frac{\alpha v_1}{\rho\beta^2} & 1 & 0 & 0 \\ \frac{\alpha v_2}{\rho\beta^2} & 0 & 1 & 0 \\ \frac{1}{p}\left(\frac{c^2-1}{\beta^2}\right) & 0 & 0 & 1 \end{bmatrix}. \tag{4.54}$$

Hence, with the preconditioning scheme derived in the $\boldsymbol{q}_5$ notation, the entropy equation is no longer decoupled.

Another approach is taken by Briley et al. [9]. Their preconditioning matrix is derived in $\boldsymbol{q}_1$ variables and applied to the isoenergetic Navier Stokes equations. The preconditioning matrix takes the following form:

$$\boldsymbol{P}(\boldsymbol{q}_1) = \begin{bmatrix} 1 & 0 & 0 & 0 \\ 0 & 1 & 0 & 0 \\ 0 & 0 & 1 & 0 \\ 0 & 0 & 0 & \beta \end{bmatrix}$$

Here, the rate of change of the pressure contribution is decreased by a factor β. For this preconditioner, β is proportional to a parameter that resembles the square of the reference Mach number. It is given by

$$\beta = \begin{cases} M_{\text{ref}}^2, & M_{\text{ref}} < 1 \\ 1, & M_{\text{ref}} \geq 1, \end{cases}$$

where $M_{\text{ref}} = v_{\text{ref}}/\sqrt{\gamma R T_{\text{ref}}}$ with the isentropic exponent γ. The reference values v_{ref} and T_{ref} should be chosen such that they represent the global flow properties for the considered test case. For external flows, it is recommended to use the freestream values. Briley shows that the use of this preconditioner greatly improves the convergence rate at a reference Mach number of 0.05 for a turbulent flow through a ninety-degree channel bend.

Choi and Merkle [12],[11] study the convergence of implicit solutions of the Euler equations and introduce a similar preconditioning matrix. In conservative variables it takes the form

$$\boldsymbol{\Gamma}(\boldsymbol{u}) = \begin{bmatrix} 1 & 0 & 0 & 0 \\ 0 & 1 & 0 & 0 \\ 0 & 0 & 1 & 0 \\ \frac{q}{2}\left(Ma^{-2}-1\right) & v_1\left(1-Ma^{-2}\right) & v_2\left(1-Ma^{-2}\right) & Ma^{-2} \end{bmatrix}$$

when it is transformed from primitive variables using the ideal gas law. Here, Ma resembles the local Mach number. The preconditioner by Choi and Merkle is similar to the one by Briley, but a progress in the sence that it is no longer restricted to isoenergetic flows. In addition, it is implemented in conservative variables.

Erikson [22] presents an extension of the preconditioning matrix by Briley. They adapt the matrix so that the entropy of the system is preserved. This leads to the following preconditioning matrix:

$$\boldsymbol{P}(\boldsymbol{q}_1) = \begin{bmatrix} 1 & 0 & 0 & -\frac{1-\beta}{c^2} \\ 0 & 1 & 0 & 0 \\ 0 & 0 & 1 & 0 \\ 0 & 0 & 0 & \beta \end{bmatrix}$$

Erikson suggests a value for β of

$$\beta \approx \frac{v_1^2 + v_2^2}{c^2}.$$

Van Leer et al. [40] also present a family of preconditioning schemes in $\boldsymbol{q}_4$ variables and a flow-aligned coordinate system. However, these preconditioners require a well-defined flow angle. This can become a problem in the vicinity of the stagnation point or on unstructured meshes.

Weiss and Smith [77] take a different approach on the derivation of a preconditioning scheme formulated in $\boldsymbol{q}_2$ variables. Instead of multiplying a separate matrix $\boldsymbol{P}(\boldsymbol{q}_2)$ to the transformation matrices in equation (4.47), the product $\boldsymbol{P}(\boldsymbol{q}_2)\frac{\partial \boldsymbol{q}_2}{\partial \boldsymbol{u}}$ is replaced by the preconditioning matrix

$$\begin{bmatrix} \theta & 0 & 0 & \frac{\partial \rho}{\partial T} \\ 0 & \rho & 0 & 0 \\ 0 & 0 & \rho & 0 \\ -1 & 0 & 0 & \rho c_p \end{bmatrix},$$

where θ is given by

$$\theta = \left(\frac{1}{v_{\text{ref}}^2} - \frac{1}{\rho c_p} \frac{\partial \rho}{\partial T} \right)$$

with the reference velocity v_{ref} which is defined as follows:

$$v_{\text{ref}} = \begin{cases} \epsilon c, & |q| < \epsilon c \\ |\boldsymbol{v}|, & \epsilon c \leq |q| < c, \quad \epsilon = 10^{-5} \\ c, & |q| \geq c \end{cases} \tag{4.55}$$

Hence, the preconditioning matrix in conservative variables is given by

$$\boldsymbol{\Gamma}(\boldsymbol{u}) = \begin{bmatrix} \theta & 0 & 0 & \frac{\partial \rho}{\partial T} \\ \theta v_1 & \rho & 0 & v_1 \frac{\partial \rho}{\partial T} \\ \theta v_2 & 0 & \rho & v_2 \frac{\partial \rho}{\partial T} \\ \theta H - 1 & \rho v_1 & \rho v_2 & H \frac{\partial \rho}{\partial T} + \rho c_p \end{bmatrix}.$$

A similar approach is taken by Diangui [17] where a preconditioning matrix in $\boldsymbol{q}_3$ variables is constructed. The final form of this preconditioning matrix in conservative variables is

$$\boldsymbol{\Gamma}(\boldsymbol{u}) = \begin{bmatrix} \theta & 0 & 0 & \frac{\partial \rho}{\partial h} \\ \theta v_1 & \rho & 0 & v_1 \frac{\partial \rho}{\partial h} \\ \theta v_2 & 0 & \rho & v_2 \frac{\partial \rho}{\partial h} \\ \theta H - 1 & \rho v_1 & \rho v_2 & H \frac{\partial \rho}{\partial h} + \rho \end{bmatrix}, \tag{4.56}$$

where θ is given by

$$\theta = \left(\frac{1}{v_{\text{ref}}^2} - \frac{1}{\rho} \frac{\partial \rho}{\partial h} \right)$$

and v_{ref} is defined by equation (4.55).

4.3.1.1. Approaches for Real Gases

The preconditioning schemes described in the previous section are only designed for ideal gases. However, many relevant applications require a preconditioner that is applicable to a real gas, like the simulation of refrigerants in cooling channels or combustion processes that involve real gas thermodynamics. Hence, we review approaches to use preconditioners for real gases.

Especially the modeling of two-phase flows in the region of low Mach numbers is challenging, since the speed of sound can vary by multiple orders of magnitude between the different phases of the fluid, see for example Eddington [19]. This increases the difference between the eigenvalues of the system and hence intensifies the need for a preconditioning scheme. Particularly flows covering cavitation phenomena include both a wide range of thermodynamic states and compressible effects. The physics of cavitation are described in detail in Reisman et al. [57].

There are many approaches in the literature to apply preconditioning schemes to two

phase flows, e.g. for the simulation of cavitating flows. However, in these cases the gaseous and liquid phases are described by two different equations of state. Typically, the gas phase is assumed to follow the ideal gas law and the liquid phase is either modeled to be incompressible or is described by a stiffened equation of state. The latter is designed for water under very high pressures and treats the fluid as if it was an ideal gas that is already under a very high pressure. A detailed description of the stiffened equation of state and further developments can be found in O Le Métayer and Saurel [39].
In the work of Merkle et al. [50], a preconditioning scheme for ideal gases is applied to a two-phase flow by using the mass fraction of one fluid as the dependent variable. A similar path is taken by Kunz et al. [37] with the difference that the volume fraction is taken as a variable. In these approaches, the densities for both the liquid and vapor phases are assumed to be constant and hence no real gas effects are considered.
More detailed models for two phase flows apply separate continuity equations for the different phases including special mass transfer terms that account for the phase change. The work of Venkateswaran et al. [71], [72] is an example for such a scheme. These models are usually called homogeneous mixture model since the interface between the liquid and the gaseous phase is assumed to be in dynamic and thermal equilibrium and hence the momentum and energy equations are formulated for the mixture. In their work, Venkateswaran et al. use a preconditioning method to model compressible cavitation. However, the densities of the different phases are kept constant in the earlier work. In the more recent publication the density varies with pressure but is independent of the other thermodynamic properties. So again, real gas effects are not examined.
There are many more schemes that apply ideal gas preconditioners to two phase flows, for example the work of Murrone and Guillard [52], Chen at al. [10] and Goncalves and Patella [26]. But in these works, the different fluids are treated either as an ideal gas or are described by a simplified equation. Hence, these approaches do not consider the mathematical properties of a real gas equation of state.
Zong and Yang [79], on the other hand, adapt the preconditioning scheme by Weiss and Smith to a cubic equation of state. Since the formulation of this preconditioner requires thermodynamic derivatives of the state variables instead of applying the ideal gas assumptions, it is in general possible to apply it to a real gas equation of state.
In their work, Zong and Yang present a detailed derivation of all required thermodynamic quantities and derivatives. However, they only apply their preconditioning scheme to supercritical flows. In a test case of a flow around the NACA0012 profile at subcritical conditions, we find that a numerical scheme with this specific preconditioner does not converge to a steady state solution below an inflow Mach number of about 0.05. There-

fore, this preconditioning scheme is not suitable for our purposes, while it works well for supercritical conditions and a Mach number around 10^{-1}, which is sufficient for some applications.

4.3.2. Different Requirements for a Van der Waals gas

The purpose of multiplying a preconditioning matrix to the flux Jacobi matrix is to gain a condition number close to one. Hence, an ideal preconditioning matrix would be the inverse of the flux Jacobi matrix. But it is numerically expensive to calculate this inverse at every grid point. In addition, the exact form of the flux Jacobi matrix is generally not known and hence the direct calculation of the inverse is not possible. Therefore, preconditioning matrices are approximations of the inverse of the flux Jacobi matrices, that are numerically more easily calculated and have one general form for every grid cell. In section 4.2.3 starting on page 49, we show that the differences in the equation of state lead to different behaviors of the entries of the flux Jacobi matrix as the Mach number approaches zero. The derivative of pressure with respect to density strongly depends on the chosen state equation. For an ideal gas it is of order $\mathcal{O}(M^2)$ as the Mach number approaches zero while for a Van der Waals gas it is of order $\mathcal{O}(1)$. This difference leads to a different behavior of certain terms of the flux Jacobi matrix.
Since the preconditioning matrix approximates the inverse flux Jacobi matrix, a preconditioner built for the ideal gas Euler equations cannot, in general, lead to a favorable condition number of the Van der Waals gas flux Jacobi matrix. The different behavior of the terms of the flux Jacobi matrix as the Mach number approaches zero need to be considered when the preconditioning scheme is built. Hence, in general, for an ideal gas and a Van der Waals gas, different preconditioning schemes are required.
In section 4.2.3, we analyze the continuous flux Jacobi matrix of the Euler equations in x_1-direction. There we also refer to the differences between this matrix and the one in x_2-direction. The flux Jacobi matrix representing the flux function contains the properties of all directional Jacobi matrices of the Euler equations.
Since the preconditioning matrix is applied to the Jacobi matrix representing the flux function, we cannot build separate preconditioning schemes for the different spatial directions but have to include all properties in one single matrix as well. The differences between the continuous Jacobi matrices in the different spatial directions only concern the momentum equations. From this, we can formulate requirements for a preconditioning scheme that contains the properties of the inverses of all directional matrices:

- For the rows of the matrix that represent the momentum equations, both the terms multiplied by $\triangle\rho$ and the ones multiplied by $\triangle(\rho E)$ only differ by the respective

Cartesian velocity.

- The terms on the principal axis in the two rows of the momentum equations are identical. They only vary in the square of the respective Cartesian velocity, if at all.
- The same holds for the terms that are multiplied by $\triangle(\rho v_1)$ and $\triangle(\rho v_2)$ of these two rows that are not on the principal axis.
- The terms multiplied by momentum differences in both the mass and energy equation only differ by the respective Cartesian velocity each

Hence, the preconditioning matrix takes the form

$$\boldsymbol{\Gamma}(\boldsymbol{u}) = \begin{bmatrix} \eta_1 & \eta_2 v_1 & \eta_2 v_2 & \eta_3 \\ \eta_4 v_1 & \eta_5 v_1^2 & \eta_6 v_1 v_2 & \eta_7 v_1 \\ \eta_4 v_2 & \eta_6 v_1 v_2 & \eta_5 v_2^2 & \eta_7 v_2 \\ \eta_8 & \eta_9 v_1 & \eta_9 v_2 & \eta_{10} \end{bmatrix} \tag{4.57}$$

with the ten functions η_1 to η_{10} that need to be defined. These functions are in terms of the thermodynamic properties pressure, density and enthalpy or temperature as well as properties of the fluid but independent of the velocity. So, the requirements we define for the preconditioner reduce the entries of the matrix we need to define to ten. Note that no additional entry is necessary to transfer this scheme to three spatial dimensions. If a preconditioning matrix fulfills these requirements, the resulting matrices of a preconditioning of the flux Jacobi matrix of the Euler equations in any spatial direction have similar condition numbers. They only differ due to the specific flow situation. Hence, we can limit the analysis of preconditioning matrices to the effect on the flux Jacobi matrix in only one spatial direction and still get a generally valid result.
In addition, with these requirements an approximation of the inverse of the continuous flux Jacobi matrix of the Euler equations has comparable effects to an approximation of the inverse of the Jacobi matrix of a numerical flux function. That means that the resulting condition numbers are within a small range when both approximated matrices are used to precondition either the continuous Jacobi matrix of the Euler equations or a Jacobi matrix that represents a numerical flux function. Since the continuous flux Jacobi matrix has a simpler form compared to the MAPS+ flux Jacobi matrix, we choose the former as the base for the construction of a preconditioning scheme applicable to a Van der Waals gas. The resulting preconditioner is presented in the following section.

4.3.2.1. Analytical Demonstration

To demonstrate the different requirements on an ideal gas and a Van der Waals gas preconditioner, we look at their effects on a flux Jacobi matrix. For the ideal gas preconditioning scheme, we take the preconditioner presented by Turkel in $\boldsymbol{q}_2 = (p, v_1, v_2, T)$ variables

$$\boldsymbol{P}(\boldsymbol{q}_2)_{Turkel} = \begin{bmatrix} \frac{1}{\beta^2} - (\gamma - 1)\delta & 0 & 0 & \frac{\gamma p}{T}\delta \\ \frac{\alpha v_1}{\rho\beta^2 c^2} & 1 & 0 & 0 \\ \frac{\alpha v_2}{\rho\beta^2 c^2} & 0 & 1 & 0 \\ \frac{1}{\rho c_p}\left(\frac{1}{\beta^2} - g\right) & 0 & 0 & g \end{bmatrix},$$

with $g = 1 + (\gamma - 1)\,\delta$. Here, we set $\alpha = 0$ and $\delta = 1$ since this combination shows to be a good choice for flows that are at an overall low Mach number, see Turkel et al. [69]. For β we choose the relation

$$\beta = \min\left[\max\left(|q|^2, K|q_\infty|^2\right), c^2\right],$$

where K is a constant which is set to one and $|q_\infty|$ is the absolute value of the inflow velocity.
To transfer the matrix to conservative variables, we multiply it by the two transformation matrices for an ideal gas:

$$\begin{aligned} \boldsymbol{\Gamma}(\boldsymbol{u})_{Turkel} &= \left(\frac{\partial \boldsymbol{u}}{\partial \boldsymbol{q}_2}\right)_{id} \boldsymbol{P}(\boldsymbol{q}_2)_{Turkel} \left(\frac{\partial \boldsymbol{q}_2}{\partial \boldsymbol{u}}\right)_{id} \\ &= \begin{bmatrix} 1 + \xi_1 & \xi_2 v_1 & \xi_2 v_2 & -\xi_2 \\ \xi_1 v_1 & 1 + \xi_2 v_1^2 & \xi_2 v_1 v_2 & -\xi_2 v_1 \\ \xi_1 v_2 & \xi_2 v_1 v_2 & 1 + \xi_2 v_2^2 & -\xi_2 v_2 \\ \frac{c^2}{\gamma - 1}\xi\xi_1 & \xi v_1 & \xi v_2 & 1 - \xi \end{bmatrix} \end{aligned}$$

with

$$\xi = 1 + \frac{\gamma - 1}{2} Ma^2,$$

$$\xi_1 = \frac{\beta}{c^2} - \frac{q^2}{2}\xi_2$$

and

$$\xi_2 = \frac{\gamma - 1}{c^2}.$$

If we compare this matrix to the requirements for a preconditioning scheme we list at the beginning of section 4.3.2, we see that all requirements are indeed met.
For the Van der Waals gas preconditioning scheme, we take the matrix written in equation (4.57) in the slightly modified form

$$\boldsymbol{\Gamma}(\boldsymbol{u}) = \begin{bmatrix} \eta_1 & \eta_2 v_1 & \eta_2 v_2 & \eta_3 \\ \eta_4 v_1 & \eta_5 & \eta_6 v_1 v_2 & \eta_7 v_1 \\ \eta_4 v_2 & \eta_6 v_1 v_2 & \eta_5 & \eta_7 v_2 \\ \eta_8 & \eta_9 q & \eta_9 q & \eta_{10} \end{bmatrix}$$

with the following definitions of the functions η_1 to η_{10}:

$$\eta_1 = \frac{5M_w^2 p - 3M_w bp\rho + a\rho^2}{5M_w^2 p - a\rho^2},$$

$$\eta_2 = \eta_6 = \frac{2M_w^2 \rho}{5M_w^2 p - a\rho^2},$$

$$\eta_3 = \eta_7 = -\frac{2M_w^2 \rho}{5M_w^2 p - a\rho^2},$$

$$\eta_4 = -\frac{\rho\left(3M_w^2 bp - 2M_w a\rho + 9ab\rho^2\right)}{5M_w^3 p - M_w a\rho^2},$$

$$\eta_5 = 1,$$

$$\eta_8 = \frac{-15M_w^3 bp^2 + 10M_w^2 ap\rho + 9M_w^2 b^2 p^2 \rho - 54M_w abp\rho^2 + 2a^2\rho^3}{10M_w^4 p - 2M_w^2 a\rho^2},$$

$$\eta_9 = \frac{15M_w^2 p - 30M_w bp\rho + 7a\rho^2}{10M_w^2 p - 2a\rho^2}$$

and

$$\eta_{10} = \frac{\rho\left(3M_w^2 bp - 2M_w a\rho + 9ab\rho^2\right)}{5M_w^3 p - M_w a\rho^2}$$

This matrix approximates the inverse of the flux Jacobi matrix of the Euler equations for a Van der Waals gas represented by the caloric equation of state (2.14) on page 14. Since the procedure of taking an inverse of a fully occupied matrix requires many steps, we use the python library SymPy to calculate the inverse. The presented matrix is then acquired by considering the requirements stated at the beginning of section 4.3.2. It is formulated in conservative variables.
To compare the two preconditioning matrices, we multiply each matrix with both the ideal gas and the Van der Waals gas flux Jacobi matrix in x_1-direction. In the next

step, we calculate the eigenvalues of the resulting matrices and the respective condition numbers and compare them with each other. In Table 4.2, the values used for the calculations are listed. For β, we use the expression $\beta = \left(v_1^2 + v_2^2\right)$.

Table 4.2.: Conditions for the calculations of the eigenvalues

Values	Ideal Gas	Van der Waals (Oxygen)
γ	1.39502	-
M_w	-	0.0226820
a	-	$1.38191 \cdot 10^{-6}$
b	-	$3.18575 \cdot 10^{-5}$
c	1.39502	1.39502
p	1	1
ρ	-	1
T	1	-
v_1	$10^{-1}/10^{-4}$	$10^{-1}/10^{-4}$
v_2	$10^{-1}/10^{-4}$	$10^{-1}/10^{-4}$
β	$2 \cdot 10^{-2}/2 \cdot 10^{-8}$	$2 \cdot 10^{-2}/2 \cdot 10^{-8}$

In Table 4.3, the eigenvalues and corresponding condition numbers are listed for preconditioning of both the ideal gas and the Van der Waals gas flux Jacobi matrix by each preconditioning scheme. In addition, we present the values of the non-preconditioned matrices.

From the values, we see that there is only a small difference between the two preconditioning schemes at a Mach number of $M = 10^{-1}$. Both preconditioners lead to a lower condition number when they are applied to the ideal gas flux Jacobi matrix. The condition number in the case of a Van der Waals gas matrix is higher but still well below 10. Compared to the cases without preconditioning, both preconditioners improve the condition number by a factor of 6.5 in the ideal gas case and 4 in the Van der Waals gas case. However, at this Mach number, most numerical schemes converge well without a preconditioning scheme. So, the preconditioners are not yet required in this Mach number regime.

At the lower Mach number of $M = 10^{-4}$, there is a notable difference between the two schemes. The preconditioner of Turkel works as well for the ideal gas flux Jacobi matrix as it does at the Mach number of 10^{-1}. The same applies for the Van der Waals gas preconditioner applied to the corresponding flux Jacobi matrix. In both cases, the condition numbers are the same for both Mach numbers. Compared to the calculations without a preconditioning schemes the condition numbers are lowered by about four orders of magnitude in both cases. Hence, here the preconditioners produce the expected

Table 4.3.: Eigenvalues and condition numbers of the resulting matrices from the preconditioning of the ideal gas and the Van der Waals gas flux Jacobi matrix with the two preconditioning schemes at Mach numbers $M = 10^{-1}$ and $M = 10^{-4}$, as well as the values of the non-preconditioned matrices

Preconditioner	Mach Number	Flux Jacobi Matrix	Eigenvalues	Condition Number
Turkel	10^{-1}	ideal gas	-0.078, 0.1, 0.1, 0.18	2.3
Turkel	10^{-4}	ideal gas	$-7.8 \cdot 10^{-5}$, $1.0 \cdot 10^{-4}$, $1.0 \cdot 10^{-4}$, $1.8 \cdot 10^{-4}$	2.3
Turkel	10^{-1}	Van der Waals	-0.084, 0.064, 0.1, 0.22	3.5
Turkel	10^{-4}	Van der Waals	$-6.5 \cdot 10^{-9}$, $1.0 \cdot 10^{-4}$, $1.0 \cdot 10^{-4} + 0.014i$, $1.0 \cdot 10^{-4} + 0.014i$	$2.1 \cdot 10^{6}$
VdW	10^{-1}	ideal gas	-0.15, 0.1, 0.17, 0.24	2.4
VdW	10^{-4}	ideal gas	$-2.6 \cdot 10^{-8}$, $1.0 \cdot 10^{-4}$, $1.3 \cdot 10^{-4} + 0.015i$, $1.3 \cdot 10^{-4} - 0.015i$	$5.6 \cdot 10^{5}$
VdW	10^{-1}	Van der Waals	-0.15, 0.1,0.1, 0.35	3.5
VdW	10^{-4}	Van der Waals	$-1.4 \cdot 10^{-4}$, $1.0 \cdot 10^{-4}$, $1.0 \cdot 10^{-4}$, $3.5 \cdot 10^{-4}$	3.5
none	10^{-1}	ideal gas	-1.3, 0.1, 0.1, 1.5	15
none	10^{-4}	ideal gas	-1.4, $0.1 \cdot 10^{-4}$, $0.1 \cdot 10^{-4}$, 1.4	$1.4 \cdot 10^{4}$
none	10^{-1}	Van der Waals	-1.2, 0.1, 0.1, 1.4	14
none	10^{-4}	Van der Waals	-1.3, $0.1 \cdot 10^{-4}$, $0.1 \cdot 10^{-4}$, 1.3	$1.3 \cdot 10^{4}$

results.

However, if the preconditioning schemes are applied to the matrices they are not designed for, they increase the condition numbers of the matrices. So, they enlarge the stiffness of the problem. In addition, both preconditioners lead to complex eigenvalues.

So, at low Mach numbers, a preconditioning scheme that is used for a set of equations containing a different thermodynamic relation than the one enclosed in the preconditioner causes two problems. It increases the condition number and also worsens the circumstances for the numerical solver by producing complex eigenvalues. One possible effect of complex eigenvalues is that they are no longer within the stability domain of the time integration scheme and hence cause it to abort.

It is also possible to repeat this analytical investigation with the MAPS+ flux Jacobi matrix. The resulting eigenvalues are similar to the ones for the flux Jacobi matrices of

the Euler equations presented here. In addition, similar results can be obtained for other values of the variables listed in Table 4.2.
This analytical demonstration also shows that it is possible to successfully precondition a Van der Waals gas flux Jacobi matrix. The premise is that the used preconditioning scheme is designed for a Van der Waals gas. Then favorable eigenvalues can be gained. However, the thermodynamic relations the presented Van der Waals gas preconditioning scheme is based on are not the same as the ones implemented in the DLR TAU-code. This preconditioner is based on the analytic caloric equation of state as it is derived in equation (2.14) on page 14, while the real gas thermodynamics implemented in the DLR TAU-code are based on an iterative calculation of thermodynamic properties within the code. These two versions of real gas thermodynamics do not agree with each other. Hence, the behavior of the terms of the transformation matrices $\frac{\partial \boldsymbol{u}}{\partial \boldsymbol{q}}$ and $\frac{\partial \boldsymbol{q}}{\partial \boldsymbol{u}}$ as the Mach number approaches zero cannot be expected to be the same. So, the presented preconditioner cannot lead to favorable eigenvalues when it is used in the DLR TAU-code together with the implemented thermodynamics.

4.3.3. Preconditioning scheme for a Van der Waals gas

For the flux Jacobi matrices and hence for the preconditioning scheme, the transformation matrices between primitive and conservative variables are the relevant difference between an ideal gas and a Van der Waals gas. Especially in the limit of a low Mach number, some of the terms of these matrices show different behaviors depending on the applied equation of state. We discuss this in detail in section 4.2.3 starting on page 49.
This difference is why a preconditioning scheme in conservative variables that is built for an ideal gas cannot be used for a Van der Waals gas and vice versa. However, in primitive variables a preconditioning scheme is applicable to either gas, as long as no assumptions concerning the thermodynamic equations are used to build the scheme.
Therefore, the preconditioners by Turkel stated in equations (4.50) and (4.53) on page 102 are applicable to both an ideal gas and a Van der Waals gas, while the preconditioners described in equations (4.51) and (4.54) are limited to an ideal gas. All preconditioning matrices in equations (4.50) to (4.54) are derived in a similar way, but in different sets of variables. We have to consider this when we choose a preconditioning scheme.
Hence, for the following simulations, we choose the preconditioner described by equation (4.52) as it is a generalization of the scheme described in equation (4.50). However, to avoid the limitation to an ideal gas, we conduct the change from $\boldsymbol{q}_4$ to $\boldsymbol{q}_2$ variables in general terms using the derivatives of the thermodynamics implemented in the DLR TAU-code.

In a similar way, the preconditioning scheme by Diangui presented in equation (4.56) can be applied to a Van der Waals gas. Here, we simply have to evaluate the derivatives of enthalpy using the real gas thermodynamic relations implemented in the code.
In a last step, we transfer the preconditioning schemes from primitive to conservative variables. We use the numerical derivatives of the implemented thermodynamic relations to create the transformation matrices. This leads to the final preconditioning schemes formulated in conservative variables. Compared to the preconditioning scheme presented in section 4.3.2.1, this approach has the disadvantage that the numerical derivatives need to be evaluated for every grid cell at each time step. However, it has the advantage that the formulation of the preconditioner is independent of the used equation of state as long as the derivatives are defined in an appropriate way. Hence, this method can be applied to any implemented thermodynamic relation while the preconditioning scheme shown in section 4.3.2.1 is limited to one single caloric equation of state.

4.3.4. Numerical Results

We choose the inviscid flow around a NACA0012 profile as a test case for the numerical results. This is the same setup as in section 4.2.5. We also use similar initial and boundary conditions as for the computations in section 4.2.5 and the same grid. All calculations are conducted using a two-step Runge-Kutta scheme with a CFL number of 0.8.
First, we present results of the two chosen preconditioning schemes for a Van der Waals gas. We compare these results with each other and with a reference solution of an ideal gas at one set of thermodynamic conditions and for two different Mach numbers. For the ideal gas, we use the preconditioner of Turkel presented in equation (4.51) on page 101. The fluxes are calculated with the altered MAPS+ scheme for the low Mach region that we analyze in section 4.2.4. For the comparison of the schemes, we consider both field solutions of different quantities and the convergence rate. The quantities we present in the field solutions are pressure, density, the x_1-component of velocity and the local Mach number.
In the next step we compare the convergence rate of the two chosen preconditioning schemes. We present the convergence rates of both preconditioners for one set of thermodynamic properties but multiple inflow Mach numbers. This way, we can show that both preconditioning schemes have a convergence rate independent of the Mach number for $M \to 0$.
Finally, we demonstrate the capability of the preconditioning scheme of Diangui. We show the results of simulations for a wide range of thermodynamic conditions for two

different Van der Waals gases. The conditions used for the calculations are summarized in Table 4.4. Again, we present field solutions of pressure, density, the x_1-component of velocity and the Mach number.

Table 4.4.: Conditions used for the calculations

Condition	fluid	state	inflow pressure	inflow temperature
1	nitrogen	gas	$10^5 Pa$	$300K$
2	nitrogen	liquid	$10^4 Pa$	$64K$
3	nitrogen	supercritical	$10^6 Pa$	$300K$
4	ideal gas	gas	$10^5 Pa$	$273.15K$
5	oxygen	gas	$10^5 Pa$	$300K$
6	oxygen	liquid	$10^5 Pa$	$64K$
7	oxygen	supercritical	$10^6 Pa$	$300K$

4.3.4.1. Comparison of preconditioning schemes

First, we present the numerical solutions of the flow around a NACA0012 profile. The considered fluid is nitrogen modeled as a Van der Waals gas. The inflow Mach number is $M = 10^{-3}$ and condition 1 in Table 4.4 is used.

In Figures 4.5 and 4.6, the numerical results are shown. They are obtained with the preconditioning schemes by Turkel and Diangui, respectively. In both figures, the field solutions of the thermodynamic properties are presented in the upper row, with pressure on the left and density on the right-hand side. In the bottom row, the subfigure on the left-hand side shows the distribution of the x_1-component of velocity and the subfigure on the right-hand side presents the Mach number distribution. Again, the plots of the thermodynamic properties show the difference to the background values since these differences are very small in comparison.

The pressure distributions in these figures are similar to the one shown in Subfigure 4.2f on page 93 that is obtained without a preconditioning scheme. So as expected, the use of a preconditioning scheme does not change the solution.

The density distributions in Subfigures 4.5b and 4.6b show the offset to the background density of $1.284068 \frac{kg}{m^3}$. This value indicates that the modeled nitrogen is indeed at a gaseous state. The plotted density differences are of the order of $10^{-7} \frac{kg}{m^3}$ which is due to the low Mach number.

The distributions of the Mach number shown in Subfigures 4.5d and 4.6d have a slimmer shape than the x_1-velocity distributions shown in Subfigures 4.5c and 4.6c. This shows the influence of variations of thermodynamic quantities such as pressure or density on the speed of sound.

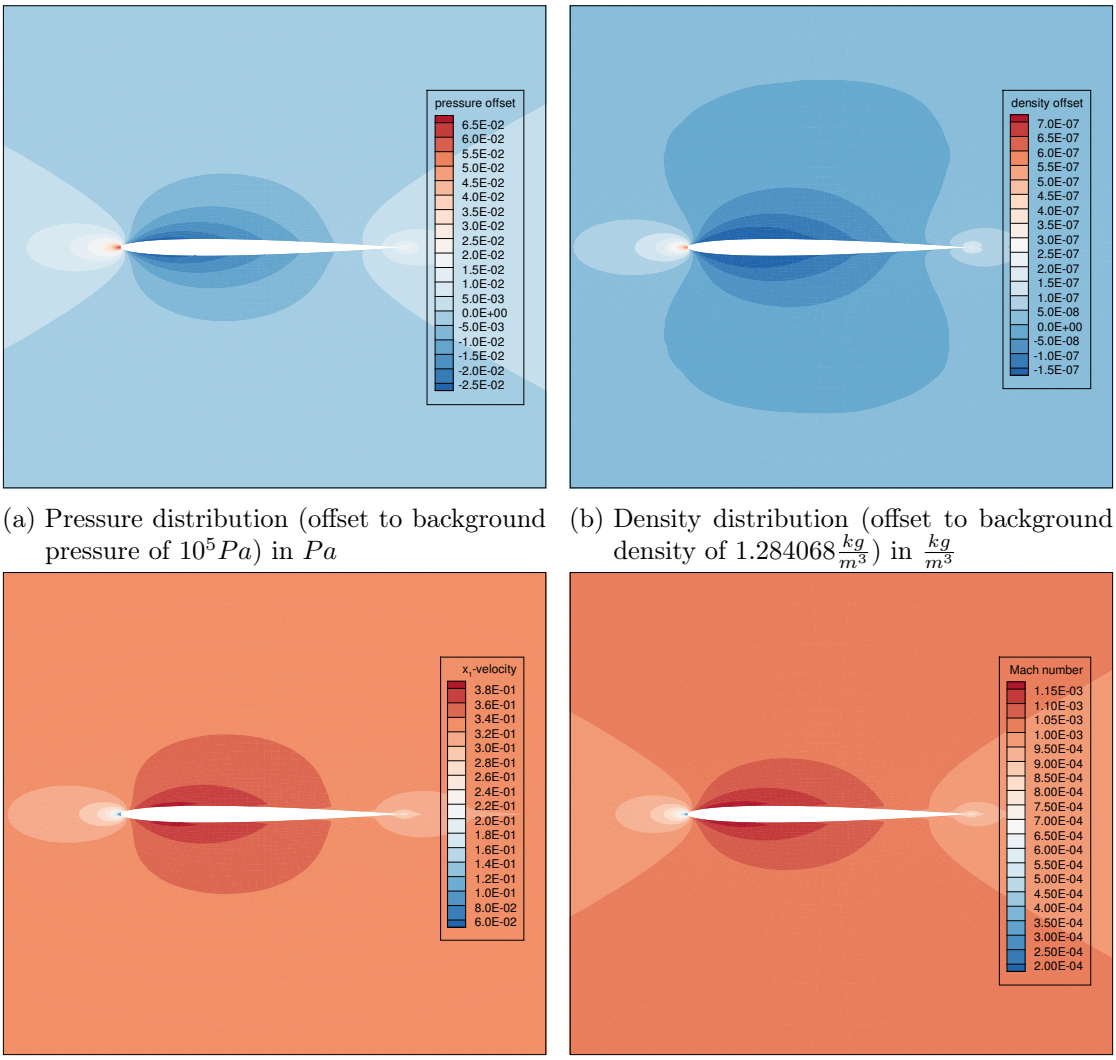

(a) Pressure distribution (offset to background pressure of $10^5 Pa$) in Pa

(b) Density distribution (offset to background density of $1.284068 \frac{kg}{m^3}$) in $\frac{kg}{m^3}$

(c) x_1-velocity distribution in $\frac{m}{s}$

(d) Mach number distribution

Figure 4.5.: Field solutions for a Van der Waals gas obtained using the preconditioning scheme by Turkel at a Mach number of $Ma_{\text{in}} = 10^{-3}$

In general, we see similar results for all plotted quantities in both figures. It can be said that the numerical scheme is able to converge to a reasonable solution using each preconditioning scheme at the presented inflow Mach number.

As a reference, in Figure 4.7 the distributions of the same quantities are shown for the flow of an ideal gas around the NACA0012 profile. The inflow Mach number is set to $Ma_{\text{in}} = 10^{-3}$ and condition 4 in Table 4.4 is used for the inflow pressure and temperature. We choose the Mach number and pressure this way to be the same as for the calculations

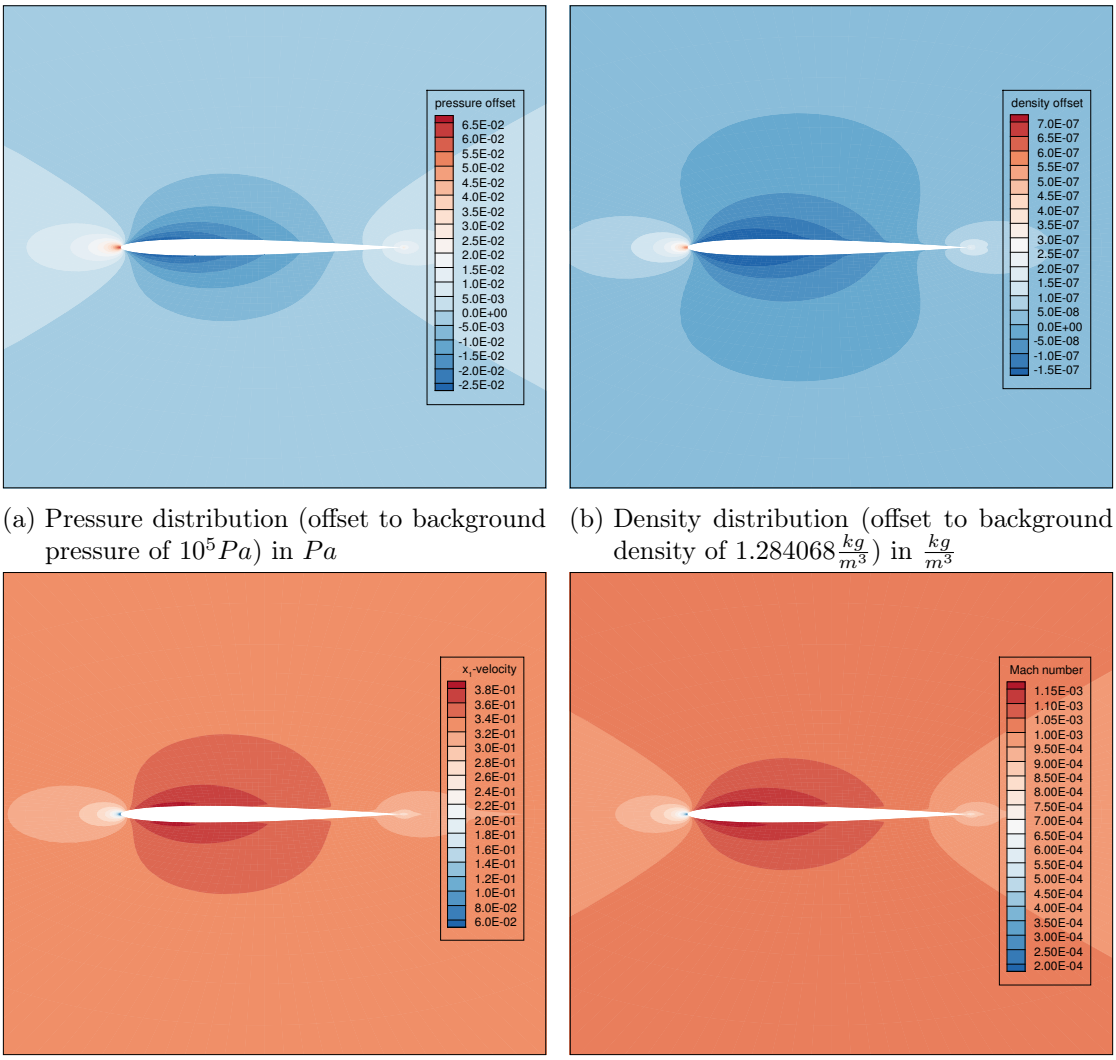

(a) Pressure distribution (offset to background pressure of $10^5 Pa$) in Pa

(b) Density distribution (offset to background density of $1.284068 \frac{kg}{m^3}$) in $\frac{kg}{m^3}$

(c) x_1-velocity distribution in $\frac{m}{s}$

(d) Mach number distribution

Figure 4.6.: Field solutions for a Van der Waals gas obtained using the preconditioning scheme by Diangui at a Mach number of $Ma_{\text{in}} = 10^{-3}$

using the Van der Waals thermodynamic modeling, while the temperature results from the ideal gas law.

As expected, the numerical solver converges to a reasonable solution for the ideal gas case. In addition, the ideal gas solution is qualitatively similar to the solutions obtained for a Van der Waals gas. This strengthens the statement that the solver converges to a reasonable solution for the Van der Waals gas.

The background density in Subfigure 4.7b is slightly lower than the one in the cases for

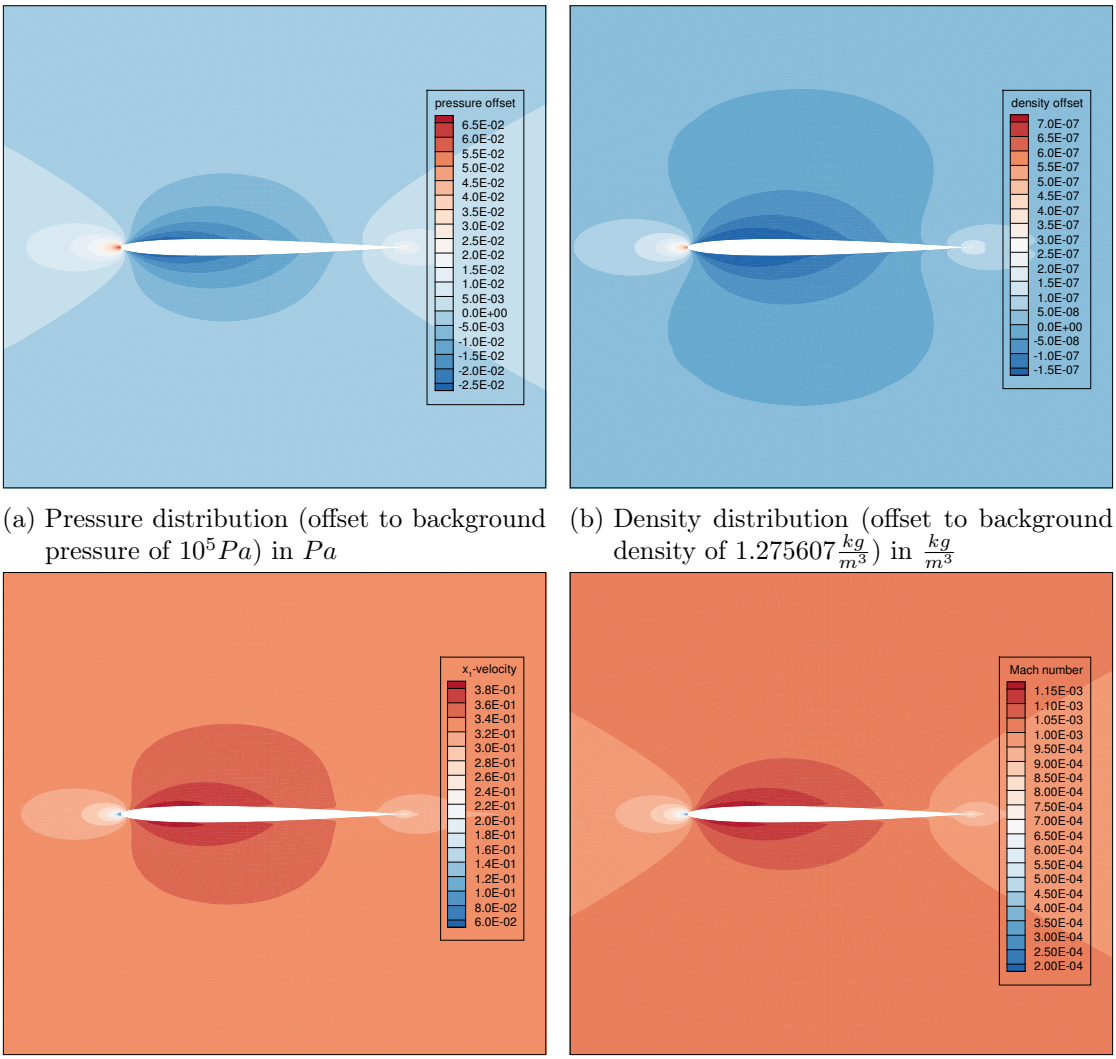

(a) Pressure distribution (offset to background pressure of $10^5 Pa$) in Pa

(b) Density distribution (offset to background density of $1.275607 \frac{kg}{m^3}$) in $\frac{kg}{m^3}$

(c) x_1-velocity distribution in $\frac{m}{s}$

(d) Mach number distribution

Figure 4.7.: Field solutions for an ideal gas obtained using the preconditioning scheme by Turkel at a Mach number of $Ma_{\text{in}} = 10^{-3}$

a Van der Waals gas shown in Subfigures 4.5b and 4.6b. The inflow temperature in the ideal gas case is slightly lower than for the calculations with a Van der Waals gas which should lead to a higher density due to the ideal gas law. The lower value of the density in comparison is due to the fact that the ideal gas does not exactly represent nitrogen and hence there are differences in the modeling compared to the modeling as a Van der Waals gas. Apart from this difference, the results of the ideal gas calculations closely resemble the ones for a Van der Waals gas. This makes sense as the chosen conditions

lay well within the region where ideal gas assumptions are valid. Hence, the deviations due to real gas effects are very small.

Now, we present the solution of a repetition of these calculations for an inflow Mach number of $Ma_{\text{in}} = 10^{-4}$ while all other parameters stay unchanged. In Figures 4.8 and 4.9, the results for the numerical simulations using the Van der Waals gas thermodynamics are shown. Again, the applied preconditioning schemes are the ones by Turkel and Diangui, respectively. The order of the subfigures is the same as in Figures 4.5 to 4.7.

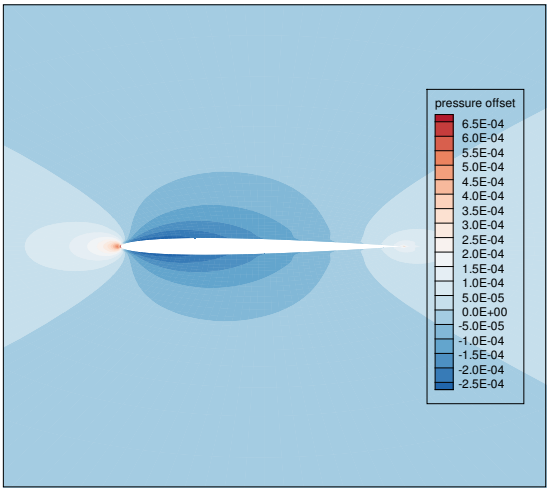

(a) Pressure distribution (offset to background pressure of $10^5 Pa$) in Pa

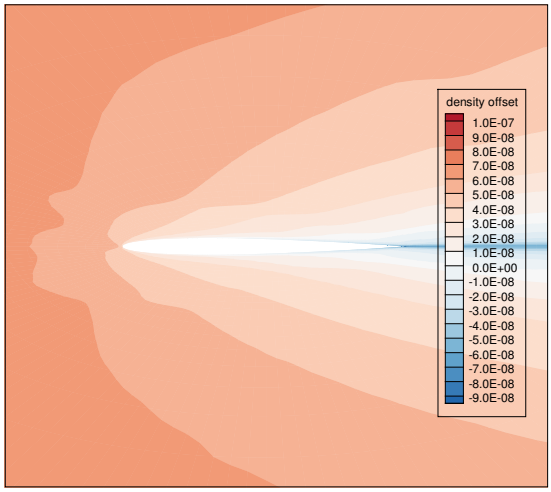

(b) Density distribution (offset to background density of $1.284068 \frac{kg}{m^3}$) in $\frac{kg}{m^3}$

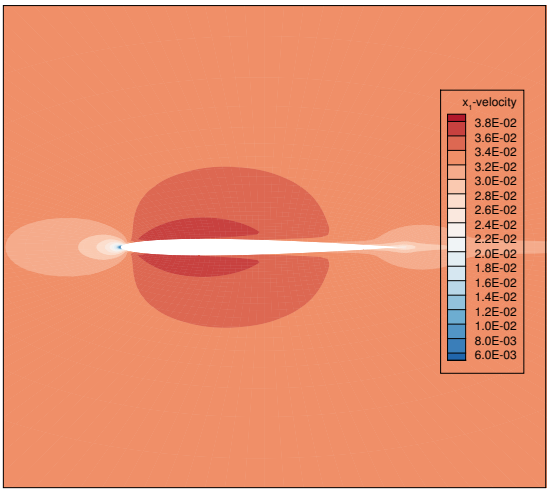

(c) x_1-velocity distribution in $\frac{m}{s}$

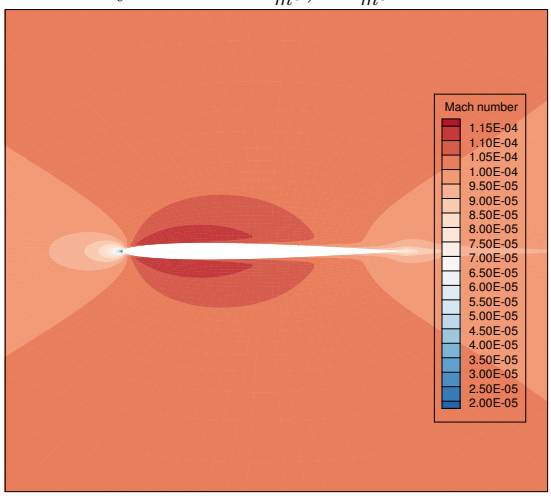

(d) Mach number distribution

Figure 4.8.: Field solutions for a Van der Waals gas obtained using the preconditioning scheme by Turkel at a Mach number of $Ma_{\text{in}} = 10^{-4}$

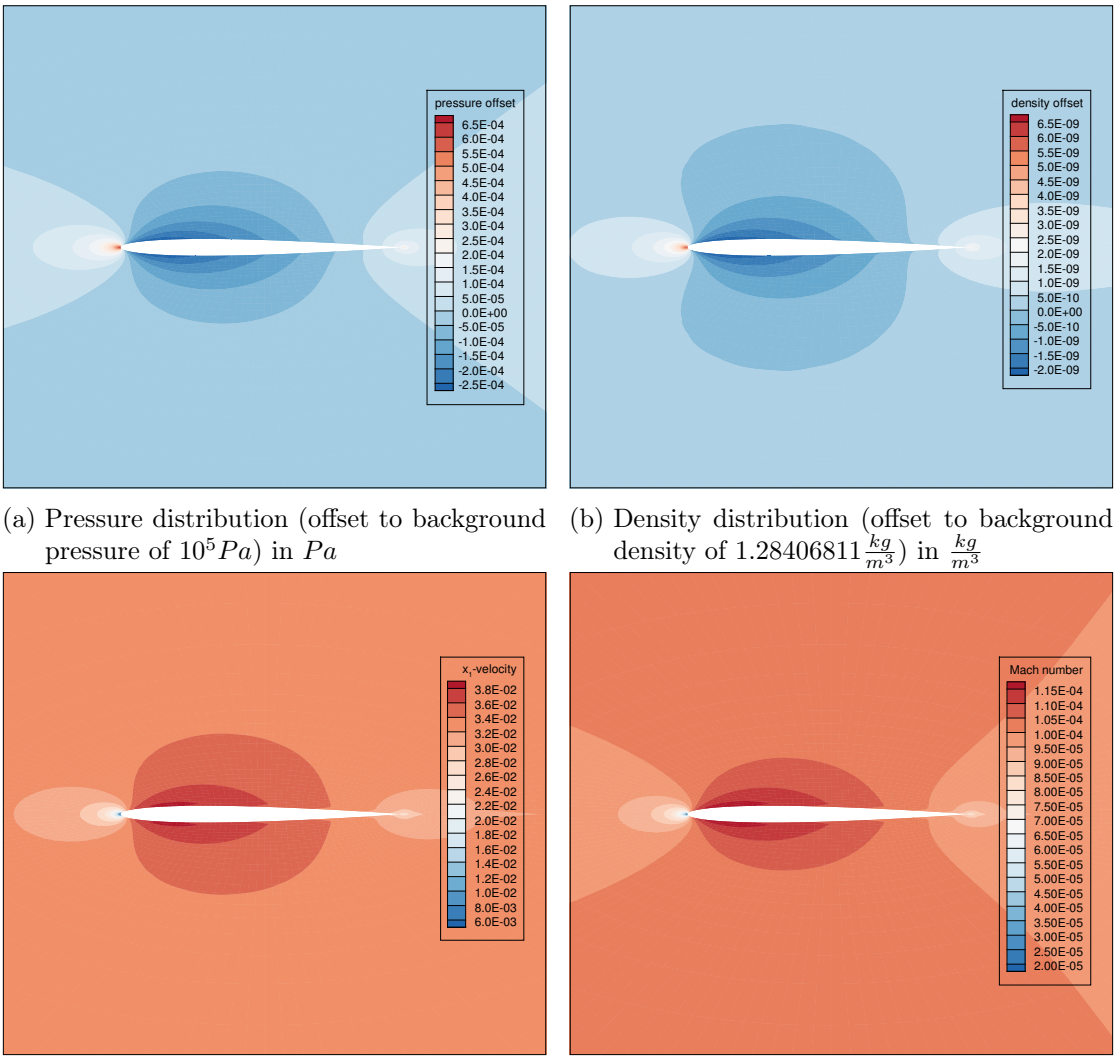

(a) Pressure distribution (offset to background pressure of $10^5 Pa$) in Pa

(b) Density distribution (offset to background density of $1.28406811 \frac{kg}{m^3}$) in $\frac{kg}{m^3}$

(c) x_1-velocity distribution in $\frac{m}{s}$

(d) Mach number distribution

Figure 4.9.: Field solutions for a Van der Waals gas obtained using the preconditioning scheme by Diangui at a Mach number of $Ma_{\text{in}} = 10^{-4}$

Both schemes produce similar results for the majority of the quantities. The pressure distribution, the flow field of the x_1-component of the velocity and the distribution of the Mach number are all alike. But only the calculations done with the preconditioning scheme by Diangui result in a reasonable distribution of density.

Looking at Subfigure 4.9b, we see that the difference of the density to the background value is of the order of $10^{-9} \frac{kg}{m^3}$. The density distribution obtained with the preconditioning scheme of Turkel shown in Subfigure 4.8b contains values of the order of $10^{-8} \frac{kg}{m^3}$. This

is the numerical error that overlies the actual density distribution. So due to this error, the preconditioning scheme by Turkel cannot produce reasonable results for the density distribution and hence is not applicable at an inflow Mach number of $Ma_{\text{in}} = 10^{-4}$ for this configuration.

Comparing the results obtained for an inflow Mach number of $Ma_{\text{in}} = 10^{-4}$ in Figures 4.8 and 4.9 with the ones for the inflow Mach number of $Ma_{\text{in}} = 10^{-3}$ in Figures 4.5 and 4.6, we notice that all distributions are qualitatively similar in both cases (except for Subfigure 4.8b). This is because the solution becomes self-similar in the incompressible limit, so the qualitative nature of the distribution of any quantity becomes independent of the Mach number as $M \to 0$. The fact that the shown distributions are qualitatively similar is a strong indication that the preconditioning schemes work as expected.

As a reference, we present the results of the ideal gas simulations at an inflow Mach number of $Ma_{\text{in}} = 10^{-4}$ in Figure 4.10. The other inflow conditions are similar to the case of the inflow Mach number of 10^{-3}. Again, in the ideal gas case the numerical solver converges to a reasonable solution.

The distributions of pressure, x_1-component of velocity and Mach number shown in Subfigures 4.10a, 4.10c and 4.10d are similar to the ones obtained with the two Van der Waals gas preconditioners in the real gas case. The density distribution in Subfigure 4.10b is similar to the one shown in Subfigure 4.9b that is obtained with the preconditioning scheme by Diangui. This underlines the quality of the solution obtained with the preconditioning scheme by Diangui.

In addition to the flow field, we compare the convergence rates for all three preconditioning schemes in Figure 4.11. In the three subfigures, the normalized density residuum is plotted over the number of iterations for both Van der Waals gas preconditioning schemes in the upper and middle plot and the ideal gas scheme as a reference in the bottom plot. The convergence rates belong to the calculations done at an inflow Mach number of $Ma_{\text{in}} = 10^{-3}$ with the results shown in Figures 4.5 to 4.7.

At these conditions, both preconditioning schemes for a Van der Waals gas take approximately the same number of iterations of about $10,000$ for the convergence rate to reach the fully converged state. For the preconditioner of Turkel, the fully converged state is at a density residuum of $3 \cdot 10^{-3}$ which is slightly higher then the final residuum of the preconditioner of Diangui which is at $1 \cdot 10^{-3}$. Both preconditioners have a convergence rate comparable to the one of the ideal gas preconditioning scheme we use as a reference. In the ideal gas case, the solver needs approximately $10,000$ iterations as well and the fully converged state is reached at a density residuum of $1 \cdot 10^{-3}$. So, there is only a small difference between the convergence behavior of the three considered preconditioning

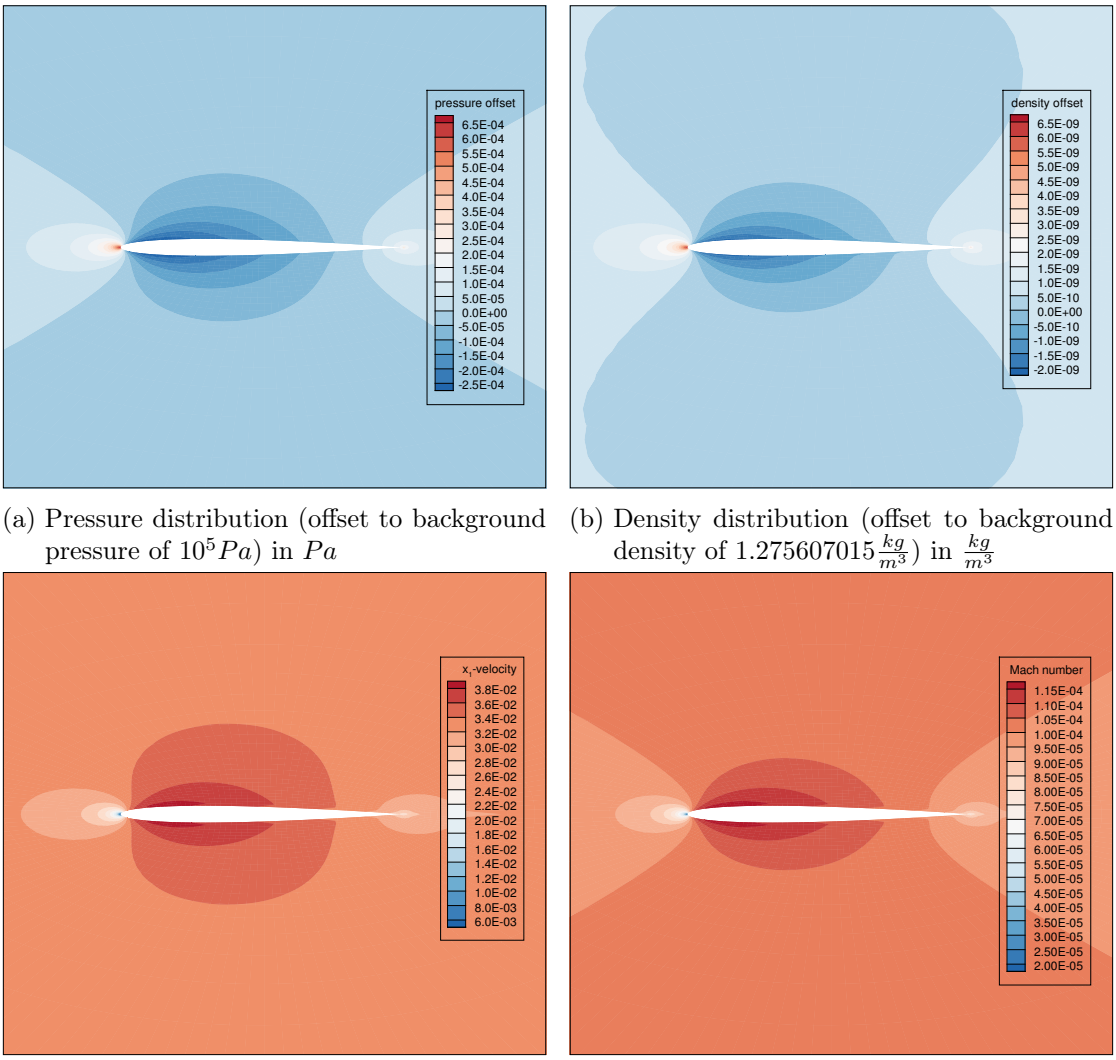

(a) Pressure distribution (offset to background pressure of $10^5 Pa$) in Pa

(b) Density distribution (offset to background density of $1.275607015 \frac{kg}{m^3}$) in $\frac{kg}{m^3}$

(c) x_1-velocity distribution in $\frac{m}{s}$

(d) Mach number distribution

Figure 4.10.: Field solutions for an ideal gas obtained using the preconditioning scheme by Turkel at a Mach number of $Ma_{\text{in}} = 10^{-4}$

schemes.

From the shown results it can be said that both Van der Waals gas preconditioning schemes work equally well in the region for an inflow Mach number of $Ma_{\text{in}} = 10^{-1}$ to $Ma_{\text{in}} = 10^{-3}$. In the region from $Ma_{\text{in}} = 10^{-3}$ to $Ma_{\text{in}} = 10^{-4}$, however, only the preconditioning scheme by Diangui converges to a stable solution while for the preconditioner of Turkel the solution deteriorates due to numerical errors. Hence, for the demonstration of the capability of the preconditioning scheme in section 4.3.4.3, we only

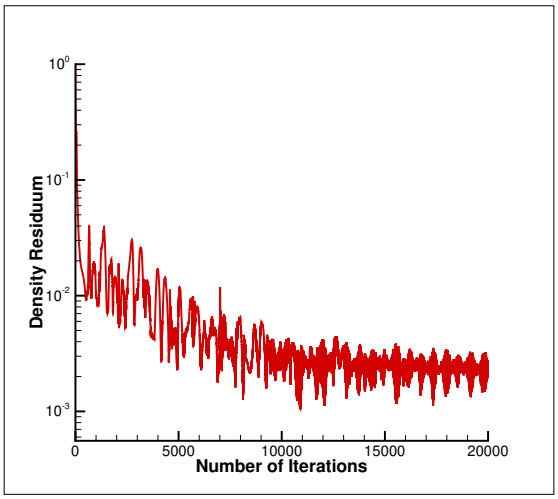

(a) Convergence rate of the preconditioning scheme of Turkel for a Van der Waals gas

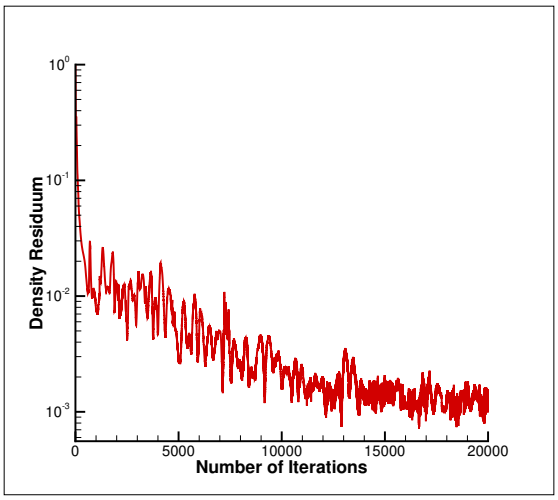

(b) Convergence rate of the preconditioning scheme of Diangui for a Van der Waals gas

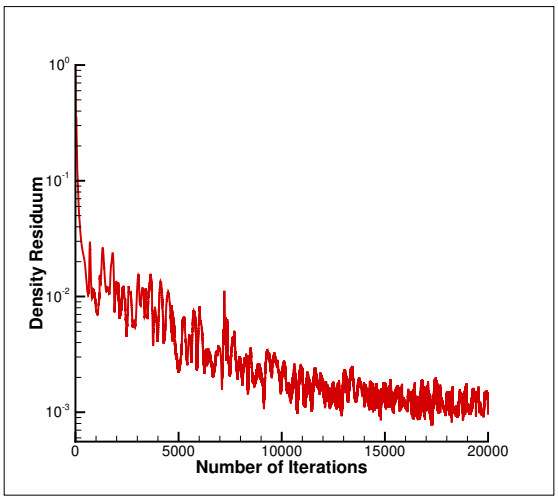

(c) Convergence rate of the preconditioning scheme of Turkel for an ideal gas

Figure 4.11.: Convergence rates of all preconditioning schemes at $Ma_{\text{in}} = 10^{-3}$

consider the scheme by Diangui.

4.3.4.2. Comparison of the convergence rates of both preconditioning schemes

Now we compare the convergence rates of the two preconditioning schemes for a Van der Waals gas. We use one set of thermodynamic conditions and multiple inflow Mach numbers. In Figures 4.12 and 4.13, the normalized density residua are plotted over the number of iterations for the calculations using the preconditioning scheme by Turkel and Diangui, respectively. We compare the convergence rates at the inflow Mach numbers of $Ma_{\text{in}} = 10^{-1}$, $Ma_{\text{in}} = 10^{-2}$, $Ma_{\text{in}} = 10^{-3}$ and, for the scheme by Diangui, of $Ma_{\text{in}} = 10^{-4}$. The considered calculations are again flows of gaseous nitrogen around a NACA0012 profile at condition 1 in Table 4.4 on page 115.
In both figures, the plots at all considered Mach numbers agree well. The density residuum of the fully converged solution stays at a value of $3 \cdot 10^{-3}$ for the preconditioning scheme of Turkel and at $1 \cdot 10^{-3}$ for the one of Diangui as the Mach number decreases. Both schemes need approximately $10,000$ iterations to reach the fully converged stage for either inflow Mach number. So, both preconditioning schemes have a convergence rate that is independent of the Mach number as $M \to 0$.

4.3.4.3. Demonstration of the capability of the preconditioning scheme

In this section, we present the results of numerical simulations using the preconditioning scheme of Diangui. In each simulation, we consider the flow of a fluid modeled as a Van der Waals gas around the NACA0012 profile. The inflow Mach number is set to $Ma_{\text{in}} = 10^{-4}$ for all calculations, while the inflow pressure and temperature vary. The specific conditions used are listed in Table 4.4 on page 115. We consider both nitrogen and oxygen, modeled by the Van der Waals gas implementation in the DLR TAU-code.
First, we continue with the calculations using nitrogen as a gas. In Figure 4.14, the flow of supercritical nitrogen at condition 2 in Table 4.4 is presented. Again, the figure shows the field solutions of pressure and density in the upper row and the x_1-component of velocity and the Mach number in the bottom row.
These results are qualitatively similar to the ones for gaseous nitrogen presented in Figure 4.9. The distribution of the pressure offset shown in Subfigure 4.14a is lower than the one for gaseous nitrogen in Subfigure 4.9a by a factor of 10 since the background pressure is lower by this factor as well due to the different inflow conditions. For the same reason the distribution of the density offset shown in Subfigure 4.14b is lower than the one in Subfigure 4.9b. The value of the background density of $0.6039360338 \frac{kg}{m^3}$ agrees well with the expected value for supercritical nitrogen. The velocity distribution shown

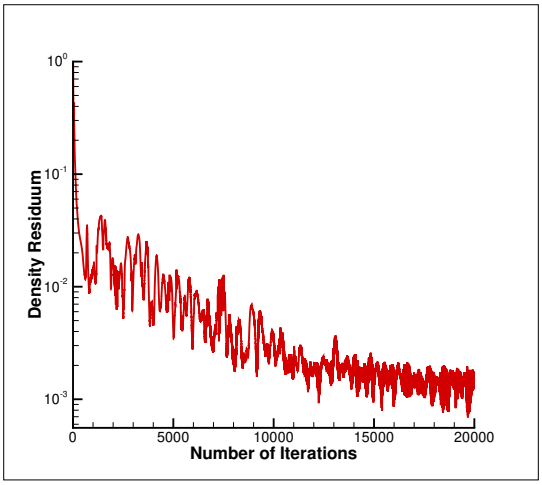

(a) Convergence rate at $Ma_{\text{in}} = 10^{-1}$

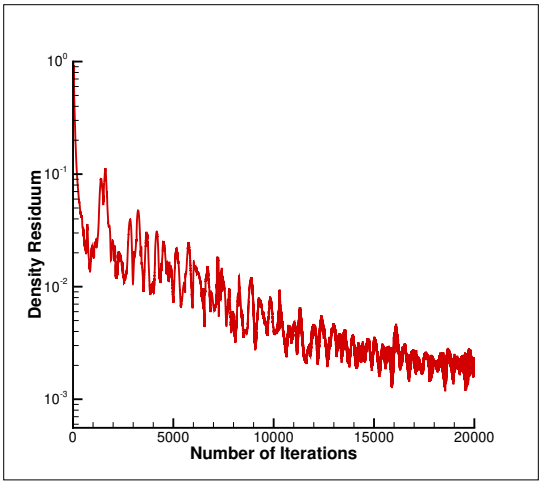

(b) Convergence rate at $Ma_{\text{in}} = 10^{-2}$

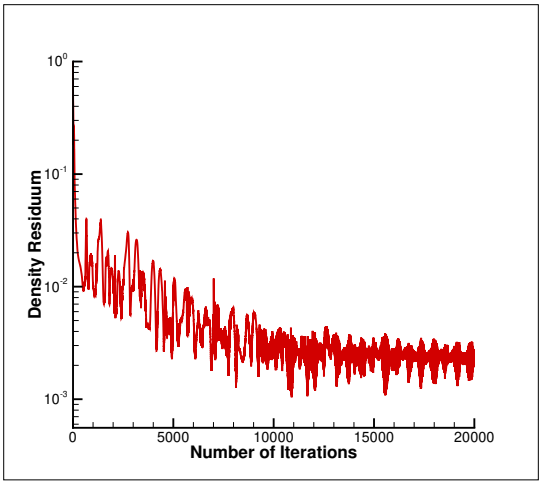

(c) Convergence rate at $Ma_{\text{in}} = 10^{-3}$

Figure 4.12.: Convergence rates at different Mach numbers for calculations using the preconditioning scheme by Turkel for a Van der Waals gas

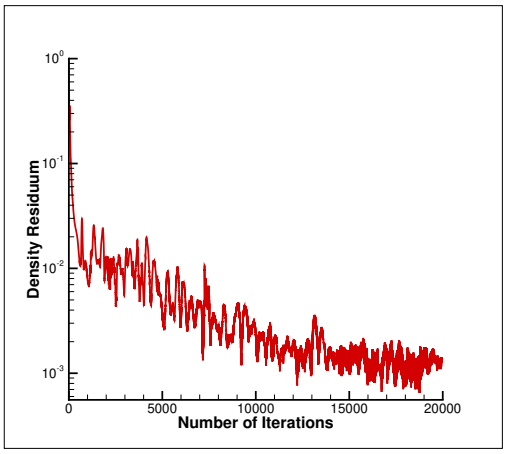

(a) Convergence rate at $Ma_{\text{in}} = 10^{-1}$

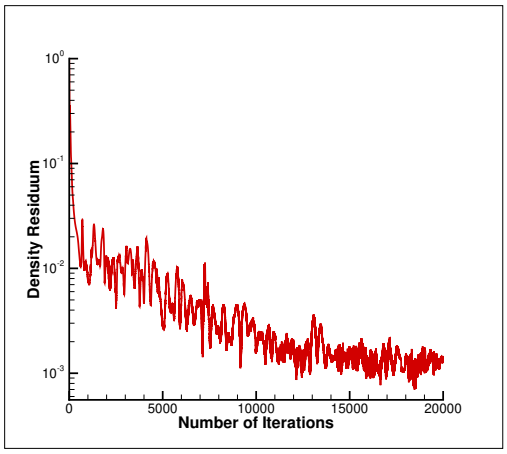

(b) Convergence rate at $Ma_{\text{in}} = 10^{-2}$

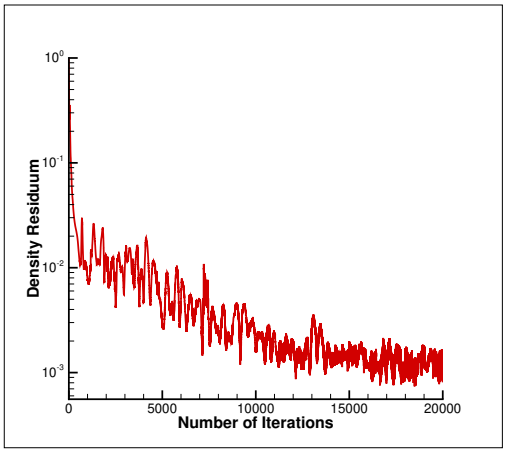

(c) Convergence rate at $Ma_{\text{in}} = 10^{-3}$

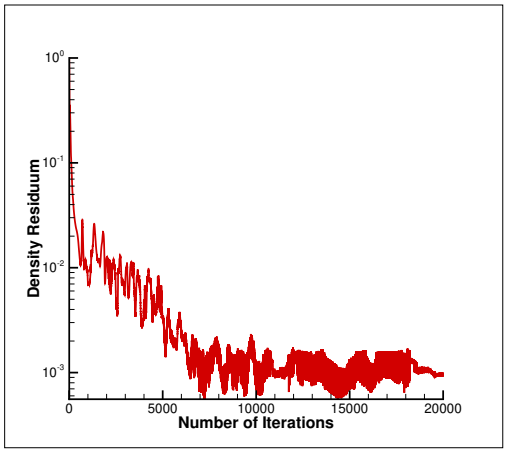

(d) Convergence rate at $Ma_{\text{in}} = 10^{-4}$

Figure 4.13.: Convergence rates at different Mach numbers for calculations using the preconditioning scheme by Diangui for a Van der Waals gas

in Subfigure 4.14c is lower than the one for gaseous nitrogen shown in Subfigure 4.9c by a factor of 2 while the Mach number distributions in Subfigures 4.14d and 4.9d agree well. This is due to the lower value of the speed of sound for a supercritical fluid. So, the distributions shown in Figure 4.14 agree well with the expectations for supercritical nitrogen. Hence, we can conclude that the preconditioning scheme works as well for supercritical nitrogen as it does in the gaseous case.

In addition, we consider liquid nitrogen at condition 3 in Table 4.4. The results of this calculation are presented in Figure 4.15. Again, we show the four different field solutions. The presented results are qualitatively similar to the ones for gaseous and supercritical nitrogen presented in Figures 4.9 and 4.14.

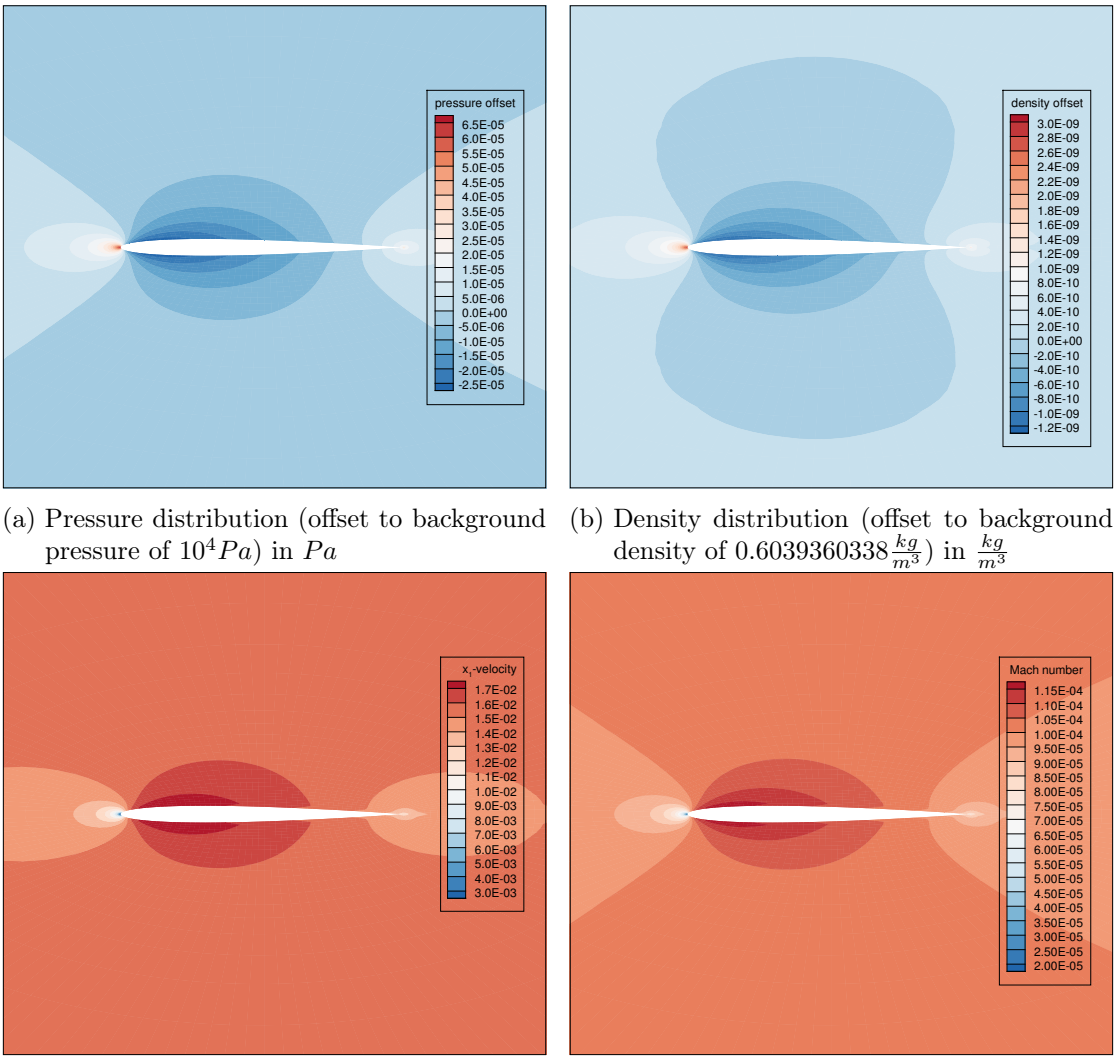

(a) Pressure distribution (offset to background pressure of $10^4 Pa$) in Pa

(b) Density distribution (offset to background density of $0.6039360338 \frac{kg}{m^3}$) in $\frac{kg}{m^3}$

(c) x_1-velocity distribution in $\frac{m}{s}$

(d) Mach number distribution

Figure 4.14.: Field solutions for a Van der Waals gas obtained using the preconditioning scheme by Diangui at a Mach number of $Ma_{\text{in}} = 10^{-4}$ and condition 2

Similar to the difference between the gaseous and supercritical case, the pressure offset distribution shown in Figure 4.15 is at a higher level than the other presented distributions. This difference agrees with the different inflow pressure due to the used condition. The same applies to the distribution of the density offset shown in Subfigure 4.15b. The value of the background density is $12.9497796 \frac{kg}{m^3}$ which is a reasonable value for liquid nitrogen at this elevated pressure.

Overall, the distributions shown in Figure 4.15 agree well with the expectations for liquid

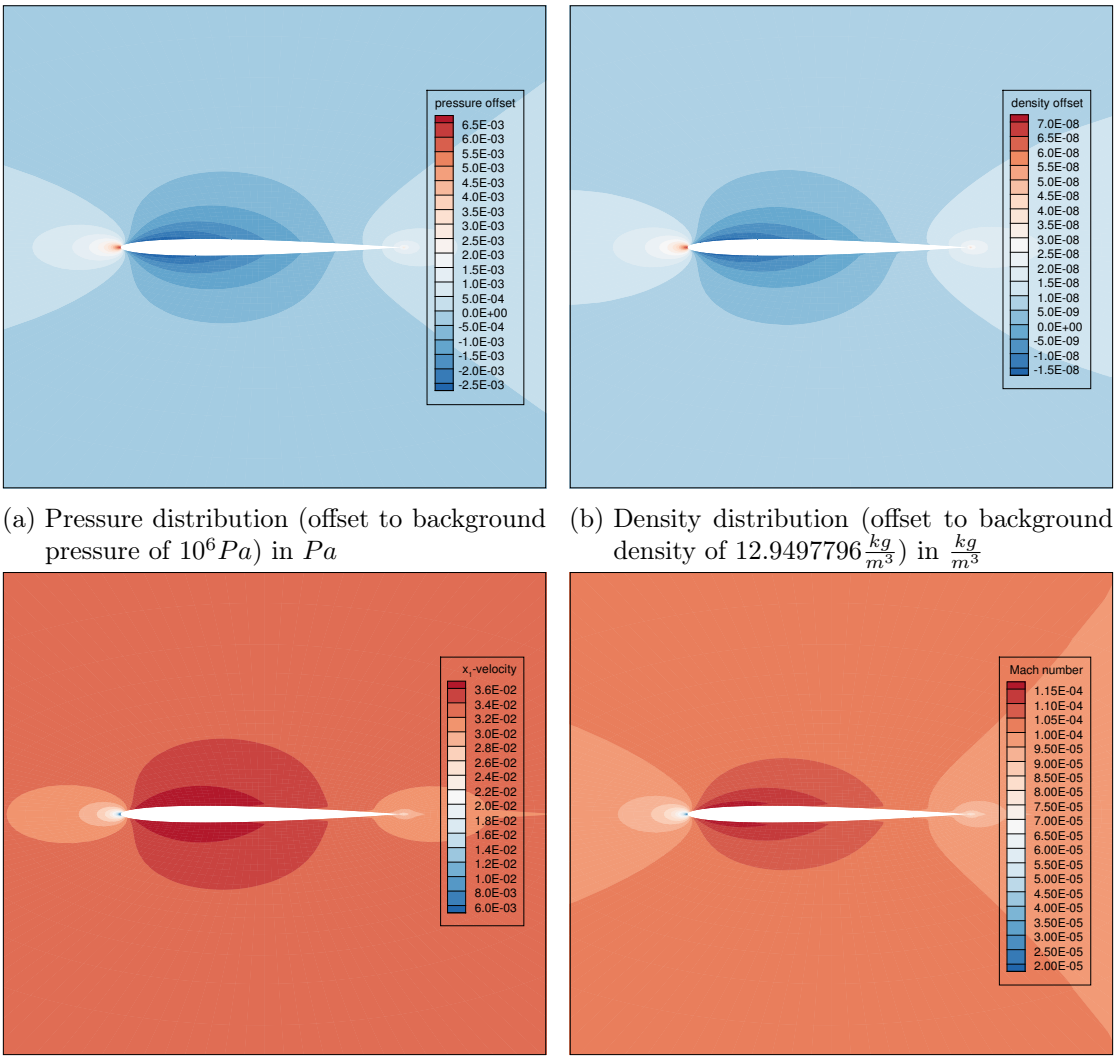

(a) Pressure distribution (offset to background pressure of $10^6 Pa$) in Pa

(b) Density distribution (offset to background density of $12.9497796 \frac{kg}{m^3}$) in $\frac{kg}{m^3}$

(c) x_1-velocity distribution in $\frac{m}{s}$

(d) Mach number distribution

Figure 4.15.: Field solutions for a Van der Waals gas obtained using the preconditioning scheme by Diangui at a Mach number of $Ma_{\text{in}} = 10^{-4}$ and condition 3

nitrogen. So, the preconditioning scheme of Diangui is applicable to nitrogen modeled as a Van der Waals gas at a liquid, a gaseous and a supercritical state.

The next fluid we consider is oxygen. We present the numerical results of calculations with gaseous, supercritical and liquid oxygen in Figures 4.16, 4.17 and 4.18, respectively. For all calculations the inflow Mach number is $Ma_{\text{in}} = 10^{-4}$. For the flow of gaseous oxygen, condition 4 in Table 4.4 is used while conditions 5 and 6 are used for the flow of supercritical and liquid oxygen, respectively. In all cases, oxygen is modeled as a

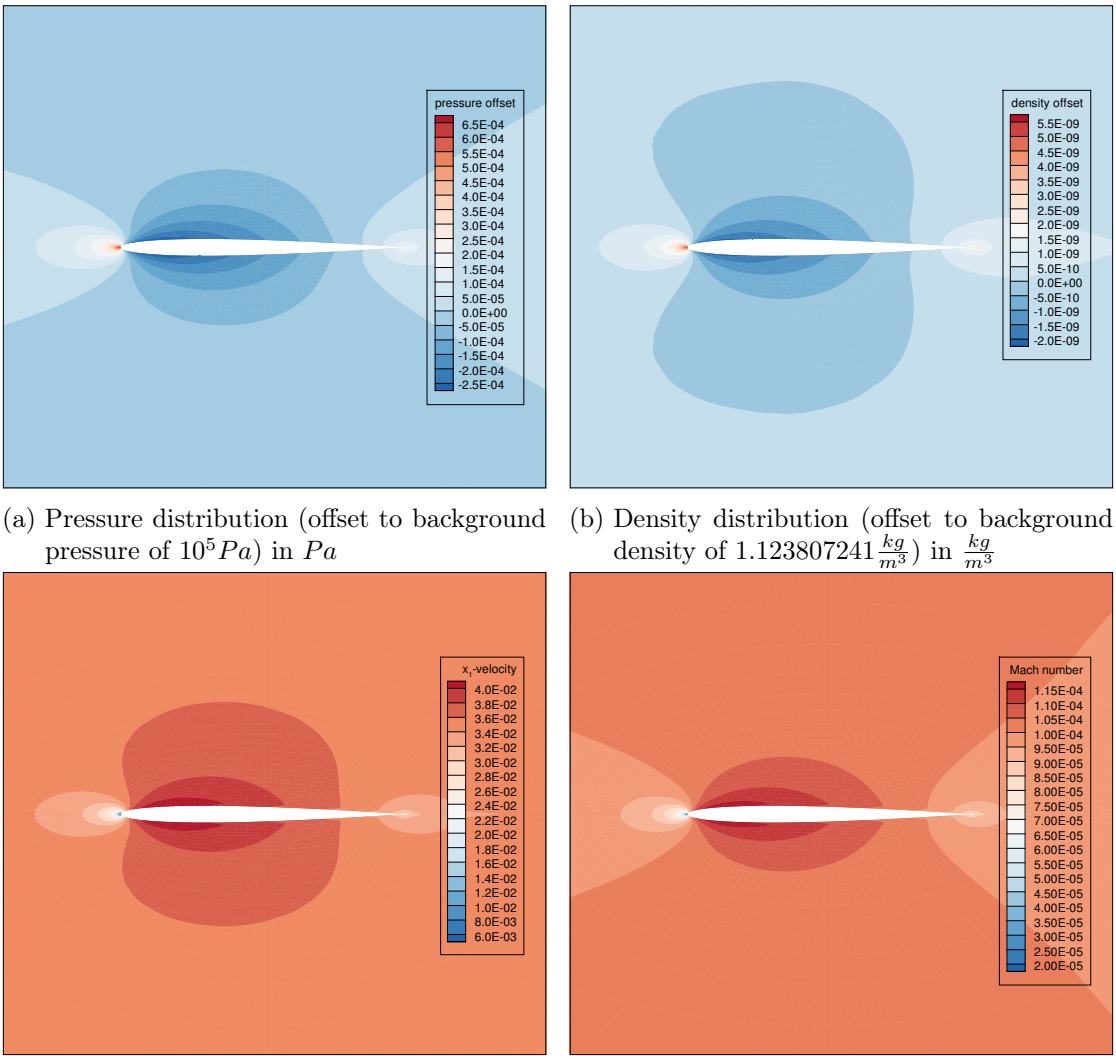

(a) Pressure distribution (offset to background pressure of $10^5 Pa$) in Pa

(b) Density distribution (offset to background density of $1.123807241 \frac{kg}{m^3}$) in $\frac{kg}{m^3}$

(c) x_1-velocity distribution in $\frac{m}{s}$

(d) Mach number distribution

Figure 4.16.: Field solutions for a Van der Waals gas obtained using the preconditioning scheme by Diangui at a Mach number of $Ma_{\text{in}} = 10^{-4}$ and condition 5

Van der Waals gas. For all results, we present the field solutions of pressure, density, x_1-component of velocity and Mach number.

The results are qualitatively similar to the ones we obtain for nitrogen. All three pressure offset distributions are qualitatively similar while representing the respective inflow condition. The distributions of the density offsets are similar as well and the values of the background density represent the respective state of the oxygen, namely the gaseous, supercritical and liquid state.

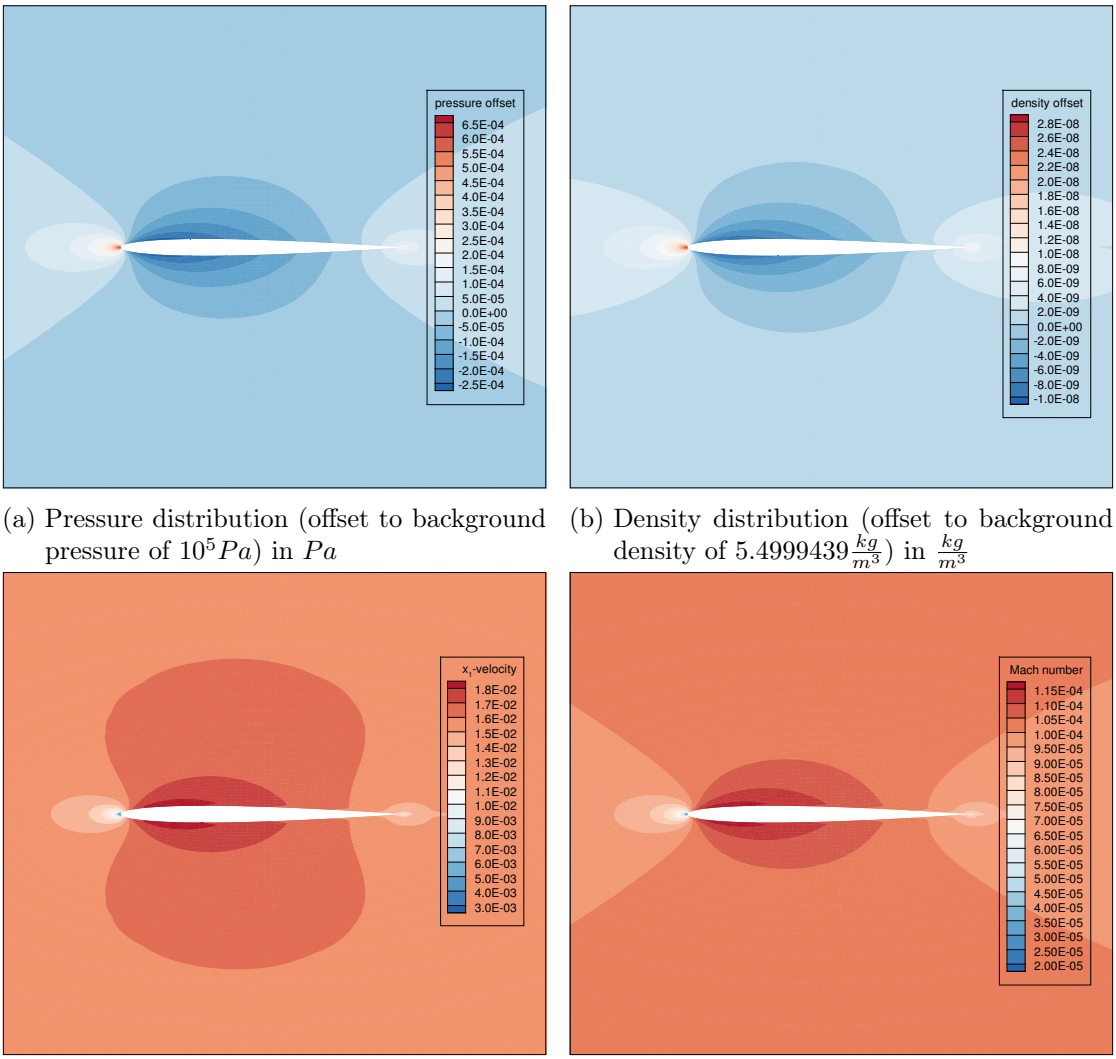

(a) Pressure distribution (offset to background pressure of $10^5 Pa$) in Pa

(b) Density distribution (offset to background density of $5.4999439 \frac{kg}{m^3}$) in $\frac{kg}{m^3}$

(c) x_1-velocity distribution in $\frac{m}{s}$

(d) Mach number distribution

Figure 4.17.: Field solutions for a Van der Waals gas obtained using the preconditioning scheme by Diangui at a Mach number of $Ma_{\text{in}} = 10^{-4}$ and condition 6

The Mach number distributions are similar both in a qualitative and a quantitative manner in all three cases since the inflow Mach number is the same. The x_1-velocity distributions are qualitatively similar but vary in magnitude. This is due to the different values of the speed of sound that is caused by the different condition of pressure and temperature and the differences in the states of oxygen.

So overall this preconditioning scheme leads to the expected results both for nitrogen and oxygen modeled as a Van der Waals gas. From this it can be expected that the

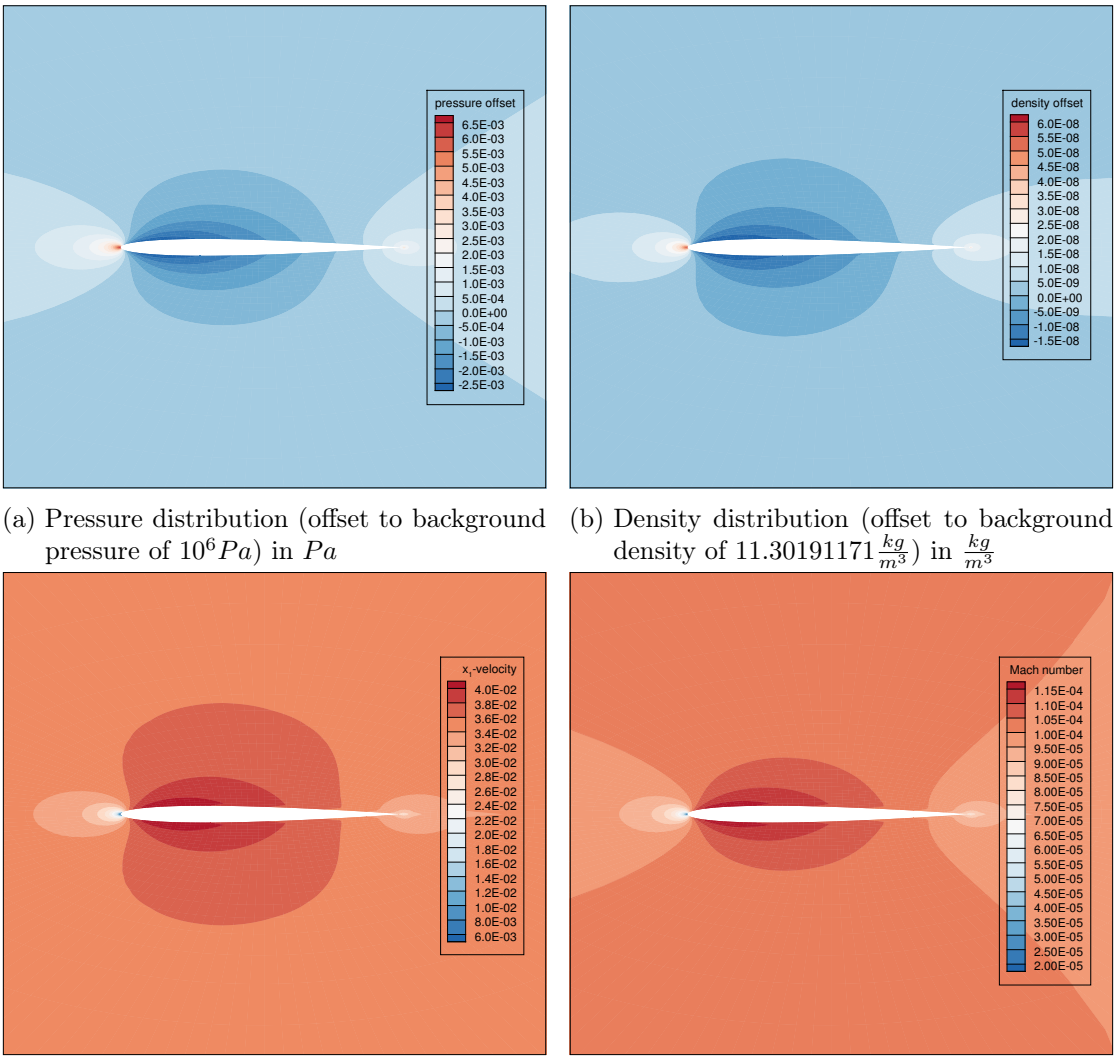

(a) Pressure distribution (offset to background pressure of $10^6 Pa$) in Pa

(b) Density distribution (offset to background density of $11.30191171 \frac{kg}{m^3}$) in $\frac{kg}{m^3}$

(c) x_1-velocity distribution in $\frac{m}{s}$

(d) Mach number distribution

Figure 4.18.: Field solutions for a Van der Waals gas obtained using the preconditioning scheme by Diangui at a Mach number of $Ma_{\text{in}} = 10^{-4}$ and condition 7

preconditioning scheme by Diangui works well for any fluid modeled by a Van der Waals gas to an inflow Mach number as low as 10^{-4} in comparable cases or a local Mach number as low as 10^{-5} in general.

5. Summary and Outlook

This work is concerned with the analysis and application of numerical schemes.
The Euler equations describing the flow of an inviscid fluid are described. To close the system of equations, the Van der Waals equation of state is used. From the definition of the thermal equation of state, a caloric state equation is derived, assuming the specific heat at constant pressure c_p to be constant. In the process of the derivation, it is proven that c_p is independent of the specific volume for a Van der Waals gas. Next, the nondimensionalization is described which introduces the Mach number into the governing equations. Then the boundary and initial conditions used within this work are stated.
In the next step, the properties of asymptotic functions are described and the process of an asymptotic expansion is explained. Then an asymptotic expansion of the governing equations for a Van der Waals gas is conducted for the first time to analyze their behavior in the limit of a small Mach number. As a result, the pressure distribution is found to be spatially constant in the limit of a vanishing Mach number. This agrees with the behavior in the ideal gas case. Additionally, the behavior of the change of pressure with time is analyzed. It is found that the leading order of the pressure is governed by compression or expansion of the gas over the boundary of the flow domain like in the case of an ideal gas, but that the real gas effects present in the Van der Waals equation of state can alter this influence.
Next, numerical schemes are considered. Finite volume schemes are defined and the discretization of both the computational domain and the convective fluxes is described. The MAPS+ flux function is chosen for the analysis. It consists of a general part and special adaptations for the low Mach number region and is described in detail. Then the different terms in the flux Jacobi matrix representing MAPS+ and the flux Jacobi matrix representing the continuous flux function are compared. By showing that their behavior for a vanishing Mach number is similar, it is concluded that the MAPS+ flux function is a close approximation of the continuous flux function. This analysis is conducted for both an ideal gas and a Van der Waals gas with the result that MAPS+ approximates both gases equally well.
In the next step, a discrete asymptotic analysis of the MAPS+ flux function is conducted. This results in the statement that the general MAPS+ scheme can lead to fluctuations

of the first order pressure term on a length scale independent of the Mach number while no such fluctuations are possible with the altered MAPS+ scheme which includes the adaptations for the low Mach number region. These variations in the first order pressure terms contradict the results of the continuous asymptotic analysis. The result of this finding is that only the altered MAPS+ scheme is suitable for the simulation of low Mach number flows. To complete this section, numerical results are shown which confirm that the altered MAPS+ scheme produces reasonable results in the limit of a low Mach number while the general MAPS+ scheme deteriorates as the Mach number decreases.
Finally, preconditioning schemes are analyzed. A detailed overview over the currently available schemes is given and the different requirements of ideal and Van der Waals gases concerning preconditioners are discussed. The differences in the properties of the flux Jacobi matrices in both cases are analyzed with the result that an ideal gas preconditioning scheme cannot, in general, lead to favorable results in the case of a Van der Waals gas. This is then demonstrated by the analytical preconditioning of both the ideal gas and the Van der Waals gas flux Jacobi matrix. For this demonstration, an ideal gas preconditioning scheme by Turkel is compared to a Van der Waals gas preconditioner that is constructed by simplifying the inverse of the Van der Waals gas flux Jacobi matrix. The demonstration shows that the Van der Waals gas preconditioner works as expected for the corresponding flux Jacobi matrix while the ideal gas preconditioning scheme leads to complex eigenvalues and an increased condition number when used in the Van der Waals gas case.
However, the constructed preconditioning matrix is limited to the analytical caloric equation of state for a Van der Waals gas and hence cannot be used with a numerical estimation of the thermodynamic properties as it is implemented in most CFD codes. Hence, the DLR TAU-code is used in combination with two suitable preconditioning schemes by other authors to demonstrate the capability of preconditioners for a Van der Waals gas using the TAU-code. The preconditioning schemes are implemented into the code using derivatives of the thermodynamic modules within the code for the transformation from primitive to conservative variables. The simulations with these preconditioners show that flows of a real gas described by the Van der Waals gas equation of state can be successfully simulated to a local Mach number as low as 10^{-5} for liquid, gaseous and supercritical states. In addition, the convergence rates of these preconditioning schemes are found to be independent of the Mach number as $M \to 0$.
The work conducted in this thesis is intended as a baseline for further investigation of preconditioning schemes for real gases. The analysis done for an inviscid fluid can be extended to viscous calculations. In addition, the investigations done in this work are

not limited to a Van der Waals gas but can be extended to other, more detailed cubic equations of state.

A. Appendix

A.1. Behavior of Jacobi matrices for a vanishing Mach number

The continuous Jacobi matrix in x_1-direction $\boldsymbol{A}_{\boldsymbol{u}}^{(1)} = \frac{\partial \boldsymbol{f}_1(\boldsymbol{u})}{\partial \boldsymbol{u}}$ is defined in equation (2.4) on page 8. The convective flux in x_1-direction is given by

$$\boldsymbol{f}_1(\boldsymbol{u}) = \begin{pmatrix} \rho v_1 \\ \rho v_1^2 + p \\ \rho v_1 v_2 \\ \rho H v_1 \end{pmatrix}.$$

In a similar way as in subsection 4.2.3 on page 49 we can write this vector in terms of the conservative variables $\boldsymbol{u} = (u_1, u_2, u_3, u_4)^T = (\rho, \rho v_1, \rho v_2, \rho E)^T$. This leads to

$$\boldsymbol{f}_1(\boldsymbol{u}) = \begin{pmatrix} u_2 \\ \frac{u_2^2}{u_1} + (\gamma - 1)\left(u_4 - \frac{1}{2}\frac{u_2^2 + u_3^2}{u_1}\right) \\ \frac{u_2 u_3}{u_1} \\ \gamma \frac{u_2 u_4}{u_1} - \frac{(\gamma - 1)}{2}\left(\frac{u_2^3 + u_2 u_3^2}{u_1^2}\right) \end{pmatrix}. \tag{A.1}$$

For the representation of pressure see equation (4.11) on page 50. The term $\rho H v_1$ can be rewritten as

$$\rho H v_1 = \rho v_1 \left(E + \frac{p}{\rho}\right) = \rho v_1 E + v_1 p. \tag{A.2}$$

If we insert the conservative variables into this relation we get

$$\rho H v_1 = \frac{u_2 u_4}{u_1} + (\gamma - 1)\left(\frac{u_2 u_4}{u_1} - \frac{1}{2}\frac{u_2^3 + u_2 u_3^2}{u_1^2}\right)$$

which can be simplified to the last entry in equation A.1.

Taking the derivative, we arrive at

$$\boldsymbol{A}_{\boldsymbol{u}}^{(1)} = \begin{bmatrix} 0 & 1 & 0 & 0 \\ -\frac{u_2^2}{u_1^2} + \frac{1}{2}\xi\frac{u_2^2+u_3^2}{u_1^2} & 2\frac{u_2}{u_1} - \xi\frac{u_2}{u_1} & -\xi\frac{u_3}{u_1} & \xi \\ -\frac{u_2 u_3}{u_1^2} & \frac{u_3}{u_1} & \frac{u_2}{u_1} & 0 \\ -\gamma\frac{u_2 u_4}{u_1^2} + \xi\left(\frac{u_2^3+u_2 u_3^2}{u_1^3}\right) & \gamma\frac{u_4}{u_1} - \frac{\xi}{2}\left(\frac{3u_2^2+u_3^2}{u_1^2}\right) & -\xi\left(\frac{u_2 u_3}{u_1^2}\right) & \gamma\frac{u_2}{u_1} \end{bmatrix}$$

with

$$\xi = \gamma - 1.$$

In the next step we replace the conservative variables. This leads to

$$\boldsymbol{A}_{\boldsymbol{u}}^{(1)} = \begin{bmatrix} 0 & 1 & 0 & 0 \\ -v_1^2 + \frac{1}{2}\xi|\boldsymbol{v}|^2 & (3-\gamma)\,v_1 & -\xi v_2 & \xi \\ -v_1 v_2 & v_2 & v_1 & 0 \\ -\gamma v_1 E + \xi\left(v_1^3 + v_1 v_2^2\right) & \gamma E - \frac{\xi}{2}\left(3v_1^2 + v_2^2\right) & -\xi\left(v_2 v_3\right) & \gamma v_2 \end{bmatrix}. \tag{A.3}$$

For $M \to 0$, γ and E are of $\mathcal{O}(1)$ while v_1, v_2 and $|\boldsymbol{v}|$ are of $\mathcal{O}(M)$. Hence, in the limit of a vanishing Mach number we get the following behavior of the different terms in the Jacobi matrix:

$$\boldsymbol{A}_{\boldsymbol{u}}^{(1)} = \begin{bmatrix} 0 & 1 & 0 & 0 \\ \mathcal{O}(M^2) & \mathcal{O}(M) & \mathcal{O}(M) & \mathcal{O}(1) \\ \mathcal{O}(M^2) & \mathcal{O}(M) & \mathcal{O}(M) & 0 \\ \mathcal{O}(M) & \mathcal{O}(1) & \mathcal{O}(M^2) & \mathcal{O}(M) \end{bmatrix} \tag{A.4}$$

Now we repeat this derivation for a Van der Waals gas. From the representation of the primitive variables in terms of the conservative variables in equation (4.13) we take the pressure of a Van der Waals gas written in conservative variables. For the enthalpy flux, we take equation (A.2) and insert the conservative variables. This leads to

$$\rho H v_1 = \frac{u_2 u_4}{u_1} + \frac{2M_w u_2 u_4 - M_w\frac{u_2^3+u_2 u_3^2}{u_1} + 2\frac{a u_1^2 u_2}{M_w}}{3u_1\left(M_w - b u_1\right)} - \frac{a u_1 u_2}{M_w^2}.$$

Hence, the convective flux in x_1-direction for a Van der Waals gas is given by

$$\boldsymbol{f}_1(\boldsymbol{u}) = \begin{pmatrix} u_2 \\ \frac{u_2^2}{u_1} + \frac{2M_w u_4 - M_w \frac{u_2^2+u_3^2}{u_1} + 2\frac{au_1^2}{M_w}}{3M_w - 3bu_1} - \frac{au_1^2}{M_w^2} \\ \frac{u_2 u_3}{u_1} \\ \frac{u_2 u_4}{u_1} + \frac{2M_w u_2 u_4}{3u_1(M_w - bu_1)} - \frac{M_w\left(u_2^3 + u_2 u_3^2\right)}{3u_1^2(M_w - bu_1)} + \frac{2au_1 u_2}{3M_w(M_w - bu_1)} - \frac{au_1 u_2}{M_w^2} \end{pmatrix}. \tag{A.5}$$

Now, we take the derivative to arrive at the Jacobi matrix. The first and third entry of the convective flux vector are identical to the ideal gas case, hence the first and third line of the Jacobi matrix are identical to the matrix in equation (A.3). The second row can be deduced with the help of the fourth row of the matrix in equation (4.14). For the first entry of the last row we get

$$\begin{aligned} \frac{\partial \left(f_1\left(\boldsymbol{u}\right)\right)_4}{\partial u_1} =& -\frac{u_2 u_4}{u_1^2} + \frac{-2M_w u_2 u_4 \left(3M_w - 6bu_1\right)}{9u_1^2 \left(M_w - bu_1\right)^2} + \frac{M_w\left(u_2^3 + u_2 u_3^2\right)\left(6M_w u_1 - 9bu_1^2\right)}{9u_1^4 \left(M_w - bu_1\right)^2} \\ &+ \frac{6aM_w u_2 \left(M_w - bu_1\right) + 6abM_w u_1 u_2}{9M_w^2 \left(M_w - bu_1\right)^2} - \frac{au_2}{M_w^2}. \end{aligned}$$

Now we replace the conservative variables and arrive at

$$\begin{aligned} \frac{\partial \left(f_1\left(\boldsymbol{u}\right)\right)_4}{\partial u_1} &= -v_1 E + \frac{-2M_w v_1 E \left(3M_w - 6b\rho\right)}{9\left(M_w - b\rho\right)^2} + \frac{M_w\left(v_1^3 + v_1 v_2^2\right)\left(2M_w\rho - 3b\rho^2\right)}{3\rho\left(M_w - b\rho\right)^2} \\ &\quad + \frac{2aM_w\rho v_1 \left(M_w - b\rho\right) + 2abM_w\rho^2 v_1}{3M_w^2 \left(M_w - b\rho\right)^2} - \frac{a\rho v_1}{M_w^2} \\ &= -v_1 E + \frac{-2M_w v_1 E \left(M_w - 2b\rho\right)}{3\left(M_w - b\rho\right)^2} + \frac{2M_w v_1 |\boldsymbol{v}|^2 \left(M_w - 2b\rho\right) + bM_w\rho v_1 |\boldsymbol{v}|^2}{3\left(M_w - b\rho\right)^2} \\ &\quad + \frac{2aM_w\rho v_1 \left(M_w - b\rho\right) + 2abM_w\rho^2 v_1}{3M_w^2 \left(M_w - b\rho\right)^2} - \frac{a\rho v_1}{M_w^2} \\ &= -v_1 E + \frac{2M_w v_1 \left(2b\rho - M_w\right)\left(E - |\boldsymbol{v}|^2\right) + bM_w\rho v_1 |\boldsymbol{v}|^2}{3\left(M_w - b\rho\right)^2} \\ &\quad + \frac{2aM_w\rho v_1 \left(M_w - b\rho\right) + 2abM_w\rho^2 v_1}{3M_w^2 \left(M_w - b\rho\right)^2} - \frac{a\rho v_1}{M_w^2}. \end{aligned}$$

For the second entry in the last row we get

$$\frac{\partial\left(f_1\left(\boldsymbol{u}\right)\right)_4}{\partial u_2} = \frac{u_4}{u_1} + \frac{2M_w u_4}{3u_1\left(M_w - bu_1\right)} - \frac{M_w\left(3u_2^2 + u_3^2\right)}{3u_1^2\left(M_w - bu_1\right)} + \frac{2au_1}{3M_w\left(M_w - bu_1\right)} - \frac{au_1}{M_w^2}.$$

Replacing the conservative variables this becomes

$$\begin{aligned}\frac{\partial\left(f_1\left(\boldsymbol{u}\right)\right)_4}{\partial u_2} &= E + \frac{2M_w E}{3\left(M_w - b\rho\right)} - \frac{M_w\left(3v_1^2 + v_2^2\right)}{3\left(M_w - b\rho\right)} + \frac{2a\rho}{3M_w\left(M_w - b\rho\right)} - \frac{a\rho}{M_w^2} \\ &= E + \frac{\left(2E - |\boldsymbol{v}|^2 - 2v_1^2\right) + 2\frac{a\rho}{M_w^2}}{\frac{3(M_w - b\rho)}{M_w}} - \frac{a\rho}{M_w^2}.\end{aligned}$$

The third entry in the last row can be written as

$$\frac{\partial\left(f_1\left(\boldsymbol{u}\right)\right)_4}{\partial u_3} = -\frac{2M_w u_2 u_3}{3u_1^2\left(M_w - bu_1\right)},$$

replacing the conservative variables we get

$$\frac{\partial\left(f_1\left(\boldsymbol{u}\right)\right)_4}{\partial u_3} = -\frac{2M_w v_1 v_2}{3\left(M_w - b\rho\right)}.$$

And finally, the fourth entry of the last row is

$$\frac{\partial\left(f_1\left(\boldsymbol{u}\right)\right)_4}{\partial u_4} = \frac{u_2}{u_1} + \frac{2M_w u_2}{3u_1\left(M_w - bu_1\right)}.$$

If we replace the conservative variables we get

$$\frac{\partial\left(f_1\left(\boldsymbol{u}\right)\right)_4}{\partial u_4} = v_1 + \frac{2M_w v_1}{3\left(M_w - b\rho\right)}.$$

Combining all these results, we can write the Jacobi matrix for a Van der Waals gas:

$$\boldsymbol{A}_{\boldsymbol{u}}^{(1)} = \begin{bmatrix} 0 & 1 & 0 & 0 \\ -v_1^2 + \frac{2bM_w\rho\left(E - |\boldsymbol{v}|^2\right) + M_w^2|\boldsymbol{v}|^2 - \xi_2}{3\xi_1^2} & 2v_1 + \frac{-2M_w v_1}{3\xi_1} & \frac{-2M_w v_2}{3\xi_1} & \frac{2M_w}{3\xi_1} \\ -v_1 v_2 & v_2 & v_1 & 0 \\ -v_1 E + \frac{2M_w v_1(2b\rho - M_w)\left(E - |\boldsymbol{v}|^2\right) + bM_w\rho v_1|\boldsymbol{v}|^2}{3\xi_1^2} + v_1\xi_3 - v_1\xi_4 & E + \frac{\left(2E - |\boldsymbol{v}|^2 - 2v_1^2\right) + 2\xi_4}{\frac{3\xi_1}{M_w}} - \xi_4 & -\frac{2M_w v_1 v_2}{3\xi_1} & v_1 + \frac{2M_w v_1}{3\xi_1} \end{bmatrix} \tag{A.6}$$

with

$$\xi_1 = M_w - b\rho,$$

$$\xi_2 = 6\frac{ab^2}{M_w^2}\rho^3 - 10\frac{ab}{M_w}\rho^2 + 2a\rho,$$

$$\xi_3 = \frac{2aM_w\rho\xi_1 + 2abM_w\rho^2}{3M_w^2\xi_1^2}$$

and

$$\xi_4 = \frac{a\rho}{M_w^2}$$

For $M \to 0$, a, b, M_w, ρ and E are of $\mathcal{O}(1)$ while v_1, v_2 and $|\boldsymbol{v}|$ are of $\mathcal{O}(M)$. Hence, in the limit of a vanishing Mach number we get the following behavior of the different terms in the Jacobi matrix for a Van der Waals gas:

$$\boldsymbol{A}_{\boldsymbol{u}}^{(1)} = \begin{bmatrix} 0 & 1 & 0 & 0 \\ \mathcal{O}(1) & \mathcal{O}(M) & \mathcal{O}(M) & \mathcal{O}(1) \\ \mathcal{O}(M^2) & \mathcal{O}(M) & \mathcal{O}(M) & 0 \\ \mathcal{O}(M) & \mathcal{O}(1) & \mathcal{O}(M^2) & \mathcal{O}(M) \end{bmatrix}. \tag{A.7}$$

A.2. Transformation of flux Jacobi matrix

Here, we want to transform the flux Jacobi matrix into a form similar to the Jacobi matrix of the MAPS+ scheme presented in equation (4.19) on page 55. Hence, we want to write the flux Jacobi matrix as

$$\boldsymbol{A}_{\boldsymbol{u}}^{(1)} = \boldsymbol{A}_{\text{prim}}\frac{\partial \boldsymbol{q}_1}{\partial \boldsymbol{u}} + \begin{bmatrix} v_1 & 0 & 0 & 0 \\ 0 & v_1 & 0 & 0 \\ 0 & 0 & v_1 & 0 \\ 0 & 0 & 0 & v_1 \end{bmatrix}. \tag{A.8}$$

In a first step, we transform the matrix for an ideal gas, followed by the transformation for a Van der Waals gas.

A.2.1. Jacobi matrix of an ideal gas

In terms of the conservative variables, the flux Jacobi matrix of an ideal gas is given by equation (A.1).
To attain the matrix $\boldsymbol{A}_{\text{prim}}$, we first need to subtract the last matrix in equation (A.8) from the flux Jacobi matrix. In terms of the conservative variables we get

$$\boldsymbol{A}_{\text{prim}} = \begin{bmatrix} 0 & 1 & 0 & 0 \\ -\frac{u_2^2}{u_1^2} + \frac{1}{2}\xi\frac{u_2^2+u_3^2}{u_1^2} & 2\frac{u_2}{u_1} - \xi\frac{u_2}{u_1} & -\xi\frac{u_3}{u_1} & \xi \\ -\frac{u_2 u_3}{u_1^2} & \frac{u_3}{u_1} & \frac{u_2}{u_1} & 0 \\ -\gamma\frac{u_2 u_4}{u_1^2} + \xi\left(\frac{u_2^3+u_2 u_3^2}{u_1^3}\right) & \gamma\frac{u_4}{u_1} - \frac{\xi}{2}\left(\frac{3u_2^2+u_3^2}{u_1^2}\right) & -\xi\left(\frac{u_2 u_3}{u_1^2}\right) & \gamma\frac{u_2}{u_1} \end{bmatrix} - \begin{bmatrix} \frac{u_2}{u_1} & 0 & 0 & 0 \\ 0 & \frac{u_2}{u_1} & 0 & 0 \\ 0 & 0 & \frac{u_2}{u_1} & 0 \\ 0 & 0 & 0 & \frac{u_2}{u_1} \end{bmatrix}$$
$$= \begin{bmatrix} -\frac{u_2}{u_1} & 1 & 0 & 0 \\ -\frac{u_2^2}{u_1^2} + \frac{1}{2}\xi\frac{u_2^2+u_3^2}{u_1^2} & \frac{u_2}{u_1} - \xi\frac{u_2}{u_1} & -\xi\frac{u_3}{u_1} & \xi \\ -\frac{u_2 u_3}{u_1^2} & \frac{u_3}{u_1} & 0 & 0 \\ -\gamma\frac{u_2 u_4}{u_1^2} + \xi\left(\frac{u_2^3+u_2 u_3^2}{u_1^3}\right) & \gamma\frac{u_4}{u_1} - \frac{\xi}{2}\left(\frac{3u_2^2+u_3^2}{u_1^2}\right) & -\xi\left(\frac{u_2 u_3}{u_1^2}\right) & \xi\frac{u_2}{u_1} \end{bmatrix} \tag{A.9}$$

with

$$\xi = \gamma - 1.$$

Next, we need to multiply this matrix with the transformation matrix from conservative to primitive variables. In order to attain the transformation matrix, we write the vector of conservative variables in terms of the primitive variables $\boldsymbol{q}_1 = (q_1, q_2, q_3, q_4)^T = (\rho, v_1, v_2, p)^T$. For the representation of pressure we first rewrite the dimensionless version of the caloric ideal gas equation (2.5) on page 9 to

$$\rho E = \frac{p}{\xi} + \frac{1}{2}\rho \boldsymbol{v}^2.$$

We get the vector of conservative variables:

$$\boldsymbol{u} = \left(q_1, q_1 q_2, q_1 q_3, \frac{q_4}{\xi} + \frac{1}{2} q_1 \left(q_2^2 + q_3^2\right)\right)^T$$

With this, we can write the transformation matrix as

$$\left(\frac{\partial \boldsymbol{u}}{\partial \boldsymbol{q}_1}\right) = \begin{bmatrix} 1 & 0 & 0 & 0 \\ q_2 & q_1 & 0 & 0 \\ q_3 & 0 & q_1 & 0 \\ \frac{q_2^2+q_3^2}{2} & q_1 q_2 & q_1 q_3 & \frac{1}{\xi} \end{bmatrix}.$$

For the multiplication, it is helpful to rewrite this matrix in terms of conservative variables. This gives us

$$\left(\frac{\partial \boldsymbol{u}}{\partial \boldsymbol{q}_1}\right) = \begin{bmatrix} 1 & 0 & 0 & 0 \\ \frac{u_2}{u_1} & u_1 & 0 & 0 \\ \frac{u_3}{u_1} & 0 & u_1 & 0 \\ \frac{u_2^2+u_3^2}{2u_1^2} & u_2 & u_3 & \frac{1}{\xi} \end{bmatrix}.$$

Now, we multiply the result of equation (A.9) with the transformation matrix from conservative to primitive variables. This gives us the following form of the matrix A_{prim}:

$$A_{\text{prim}} = \begin{bmatrix} -\frac{u_2}{u_1} & 1 & 0 & 0 \\ -\frac{u_2^2}{u_1^2} + \frac{1}{2}\xi\frac{u_2^2+u_3^2}{u_1^2} & \frac{u_2}{u_1} - \xi\frac{u_2}{u_1} & -\xi\frac{u_3}{u_1} & \xi \\ -\frac{u_2 u_3}{u_1^2} & \frac{u_3}{u_1} & 0 & 0 \\ -\gamma\frac{u_2 u_4}{u_1^2} + \xi\left(\frac{u_2^3+u_2 u_3^2}{u_1^3}\right) & \gamma\frac{u_4}{u_1} - \frac{\xi}{2}\left(\frac{3u_2^2+u_3^2}{u_1^2}\right) & -\xi\left(\frac{u_2 u_3}{u_1^2}\right) & \xi\frac{u_2}{u_1} \end{bmatrix}$$
$$\cdot \begin{bmatrix} 1 & 0 & 0 & 0 \\ \frac{u_2}{u_1} & u_1 & 0 & 0 \\ \frac{u_3}{u_1} & 0 & u_1 & 0 \\ \frac{u_2^2+u_3^2}{2u_1^2} & u_2 & u_3 & \frac{1}{\xi} \end{bmatrix} = \begin{bmatrix} 0 & u_1 & 0 & 0 \\ 0 & u_2 & 0 & 1 \\ 0 & u_3 & 0 & 1 \\ 0 & \gamma u_4 - \frac{\xi}{2}\frac{u_2^2+u_3^2}{u_1} & 0 & \frac{u_2}{u_1} \end{bmatrix}$$

Replacing the conservative variables, we can get

$$A_{\text{prim}} = \begin{bmatrix} 0 & \rho & 0 & 0 \\ 0 & \rho v_1 & 0 & 1 \\ 0 & \rho v_2 & 0 & 1 \\ 0 & \gamma\rho E - \frac{\xi}{2}\rho|\boldsymbol{v}|^2 & 0 & v_1 \end{bmatrix}. \tag{A.10}$$

The second term in the last row can be reformulated which results in

$$\gamma\rho E - \frac{\xi}{2}\rho|\boldsymbol{v}|^2 = (\gamma-1)\,\rho E - \frac{1}{2}(\gamma-1)\,\rho|\boldsymbol{v}|^2 + \rho E$$

With the caloric equation of state (2.5) we can introduce pressure into the equation which gives us

$$(\gamma-1)\,\rho E - \frac{1}{2}(\gamma-1)\,\rho|\boldsymbol{v}|^2 + \rho E = p + \rho E.$$

Now, we can write the Jacobi matrix for an ideal gas in its final form

$$\boldsymbol{A}_{\boldsymbol{u}}^{(1)} = \begin{bmatrix} 0 & \rho & 0 & 0 \\ 0 & \rho v_1 & 0 & 1 \\ 0 & \rho v_2 & 0 & 0 \\ 0 & \rho(E + \frac{p}{\rho}) & 0 & v_1 \end{bmatrix} \frac{\partial \boldsymbol{q_1}}{\partial \boldsymbol{u}} + \begin{bmatrix} v_1 & 0 & 0 & 0 \\ 0 & v_1 & 0 & 0 \\ 0 & 0 & v_1 & 0 \\ 0 & 0 & 0 & v_1 \end{bmatrix}. \tag{A.11}$$

A.2.2. Jacobi matrix of a Van der Waals gas

The flux Jacobi matrix of a Van der Waals gas is given by equation (A.6). In terms of the conservative variables, we can write it as

$$\boldsymbol{A}_{\boldsymbol{u}}^{(1)} = \begin{bmatrix} 0 & 1 & 0 & 0 \\ -\frac{u_2^2}{u_1^2} + \frac{2bM_w\xi_5 + M_w^2\frac{u_2^2+u_3^2}{u_1^2} - \xi_2}{3\xi_1^2} & 2\frac{u_2}{u_1} + \frac{-2M_w\frac{u_2}{u_1}}{3\xi_1} & \frac{-2M_w\frac{u_3}{u_1}}{3\xi_1} & \frac{2M_w}{3\xi_1} \\ -\frac{u_2u_3}{u_1^2} & \frac{u_3}{u_1} & \frac{u_2}{u_1} & 0 \\ \frac{2M_w\frac{u_2}{u_1}(2bu_1 - M_w)\frac{\xi_5}{u_1} + bM_wu_1\frac{u_2^3+u_2u_3^2}{u_1^3}}{3\xi_1^2} & \frac{u_4}{u_1} + \frac{\left(2\frac{u_4}{u_1} - \frac{3u_2^2+u_3^2}{u_1^2}\right)+2\xi_4}{\frac{3\xi_1}{M_w}} - \xi_4 & -\frac{2M_w\frac{u_2u_3}{u_1^2}}{3\xi_1} & \frac{u_2}{u_1} + \frac{2M_wu_2}{3u_1\xi_1} \\ -\frac{u_2u_4}{u_1^2} + \frac{u_2}{u_1}\xi_3 - \frac{u_2}{u_1}\xi_4 & & & \end{bmatrix}$$

with

$$\xi_1 = M_w - bu_1,$$

$$\xi_2 = 6\frac{ab^2}{M_w^2}u_1^3 - 10\frac{ab}{M_w}u_1^2 + 2au_1,$$

$$\xi_3 = \frac{2aM_wu_1\xi_1 + 2abM_wu_1^2}{3M_w^2\xi_1^2},$$

$$\xi_4 = \frac{au_1}{M_w^2}$$

and

$$\xi_5 = u_4 - \frac{u_2^2 + u_3^2}{u_1}.$$

Now, we subtract the last matrix in equation (A.8) from the flux Jacobi matrix:

$$
\begin{aligned}
&\begin{bmatrix}
0 & 1 & 0 & 0 \\
-\frac{u_2^2}{u_1^2} + \frac{2bM_w\xi_5 + M_w^2\frac{u_2^2+u_3^2}{u_1^2} - \xi_2}{3\xi_1^2} & 2\frac{u_2}{u_1} + \frac{-2M_w\frac{u_2}{u_1}}{3\xi_1} & \frac{-2M_w\frac{u_3}{u_1}}{3\xi_1} & \frac{2M_w}{3\xi_1} \\
-\frac{u_2u_3}{u_1^2} & \frac{u_3}{u_1} & \frac{u_2}{u_1} & 0 \\
\frac{2M_w\frac{u_2}{u_1}(2bu_1 - M_w)\frac{\xi_5}{u_1} + bM_wu_1\frac{u_2^3+u_2u_3^2}{u_1^3}}{3\xi_1^2} & \frac{u_4}{u_1} + \frac{\left(2\frac{u_4}{u_1} - \frac{3u_2^2+u_3^2}{u_1^2}\right)+2\xi_4}{\frac{3\xi_1}{M_w}} - \xi_4 & -\frac{2M_w\frac{u_2u_3}{u_1^2}}{3\xi_1} & \frac{u_2}{u_1} + \frac{2M_wu_2}{3u_1\xi_1} \\
-\frac{u_2u_4}{u_1^2} + \frac{u_2}{u_1}\xi_3 - \frac{u_2}{u_1}\xi_4 & & &
\end{bmatrix} \\
&- \begin{bmatrix}
\frac{u_2}{u_1} & 0 & 0 & 0 \\
0 & \frac{u_2}{u_1} & 0 & 0 \\
0 & 0 & \frac{u_2}{u_1} & 0 \\
0 & 0 & 0 & \frac{u_2}{u_1}
\end{bmatrix} \\
&= \begin{bmatrix}
-\frac{u_2}{u_1} & 1 & 0 & 0 \\
-\frac{u_2^2}{u_1^2} + \frac{2bM_w\xi_5 + M_w^2\frac{u_2^2+u_3^2}{u_1^2} - \xi_2}{3\xi_1^2} & \frac{u_2}{u_1} + \frac{-2M_w\frac{u_2}{u_1}}{3\xi_1} & \frac{-2M_w\frac{u_3}{u_1}}{3\xi_1} & \frac{2M_w}{3\xi_1} \\
-\frac{u_2u_3}{u_1^2} & \frac{u_3}{u_1} & 0 & 0 \\
\frac{2M_w\frac{u_2}{u_1}(2bu_1 - M_w)\frac{\xi_5}{u_1} + bM_wu_1\frac{u_2^3+u_2u_3^2}{u_1^3}}{3\xi_1^2} & \frac{u_4}{u_1} + \frac{\left(2\frac{u_4}{u_1} - \frac{3u_2^2+u_3^2}{u_1^2}\right)+2\xi_4}{\frac{3\xi_1}{M_w}} - \xi_4 & -\frac{2M_w\frac{u_2u_3}{u_1^2}}{3\xi_1} & \frac{2M_wu_2}{3u_1\xi_1} \\
-\frac{u_2u_4}{u_1^2} + \frac{u_2}{u_1}\xi_3 - \frac{u_2}{u_1}\xi_4 & & &
\end{bmatrix}
\end{aligned}
\tag{A.12}
$$

For the next step, we need the transformation matrix from conservative to primitive variables for a Van der Waals gas. First, we write the vector of conservative variables in terms of the primitive variables $\boldsymbol{q}_1 = (q_1, q_2, q_3, q_4)^T = (\rho, v_1, v_2, p)^T$. For this purpose, we rewrite the caloric Van der Waals equation of state (4.4) on page 45 as

$$\rho E = \frac{3}{2M_w}\left(p + \frac{a\rho^2}{M_w^2}\right)(M_w - b\rho) + \frac{1}{2}\rho|\boldsymbol{v}|^2 - \frac{a\rho^2}{M_w^2}$$

With this, we get the vector of conservative variable as

$$\boldsymbol{u} = \left(q_1, q_1q_2, q_1q_3, \frac{3}{2M_w}\left(q_4 + \frac{aq_1^2}{M_w^2}\right)(M_w - bq_1) + \frac{1}{2}q_1\left(q_2^2 + q_3^2\right) - \frac{aq_1^2}{M_w^2}\right)^T$$

Now, we can write the transformation matrix as

$$\left(\frac{\partial \boldsymbol{u}}{\partial \boldsymbol{q}_1}\right) = \begin{bmatrix} 1 & 0 & 0 & 0 \\ q_2 & q_1 & 0 & 0 \\ q_3 & 0 & q_1 & 0 \\ \frac{-9ab}{2M_w^3}q_1^2 + \frac{a}{M_w^2}q_1 + \frac{1}{2}\left(q_2^2+q_3^2\right) - \frac{3b}{2M_w}q_4 & q_1q_2 & q_1q_3 & \frac{3}{2M_w}\left(M_w - bq_1\right) \end{bmatrix}.$$

To gain the first entry in the last row, we transform the derivative to

$$\begin{aligned} \left(\frac{\partial u_4}{\partial \left(\boldsymbol{q}_1\right)_1}\right) &= \frac{-3b}{2M_w}\left(q_4 + \frac{aq_1^2}{M_w^2}\right) + \frac{3aq_1}{M_w^3}\left(M_w - bq_1\right) + \frac{1}{2}\left(q_2^2+q_3^2\right) - 2\frac{aq_1}{M_w^2} \\ &= \frac{-3b}{2M_w}q_4 - \frac{3ab}{2M_w^3}q_1^2 + \frac{3a}{M_w^2}q_1 - \frac{3ab}{M_w^3}q_1^2 + \frac{1}{2}\left(q_2^2+q_3^2\right) - \frac{2a}{M_w^2}q_1 \\ &= \frac{-9ab}{2M_w^3}q_1^2 + \frac{a}{M_w^2}q_1 + \frac{1}{2}\left(q_2^2+q_3^2\right) - \frac{3b}{2M_w}q_4. \end{aligned}$$

For the multiplication we rewrite the transformation matrix in terms of conservative variables. For the first term in the last row, we use the representation of pressure in terms of the conservative variables that is given in equation (4.13) on page 51 to get

$$
\begin{aligned}
\left(\frac{\partial u_4}{\partial\left(\boldsymbol{q}_1\right)_1}\right) &= \frac{-9ab}{2M_w^3}u_1^2 + \frac{a}{M_w^2}u_1 + \frac{u_2^2+u_3^2}{2u_1^2} \\
&\quad - \frac{3b}{2M_w}\left(\frac{2M_w u_4 - M_w\frac{u_2^2+u_3^2}{u_1} + 2\frac{au_1^2}{M_w}}{3\left(M_w - bu_1\right)} - \frac{au_1^2}{M_w^2}\right) \\
&= \frac{-9ab}{2M_w^3}u_1^2 + \frac{a}{M_w^2}u_1 + \frac{u_2^2+u_3^2}{2u_1^2} - \frac{b}{M_w - bu_1}u_4 + \frac{b}{2\left(M_w - bu_1\right)}\frac{u_2^2+u_3^2}{u_1} \\
&\quad - \frac{ab}{M_w^2\left(M_w - bu_1\right)}u_1^2 + \frac{3ab}{2M_w^3}u_1^2 \\
&= \frac{-9abu_1^2\left(M_w - bu_1\right) + 2aM_w u_1\left(M_w - bu_1\right) - 2abM_w u_1^2}{2M_w^3\left(M_w - bu_1\right)} \\
&\quad + \frac{3ab\left(M_w - bu_1\right)u_1^2}{2M_w^3\left(M_w - bu_1\right)} + \frac{\left(u_2^2+u_3^2\right)\left(M_w - bu_1\right) + bu_1\left(u_2^2+u_3^2\right)}{2u_1^2\left(M_w - bu_1\right)} \\
&\quad - \frac{b}{M_w - bu_1}u_4 \\
&= \frac{-9abM_w u_1^2 + 9ab^2u_1^3 + 2aM_w^2u_1 - 2abM_w u_1^2 - 2abM_w u_1^2 + 3abM_w u_1^2}{2M_w^3\left(M_w - bu_1\right)} \\
&\quad - \frac{3ab^2u_1^3}{2M_w^3\left(M_w - bu_1\right)} + \frac{M_w\left(u_2^2+u_3^2\right)}{2u_1^2\left(M_w - bu_1\right)} - \frac{b}{M_w - bu_1}u_4 \\
&= \frac{6ab^2u_1^3 - 10abM_w u_1^2 + 2aM_w^2u_1}{2M_w^3\left(M_w - bu_1\right)} + \frac{M_w\left(u_2^2+u_3^2\right)}{2u_1^2\left(M_w - bu_1\right)} - \frac{b}{M_w - bu_1}u_4.
\end{aligned}
$$

We arrive at

$$
\left(\frac{\partial \boldsymbol{u}}{\partial \boldsymbol{q}_1}\right) = \begin{bmatrix}
1 & 0 & 0 & 0 \\
\frac{u_2}{u_1} & u_1 & 0 & 0 \\
\frac{u_3}{u_1} & 0 & u_1 & 0 \\
\frac{6ab^2u_1^3 - 10abM_w u_1^2 + 2aM_w^2u_1}{2M_w^3(M_w - bu_1)} + \frac{M_w\left(u_2^2+u_3^2\right)}{2u_1^2(M_w - bu_1)} - \frac{b}{M_w - bu_1}u_4 & u_2 & u_3 & \frac{3(M_w - bu_1)}{2M_w}
\end{bmatrix}.
$$

Now, we multiply the result of equation (A.12) with the transformation matrix from conservative to primitive variables. This gives us the following form of the matrix A_{prim}:

$$
A_{\text{prim}} = \begin{bmatrix}
-\frac{u_2}{u_1} & 1 & 0 & 0 \\
-\frac{u_2^2}{u_1^2} + \frac{2bM_w\xi_5 + M_w^2\frac{u_2^2+u_3^2}{u_1^2} - \xi_2}{3\xi_1^2} & \frac{u_2}{u_1} + \frac{-2M_w\frac{u_2}{u_1}}{3\xi_1} & \frac{-2M_w\frac{u_3}{u_1}}{3\xi_1} & \frac{2M_w}{3\xi_1} \\
-\frac{u_2u_3}{u_1^2} & \frac{u_3}{u_1} & 0 & 0 \\
\frac{2M_w\frac{u_2}{u_1}(2bu_1 - M_w)\frac{\xi_5}{u_1} + bM_wu_1\frac{u_2^3+u_2u_3^2}{u_1^3}}{3\xi_1^2} & \frac{u_4}{u_1} + \frac{\left(2\frac{u_4}{u_1} - \frac{3u_2^2+u_3^2}{u_1^2}\right)+2\xi_4}{\frac{3\xi_1}{M_w}} - \xi_4 & -\frac{2M_w\frac{u_2u_3}{u_1^2}}{3\xi_1} & \frac{2M_wu_2}{3u_1\xi_1} \\
-\frac{u_2u_4}{u_1^2} + \frac{u_2}{u_1}\xi_3 - \frac{u_2}{u_1}\xi_4 & & &
\end{bmatrix}
$$

$$
\cdot \begin{bmatrix}
1 & 0 & 0 & 0 \\
\frac{u_2}{u_1} & u_1 & 0 & 0 \\
\frac{u_3}{u_1} & 0 & u_1 & 0 \\
\frac{6ab^2u_1^3 - 10abM_wu_1^2 + 2aM_w^2u_1}{2M_w^3(M_w - bu_1)} + \frac{M_w\left(u_2^2+u_3^2\right)}{2u_1^2(M_w - bu_1)} - \frac{b}{M_w - bu_1}u_4 & u_2 & u_3 & \frac{3(M_w - bu_1)}{2M_w}
\end{bmatrix}
$$

$$
= \begin{bmatrix}
0 & u_1 & 0 & 0 \\
0 & u_2 & 0 & 1 \\
0 & u_3 & 0 & 0 \\
0 & \frac{-aM_wu_1^2 + 3abu_1^3}{3M_w^2(M_w - bu_1)} - \frac{M_w}{3(M_w - bu_1)}\frac{u_2^2+u_3^2}{u_1} + \frac{5M_w - 3bu_1}{3(M_w - bu_1)}u_4 & 0 & \frac{u_2}{u_1}
\end{bmatrix}
$$

In the following, we present the simplification of some of the entries of this matrix. We refer to the entry in row i and column j of A_{prim} as a_{ij}.

$$
\begin{aligned}
a_{21} = &-\frac{u_2^2}{u_1^2} + \frac{2bM_w\xi_5 + M_w^2\frac{u_2^2+u_3^2}{u_1^2} - \xi_2}{3\xi_1^2} + \frac{u_2^2}{u_1^2} - \frac{2M_w}{3\xi_1}\frac{u_2^2}{u_1^2} - \frac{2M_w}{3\xi_1}\frac{u_3^2}{u_1^2} \\
&+ \frac{2M_w}{3\xi_1}\left(\frac{6ab^2u_1^3 - 10abM_wu_1^2 + 2aM_w^2u_1}{2M_w^3\left(M_w - bu_1\right)} + \frac{M_w\left(u_2^2+u_3^2\right)}{2u_1^2\left(M_w - bu_1\right)} - \frac{b}{M_w - bu_1}u_4\right)
\end{aligned}
$$

To simplify this entry, we substitute the abbreviations ξ_1 to ξ_5 by the corresponding expressions:

$$
\begin{aligned}
a_{21} = & \frac{2bM_w}{3\left(M_w - bu_1\right)^2}\left(u_4 - \frac{u_2^2+u_3^2}{u_1}\right) + \frac{M_w^2}{3\left(M_w-bu_1\right)^2}\frac{u_2^2+u_3^2}{u_1^2} \\
& - \frac{6\frac{ab^2}{M_w^2}u_1^3 - 10\frac{ab}{M_w}u_1^2 + 2au_1}{3\left(M_w-bu_1\right)^2} - \frac{2M_w}{3\left(M_w-bu_1\right)}\frac{u_2^2+u_3^2}{u_1^2} \\
& + \frac{2M_w}{3\left(M_w-bu_1\right)}\frac{6ab^2u_1^3 - 10abM_wu_1^2 + 2aM_w^2u_1}{2M_w^3\left(M_w-bu_1\right)} + \frac{2M_w}{3\left(M_w-bu_1\right)}\frac{M_w\left(u_2^2+u_3^2\right)}{2u_1^2\left(M_w-bu_1\right)} \\
& - \frac{2M_w}{3\left(M_w-bu_1\right)}\frac{b}{\left(M_w-bu_1\right)}u_4 \\
= & -\frac{6ab^2M_wu_1^3 - 10abM_w^2u_1^2 + 2aM_w^3u_1}{3M_w^3\left(M_w-bu_1\right)^2} + \frac{6ab^2M_wu_1^3 - 10abM_w^2u_1^2 + 2aM_w^3u_1}{3M_w^3\left(M_w-bu_1\right)^2} \\
& - \frac{2bM_wu_1}{3\left(M_w-bu_1\right)^2}\frac{u_2^2+u_3^2}{u_1^2} + \frac{2M_w^2}{3\left(M_w-bu_1\right)^2}\frac{u_2^2+u_3^2}{u_1^2} - \frac{2M_w\left(M_w-bu_1\right)}{3\left(M_w-bu_1\right)^2}\frac{u_2^2+u_3^2}{u_1^2} \\
= & \frac{2M_w^2-2bM_wu_1}{3\left(M_w-bu_1\right)^2}\frac{u_2^2+u_3^2}{u_1^2} - \frac{2M_w^2-2bM_wu_1}{3\left(M_w-bu_1\right)^2}\frac{u_2^2+u_3^2}{u_1^2} = 0
\end{aligned}
$$

$$
\begin{aligned}
a_{41} = & \frac{2M_w\frac{u_2}{u_1}\left(2bu_1-M_w\right)\frac{\xi_5}{u_1} + bM_wu_1\frac{u_2^3+u_2u_3^2}{u_1^3}}{3\xi_1^2} - \frac{u_2u_4}{u_1^2} + \frac{u_2}{u_1}\xi_3 - \frac{u_2}{u_1}\xi_4 + \frac{u_2u_4}{u_1^2} \\
& + \frac{u_2}{u_1}\frac{\left(2\frac{u_4}{u_1} - \frac{3u_2^2+u_3^2}{u_1^2}\right) + 2\xi_4}{\frac{3\xi_1}{M_w}} - \frac{u_2}{u_1}\xi_4 - \frac{2M_w\frac{u_2u_3^2}{u_1^3}}{3\xi_1} \\
& + \frac{2M_wu_2}{3u_1\xi_1}\left(\frac{6ab^2u_1^3 - 10abM_wu_1^2 + 2aM_w^2u_1}{2M_w^3\left(M_w-bu_1\right)} + \frac{M_w\left(u_2^2+u_3^2\right)}{2u_1^2\left(M_w-bu_1\right)} - \frac{b}{M_w-bu_1}u_4\right)
\end{aligned}
$$

Again, we substitute the corresponding expressions for ξ_1 to ξ_5. This leads to

$$
\begin{aligned}
a_{41} = & \frac{2M_w\left(2bu_1-M_w\right)}{3\left(M_w-bu_1\right)^2}\frac{u_2}{u_1^2}\left(u_4 - \frac{u_2^2+u_3^2}{u_1}\right) + \frac{bM_wu_1}{3\left(M_w-bu_1\right)^2}\frac{u_2^3+u_2u_3^2}{u_1^3} \\
& + \frac{u_2}{u_1}\frac{2aM_wu_1\left(M_w-bu_1\right) + 2abM_wu_1^2}{3M_w^2\left(M_w-bu_1\right)^2} - \frac{u_2}{u_1}\frac{au_1}{M_w^2} + \frac{2M_w}{3\left(M_w-bu_1\right)}\frac{u_2u_4}{u_1^2} \\
& - \frac{M_w}{3\left(M_w-bu_1\right)}\frac{u_2}{u_1}\frac{3u_2^2+u_3^2}{u_1^2} + \frac{2M_w}{3\left(M_w-bu_1\right)}\frac{u_2}{u_1}\frac{au_1}{M_w^2} - \frac{u_2}{u_1}\frac{au_1}{M_w^2} - \frac{2M_w}{3\left(M_w-bu_1\right)}\frac{u_2u_3^2}{u_1^3} \\
& + \frac{2M_wu_2}{3u_1\left(M_w-bu_1\right)}\frac{6ab^2u_1^3 - 10abM_wu_1^2 + 2aM_w^2u_1}{2M_w^3\left(M_w-bu_1\right)} \\
& + \frac{2M_wu_2}{3u_1\left(M_w-bu_1\right)}\frac{M_w\left(u_2^2+u_3^2\right)}{2u_1^2\left(M_w-bu_1\right)} - \frac{2M_wu_2}{3u_1\left(M_w-bu_1\right)}\frac{b}{\left(M_w-bu_1\right)}u_4,
\end{aligned}
$$

which we can further simplify to

$$
\begin{aligned}
a_{41} &= u_2\frac{2aM_w^2-2abM_wu_1+2abM_wu_1}{3M_w^2\left(M_w-bu_1\right)^2}-u_2\frac{2a}{M_w^2}+\frac{2M_w}{3\left(M_w-bu_1\right)}u_2\frac{a}{M_w^2}\\
&+\frac{2M_wu_2}{3\left(M_w-bu_1\right)}\frac{6ab^2u_1^2-10abM_wu_1+2aM_w^2}{2M_w^3\left(M_w-bu_1\right)}-\frac{4bM_wu_1-2M_w^2}{3\left(M_w-bu_1\right)^2}\frac{u_2^3+u_2u_3^2}{u_1^3}\\
&+\frac{bM_wu_1}{3\left(M_w-bu_1\right)^2}\frac{u_2^3+u_2u_3^2}{u_1^3}-\frac{M_w}{3\left(M_w-bu_1\right)}\frac{3u_2^3+u_2u_3^2}{u_1^3}-\frac{2M_w}{3\left(M_w-bu_1\right)}\frac{u_2u_3^2}{u_1^3}\\
&+\frac{2M_w^2}{3\left(M_w-bu_1\right)^2}\frac{u_2^3+u_2u_3^2}{2u_1^3}+\frac{4bM_wu_1-2M_w^2}{3\left(M_w-bu_1\right)^2}\frac{u_2}{u_1^2}u_4+\frac{2M_w}{3\left(M_w-bu_1\right)}\frac{u_2u_4}{u_1^2}\\
&-\frac{2bM_w}{3\left(M_w-bu_1\right)^2}\frac{u_2u_4}{u_1}\\
&=u_2\frac{2aM_w^3-2abM_w^2u_1+2abM_w^2u_1}{3M_w^3\left(M_w-bu_1\right)^2}-u_2\frac{2aM_w\left(M_w^2-2bM_wu_1+b^2u_1^2\right)}{3M_w^3\left(M_w-bu_1\right)^2}\\
&+\frac{2aM_w^2\left(M_w-bu_1\right)}{3M_w^3\left(M_w-bu_1\right)^2}u_2+\frac{M_wu_2}{3\left(M_w-bu_1\right)}\frac{6ab^2u_1^2-10abM_wu_1+2aM_w^2}{M_w^3\left(M_w-bu_1\right)}\\
&-\frac{4bM_wu_1-2M_w^2}{3\left(M_w-bu_1\right)^2}\frac{u_2^3+u_2u_3^2}{u_1^3}+\frac{bM_wu_1}{3\left(M_w-bu_1\right)^2}\frac{u_2^3+u_2u_3^2}{u_1^3}\\
&-\frac{M_w}{3\left(M_w-bu_1\right)}\frac{3u_2^3+u_2u_3^2}{u_1^3}-\frac{2M_w}{3\left(M_w-bu_1\right)}\frac{u_2u_3^2}{u_1^3}+\frac{2M_w^2}{3\left(M_w-bu_1\right)^2}\frac{u_2^3+u_2u_3^2}{2u_1^3}\\
&+\frac{4bM_wu_1-2M_w^2}{3\left(M_w-bu_1\right)^2}\frac{u_2}{u_1^2}u_4+\frac{2M_w}{3\left(M_w-bu_1\right)}\frac{u_2u_4}{u_1^2}-\frac{2bM_w}{3\left(M_w-bu_1\right)^2}\frac{u_2u_4}{u_1}\\
&=\frac{2aM_w^3u_2-6aM_w^3u_2+12abM_w^2u_1u_2-6ab^2M_wu_1^2u_2+2aM_w^3u_2-2abM_w^2u_1u_2}{3M_w^3\left(M_w-bu_1\right)^2}\\
&+\frac{+6ab^2M_wu_1^2u_2-10abM_w^2u_1u_2+2aM_w^3u_2}{3M_w^3\left(M_w-bu_1\right)^2}-\frac{3bM_wu_1-M_w^2}{3\left(M_w-bu_1\right)^2}\frac{u_2}{u_1^2}\frac{u_2^2+u_3^2}{u_1}\\
&-\frac{M_w}{\left(M_w-bu_1\right)}\frac{u_2}{u_1}\frac{u_2^2+u_3^2}{u_1^2}+\frac{2bM_wu_1-2M_w^2}{3\left(M_w-bu_1\right)^2}\frac{u_2}{u_1^2}u_4+\frac{2M_w}{3\left(M_w-bu_1\right)}\frac{u_2u_4}{u_1^2}\\
&=\frac{\left(3bM_wu_1-M_w^2\right)u_2\left(u_2^2+u_3^2\right)-\left(3M_w^2-3bM_wu_1\right)u_2\left(u_2^2+u_3^2\right)}{3\left(M_w-bu_1\right)^2u_1^3}=0.
\end{aligned}
$$

$$
a_{42}=u_4+\frac{\left(2u_4-\frac{3u_2^2+u_3^2}{u_1}\right)+2\xi_4u_1}{\frac{3\xi_1}{M_w}}-\xi_4u_1+\frac{2M_wu_2^2}{3u_1\xi_1}
$$

First, we replace ξ_1 and ξ_4 by the corresponding expressions, which leads to

$$\begin{aligned}
a_{42} &= u_4 + \frac{2M_w}{3\left(M_w - bu_1\right)}u_4 - \frac{M_w}{3\left(M_w - bu_1\right)}\frac{3u_2^2 + u_3^2}{u_1} + \frac{2\frac{au_1^2}{M_w}}{3\left(M_w - bu_1\right)} - \frac{au_1^2}{M_w^2} \\
&\quad + \frac{2M_w u_2^2}{3u_1\left(M_w - bu_1\right)} \\
&= \frac{2aM_w u_1^2 - 3aM_w u_1^2 + 3abu_1^3}{3M_w^2\left(M_w - bu_1\right)} - \frac{M_w}{3\left(M_w - bu_1\right)}\frac{u_2^2 + u_3^2}{u_1} + \frac{2M_w + 3M_w - 3bu_1}{3\left(M_w - bu_1\right)}u_4 \\
&= \frac{-aM_w u_1^2 + 3abu_1^3}{3M_w^2\left(M_w - bu_1\right)} - \frac{M_w}{3\left(M_w - bu_1\right)}\frac{u_2^2 + u_3^2}{u_1} + \frac{5M_w - 3bu_1}{3\left(M_w - bu_1\right)}u_4.
\end{aligned}$$

Now, we replace the conservative variables in A_{prim}. For the second entry in the last row we can also insert pressure from the caloric equation of state for a Van der Waals gas (4.4) on page 45:

$$\begin{aligned}
a_{42} &= \frac{-aM_w u_1^2 + 3abu_1^3}{3M_w^2\left(M_w - bu_1\right)} - \frac{M_w}{3\left(M_w - bu_1\right)}\frac{u_2^2 + u_3^2}{u_1} + \frac{5M_w - 3bu_1}{3\left(M_w - bu_1\right)}u_4 \\
&= \frac{-aM_w\rho^2 + 3ab\rho^3}{3M_w^2\left(M_w - b\rho\right)} - \frac{M_w}{3\left(M_w - b\rho\right)}\rho|\boldsymbol{v}|^2 + \frac{5M_w - 3b\rho}{3\left(M_w - b\rho\right)}\rho E \\
&= \frac{\frac{-a\rho^2}{M_w} + \frac{3ab\rho^3}{M_w^2} - M_w\rho|\boldsymbol{v}|^2 + 2M_w\rho E}{3\left(M_w - b\rho\right)} + \rho E \\
&= \frac{\frac{-a\rho^2}{M_w^2}\cdot 3\left(M_w - b\rho\right) + \frac{2a\rho^2}{M_w} - M_w\rho|\boldsymbol{v}|^2 + 2M_w\rho E}{3\left(M_w - b\rho\right)} + \rho E \\
&= \frac{\frac{2a\rho^2}{M_w} - M_w\rho|\boldsymbol{v}|^2 + 2M_w\rho E}{3\left(M_w - b\rho\right)} - \frac{a\rho^2}{M_w^2} + \rho E = p + \rho E
\end{aligned}$$

With this, we get

$$A_{\text{prim}} = \begin{bmatrix} 0 & \rho & 0 & 0 \\ 0 & \rho v_1 & 0 & 1 \\ 0 & \rho v_2 & 0 & 0 \\ 0 & \rho\left(E + \frac{p}{\rho}\right) & 0 & v_1 \end{bmatrix}. \tag{A.13}$$

Now, we can write the Jacobi matrix for a Van der Waals gas in its final form

$$\boldsymbol{A}_{\boldsymbol{u}}^{(1)} = \begin{bmatrix} 0 & \rho & 0 & 0 \\ 0 & \rho v_1 & 0 & 1 \\ 0 & \rho v_2 & 0 & 0 \\ 0 & \rho(E + \frac{p}{\rho}) & 0 & v_1 \end{bmatrix} \frac{\partial \boldsymbol{q_1}}{\partial \boldsymbol{u}} + \begin{bmatrix} v_1 & 0 & 0 & 0 \\ 0 & v_1 & 0 & 0 \\ 0 & 0 & v_1 & 0 \\ 0 & 0 & 0 & v_1 \end{bmatrix}. \tag{A.14}$$

This matrix is identical to the one in equation (A.11) on page VIII for an ideal gas. The multiplication with $\frac{\partial \boldsymbol{q_1}}{\partial \boldsymbol{u}}$ introduces the differences due to the different equations of state. So, for our purpose, we can use equation (A.11) regardless of the equation of state.

A.3. Behavior of the MAPS+ Jacobi matrix for a vanishing Mach number

In this section, we analyze the different entries of matrix (4.21) on page 57 as the Mach number approaches zero for both an ideal and a Van der Waals gas. As $M \to 0$, ρ, p and E are of $\mathcal{O}(1)$ while v_1 is of $\mathcal{O}(M)$. In subsection 4.2.4.3 on page 73 we see that $c_{\text{max,mod}} = \mathcal{O}(M)$ and $(1 - |Ma_0|) = \mathcal{O}(1)$ as $M \to 0$. For the behavior of the transformations matrices, we take the results in equation (4.15) and (4.16) for the ideal and Van der Waals gas case, respectively.

For an ideal gas, we get

$$
\begin{aligned}
\boldsymbol{A}_{\boldsymbol{u},MAPS+} &= \begin{bmatrix} 0 & 0 & 0 & \mathcal{O}(M^{-1}) \\ 0 & \mathcal{O}(M) & 0 & \mathcal{O}(1) \\ 0 & \mathcal{O}(M) & 0 & \mathcal{O}(1) \\ 0 & 0 & 0 & \mathcal{O}(M^{-1}) \end{bmatrix} \cdot \begin{bmatrix} 1 & 0 & 0 & 0 \\ \mathcal{O}(M) & \mathcal{O}(1) & 0 & 0 \\ \mathcal{O}(M) & 0 & \mathcal{O}(1) & 0 \\ \mathcal{O}(M^2) & \mathcal{O}(M) & \mathcal{O}(M) & \mathcal{O}(1) \end{bmatrix} \\
&+ \begin{bmatrix} \mathcal{O}(M) & 0 & 0 & 0 \\ 0 & \mathcal{O}(M) & 0 & 0 \\ 0 & 0 & \mathcal{O}(M) & 0 \\ 0 & 0 & 0 & \mathcal{O}(M) \end{bmatrix} \\
&= \begin{bmatrix} \mathcal{O}(M) & \mathcal{O}(1) & \mathcal{O}(1) & \mathcal{O}(M^{-1}) \\ \mathcal{O}(M^2) & \mathcal{O}(M) & \mathcal{O}(M) & \mathcal{O}(1) \\ \mathcal{O}(M^2) & \mathcal{O}(M) & \mathcal{O}(M) & \mathcal{O}(1) \\ \mathcal{O}(M) & \mathcal{O}(1) & \mathcal{O}(1) & \mathcal{O}(M^{-1}) \end{bmatrix} \\
&+ \begin{bmatrix} \mathcal{O}(M) & 0 & 0 & 0 \\ 0 & \mathcal{O}(M) & 0 & 0 \\ 0 & 0 & \mathcal{O}(M) & 0 \\ 0 & 0 & 0 & \mathcal{O}(M) \end{bmatrix} \\
&= \begin{bmatrix} \mathcal{O}(M) & \mathcal{O}(1) & \mathcal{O}(1) & \mathcal{O}(M^{-1}) \\ \mathcal{O}(M^2) & \mathcal{O}(M) & \mathcal{O}(M) & \mathcal{O}(1) \\ \mathcal{O}(M^2) & \mathcal{O}(M) & \mathcal{O}(M) & \mathcal{O}(1) \\ \mathcal{O}(M) & \mathcal{O}(1) & \mathcal{O}(1) & \mathcal{O}(M^{-1}) \end{bmatrix}.
\end{aligned}
$$

While the usage of a Van der Waals gas leads to

$$
\begin{aligned}
\boldsymbol{A}_{\boldsymbol{u},MAPS+} &= \begin{bmatrix} 0 & 0 & 0 & \mathcal{O}(M^{-1}) \\ 0 & \mathcal{O}(M) & 0 & \mathcal{O}(1) \\ 0 & \mathcal{O}(M) & 0 & \mathcal{O}(1) \\ 0 & 0 & 0 & \mathcal{O}(M^{-1}) \end{bmatrix} \cdot \begin{bmatrix} 1 & 0 & 0 & 0 \\ \mathcal{O}(M) & \mathcal{O}(1) & 0 & 0 \\ \mathcal{O}(M) & 0 & \mathcal{O}(1) & 0 \\ \mathcal{O}(1) & \mathcal{O}(M) & \mathcal{O}(M) & \mathcal{O}(1) \end{bmatrix} \\
&+ \begin{bmatrix} \mathcal{O}(M) & 0 & 0 & 0 \\ 0 & \mathcal{O}(M) & 0 & 0 \\ 0 & 0 & \mathcal{O}(M) & 0 \\ 0 & 0 & 0 & \mathcal{O}(M) \end{bmatrix} \\
&= \begin{bmatrix} \mathcal{O}(M^{-1}) & \mathcal{O}(1) & \mathcal{O}(1) & \mathcal{O}(M^{-1}) \\ \mathcal{O}(1) & \mathcal{O}(M) & \mathcal{O}(M) & \mathcal{O}(1) \\ \mathcal{O}(1) & \mathcal{O}(M) & \mathcal{O}(M) & \mathcal{O}(1) \\ \mathcal{O}(M^{-1}) & \mathcal{O}(1) & \mathcal{O}(1) & \mathcal{O}(M^{-1}) \end{bmatrix} \\
&+ \begin{bmatrix} \mathcal{O}(M) & 0 & 0 & 0 \\ 0 & \mathcal{O}(M) & 0 & 0 \\ 0 & 0 & \mathcal{O}(M) & 0 \\ 0 & 0 & 0 & \mathcal{O}(M) \end{bmatrix} \\
&= \begin{bmatrix} \mathcal{O}(M^{-1}) & \mathcal{O}(1) & \mathcal{O}(1) & \mathcal{O}(M^{-1}) \\ \mathcal{O}(1) & \mathcal{O}(M) & \mathcal{O}(M) & \mathcal{O}(1) \\ \mathcal{O}(1) & \mathcal{O}(M) & \mathcal{O}(M) & \mathcal{O}(1) \\ \mathcal{O}(M^{-1}) & \mathcal{O}(1) & \mathcal{O}(1) & \mathcal{O}(M^{-1}) \end{bmatrix}.
\end{aligned}
$$

A.4. Taylor series

In general, a Taylor series is defined as follows.

Definition A.4.1.
The Taylor series of the function $f(x)$ at the point a is the power series

$$\sum_{n=0}^{\infty} \frac{f^{(n)}(a)}{n!},$$

where $f^{(n)}(a)$ denotes the nth derivative of the function $f(x)$ evaluated at the point a and $n!$ is the factorial of n.

In the following, we only consider Taylor series up to the second power.

A.4.1. Taylor series of the caloric Van der Waals equation of state

Inserting the asymptotic sequence into the caloric Van der Waals equation of state (2.19) on page 17, we get

$$\begin{aligned} p^{(0)} + Mp^{(1)} + M^2p^{(2)} = & \frac{2M_w\left(\rho^{(0)} + M\rho^{(1)} + M^2\rho^{(2)}\right)\left(E^{(0)} + ME^{(1)} + M^2E^{(2)}\right)}{3M_w - 3b\left(\rho^{(0)} + M\rho^{(1)} + M^2\rho^{(2)}\right)} \\ & - \frac{M^2M_w\left(\rho^{(0)} + M\rho^{(1)} + M^2\rho^{(2)}\right)\left(|\boldsymbol{v}^{(0)}| + M|\boldsymbol{v}^{(1)}| + M^2|\boldsymbol{v}^{(2)}|\right)^2}{3M_w - 3b\left(\rho^{(0)} + M\rho^{(1)} + M^2\rho^{(2)}\right)} \\ & + \frac{\frac{2a}{M_w}\left(\rho^{(0)} + M\rho^{(1)} + M^2\rho^{(2)}\right)^2}{3M_w - 3b\left(\rho^{(0)} + M\rho^{(1)} + M^2\rho^{(2)}\right)} - \frac{a\left(\rho^{(0)} + M\rho^{(1)} + M^2\rho^{(2)}\right)^2}{M_w^2}. \end{aligned}$$

Now we expand the right hand side of this equation into a Taylor series around $M = 0$. Since we are only interested in the $\mathcal{O}(1)$ part of the expression, we only consider the function $f(M)$ and neglect the derivatives. Hence, we can write

$$p^{(0)} = f(0) = \frac{2M_w\left(\rho E\right)^{(0)} + \frac{2a}{M_w}[\rho^{(0)}]^2}{3M_w - 3b\rho^{(0)}} - \frac{a[\rho^{(0)}]^2}{M_w^2}. \tag{A.15}$$

A.4.2. Taylor series of the density flux function of the general MAPS+ scheme

If we insert the asymptotic sequence into the density flux function of the general MAPS+ scheme presented in equation (4.25) on page 62 we get

$$\begin{aligned} \mathcal{H}^{\rho}_{MAPS+}\left(\widetilde{\boldsymbol{u}}_i, \widetilde{\boldsymbol{u}}_j; \boldsymbol{n}\right) = & \underbrace{\frac{\sum_{k=0}^{2} M^k \triangle_{ij} p^{(k)}}{2\sum_{k=0}^{2} M^k c^{(k)}_{\max,ij}}}_{f_1(M)} \\ & \underbrace{- M\left(\frac{\sum_{k=0}^{2} M^k |q^{(k)}|_{\max,ij}}{\sum_{k=0}^{2} M^k c^{(k)}_{\min,ij}} \frac{\sum_{k=0}^{2} M^k \triangle_{ij} p^{(k)}}{\sum_{k=0}^{2} M^k c_i^{(k)} + \sum_{k=0}^{2} M^k c_j^{(k)}}\right)}_{f_2(M)} \\ & + M\frac{\sum_{k=0}^{2} M^k |q^{(k)}|_{\max,ij}}{2}\left(\sum_{k=0}^{2} M^k \triangle_{ij}\rho^{(k)}\right) \\ & + M\sum_{k=0}^{2}\left(M^k q_i^{(k)} + M^k q_j^{(k)}\right)\frac{\sum_{k=0}^{2}\left(M^k\rho_i^{(k)} + M^k\rho_j^{(k)}\right)}{4}. \end{aligned} \tag{A.16}$$

We expand the right hand side of this equation into a Taylor series around $M = 0$. The part of $\mathcal{O}(1)$ is given by

$$\mathcal{H}^{\rho}_{MAPS+}\left(\widetilde{\boldsymbol{u}}_i, \widetilde{\boldsymbol{u}}_j; \boldsymbol{n}\right) = \frac{\triangle_{ij} p^{(0)}}{2 c^{(0)}_{\max,ij}}. \tag{A.17}$$

For the part of $\mathcal{O}(M)$, we need to consider the derivative $f'(M)$. In a first step, we only look at the first summand, so

$$f_1(M) = \frac{\sum_{k=0}^{2} M^k \triangle_{ij} p^{(k)}}{2 \sum_{k=0}^{2} M^k c^{(k)}_{\max,ij}}.$$

Now, we can write the derivative as

$$f_1'(M) = \frac{\triangle_{ij} p^{(1)} + 2M \triangle_{ij} p^{(2)}}{2 \sum_{k=0}^{2} M^k c^{(k)}_{\max,ij}} - \frac{\left(\sum_{k=0}^{2} M^k \triangle_{ij} p^{(k)}\right)\left(c^{(1)}_{\max,ij} + 2M c^{(2)}_{\max,ij}\right)}{2\left(\sum_{k=0}^{2} M^k c^{(k)}_{\max,ij}\right)^2}.$$

For $M = 0$ we get

$$f_1'(0) = \frac{\triangle_{ij} p^{(1)}}{2 c^{(0)}_{\max,ij}} - \frac{c^{(1)}_{\max,ij} \triangle_{ij} p^{(0)}}{2\left(c^{(0)}_{\max,ij}\right)^2}$$

Next, we look at the second summand. We can simplify the process of taking the derivative when we remember that we are only interested in the expression for $M = 0$. With this, we can deduce

$$f_2'(0) = \frac{|q^{(0)}|_{\max,ij}}{c^{(0)}_{\min,ij}} \frac{\triangle_{ij} p^{(0)}}{c^{(0)}_i + c^{(0)}_j}.$$

In a similar way we obtain the results for the remaining terms in equation (A.16). Combining all these expressions, we get

$$\begin{aligned} f(0) = {} & \frac{\triangle_{ij} p^{(1)}}{2 c^{(0)}_{\max,ij}} - \frac{c^{(1)}_{\max,ij} \triangle_{ij} p^{(0)}}{2\left(c^{(0)}_{\max,ij}\right)^2} - \frac{|q^{(0)}|_{\max,ij}}{c^{(0)}_{\min,ij}} \frac{\triangle_{ij} p^{(0)}}{c^{(0)}_i + c^{(0)}_j} + \frac{|q^{(0)}|_{\max,ij}}{2} \triangle_{ij} \rho^{(0)} \\ & + \frac{\left(q^{(0)}_i + q^{(0)}_j\right)\left(\rho^{(0)}_i + \rho^{(0)}_j\right)}{4}. \end{aligned} \tag{A.18}$$

A.4.3. Taylor series of the momentum flux functions of the general MAPS+ scheme

We insert the asymptotic sequence into the momentum flux functions of the general MAPS+ scheme presented in equation (4.26) on page 63. This results in

$$\begin{aligned}
\mathcal{H}^{\rho v_\zeta}_{MAPS+}(\widetilde{\boldsymbol{u}}_i, \widetilde{\boldsymbol{u}}_j; \boldsymbol{n}) = {} & n_\zeta \frac{\sum_{k=0}^{2}\left(M^k p_i^{(k)} + M^k p_j^{(k)}\right)}{2} \\
& + \underbrace{M \frac{\sum_{k=0}^{2}\left[M^k \left(v_\zeta\right)_i^{(k)} + M^k \left(v_\zeta\right)_j^{(k)}\right]}{\sum_{k=0}^{2} M^k 4 c_{\max,ij}^{(k)}} \sum_{k=0}^{2} M^k \triangle_{ij} p^{(k)}}_{f_1(M)} \\
& + \underbrace{n_\zeta M \frac{\sum_{k=0}^{2}\left(M^k \rho_i^{(k)} + M^k \rho_j^{(k)}\right)}{4} \sum_{k=0}^{2} M^k c_{\min,ij}^{(k)} \sum_{k=0}^{2} M^k \triangle_{ij} q^{(k)}}_{f_2(M)} \\
& - \underbrace{M^2 \frac{\sum_{k=0}^{2} M^k |q^{(k)}|_{\max,ij}}{2\sum_{k=0}^{2} M^k c_{\min,ij}^{(k)}} \frac{\sum_{k=0}^{2}\left[M^k \left(v_\zeta\right)_i^{(k)} + M^k \left(v_\zeta\right)_j^{(k)}\right]}{\sum_{k=0}^{2}\left(M^k c_i^{(k)} + M^k c_j^{(k)}\right)} \sum_{k=0}^{2} M^k \triangle_{ij} p^{(k)}}_{f_3(M)} \\
& - \underbrace{n_\zeta M^2 \frac{\sum_{k=0}^{2} M^k |q^{(k)}|_{\max,ij} \sum_{k=0}^{2} M^k c_{\max,ij}^{(k)}}{2}}_{f_4(M)} \\
& \underbrace{\cdot \frac{\sum_{k=0}^{2}\left(M^k \rho_i^{(k)} + M^k \rho_j^{(k)}\right)}{\sum_{k=0}^{2}\left(M^k c_i^{(k)} + M^k c_j^{(k)}\right)} \sum_{k=0}^{2} M^k \triangle_{ij} q^{(k)}}_{f_4(M)} \\
& + M^2 \frac{\sum_{k=0}^{2} M^k |q^{(k)}|_{\max,ij}}{2} \sum_{k=0}^{2} M^k \triangle_{ij} \left(\rho v_\zeta\right)^{(k)} \\
& + M^2 \frac{\sum_{k=0}^{2}\left(M^k q_i^{(k)} + M^k q_j^{(k)}\right)}{4} \sum_{k=0}^{2}\left[M^k \left(\rho v_\zeta\right)_i^{(k)} + M^k \left(\rho v_\zeta\right)_j^{(k)}\right].
\end{aligned} \tag{A.19}$$

We expand the right hand side of this equation into a Taylor series around $M = 0$. For the $\mathcal{O}(1)$ part we get

$$f(0) = \frac{p_i^{(0)} + p_j^{(0)}}{2}. \tag{A.20}$$

For the part of $\mathcal{O}(M)$, we consider the derivative $f'(M)$. In a first step, we only need the derivative at $M = 0$, which we can deduce as

$$f'(0) = n_\zeta \frac{p_i^{(1)} + p_j^{(1)}}{2} + \frac{(v_\zeta)_i^{(0)} + (v_\zeta)_j^{(0)}}{4c_{\max,ij}^{(0)}} \triangle_{ij} p^{(0)} + n_\zeta \frac{\rho_i^{(0)} + \rho_j^{(0)}}{4} c_{\min,ij}^{(0)} \triangle_{ij} q^{(0)}. \quad \text{(A.21)}$$

For the part of $\mathcal{O}(M^2)$, we need to calculate the second derivative $f''(M)$. In a first step, we consider the summand $f_1(M)$. The first derivative can be calculated as

$$\begin{aligned}
f_1'(M) = {} & M \frac{\sum_{k=0}^{2} \left[M^k (v_\zeta)_i^{(k)} + M^k (v_\zeta)_j^{(k)} \right]}{\sum_{k=0}^{2} M^k 4c_{\max,ij}^{(k)}} \left(\triangle_{ij} p^{(1)} + 2M \triangle_{ij} p^{(2)} \right) \\
& + M \frac{(v_\zeta)_i^{(1)} + 2M (v_\zeta)_i^{(2)} + (v_\zeta)_j^{(1)} + 2M (v_\zeta)_j^{(2)}}{\sum_{k=0}^{2} M^k 4c_{\max,ij}^{(k)}} \sum_{k=0}^{2} M^k \triangle_{ij} p^{(k)} \\
& - M \frac{\sum_{k=0}^{2} \left[M^k (v_\zeta)_i^{(k)} + M^k (v_\zeta)_j^{(k)} \right]}{\left(\sum_{k=0}^{2} M^k 4c_{\max,ij}^{(k)} \right)^2} \left(4c_{\max,ij}^{(1)} + 8M c_{\max,ij}^{(2)} \right) \sum_{k=0}^{2} M^k \triangle_{ij} p^{(k)} \\
& + \frac{\sum_{k=0}^{2} \left[M^k (v_\zeta)_i^{(k)} + M^k (v_\zeta)_j^{(k)} \right]}{\sum_{k=0}^{2} M^k 4c_{\max,ij}^{(k)}} \sum_{k=0}^{2} M^k \triangle_{ij} p^{(k)}.
\end{aligned}$$

From the second derivative, we only consider the part $f_1''(0)$. We can deduce this as

$$\begin{aligned}
f_1''(0) = {} & \frac{(v_\zeta)_i^{(0)} + (v_\zeta)_j^{(0)}}{2c_{\max,ij}^{(0)}} \triangle_{ij} p^{(1)} + \frac{(v_\zeta)_i^{(1)} + (v_\zeta)_j^{(1)}}{2c_{\max,ij}^{(0)}} \triangle_{ij} p^{(0)} \\
& - \frac{(v_\zeta)_i^{(0)} + (v_\zeta)_j^{(0)}}{2 \left(c_{\max,ij}^{(0)} \right)^2} c_{\max,ij}^{(1)} \triangle_{ij} p^{(0)}.
\end{aligned}$$

Now, we take the first derivative of the summand $f_2(M)$. We get

$$\begin{aligned}
f_2'(M) = n_\zeta M \frac{\sum_{k=0}^{2}\left(M^k\rho_i^{(k)} + M^k\rho_j^{(k)}\right)}{4} \sum_{k=0}^{2} M^k c_{\min,ij}^{(k)} \left(\triangle_{ij}q^{(1)} + 2M\triangle_{ij}q^{(2)}\right) \\
+n_\zeta M \frac{\sum_{k=0}^{2}\left(M^k\rho_i^{(k)} + M^k\rho_j^{(k)}\right)}{4} \left(c_{\min,ij}^{(1)} + 2Mc_{\min,ij}^{(2)}\right) \sum_{k=0}^{2} M^k \triangle_{ij}q^{(k)} \\
+n_\zeta M \frac{\rho_i^{(1)} + 2M\rho_i^{(2)} + \rho_j^{(1)} + 2M\rho_j^{(2)}}{4} \sum_{k=0}^{2} M^k c_{\min,ij}^{(k)} \sum_{k=0}^{2} M^k \triangle_{ij}q^{(k)} \\
+n_\zeta \frac{\sum_{k=0}^{2}\left(M^k\rho_i^{(k)} + M^k\rho_j^{(k)}\right)}{4} \sum_{k=0}^{2} M^k c_{\min,ij}^{(k)} \sum_{k=0}^{2} M^k \triangle_{ij}q^{(k)}.
\end{aligned}$$

For the second derivative at $M = 0$ we get

$$\begin{aligned}
f_2''(0) = n_\zeta \frac{\rho_i^{(0)} + \rho_j^{(0)}}{2} c_{\min,ij}^{(0)} \triangle_{ij}q^{(1)} + n_\zeta \frac{\rho_i^{(0)} + \rho_j^{(0)}}{2} c_{\min,ij}^{(1)} \triangle_{ij}q^{(0)} \\
+n_\zeta \frac{\rho_i^{(1)} + \rho_j^{(1)}}{2} c_{\min,ij}^{(0)} \triangle_{ij}q^{(0)}.
\end{aligned}$$

Next, we look at the summand $f_3(M)$. We write the first derivative as

$$
\begin{aligned}
&f_3'(M) = \\
&M^2 \frac{\sum_{k=0}^{2} M^k |q^{(k)}|_{\max,ij}}{2\sum_{k=0}^{2} M^k c_{\min,ij}^{(k)}} \frac{\sum_{k=0}^{2}\left[M^k (v_\zeta)_i^{(k)} + M^k (v_\zeta)_j^{(k)}\right]}{\sum_{k=0}^{2}\left(M^k c_i^{(k)} + M^k c_j^{(k)}\right)} \left(\triangle_{ij} p^{(1)} + 2M \triangle_{ij} p^{(2)}\right) \\
&+ M^2 \frac{\sum_{k=0}^{2} M^k |q^{(k)}|_{\max,ij}}{2\sum_{k=0}^{2} M^k c_{\min,ij}^{(k)}} \frac{(v_\zeta)_i^{(1)} + 2M (v_\zeta)_i^{(2)} (v_\zeta)_j^{(1)} + 2M (v_\zeta)_j^{(2)}}{\sum_{k=0}^{2}\left(M^k c_i^{(k)} + M^k c_j^{(k)}\right)} \sum_{k=0}^{2} M^k \triangle_{ij} p^{(k)} \\
&- M^2 \frac{\sum_{k=0}^{2} M^k |q^{(k)}|_{\max,ij}}{2\sum_{k=0}^{2} M^k c_{\min,ij}^{(k)}} \frac{\sum_{k=0}^{2}\left[M^k (v_\zeta)_i^{(k)} + M^k (v_\zeta)_j^{(k)}\right]}{\left(\sum_{k=0}^{2}\left(M^k c_i^{(k)} + M^k c_j^{(k)}\right)\right)^2} \\
&\quad \cdot \left(c_i^{(1)} + 2M c_i^{(2)} + c_j^{(1)} + 2M c_j^{(2)}\right) \sum_{k=0}^{2} M^k \triangle_{ij} p^{(k)} \\
&+ M^2 \frac{|q^{(1)}|_{\max,ij} + 2M |q^{(2)}|_{\max,ij}}{2\sum_{k=0}^{2} M^k c_{\min,ij}^{(k)}} \frac{\sum_{k=0}^{2}\left[M^k (v_\zeta)_i^{(k)} + M^k (v_\zeta)_j^{(k)}\right]}{\sum_{k=0}^{2}\left(M^k c_i^{(k)} + M^k c_j^{(k)}\right)} \sum_{k=0}^{2} M^k \triangle_{ij} p^{(k)} \\
&- M^2 \frac{\sum_{k=0}^{2} M^k |q^{(k)}|_{\max,ij}}{2\left(\sum_{k=0}^{2} M^k c_{\min,ij}^{(k)}\right)^2} \left(c_{\min,ij}^{(1)} + 2M c_{\min,ij}^{(2)}\right) \\
&\quad \cdot \frac{\sum_{k=0}^{2}\left[M^k (v_\zeta)_i^{(k)} + M^k (v_\zeta)_j^{(k)}\right]}{\sum_{k=0}^{2}\left(M^k c_i^{(k)} + M^k c_j^{(k)}\right)} \sum_{k=0}^{2} M^k \triangle_{ij} p^{(k)} \\
&+ 2M \frac{\sum_{k=0}^{2} M^k |q^{(k)}|_{\max,ij}}{2\sum_{k=0}^{2} M^k c_{\min,ij}^{(k)}} \frac{\sum_{k=0}^{2}\left[M^k (v_\zeta)_i^{(k)} + M^k (v_\zeta)_j^{(k)}\right]}{\sum_{k=0}^{2}\left(M^k c_i^{(k)} + M^k c_j^{(k)}\right)} \sum_{k=0}^{2} M^k \triangle_{ij} p^{(k)}.
\end{aligned}
$$

From the second derivative $f_3''(M)$, we only consider the part $f_3''(0)$. Hence, we can write

$$
f_3''(0) = \frac{|q^{(0)}|_{\max,ij}}{c_{\min,ij}^{(0)}} \frac{(v_\zeta)_i^{(0)} + (v_\zeta)_j^{(0)}}{c_i^{(0)} + c_j^{(0)}} \triangle_{ij} p^{(0)}.
$$

In the next step, we consider the summand $f_4(M)$ which is given by

$$
\begin{aligned}
f_4(M) = n_\zeta M^2 &\frac{\sum_{k=0}^{2} M^k |q^{(k)}|_{\max,ij} \sum_{k=0}^{2} M^k c_{\max,ij}^{(k)}}{2} \\
&\cdot \frac{\sum_{k=0}^{2}\left(M^k \rho_i^{(k)} + M^k \rho_j^{(k)}\right)}{\sum_{k=0}^{2}\left(M^k c_i^{(k)} + M^k c_j^{(k)}\right)} \sum_{k=0}^{2} M^k \triangle_{ij} q^{(k)}.
\end{aligned}
$$

If we look at the second derivative of $f_3(M)$, we see that the $\mathcal{O}(M^2)$-part of $f_3'(M)$ is not considered in $f_3''(0)$. Hence, we write the first derivative of $f_4(M)$ as

$$f_4'(M) = n_\zeta M \sum_{k=0}^{2} M^k |q^{(k)}|_{\max,ij} \sum_{k=0}^{2} M^k c_{\max,ij}^{(k)} \cdot \frac{\sum_{k=0}^{2} \left(M^k \rho_i^{(k)} + M^k \rho_j^{(k)} \right)}{\sum_{k=0}^{2} \left(M^k c_i^{(k)} + M^k c_j^{(k)} \right)} \sum_{k=0}^{2} M^k \triangle_{ij} q^{(k)} + \mathcal{O}(M^2).$$

Next, we derive the second derivative for $M = 0$. This leads us to

$$f_4''(0) = n_\zeta |q^{(0)}|_{\max,ij} c_{\max,ij}^{(0)} \frac{\rho_i^{(0)} + \rho_j^{(0)}}{c_i^{(0)} + c_j^{(0)}} \triangle_{ij} q^{(0)}.$$

Combining these intermediate results and taking the second derivative of the remaining terms in equation (A.19), we arrive at

$$\begin{aligned} f''(0) = {} & n_\zeta \left(p_i^{(2)} + p_j^{(2)} \right) + \frac{(v_\zeta)_i^{(0)} + (v_\zeta)_j^{(0)}}{2 c_{\max,ij}^{(0)}} \triangle_{ij} p^{(1)} + \frac{(v_\zeta)_i^{(1)} + (v_\zeta)_j^{(1)}}{2 c_{\max,ij}^{(0)}} \triangle_{ij} p^{(0)} \\ & - \frac{(v_\zeta)_i^{(0)} + (v_\zeta)_j^{(0)}}{2 \left(c_{\max,ij}^{(0)} \right)^2} c_{\max,ij}^{(1)} \triangle_{ij} p^{(0)} + n_\zeta \frac{\rho_i^{(0)} + \rho_j^{(0)}}{2} c_{\min,ij}^{(0)} \triangle_{ij} q^{(1)} \\ & + n_\zeta \frac{\rho_i^{(0)} + \rho_j^{(0)}}{2} c_{\min,ij}^{(1)} \triangle_{ij} q^{(0)} + n_\zeta \frac{\rho_i^{(1)} + \rho_j^{(1)}}{2} c_{\min,ij}^{(0)} \triangle_{ij} q^{(0)} \\ & - \frac{|q^{(0)}|_{\max,ij}}{c_{\min,ij}^{(0)}} \frac{(v_\zeta)_i^{(0)} + (v_\zeta)_j^{(0)}}{c_i^{(0)} + c_j^{(0)}} \triangle_{ij} p^{(0)} - n_\zeta |q^{(0)}|_{\max,ij} c_{\max,ij}^{(0)} \frac{\rho_i^{(0)} + \rho_j^{(0)}}{c_i^{(0)} + c_j^{(0)}} \triangle_{ij} q^{(0)} \\ & + \| q^{(0)} |_{\max,ij} \triangle_{ij} \left(\rho v_\zeta \right)^{(0)} + \frac{q_i^{(0)} + q_j^{(0)}}{2} \left[(\rho v_\zeta)_i^{(0)} + (\rho v_\zeta)_j^{(0)} \right], \end{aligned}$$

which leads us to the final result of

$$
\begin{aligned}
\mathcal{H}^{\rho v_\zeta}_{MAPS+}\left(\widetilde{\boldsymbol{u}}_i, \widetilde{\boldsymbol{u}}_j; \boldsymbol{n}\right) = & \frac{p_i^{(0)} + p_j^{(0)}}{2} \\
& + M \Bigg(n_\zeta \frac{p_i^{(1)} + p_j^{(1)}}{2} + \frac{(v_\zeta)_i^{(0)} + (v_\zeta)_j^{(0)}}{4 c_{\max,ij}^{(0)}} \triangle_{ij} p^{(0)} \\
& \qquad + n_\zeta \frac{\rho_i^{(0)} + \rho_j^{(0)}}{4} c_{\min,ij}^{(0)} \triangle_{ij} q^{(0)} \Bigg) \\
& + M^2 \Bigg(n_\zeta \frac{p_i^{(2)} + p_j^{(2)}}{2} + \frac{(v_\zeta)_i^{(0)} + (v_\zeta)_j^{(0)}}{4 c_{\max,ij}^{(0)}} \triangle_{ij} p^{(1)} \\
& \quad + \frac{(v_\zeta)_i^{(1)} + (v_\zeta)_j^{(1)}}{4 c_{\max,ij}^{(0)}} \triangle_{ij} p^{(0)} \\
& \quad - \frac{(v_\zeta)_i^{(0)} + (v_\zeta)_j^{(0)}}{4 \left(c_{\max,ij}^{(0)} \right)^2} c_{\max,ij}^{(1)} \triangle_{ij} p^{(0)} \\
& \quad + n_\zeta \frac{\rho_i^{(0)} + \rho_j^{(0)}}{4} c_{\min,ij}^{(0)} \triangle_{ij} q^{(1)} + n_\zeta \frac{\rho_i^{(0)} + \rho_j^{(0)}}{2} c_{\min,ij}^{(1)} \triangle_{ij} q^{(0)} \\
& \quad + n_\zeta \frac{\rho_i^{(1)} + \rho_j^{(1)}}{2} c_{\min,ij}^{(0)} \triangle_{ij} q^{(0)} \\
& \quad - \frac{|q^{(0)}|_{\max,ij}}{2 c_{\min,ij}^{(0)}} \frac{(v_\zeta)_i^{(0)} + (v_\zeta)_j^{(0)}}{c_i^{(0)} + c_j^{(0)}} \triangle_{ij} p^{(0)} \\
& \quad - n_\zeta \frac{|q^{(0)}|_{\max,ij}}{2} c_{\max,ij}^{(0)} \frac{\rho_i^{(0)} + \rho_j^{(0)}}{c_i^{(0)} + c_j^{(0)}} \triangle_{ij} q^{(0)} \\
& \quad + \frac{|q^{(0)}|_{\max,ij}}{2} \triangle_{ij} \left(\rho v_\zeta \right)^{(0)} \\
& \quad + \frac{q_i^{(0)} + q_j^{(0)}}{4} \left[(\rho v_\zeta)_i^{(0)} + (\rho v_\zeta)_j^{(0)} \right] \Bigg) + \mathcal{O}(M^3).
\end{aligned}
\tag{A.22}
$$

A.4.4. Taylor series of the density enthalpy flux function of the general MAPS+ scheme

Now we insert the asymptotic sequence into the density enthalpy flux function of the general MAPS+ scheme presented in equation (4.27) on page 63. The result is

$$\begin{aligned}
\mathcal{H}^{\rho h}_{MAPS+}\left(\widetilde{\boldsymbol{u}}_i, \widetilde{\boldsymbol{u}}_j; \boldsymbol{n}\right) = & \underbrace{\frac{\sum_{k=0}^{2}\left(M^k h_i^{(k)} + M^k h_j^{(k)}\right)}{4\sum_{k=0}^{2} M^k c^{(k)}_{\max,ij}} \sum_{k=0}^{2} M^k \triangle_{ij} p^{(k)}}_{f_1(M)} \\
& \underbrace{- M \frac{\sum_{k=0}^{2} M^k |q^{(k)}|_{\max,ij}}{2\sum_{k=0}^{2} M^k c^{(k)}_{\min,ij}} \frac{\sum_{k=0}^{2}\left(M^k h_i^{(k)} + M^k h_j^{(k)}\right)}{\sum_{k=0}^{2}\left(M^k c_i^{(k)} + M^k c_j^{(k)}\right)} \sum_{k=0}^{2} M^k \triangle_{ij} p^{(k)}}_{f_2(M)} \\
& + M \sum_{k=0}^{2} M^k \frac{|q^{(k)}|_{\max,ij}}{2} \triangle_{ij} \left(\sum_{k=0}^{2} M^k \rho^{(k)} \sum_{k=0}^{2} M^k h^{(k)}\right) \\
& + M \frac{\sum_{k=0}^{2}\left(M^k q_i^{(k)} + M^k q_j^{(k)}\right)}{4} \\
& \quad \cdot \left[\left(\sum_{k=0}^{2} M^k \rho_i^{(k)} \sum_{k=0}^{2} M^k h_i^{(k)}\right) + \left(\sum_{k=0}^{2} M^k \rho_j^{(k)} \sum_{k=0}^{2} M^k h_j^{(k)}\right)\right].
\end{aligned} \tag{A.23}$$

We expand the right hand side of this equation into a Taylor series around $M = 0$. The part of $\mathcal{O}(1)$ is given by

$$f(0) = \frac{h_i^{(0)} + h_j^{(0)}}{4c^{(0)}_{\max,ij}} \triangle_{ij} p^{(0)}. \tag{A.24}$$

For the part of $\mathcal{O}(M)$, we consider the derivative $f'(M)$. In a first step, we look at the first summand $f_1(M)$. We can write the derivative as

$$\begin{aligned}
f_1'(M) = & \frac{\sum_{k=0}^{2}\left(M^k h_i^{(k)} + M^k h_j^{(k)}\right)}{4\sum_{k=0}^{2} M^k c^{(k)}_{\max,ij}} \left(\triangle_{ij} p^{(1)} + 2M \triangle_{ij} p^{(2)}\right) \\
& + \frac{h_i^{(1)} + 2M h_i^{(2)} + h_j^{(1)} + 2M h_j^{(2)}}{4\sum_{k=0}^{2} M^k c^{(k)}_{\max,ij}} \sum_{k=0}^{2} M^k \triangle_{ij} p^{(k)} \\
& - \frac{\left(c^{(1)}_{\max,ij} + 2M c^{(2)}_{\max,ij}\right)\sum_{k=0}^{2}\left(M^k h_i^{(k)} + M^k h_j^{(k)}\right)}{4\left(\sum_{k=0}^{2} M^k c^{(k)}_{\max,ij}\right)^2} \sum_{k=0}^{2} M^k \triangle_{ij} p^{(k)}.
\end{aligned}$$

For $M = 0$, we get

$$f_1'(0) = \frac{h_i^{(0)} + h_j^{(0)}}{4c_{\max,ij}^{(0)}} \triangle_{ij} p^{(1)} + \frac{h_i^{(1)} + h_j^{(1)}}{4c_{\max,ij}^{(0)}} \triangle_{ij} p^{(0)} - \frac{c_{\max,ij}^{(1)} \left(h_i^{(0)} + h_j^{(0)} \right)}{4 \left(c_{\max,ij}^{(0)} \right)^2} \triangle_{ij} p^{(0)}.$$

For the second summand $f_2(M)$, we only consider $f'(0)$. Hence, we arrive at

$$f_2'(0) = \frac{|q^{(0)}|_{\max,ij}}{2c_{\min,ij}^{(0)}} \frac{h_i^{(0)} + h_j^{(0)}}{c_i^{(0)} + c_j^{(0)}} \triangle_{ij} p^{(0)}.$$

In a similar way we obtain the results for the remaining terms in equation (A.23). Combining all these expressions, we get

$$\begin{aligned} f'(0) = & \frac{h_i^{(0)} + h_j^{(0)}}{4c_{\max,ij}^{(0)}} \triangle_{ij} p^{(1)} + \frac{h_i^{(1)} + h_j^{(1)}}{4c_{\max,ij}^{(0)}} \triangle_{ij} p^{(0)} - \frac{c_{\max,ij}^{(1)} \left(h_i^{(0)} + h_j^{(0)} \right)}{4 \left(c_{\max,ij}^{(0)} \right)^2} \triangle_{ij} p^{(0)} \\ & - \frac{|q^{(0)}|_{\max,ij}}{2c_{\min,ij}^{(0)}} \frac{h_i^{(0)} + h_j^{(0)}}{c_i^{(0)} + c_j^{(0)}} \triangle_{ij} p^{(0)} + \frac{|q^{(0)}|_{\max,ij}}{2} \triangle_{ij} \left(\rho h \right)^{(0)} \\ & + \frac{q_i^{(0)} + q_j^{(0)}}{4} \left[\left(\rho h \right)_i + \left(\rho h \right)_j \right]. \end{aligned} \tag{A.25}$$

A.4.5. Taylor series of the density flux function of the altered MAPS+ scheme

Now we insert the asymptotic sequence into the density flux function of the altered MAPS+ scheme presented in equation (4.40) on page 80. To expand it into a Taylor series, we multiply the expression by the Mach number. This gives us

$$\begin{aligned} M \cdot \mathcal{H}_{MAPS+}^{\rho} \left(\widetilde{\boldsymbol{u}}_i, \widetilde{\boldsymbol{u}}_j; \boldsymbol{n} \right) = & \frac{1}{2} \left(\frac{\sum_{k=0}^{2} \left(M^k c_i^{(k)} + M^k c_j^{(k)} \right)}{\xi} \right. \\ & \left. - \frac{\sum_{k=0}^{2} M^k c_{\max,ij}^{(k)} \sum_{k=0}^{2} M^k |q^{(k)}|_{\max,ij} \sum_{k=0}^{2} \left(M^k c_i^{(k)} + M^k c_j^{(k)} \right)}{\xi^2} \right) \sum_{k=0}^{2} M^k \triangle_{ij} p^{(k)} \\ & + \mathcal{O}(M^2) \end{aligned}$$

with

$$\xi = \left[\left(\sum_{k=0}^{2} M^k c_{\max,ij}^{(k)} \right)^2 \left(\sum_{k=0}^{2} M^k |q^{(k)}|_{\max,ij} \right)^2 + \left(\sum_{k=0}^{2} M^k q_{\text{ref},ij}^{(k)} \right)^2 \left(\sum_{k=0}^{2} \left[M^k c_i^{(k)} + M^k c_j^{(k)} \right] \right)^2 \right]^{\frac{1}{2}}. \tag{A.26}$$

We expand the right hand side of this equation into a Taylor series around $M = 0$. The part of $\mathcal{O}(1)$ is given by

$$f(0) = \frac{1}{2} \left(\frac{\left(c_i^{(0)} + c_j^{(0)} \right)}{\sqrt{\left(c_{\max,ij}^{(0)} \right)^2 \left(|q^{(0)}|_{\max,ij} \right)^2 + \left(q_{\text{ref},ij}^{(0)} \right)^2 \left(c_i^{(0)} + c_j^{(0)} \right)^2}} - \frac{c_{\max,ij}^{(0)} |q^{(0)}|_{\max,ij} \left(c_i^{(0)} + c_j^{(0)} \right)}{\left(c_{\max,ij}^{(0)} \right)^2 \left(|q^{(0)}|_{\max,ij} \right)^2 + \left(q_{\text{ref},ij}^{(0)} \right)^2 \left(c_i^{(0)} + c_j^{(0)} \right)^2} \right) \triangle_{ij} p^{(0)}.$$

For the part of $\mathcal{O}(M)$, we calculate the derivative $f'(M)$. Here, we are only interested in the part of $M = 0$. Hence, we get

$$
\begin{aligned}
f'(0) = \frac{1}{2}\Bigg(& \frac{\left(c_i^{(0)} + c_j^{(0)}\right)}{\sqrt{\xi_1^2 + \left(q_{\mathrm{ref},ij}^{(0)}\right)^2 \left(c_i^{(0)} + c_j^{(0)}\right)^2}} - \frac{\xi_1 \left(c_i^{(0)} + c_j^{(0)}\right)}{\xi_1^2 + \left(q_{\mathrm{ref},ij}^{(0)}\right)^2 \left(c_i^{(0)} + c_j^{(0)}\right)^2} \Bigg) \triangle_{ij} p^{(1)} \\
& + \frac{1}{2}\Bigg(\frac{\left(c_i^{(1)} + c_j^{(1)}\right)}{\sqrt{\xi_1^2 + \left(q_{\mathrm{ref},ij}^{(0)}\right)^2 \left(c_i^{(0)} + c_j^{(0)}\right)^2}} - \frac{\left(c_i^{(0)} + c_j^{(0)}\right)}{2\left[\xi_1^2 + \left(q_{\mathrm{ref},ij}^{(0)}\right)^2 \left(c_i^{(0)} + c_j^{(0)}\right)^2\right]^{\frac{3}{2}}} \\
& \quad \cdot \Big[2c_{\max,ij}^{(0)} \xi_1 |q^{(1)}|_{\max,ij} + 2c_{\max,ij}^{(1)} |q^{(0)}|_{\max,ij} \xi_1 \\
& \qquad + 2\left(q_{\mathrm{ref},ij}^{(0)}\right)^2 \left(c_i^{(0)} + c_j^{(0)}\right)\left(c_i^{(1)} + c_j^{(1)}\right) + 2q_{\mathrm{ref},ij}^{(0)} q_{\mathrm{ref},ij}^{(1)} \left(c_i^{(0)} + c_j^{(0)}\right) \Big] \\
& \quad - \frac{\xi_1 \left(c_i^{(1)} + c_j^{(1)}\right)}{\xi_1^2 + \left(q_{\mathrm{ref},ij}^{(0)}\right)^2 \left(c_i^{(0)} + c_j^{(0)}\right)^2} - \frac{c_{\max,ij}^{(0)} |q^{(1)}|_{\max,ij} \left(c_i^{(0)} + c_j^{(0)}\right)}{\xi_1^2 + \left(q_{\mathrm{ref},ij}^{(0)}\right)^2 \left(c_i^{(0)} + c_j^{(0)}\right)^2} \\
& \quad - \frac{+c_{\max,ij}^{(1)} |q^{(0)}|_{\max,ij} \left(c_i^{(0)} + c_j^{(0)}\right)}{\xi_1^2 + \left(q_{\mathrm{ref},ij}^{(0)}\right)^2 \left(c_i^{(0)} + c_j^{(0)}\right)^2} + \frac{\xi_1 \left(c_i^{(0)} + c_j^{(0)}\right)}{\left[\xi_1^2 + \left(q_{\mathrm{ref},ij}^{(0)}\right)^2 \left(c_i^{(0)} + c_j^{(0)}\right)^2\right]^2} \\
& \quad \cdot \Big[2c_{\max,ij}^{(0)} |q^{(1)}|_{\max,ij} \xi_1 + 2c_{\max,ij}^{(1)} |q^{(0)}|_{\max,ij} \xi_1 \\
& \qquad + 2\left(q_{\mathrm{ref},ij}^{(0)}\right)^2 \left(c_i^{(0)} + c_j^{(0)}\right)\left(c_i^{(1)} + c_j^{(1)}\right) + 2q_{\mathrm{ref},ij}^{(0)} q_{\mathrm{ref},ij}^{(1)} \left(c_i^{(0)} + c_j^{(0)}\right) \Big] \Bigg) \\
& \cdot \triangle_{ij} p^{(0)}
\end{aligned}
$$

with

$$
\xi_1 = c_{\max,ij}^{(0)} |q^{(0)}|_{\max,ij}.
$$

Combining these results, we arrive at

$$
\begin{aligned}
&\mathcal{H}^{\rho}_{MAPS+}\left(\widetilde{\boldsymbol{u}}_i, \widetilde{\boldsymbol{u}}_j; \boldsymbol{n}\right) = \\
&\frac{1}{2M}\left(\frac{\left(c_i^{(0)}+c_j^{(0)}\right)}{\sqrt{\xi_1^2+\left(q_{\mathrm{ref},ij}^{(0)}\right)^2\left(c_i^{(0)}+c_j^{(0)}\right)^2}} - \frac{\xi_1\left(c_i^{(0)}+c_j^{(0)}\right)}{\xi_1^2+\left(q_{\mathrm{ref},ij}^{(0)}\right)^2\left(c_i^{(0)}+c_j^{(0)}\right)^2}\right)\triangle_{ij}p^{(0)} \\
&+\frac{1}{2}\left(\frac{\left(c_i^{(0)}+c_j^{(0)}\right)}{\sqrt{\xi_1^2+\left(q_{\mathrm{ref},ij}^{(0)}\right)^2\left(c_i^{(0)}+c_j^{(0)}\right)^2}} - \frac{\xi_1\left(c_i^{(0)}+c_j^{(0)}\right)}{\xi_1^2+\left(q_{\mathrm{ref},ij}^{(0)}\right)^2\left(c_i^{(0)}+c_j^{(0)}\right)^2}\right)\triangle_{ij}p^{(1)} \\
&+\frac{1}{2}\Bigg(\frac{\left(c_i^{(1)}+c_j^{(1)}\right)}{\sqrt{\xi_1^2+\left(q_{\mathrm{ref},ij}^{(0)}\right)^2\left(c_i^{(0)}+c_j^{(0)}\right)^2}} - \frac{\left(c_i^{(0)}+c_j^{(0)}\right)}{2\left[\xi_1^2+\left(q_{\mathrm{ref},ij}^{(0)}\right)^2\left(c_i^{(0)}+c_j^{(0)}\right)^2\right]^{\frac{3}{2}}} \\
&\quad\cdot\Big(2c_{\max,ij}^{(0)}\xi_1|q^{(1)}|_{\max,ij}+2c_{\max,ij}^{(1)}|q^{(0)}|_{\max,ij}\xi_1 \\
&\qquad+2\left(q_{\mathrm{ref},ij}^{(0)}\right)^2\left(c_i^{(0)}+c_j^{(0)}\right)\left(c_i^{(1)}+c_j^{(1)}\right)+2q_{\mathrm{ref},ij}^{(0)}q_{\mathrm{ref},ij}^{(1)}\left(c_i^{(0)}+c_j^{(0)}\right)\Big] \\
&\quad-\frac{\xi_1\left(c_i^{(1)}+c_j^{(1)}\right)}{\xi_1^2+\left(q_{\mathrm{ref},ij}^{(0)}\right)^2\left(c_i^{(0)}+c_j^{(0)}\right)^2} - \frac{c_{\max,ij}^{(0)}|q^{(1)}|_{\max,ij}\left(c_i^{(0)}+c_j^{(0)}\right)}{\xi_1^2+\left(q_{\mathrm{ref},ij}^{(0)}\right)^2\left(c_i^{(0)}+c_j^{(0)}\right)^2} \\
&\quad-\frac{c_{\max,ij}^{(1)}|q^{(0)}|_{\max,ij}\left(c_i^{(0)}+c_j^{(0)}\right)}{\xi_1^2+\left(q_{\mathrm{ref},ij}^{(0)}\right)^2\left(c_i^{(0)}+c_j^{(0)}\right)^2} + \frac{\xi_1\left(c_i^{(0)}+c_j^{(0)}\right)}{\left[\xi_1^2+\left(q_{\mathrm{ref},ij}^{(0)}\right)^2\left(c_i^{(0)}+c_j^{(0)}\right)^2\right]^2} \\
&\quad\cdot\Big[2c_{\max,ij}^{(0)}|q^{(1)}|_{\max,ij}\xi_1+2c_{\max,ij}^{(1)}|q^{(0)}|_{\max,ij}\xi_1 \\
&\qquad+2\left(q_{\mathrm{ref},ij}^{(0)}\right)^2\left(c_i^{(0)}+c_j^{(0)}\right)\left(c_i^{(1)}+c_j^{(1)}\right)+2q_{\mathrm{ref},ij}^{(0)}q_{\mathrm{ref},ij}^{(1)}\left(c_i^{(0)}+c_j^{(0)}\right)\Big]\Bigg)\triangle_{ij}p^{(0)} \\
&+\mathcal{O}(M).
\end{aligned}
\tag{A.27}
$$

A.4.6. Taylor series of the momentum flux function of the altered MAPS+ scheme

We insert the asymptotic sequence into the momentum flux function of the altered MAPS+ scheme given by equation (4.41) on page 82. This leads to

$$
\begin{aligned}
\mathcal{H}^{\rho v_\zeta}_{MAPS+}(\widetilde{\boldsymbol{u}}_i, \widetilde{\boldsymbol{u}}_j; \boldsymbol{n}) &= -n_\zeta \frac{\sum_{k=0}^{2}\left(M^k p_i^{(k)} + M^k p_j^{(k)}\right)}{2} \\
&+ \left(\frac{\sum_{k=0}^{2}\left(M^k c_i^{(k)} + M^k c_j^{(k)}\right)}{\xi} - \frac{\xi_q \sum_{k=0}^{2} M^k c_{\max,ij}^{(k)} \sum_{k=0}^{2}\left(M^k c_i^{(k)} + M^k c_j^{(k)}\right)}{\xi^2} \right) \\
&\quad \cdot \frac{\sum_{k=0}^{2}\left[M^k \left(v_\zeta\right)_i^{(k)} + M^k \left(v_\zeta\right)_j^{(k)}\right]}{4} \sum_{k=0}^{2} M^k \triangle_{ij} p^{(k)} \\
&+ \frac{M}{16} \Bigg(\frac{\xi_q^2 \left(\sum_{k=0}^{2} M^k q_{\mathrm{ref},ij}^{(k)}\right)^2 \sum_{k=0}^{2}\left(M^k c_i^{(k)} + M^k c_j^{(k)}\right)}{\xi^3} \\
&\qquad + \frac{\xi_q^3 \sum_{k=0}^{2} M^k c_{\max,ij}^{(k)} \left(\sum_{k=0}^{2} M^k q_{\mathrm{ref},ij}^{(k)}\right)^2 \sum_{k=0}^{2}\left(M^k c_i^{(k)} + M^k c_j^{(k)}\right)}{\xi^4} \\
&\qquad - \frac{\xi_q \left(\sum_{k=0}^{2} M^k q_{\mathrm{ref},ij}^{(k)}\right)^2 \sum_{k=0}^{2}\left(M^k c_i^{(k)} + M^k c_j^{(k)}\right)}{\sum_{k=0}^{2} M^k c_{\max,ij}^{(k)} \xi^4} \\
&\qquad\quad \cdot \left[2\left(\sum_{k=0}^{2} M^k c_{\max,ij}^{(k)}\right)^2 \xi_q^2 + \left(\sum_{k=0}^{2} M^k q_{\mathrm{ref},ij}^{(k)}\right)^2 \left(\sum_{k=0}^{2}\left[M^k c_i^{(k)} + M^k c_j^{(k)}\right]\right)^2 \right] \Bigg) \\
&\qquad \cdot \sum_{k=0}^{2}\left[M^k \left(v_\zeta\right)_i^{(k)} + M^k \left(v_\zeta\right)_j^{(k)}\right] \sum_{k=0}^{2} M^k \triangle_{ij} p^{(k)} \\
&+ \mathcal{O}(M^2)
\end{aligned}
\tag{A.28}
$$

with $\zeta = 1, 2$ and ξ given by equation (A.26). The abbreviation ξ_q is given by

$$
\xi_q = \sum_{k=0}^{2} M^k |q^{(k)}|_{\max,ij}.
$$

Now, we expand the right hand side of this equation into a Taylor series around $M = 0$.

In a first step, we write the part of $\mathcal{O}(1)$ as

$$f(0) = -n_\zeta \frac{p_i^{(0)} + p_j^{(0)}}{2} + \left(\frac{c_i^{(0)} + c_j^{(0)}}{\sqrt{\left(c_{\max,ij}^{(0)}\right)^2 \left(|q^{(0)}|_{\max,ij}\right)^2 + \left(q_{\mathrm{ref},ij}^{(0)}\right)^2 \left(c_i^{(0)} + c_j^{(0)}\right)^2}} \right.$$
$$\left. - \frac{|q^{(0)}|_{\max,ij} c_{\max,ij}^{(0)} \left(c_i^{(0)} + c_j^{(0)}\right)}{\left(c_{\max,ij}^{(0)}\right)^2 \left(|q^{(0)}|_{\max,ij}\right)^2 + \left(q_{\mathrm{ref},ij}^{(0)}\right)^2 \left(c_i^{(0)} + c_j^{(0)}\right)^2} \right)$$
$$\cdot \frac{(v_\zeta)_i^{(0)} + (v_\zeta)_j^{(0)}}{4} \triangle_{ij} p^{(0)}.$$

For the part of $\mathcal{O}(M)$, we calculate the derivative $f'(M)$. Here, we only consider the part of $M = 0$. Hence, we get

$$
\begin{aligned}
f'(0) = -n_\zeta \frac{p_i^{(1)} + p_j^{(1)}}{2} &+ \left(\frac{\xi_2}{\sqrt{\xi_1^2 + \left(q_{\mathrm{ref},ij}^{(0)}\right)^2 \xi_2^2}} - \frac{\xi_1 \xi_2}{\xi_1^2 + \left(q_{\mathrm{ref},ij}^{(0)}\right)^2 \xi_2^2} \right) \\
&\cdot \frac{(v_\zeta)_i^{(0)} + (v_\zeta)_j^{(0)}}{4} \triangle_{ij} p^{(1)} \\
&+ \left(\frac{\xi_2}{\sqrt{\xi_1^2 + \left(q_{\mathrm{ref},ij}^{(0)}\right)^2 \xi_2^2}} - \frac{\xi_1 \xi_2}{\xi_1^2 + \left(q_{\mathrm{ref},ij}^{(0)}\right)^2 \xi_2^2} \right) \frac{(v_\zeta)_i^{(1)} + (v_\zeta)_j^{(1)}}{4} \triangle_{ij} p^{(0)} \\
&+ \frac{1}{2} \Bigg(\frac{\left(c_i^{(1)} + c_j^{(1)}\right)}{\sqrt{\xi_1^2 + \left(q_{\mathrm{ref},ij}^{(0)}\right)^2 \xi_2^2}} - \frac{\xi_2}{2\left[\xi_1^2 + \left(q_{\mathrm{ref},ij}^{(0)}\right)^2 \xi_2^2\right]^{\frac{3}{2}}} \Big[2 c_{\max,ij}^{(0)} \xi_1 |q^{(1)}|_{\max,ij} \\
&\quad + 2 c_{\max,ij}^{(1)} |q^{(0)}|_{\max,ij} \xi_1 + 2 \left(q_{\mathrm{ref},ij}^{(0)}\right)^2 \xi_2 \left(c_i^{(1)} + c_j^{(1)}\right) + 2 q_{\mathrm{ref},ij}^{(0)} q_{\mathrm{ref},ij}^{(1)} \xi_2 \Big] \\
&\quad - \frac{\xi_1 \left(c_i^{(1)} + c_j^{(1)}\right)}{\xi_1^2 + \left(q_{\mathrm{ref},ij}^{(0)}\right)^2 \xi_2^2} - \frac{c_{\max,ij}^{(0)} |q^{(1)}|_{\max,ij} \xi_2}{\xi_1^2 + \left(q_{\mathrm{ref},ij}^{(0)}\right)^2 \xi_2^2} - \frac{+ c_{\max,ij}^{(1)} |q^{(0)}|_{\max,ij} \xi_2}{\xi_1^2 + \left(q_{\mathrm{ref},ij}^{(0)}\right)^2 \xi_2^2} \\
&\quad + \frac{\xi_1 \xi_2}{\left[\xi_1^2 + \left(q_{\mathrm{ref},ij}^{(0)}\right)^2 \xi_2^2\right]^2} \Big[2 c_{\max,ij}^{(0)} |q^{(1)}|_{\max,ij} \xi_1 + 2 c_{\max,ij}^{(1)} |q^{(0)}|_{\max,ij} \xi_1 \\
&\quad + 2 \left(q_{\mathrm{ref},ij}^{(0)}\right)^2 \xi_2 \left(c_i^{(1)} + c_j^{(1)}\right) + 2 q_{\mathrm{ref},ij}^{(0)} q_{\mathrm{ref},ij}^{(1)} \xi_2 \Big] \Bigg) \frac{(v_\zeta)_i^{(0)} + (v_\zeta)_j^{(0)}}{4} \triangle_{ij} p^{(0)} \\
&+ \frac{1}{16} \Bigg(\frac{|q^{(0)}|_{\max,ij}^2 \left(q_{\mathrm{ref},ij}^{(0)}\right)^2 \xi_2}{\left(\xi_1^2 + \left(q_{\mathrm{ref},ij}^{(0)}\right)^2 \xi_2^2\right)^{\frac{3}{2}}} + \frac{\xi_1 |q^{(0)}|_{\max,ij}^2 \left(q_{\mathrm{ref},ij}^{(0)}\right)^2 \xi_2}{\left(\xi_1^2 + \left(q_{\mathrm{ref},ij}^{(0)}\right)^2 \xi_2^2\right)^2} \\
&\quad - \frac{|q^{(0)}|_{\max,ij} \left(q_{\mathrm{ref},ij}^{(0)}\right)^2 \xi_2}{c_{\max,ij}^{(0)} \left(\xi_1^2 + \left(q_{\mathrm{ref},ij}^{(0)}\right)^2 \xi_2^2\right)^2} \left[2\xi_1^2 + \left(q_{\mathrm{ref},ij}^{(0)}\right)^2 \xi_2^2 \right] \Bigg) \\
&\quad \cdot \left[(v_\zeta)_i^{(0)} + (v_\zeta)_j^{(0)} \right] \triangle_{ij} p^{(0)}
\end{aligned}
$$

with

$$
\xi_1 = c_{\max,ij}^{(0)} |q^{(0)}|_{\max,ij}
$$

and

$$\xi_2 = c_i^{(0)} + c_j^{(0)}.$$

Finally, we get the result of

$$
\begin{aligned}
&\mathcal{H}^{\rho v_\zeta}_{MAPS+}(\widetilde{\boldsymbol{u}}_i,\widetilde{\boldsymbol{u}}_j;\boldsymbol{n}) = -n_\zeta \frac{p_i^{(0)}+p_j^{(0)}}{2} \\
&+\left(\frac{\xi_2}{\sqrt{\xi_1^2+\left(q^{(0)}_{\mathrm{ref},ij}\right)^2(\xi_2)^2}}-\frac{|q^{(0)}|_{\max,ij}c^{(0)}_{\max,ij}\xi_2}{\xi_1^2+\left(q^{(0)}_{\mathrm{ref},ij}\right)^2(\xi_2)^2}\right)\frac{(v_\zeta)_i^{(0)}+(v_\zeta)_j^{(0)}}{4}\triangle_{ij}p^{(0)} \\
&-Mn_\zeta\frac{p_i^{(1)}+p_j^{(1)}}{2}+M\left(\frac{\xi_2}{\sqrt{\xi_1^2+\left(q^{(0)}_{\mathrm{ref},ij}\right)^2\xi_2^2}}-\frac{\xi_1\xi_2}{\xi_1^2+\left(q^{(0)}_{\mathrm{ref},ij}\right)^2\xi_2^2}\right) \\
&\qquad\cdot\frac{(v_\zeta)_i^{(0)}+(v_\zeta)_j^{(0)}}{4}\triangle_{ij}p^{(1)} \\
&+M\left(\frac{\xi_2}{\sqrt{\xi_1^2+\left(q^{(0)}_{\mathrm{ref},ij}\right)^2\xi_2^2}}-\frac{\xi_1\xi_2}{\xi_1^2+\left(q^{(0)}_{\mathrm{ref},ij}\right)^2\xi_2^2}\right)\frac{(v_\zeta)_i^{(1)}+(v_\zeta)_j^{(1)}}{4}\triangle_{ij}p^{(0)} \\
&+\frac{M}{2}\Bigg(\frac{\left(c_i^{(1)}+c_j^{(1)}\right)}{\sqrt{\xi_1^2+\left(q^{(0)}_{\mathrm{ref},ij}\right)^2\xi_2^2}}-\frac{\xi_2}{2\left[\xi_1^2+\left(q^{(0)}_{\mathrm{ref},ij}\right)^2\xi_2^2\right]^{\frac{3}{2}}}\Big[2c^{(0)}_{\max,ij}\xi_1|q^{(1)}|_{\max,ij} \\
&\qquad+2c^{(1)}_{\max,ij}|q^{(0)}|_{\max,ij}\xi_1+2\left(q^{(0)}_{\mathrm{ref},ij}\right)^2\xi_2\left(c_i^{(1)}+c_j^{(1)}\right)+2q^{(0)}_{\mathrm{ref},ij}q^{(1)}_{\mathrm{ref},ij}\xi_2\Big] \\
&\qquad-\frac{\xi_1\left(c_i^{(1)}+c_j^{(1)}\right)}{\xi_1^2+\left(q^{(0)}_{\mathrm{ref},ij}\right)^2\xi_2^2}-\frac{c^{(0)}_{\max,ij}|q^{(1)}|_{\max,ij}\xi_2}{\xi_1^2+\left(q^{(0)}_{\mathrm{ref},ij}\right)^2\xi_2^2}-\frac{+c^{(1)}_{\max,ij}|q^{(0)}|_{\max,ij}\xi_2}{\xi_1^2+\left(q^{(0)}_{\mathrm{ref},ij}\right)^2\xi_2^2} \\
&\qquad+\frac{\xi_1\xi_2}{\left[\xi_1^2+\left(q^{(0)}_{\mathrm{ref},ij}\right)^2\xi_2^2\right]^2}\Big[2c^{(0)}_{\max,ij}|q^{(1)}|_{\max,ij}\xi_1+2c^{(1)}_{\max,ij}|q^{(0)}|_{\max,ij}\xi_1 \\
&\qquad+2\left(q^{(0)}_{\mathrm{ref},ij}\right)^2\xi_2\left(c_i^{(1)}+c_j^{(1)}\right)+2q^{(0)}_{\mathrm{ref},ij}q^{(1)}_{\mathrm{ref},ij}\xi_2\Big]\Bigg)\frac{(v_\zeta)_i^{(0)}+(v_\zeta)_j^{(0)}}{4}\triangle_{ij}p^{(0)} \\
&+\frac{M}{16}\Bigg(\frac{|q^{(0)}|^2_{\max,ij}\left(q^{(0)}_{\mathrm{ref},ij}\right)^2\xi_2}{\left(\xi_1^2+\left(q^{(0)}_{\mathrm{ref},ij}\right)^2\xi_2^2\right)^{\frac{3}{2}}}+\frac{\xi_1|q^{(0)}|^2_{\max,ij}\left(q^{(0)}_{\mathrm{ref},ij}\right)^2\xi_2}{\left(\xi_1^2+\left(q^{(0)}_{\mathrm{ref},ij}\right)^2\xi_2^2\right)^2} \\
&\qquad-\frac{|q^{(0)}|_{\max,ij}\left(q^{(0)}_{\mathrm{ref},ij}\right)^2\xi_2}{c^{(0)}_{\max,ij}\left(\xi_1^2+\left(q^{(0)}_{\mathrm{ref},ij}\right)^2\xi_2^2\right)^2}\left[2\xi_1^2+\left(q^{(0)}_{\mathrm{ref},ij}\right)^2\xi_2^2\right]\Bigg) \\
&\qquad\cdot\left[(v_\zeta)_i^{(0)}+(v_\zeta)_j^{(0)}\right]\triangle_{ij}p^{(0)}+\mathcal{O}(M^2).
\end{aligned}
\tag{A.29}
$$

A.4.7. Taylor series of the density enthalpy flux function of the altered MAPS+ scheme

Now, we insert the asymptotic sequence into the density enthalpy flux function of the altered MAPS+ scheme given by equation (4.42) on page 84. This leads to

$$\begin{aligned}
&\mathcal{H}^{\rho h}_{MAPS+}\left(\widetilde{\boldsymbol{u}}_i, \widetilde{\boldsymbol{u}}_j; \boldsymbol{n}\right) \\
&\qquad = \frac{1}{M} \frac{\sum_{k=0}^{2} \left(M^k h_i^{(0)} + M^k h_j^{(0)} \right)}{4} \sum_{k=0}^{2} M^k \triangle_{ij} p^{(0)} \\
&\qquad\quad \left(\frac{\sum_{k=0}^{2} \left(M^k c_i^{(0)} + M^k c_j^{(0)} \right)}{\xi} \right. \\
&\qquad\qquad \left. - \frac{\sum_{k=0}^{2} M^k c_{\max,ij}^{(0)} \sum_{k=0}^{2} M^k |q^{(0)}|_{\max,ij} \sum_{k=0}^{2} \left(M^k c_i^{(0)} + M^k c_j^{(0)} \right)}{\xi^2} \right) \\
&\qquad\quad + \mathcal{O}(M),
\end{aligned} \tag{A.30}$$

with ξ given by equation (A.26) on page XXIX.
If we multiply this equation by the Mach number, it is very similar to the second line in equation (A.28). Hence, we can apply the calculations done above and arrive at the final result of

$$
\begin{aligned}
&\mathcal{H}^{\rho h}_{MAPS+}\left(\widetilde{\boldsymbol{u}}_i, \widetilde{\boldsymbol{u}}_j; \boldsymbol{n}\right) = \\
&\frac{1}{M}\left(\frac{\xi_2}{\sqrt{\xi_1^2 + \left(q^{(0)}_{\mathrm{ref},ij}\right)^2 (\xi_2)^2}} - \frac{|q^{(0)}|_{\max,ij} c^{(0)}_{\max,ij}\xi_2}{\xi_1^2 + \left(q^{(0)}_{\mathrm{ref},ij}\right)^2 (\xi_2)^2}\right)\frac{h_i^{(0)} + h_j^{(0)}}{4}\triangle_{ij}p^{(0)} \\
&+\left(\frac{\xi_2}{\sqrt{\xi_1^2 + \left(q^{(0)}_{\mathrm{ref},ij}\right)^2 \xi_2^2}} - \frac{\xi_1\xi_2}{\xi_1^2 + \left(q^{(0)}_{\mathrm{ref},ij}\right)^2 \xi_2^2}\right)\frac{h_i^{(0)} + h_j^{(0)}}{4}\triangle_{ij}p^{(1)} \\
&+\left(\frac{\xi_2}{\sqrt{\xi_1^2 + \left(q^{(0)}_{\mathrm{ref},ij}\right)^2 \xi_2^2}} - \frac{\xi_1\xi_2}{\xi_1^2 + \left(q^{(0)}_{\mathrm{ref},ij}\right)^2 \xi_2^2}\right)\frac{h_i^{(1)} + h_j^{(1)}}{4}\triangle_{ij}p^{(0)} \\
&+\frac{1}{2}\Bigg(\frac{\left(c_i^{(1)} + c_j^{(1)}\right)}{\sqrt{\xi_1^2 + \left(q^{(0)}_{\mathrm{ref},ij}\right)^2 \xi_2^2}} - \frac{\xi_2}{2\left[\xi_1^2 + \left(q^{(0)}_{\mathrm{ref},ij}\right)^2 \xi_2^2\right]^{\frac{3}{2}}}\Big[2c^{(0)}_{\max,ij}\xi_1|q^{(1)}|_{\max,ij} \\
&\quad +2c^{(1)}_{\max,ij}|q^{(0)}|_{\max,ij}\xi_1 + 2\left(q^{(0)}_{\mathrm{ref},ij}\right)^2\xi_2\left(c_i^{(1)} + c_j^{(1)}\right) + 2q^{(0)}_{\mathrm{ref},ij}q^{(1)}_{\mathrm{ref},ij}\xi_2\Big] \\
&\quad - \frac{\xi_1\left(c_i^{(1)} + c_j^{(1)}\right)}{\xi_1^2 + \left(q^{(0)}_{\mathrm{ref},ij}\right)^2\xi_2^2} - \frac{c^{(0)}_{\max,ij}|q^{(1)}|_{\max,ij}\xi_2}{\xi_1^2 + \left(q^{(0)}_{\mathrm{ref},ij}\right)^2\xi_2^2} - \frac{+c^{(1)}_{\max,ij}|q^{(0)}|_{\max,ij}\xi_2}{\xi_1^2 + \left(q^{(0)}_{\mathrm{ref},ij}\right)^2\xi_2^2} \\
&\quad + \frac{\xi_1\xi_2}{\left[\xi_1^2 + \left(q^{(0)}_{\mathrm{ref},ij}\right)^2\xi_2^2\right]^2}\Big[2c^{(0)}_{\max,ij}|q^{(1)}|_{\max,ij}\xi_1 + 2c^{(1)}_{\max,ij}|q^{(0)}|_{\max,ij}\xi_1 \\
&\quad + 2\left(q^{(0)}_{\mathrm{ref},ij}\right)^2\xi_2\left(c_i^{(1)} + c_j^{(1)}\right) + 2q^{(0)}_{\mathrm{ref},ij}q^{(1)}_{\mathrm{ref},ij}\xi_2\Big]\Bigg)\frac{h_i^{(0)} + h_j^{(0)}}{4}\triangle_{ij}p^{(0)} + \mathcal{O}(M),
\end{aligned}
\tag{A.31}
$$

with ξ_1 and ξ_2 given by equation (A.4.6) and (A.4.6), respectively.

A.4.8. Taylor series of the Mach number $\tilde{M}a_0$

The Mach number $\tilde{M}a_0$ of the extended MAPS+ scheme is given in equation (4.36) on page 75 as

$$\tilde{M}a_0 = \min\left(\frac{\frac{|q|_{\max,ij}c_{\max,ij}}{c_i+c_j} + M^2\frac{q^2_{\mathrm{ref},ij}}{c_{\max,ij}}\frac{|q|_{\max,ij}}{c_i+c_j}}{\sqrt{\frac{|q|^2_{\max,ij}\left(M^2q^2_{\mathrm{ref},ij}-c^2_{\max,ij}\right)^2}{c^2_{\max,ij}(c_i+c_j)^2} + q^2_{\mathrm{ref},ij}}}, 1\right).$$

We expand the first term of the minimum into a Taylor series around $M = 0$. Hence, the function $f(M)$ is given as

$$f(M) = \frac{\frac{|q|_{\max,ij}c_{\max,ij}}{c_i+c_j} + M^2\frac{q^2_{\mathrm{ref},ij}}{c_{\max,ij}}\frac{|q|_{\max,ij}}{c_i+c_j}}{\sqrt{\frac{|q|^2_{\max,ij}\left(M^2q^2_{\mathrm{ref},ij}-c^2_{\max,ij}\right)^2}{c^2_{\max,ij}(c_i+c_j)^2} + q^2_{\mathrm{ref},ij}}}.$$

The first derivative with respect to M is

$$f'(M) = \frac{2M\frac{q^2_{\mathrm{ref},ij}}{c_{\max,ij}}\frac{|q|_{\max,ij}}{c_i+c_j}}{\sqrt{\frac{|q|^2_{\max,ij}\left(M^2q^2_{\mathrm{ref},ij}-c^2_{\max,ij}\right)^2}{c^2_{\max,ij}(c_i+c_j)^2} + q^2_{\mathrm{ref},ij}}} - \frac{\left(\frac{|q|_{\max,ij}c_{\max,ij}}{c_i+c_j} + M^2\frac{q^2_{\mathrm{ref},ij}}{c_{\max,ij}}\frac{|q|_{\max,ij}}{c_i+c_j}\right)\left(2Mq^2_{\mathrm{ref},ij}\frac{|q|^2_{\max,ij}\left(M^2q^2_{\mathrm{ref},ij}-c^2_{\max,ij}\right)}{c^2_{\max,ij}(c_i+c_j)^2}\right)}{\left(\frac{|q|^2_{\max,ij}\left(M^2q^2_{\mathrm{ref},ij}-c^2_{\max,ij}\right)^2}{c^2_{\max,ij}(c_i+c_j)^2} + q^2_{\mathrm{ref},ij}\right)^{3/2}}$$

while the second derivative can be written as

$$
\begin{aligned}
f''(M) = & \frac{2\frac{q_{\mathrm{ref},ij}^2}{c_{\mathrm{max},ij}}\frac{|q|_{\mathrm{max},ij}}{c_i+c_j}}{\sqrt{\frac{|q|_{\mathrm{max},ij}^2\left(M^2q_{\mathrm{ref},ij}^2-c_{\mathrm{max},ij}^2\right)^2}{c_{\mathrm{max},ij}^2(c_i+c_j)^2}+q_{\mathrm{ref},ij}^2}} - \frac{4M^2q_{\mathrm{ref},ij}^4\frac{|q|_{\mathrm{max},ij}^3\left(M^2q_{\mathrm{ref},ij}^2-c_{\mathrm{max},ij}^2\right)}{c_{\mathrm{max},ij}^3(c_i+c_j)^3}}{\left(\frac{|q|_{\mathrm{max},ij}^2\left(M^2q_{\mathrm{ref},ij}^2-c_{\mathrm{max},ij}^2\right)^2}{c_{\mathrm{max},ij}^2(c_i+c_j)^2}+q_{\mathrm{ref},ij}^2\right)^{3/2}} \\
& - \frac{\frac{|q|_{\mathrm{max},ij}c_{\mathrm{max},ij}}{c_i+c_j}+M^2\frac{q_{\mathrm{ref},ij}^2}{c_{\mathrm{max},ij}}\frac{|q|_{\mathrm{max},ij}}{c_i+c_j}}{\left(\frac{|q|_{\mathrm{max},ij}^2\left(M^2q_{\mathrm{ref},ij}^2-c_{\mathrm{max},ij}^2\right)^2}{c_{\mathrm{max},ij}^2(c_i+c_j)^2}+q_{\mathrm{ref},ij}^2\right)^{3/2}} \\
& \cdot\left(4M^2\frac{q_{\mathrm{ref},ij}^4|q|_{\mathrm{max},ij}^2}{c_{\mathrm{max},ij}^2\left(c_i+c_j\right)^2}+\frac{2q_{\mathrm{ref},ij}^2|q|_{\mathrm{max},ij}^2\left(M^2q_{\mathrm{ref},ij}^2-c_{\mathrm{max},ij}^2\right)}{c_{\mathrm{max},ij}^2\left(c_i+c_j\right)^2}\right) \\
& - \frac{4M^2q_{\mathrm{ref},ij}^4\frac{|q|_{\mathrm{max},ij}^3\left(M^2q_{\mathrm{ref},ij}^2-c_{\mathrm{max},ij}^2\right)}{c_{\mathrm{max},ij}^3(c_i+c_j)^3}}{\left(\frac{|q|_{\mathrm{max},ij}^2\left(M^2q_{\mathrm{ref},ij}^2-c_{\mathrm{max},ij}^2\right)^2}{c_{\mathrm{max},ij}^2(c_i+c_j)^2}+q_{\mathrm{ref},ij}^2\right)^{3/2}} \\
& + \frac{\left(\frac{|q|_{\mathrm{max},ij}c_{\mathrm{max},ij}}{c_i+c_j}+M^2\frac{q_{\mathrm{ref},ij}^2}{c_{\mathrm{max},ij}}\frac{|q|_{\mathrm{max},ij}}{c_i+c_j}\right)\left(6M^2q_{\mathrm{ref},ij}^4\frac{|q|_{\mathrm{max},ij}^4\left(M^2q_{\mathrm{ref},ij}^2-c_{\mathrm{max},ij}^2\right)^2}{c_{\mathrm{max},ij}^4(c_i+c_j)^4}\right)}{\left(\frac{|q|_{\mathrm{max},ij}^2\left(M^2q_{\mathrm{ref},ij}^2-c_{\mathrm{max},ij}^2\right)^2}{c_{\mathrm{max},ij}^2(c_i+c_j)^2}+q_{\mathrm{ref},ij}^2\right)^{5/2}}.
\end{aligned}
$$

Since we expand the Mach number into a Taylor series around $M = 0$, we need to evaluate the different functions at $M = 0$. This gives us

$$
f(0) = \frac{\frac{|q|_{\mathrm{max},ij}c_{\mathrm{max},ij}}{c_i+c_j}}{\sqrt{\frac{|q|_{\mathrm{max},ij}^2c_{\mathrm{max},ij}^2}{(c_i+c_j)^2}+q_{\mathrm{ref},ij}^2}},
$$

$$
f'(0) = 0
$$

and

$$
f''(0) = \frac{2\frac{q_{\mathrm{ref},ij}^2}{c_{\mathrm{max},ij}}\frac{|q|_{\mathrm{max},ij}}{c_i+c_j}}{\sqrt{\frac{|q|_{\mathrm{max},ij}^2c_{\mathrm{max},ij}^2}{(c_i+c_j)^2}+q_{\mathrm{ref},ij}^2}} + \frac{\frac{2q_{\mathrm{ref},ij}^2|q|_{\mathrm{max},ij}^3c_{\mathrm{max},ij}}{(c_i+c_j)^3}}{\left(\frac{|q|_{\mathrm{max},ij}^2c_{\mathrm{max},ij}^2}{(c_i+c_j)^2}+q_{\mathrm{ref},ij}^2\right)^{3/2}}.
$$

Hence, for the Mach number $\tilde{M}a_0$ we get

$$\begin{aligned}
\tilde{M}a_0 &= f(0) + Mf'(0) + \frac{M^2}{2}f''(0) + \mathcal{O}(M^4) \\
&= \frac{\frac{|q|_{\max,ij}c_{\max,ij}}{c_i+c_j}}{\sqrt{\frac{|q|^2_{\max,ij}c^2_{\max,ij}}{(c_i+c_j)^2} + q^2_{\mathrm{ref},ij}}} \\
&\quad + \frac{M^2}{2}\left(\frac{2\frac{q^2_{\mathrm{ref},ij}}{c_{\max,ij}}\frac{|q|_{\max,ij}}{c_i+c_j}}{\sqrt{\frac{|q|^2_{\max,ij}c^2_{\max,ij}}{(c_i+c_j)^2} + q^2_{\mathrm{ref},ij}}} + \frac{\frac{2q^2_{\mathrm{ref},ij}|q|^3_{\max,ij}c_{\max,ij}}{(c_i+c_j)^3}}{\left(\frac{|q|^2_{\max,ij}c^2_{\max,ij}}{(c_i+c_j)^2} + q^2_{\mathrm{ref},ij}\right)^{3/2}} \right) + \mathcal{O}(M^4) \\
&= \frac{c_{\max,ij}|q|_{\max,ij}}{\sqrt{c^2_{\max,ij}|q|^2_{\max,ij} + q^2_{\mathrm{ref},ij}\left(c_i+c_j\right)^2}} \\
&\quad + M^2\frac{|q|_{\max,ij}q^2_{\mathrm{ref},ij}\left(2c^2_{\max,ij}|q|^2_{\max,ij} + q^2_{\mathrm{ref},ij}\left(c_i+c_j\right)^2\right)}{c_{\max,ij}\left(c^2_{\max,ij}|q|^2_{\max,ij} + q^2_{\mathrm{ref},ij}\left(c_i+c_j\right)^2\right)^{\frac{3}{2}}} + \mathcal{O}(M^4),
\end{aligned} \tag{A.32}$$

since $f^{(3)}(0) = 0$.

A.4.9. Taylor Series for the pressure scaling $\tilde{p}_{scal}$

For the modified expressions, the pressure scaling is given by equation (4.37) on page 76 as

$$\begin{aligned}
\tilde{p}_{scal} = \frac{1}{2M}&\frac{1}{\sqrt{\frac{|q|^2_{\max,ij}\left(M^2q^2_{\mathrm{ref},ij} - c^2_{\max,ij}\right)^2}{c^2_{\max,ij}(c_i+c_j)^2} + q^2_{\mathrm{ref},ij}}} \\
&\cdot \left(1 - \frac{c_{\max,ij}|q|_{\max,ij}}{\sqrt{c^2_{\max,ij}|q|^2_{\max,ij} + q^2_{\mathrm{ref},ij}\left(c_i+c_j\right)^2}} \right. \\
&\left. - M^2\frac{|q|_{\max,ij}q^2_{\mathrm{ref},ij}\left(2c^2_{\max,ij}|q|^2_{\max,ij} + q^2_{\mathrm{ref},ij}\left(c_i+c_j\right)^2\right)}{c_{\max,ij}\left(c^2_{\max,ij}|q|^2_{\max,ij} + q^2_{\mathrm{ref},ij}\left(c_i+c_j\right)^2\right)^{\frac{3}{2}}} + \mathcal{O}(M^4) \right) \cdot \frac{p_j - p_i}{2}.
\end{aligned}$$

For the asymptotic analysis, we expand the second factor into a Taylor series around $M = 0$. Hence, the function $f(M)$ is given as

$$f(M) = \frac{1}{\sqrt{\frac{|q|^2_{\max,ij}\left(M^2 q^2_{\mathrm{ref},ij} - c^2_{\max,ij}\right)^2}{c^2_{\max,ij}(c_i+c_j)^2} + q^2_{\mathrm{ref},ij}}}.$$

The first derivative with respect to M is

$$f'(M) = -\frac{2Mq^2_{\mathrm{ref},ij}|q|^2_{\max,ij}\left(M^2 q^2_{\mathrm{ref},ij} - c^2_{\max,ij}\right)}{c^2_{\max,ij}\left(c_i+c_j\right)^2\left(\frac{|q|^2_{\max,ij}\left(M^2 q^2_{\mathrm{ref},ij} - c^2_{\max,ij}\right)^2}{c^2_{\max,ij}(c_i+c_j)^2} + q^2_{\mathrm{ref},ij}\right)^{\frac{3}{2}}}$$

and the second derivative results in

$$\begin{aligned} f''(M) = &-\frac{4M^2 q^4_{\mathrm{ref},ij}|q|^2_{\max,ij} + 2q^2_{\mathrm{ref},ij}|q|^2_{\max,ij}\left(M^2 q^2_{\mathrm{ref},ij} - c^2_{\max,ij}\right)}{c^2_{\max,ij}\left(c_i+c_j\right)^2\left(\frac{|q|^2_{\max,ij}\left(M^2 q^2_{\mathrm{ref},ij} - c^2_{\max,ij}\right)^2}{c^2_{\max,ij}(c_i+c_j)^2} + q^2_{\mathrm{ref},ij}\right)^{\frac{3}{2}}} \\ &+\frac{12M^2 q^4_{\mathrm{ref},ij}|q|^4_{\max,ij}\left(M^2 q^2_{\mathrm{ref},ij} - c^2_{\max,ij}\right)^2}{c^4_{\max,ij}\left(c_i+c_j\right)^4\left(\frac{|q|^2_{\max,ij}\left(M^2 q^2_{\mathrm{ref},ij} - c^2_{\max,ij}\right)^2}{c^2_{\max,ij}(c_i+c_j)^2} + q^2_{\mathrm{ref},ij}\right)^{\frac{5}{2}}}. \end{aligned}$$

Evaluating these expressions at $M = 0$ we get

$$f(0) = \frac{1}{\sqrt{\frac{|q|^2_{\max,ij}c^2_{\max,ij}}{(c_i+c_j)^2} + q^2_{\mathrm{ref},ij}}},$$

$$f'(0) = 0$$

and

$$f''(0) = \frac{2q^2_{\mathrm{ref},ij}|q|^2_{\max,ij}c^2_{\max,ij}}{c^2_{\max,ij}\left(c_i+c_j\right)^2\left(\frac{|q|^2_{\max,ij}c^2_{\max,ij}}{(c_i+c_j)^2} + q^2_{\mathrm{ref},ij}\right)^{\frac{3}{2}}}.$$

Combining these expressions we get

$$\begin{aligned}
\tilde{p}_{scal} &= f(0) + Mf'(0) + \frac{M^2}{2} f''(0) + \mathcal{O}(M^4) \\
&= \frac{1}{\sqrt{\frac{|q|^2_{\max,ij} c^2_{\max,ij}}{(c_i+c_j)^2} + q^2_{\mathrm{ref},ij}}} + \frac{M^2}{2} \frac{2q^2_{\mathrm{ref},ij} |q|^2_{\max,ij} c^2_{\max,ij}}{c^2_{\max,ij} (c_i+c_j)^2 \left(\frac{|q|^2_{\max,ij} c^2_{\max,ij}}{(c_i+c_j)^2} + q^2_{\mathrm{ref},ij} \right)^{\frac{3}{2}}} \\
&\quad + \mathcal{O}(M^4) \\
&= \frac{c_i + c_j}{\sqrt{c^2_{\max,ij} |q|^2_{\max,ij} + q^2_{\mathrm{ref},ij} (c_i+c_j)^2}} + M^2 \frac{q^2_{\mathrm{ref},ij} |q|^2_{\max,ij} (c_i+c_j)}{\left(c^2_{\max,ij} |q|^2_{\max,ij} + q^2_{\mathrm{ref},ij} (c_i+c_j)^2 \right)^{\frac{3}{2}}} \\
&\quad + \mathcal{O}(M^4)
\end{aligned} \tag{A.33}$$

since again $f^{(3)}(0) = 0$.

A.4.10. Taylor Series for the velocity scaling $\tilde{q}_{scal}$

For the modified expressions, the velocity scaling is given by equation (4.38) on page 77 as

$$\begin{aligned}
\tilde{q}_{scal} = \frac{\rho_i + \rho_j}{4} \Bigg(1 &- \frac{c_{\max,ij} |q|_{\max,ij}}{\sqrt{c^2_{\max,ij} |q|^2_{\max,ij} + q^2_{\mathrm{ref},ij} (c_i+c_j)^2}} \\
&- M^2 \frac{|q|_{\max,ij} q^2_{\mathrm{ref},ij} \left(2c^2_{\max,ij} |q|^2_{\max,ij} + q^2_{\mathrm{ref},ij} (c_i+c_j)^2 \right)}{c_{\max,ij} \left(c^2_{\max,ij} |q|^2_{\max,ij} + q^2_{\mathrm{ref},ij} (c_i+c_j)^2 \right)^{\frac{3}{2}}} + \mathcal{O}(M^4) \Bigg) \\
\cdot M \sqrt{\frac{|q|^2_{\max,ij} \left(M^2 q^2_{\mathrm{ref},ij} - c^2_{\max,ij} \right)^2}{c^2_{\max,ij} (c_i+c_j)^2} + q^2_{\mathrm{ref},ij}} &\cdot M (q_j - q_i) .
\end{aligned}$$

For the asymptotic analysis, we expand the last square root into a Taylor series around $M = 0$. Hence, the function $f(M)$ is given as

$$f(M) = \sqrt{\frac{|q|^2_{\max,ij} \left(M^2 q^2_{\mathrm{ref},ij} - c^2_{\max,ij} \right)^2}{c^2_{\max,ij} (c_i+c_j)^2} + q^2_{\mathrm{ref},ij}}.$$

The first derivative with respect to M is

$$f'(M) = \frac{2Mq_{\mathrm{ref},ij}^2|q|_{\mathrm{max},ij}^2\left(M^2q_{\mathrm{ref},ij}^2 - c_{\mathrm{max},ij}^2\right)}{c_{\mathrm{max},ij}^2\left(c_i+c_j\right)^2\sqrt{\frac{|q|_{\mathrm{max},ij}^2\left(M^2q_{\mathrm{ref},ij}^2-c_{\mathrm{max},ij}^2\right)^2}{c_{\mathrm{max},ij}^2\left(c_i+c_j\right)^2}+q_{\mathrm{ref},ij}^2}}$$

and the second derivative is

$$f''(M) = \frac{6M^2q_{\mathrm{ref},ij}^4|q|_{\mathrm{max},ij}^2 - 2q_{\mathrm{ref},ij}^2|q|_{\mathrm{max},ij}^2c_{\mathrm{max},ij}^2}{c_{\mathrm{max},ij}^2\left(c_i+c_j\right)^2\sqrt{\frac{|q|_{\mathrm{max},ij}^2\left(M^2q_{\mathrm{ref},ij}^2-c_{\mathrm{max},ij}^2\right)^2}{c_{\mathrm{max},ij}^2\left(c_i+c_j\right)^2}+q_{\mathrm{ref},ij}^2}} - \frac{4M^2q_{\mathrm{ref},ij}^4|q|_{\mathrm{max},ij}^4\left(M^2q_{\mathrm{ref},ij}^2-c_{\mathrm{max},ij}^2\right)^2}{c_{\mathrm{max},ij}^4\left(c_i+c_j\right)^4\left(\frac{|q|_{\mathrm{max},ij}^2\left(M^2q_{\mathrm{ref},ij}^2-c_{\mathrm{max},ij}^2\right)^2}{c_{\mathrm{max},ij}^2\left(c_i+c_j\right)^2}+q_{\mathrm{ref},ij}^2\right)^{\frac{3}{2}}}.$$

Evaluating these expressions at $M = 0$ we get

$$f(0) = \sqrt{\frac{|q|_{\mathrm{max},ij}^2c_{\mathrm{max},ij}^2}{\left(c_i+c_j\right)^2}+q_{\mathrm{ref},ij}^2},$$

$$f'(0) = 0$$

and

$$f''(M) = \frac{-2q_{\mathrm{ref},ij}^2|q|_{\mathrm{max},ij}^2c_{\mathrm{max},ij}^2}{c_{\mathrm{max},ij}^2\left(c_i+c_j\right)^2\sqrt{\frac{|q|_{\mathrm{max},ij}^2c_{\mathrm{max},ij}^2}{\left(c_i+c_j\right)^2}+q_{\mathrm{ref},ij}^2}}.$$

Combining these expressions and considering $f^{(3)}(0) = 0$ we get

$$\begin{aligned}\tilde{q}_{scal} &= f(0) + Mf'(0) + \frac{M^2}{2}f''(0) + \mathcal{O}(M^4)\\ &= \sqrt{\frac{|q|_{\mathrm{max},ij}^2c_{\mathrm{max},ij}^2}{\left(c_i+c_j\right)^2}+q_{\mathrm{ref},ij}^2} - \frac{M^2}{2}\frac{2q_{\mathrm{ref},ij}^2|q|_{\mathrm{max},ij}^2c_{\mathrm{max},ij}^2}{c_{\mathrm{max},ij}^2\left(c_i+c_j\right)^2\sqrt{\frac{|q|_{\mathrm{max},ij}^2c_{\mathrm{max},ij}^2}{\left(c_i+c_j\right)^2}+q_{\mathrm{ref},ij}^2}} + \mathcal{O}(M^4)\\ &= \sqrt{\frac{c_{\mathrm{max},ij}^2|q|_{\mathrm{max},ij}^2}{\left(c_i+c_j\right)^2}+q_{\mathrm{ref},ij}^2} - M^2\frac{q_{\mathrm{ref},ij}^2|q|_{\mathrm{max},ij}^2}{\left(c_i+c_j\right)^2\sqrt{\frac{|q|_{\mathrm{max},ij}^2c_{\mathrm{max},ij}^2}{\left(c_i+c_j\right)^2}+q_{\mathrm{ref},ij}^2}} + \mathcal{O}(M^4).\end{aligned} \tag{A.34}$$

List of Figures

List of Tables

Bibliography

[1] J. D. Anderson Jr: *Fundamentals of aerodynamics.* Tata McGraw-Hill Education, 2010.

[2] K. Asano: *On the incompressible limit of the compressible Euler equation.* Japan Journal of Applied Mathematics, 4(3):455–488, 1987.

[3] H. D. Baehr and S. Kabelac: *Thermodynamik*, volume 11. Springer, 1966.

[4] D. Banuti: *Thermodynamic analysis and numerical modeling of supercritical injection.* PhD thesis.

[5] D. T. Banuti, V. Hannemann, K. Hannemann, and B. Weigand: *An efficient multi-fluid-mixing model for real gas reacting flows in liquid propellant rocket engines.* Combustion and Flame, 168:98–112, 2016.

[6] P. Birken and A. Meister: *Stability of preconditioned finite volume schemes at low Mach numbers.* BIT Numerical Mathematics, 45(3):463–480, 2005.

[7] A. Bowyer: *Computing dirichlet tessellations.* The Computer Journal, 24(2):162–166, 1981.

[8] W. R. Briley, H. McDonald, and S. J. Shamroth: *A low Mach number Euler formulation and application to time-iterative LBI schemes.* AIAA Journal, 21(10):1467–1469, 1983.

[9] W. R. Briley, L. K. Taylor, and D. L. Whitfield: *High-resolution viscous flow simulations at arbitrary Mach number.* Journal of Computational Physics, 184(1):79–105, 2003.

[10] Y. G. Chen, W. G. Price, and P. Temarel: *Numerical simulation of liquid sloshing in LNG tanks using a compressible two-fluid flow model.* In *The Nineteenth International Offshore and Polar Engineering Conference.* OnePetro, 2009.

[11] D. Choi and C. L. Merkle: *Application of time-iterative schemes to incompressible flow.* AIAA Journal, 23(10):1518–1524, 1985.

[12] Y. H. Choi and C. L. Merkle: *The application of preconditioning in viscous flows.* Journal of Computational Physics, 105(2):207–223, 1993.

[13] A. J. Chorin: *The numerical solution of the Navier-Stokes equations for an incompressible fluid.* Bulletin of the American Mathematical Society, 73(6):928–931, 1967.

[14] M. Cismondi and J. Mollerup: *Development and application of a three-parameter RK-PR equation of state.* Fluid Phase Equilibria, 232(1-2):74–89, 2005.

[15] F. Cordier, P. Degond, and A. Kumbaro: *An asymptotic-preserving all-speed scheme for the Euler and Navier-Stokes equations.* Journal of Computational Physics, 231(17):5685–5704, 2012.

[16] S. Dellacherie: *Analysis of Godunov type schemes applied to the compressible Euler system at low Mach number.* Journal of Computational Physics, 229(4):978–1016, 2010.

[17] H. Diangui: *A new preconditioning technology for fluid dynamics.* Journal of Engineering Thermophysics, 26(4):593–595, 2005.

[18] D. G. Ebin: *Motion of slightly compressible fluids in a bounded domain. I.* Communications on Pure and Applied Mathematics, 35(4):451–485, 1982.

[19] R. B. Eddington: *Investigation of supersonic phenomena in a two-phase liquid-gas tunnel.* AIAA Journal, 8(1):65–74, 1970.

[20] J. R. Edwards and M. S. Liou: *Low-diffusion flux-splitting methods for flows at all speeds.* AIAA Journal, 36(9):1610–1617, 1998.

[21] G. Emanuel: *Advanced classical thermodynamics.* AIAA, 1988.

[22] L. E. Eriksson: *A preconditioned Navier-Stokes solver for low Mach number flows.* In *Computational fluid dynamics' 96 (Paris, 9-13 September 1996)*, pages 199–205, 1996.

[23] O. Friedrich: *A new method for generating inner points of triangulations in two dimensions.* Computer Methods in Applied Mechanics and Engineering, 104(1):77–86, 1993.

[24] T. Gerhold: *Overview of the hybrid RANS code TAU.* In *MEGAFLOW-numerical flow simulation for aircraft design*, pages 81–92. Springer, 2005.

[25] S. Godunov and I. Bohachevsky: *Finite difference method for numerical computation of discontinuous solutions of the equations of fluid dynamics.* Matematičeskij sbornik, 47(3):271–306, 1959.

[26] E. Goncalves and R. F. Patella: *Numerical simulation of cavitating flows with homogeneous models.* Computers & Fluids, 38(9):1682–1696, 2009.

[27] H. Guillard and B. Nkonga: *On the behaviour of upwind schemes in the low Mach number limit: A review.* Handbook of Numerical Analysis, 18:203–231, 2017.

[28] T. L. Hill: *An introduction to statistical thermodynamics.* Courier Corporation, 1986.

[29] A. Jameson: *Time dependent calculations using multigrid with applications to unsteady flows past airfoils and wings.* In *10th Computational Fluid Dynamics Conference*, page 1596, 1991.

[30] J. K. Kevorkian and J. D. Cole: *Multiple scale and singular perturbation methods*, volume 114. Springer Science & Business Media, 2012.

[31] S. K. Kim, H. S. Choi, and Y. Kim: *Thermodynamic modeling based on a generalized cubic equation of state for kerosene/LOx rocket combustion.* Combustion and Flame, 159(3):1351–1365, 2012.

[32] W. Kimmerle and M. Stroppel: *Analysis für Ingenieure, Mathematiker und Physiker.* Ed. Delkhofen, 2007.

[33] S. Klainerman and A. Majda: *Singular limits of quasilinear hyperbolic systems with large parameters and the incompressible limit of compressible fluids.* Communications on Pure and Applied Mathematics, 34(4):481–524, 1981.

[34] S. Klainerman and A. Majda: *Compressible and incompressible fluids.* Communications in Pure and Applied Mathematics, 35:629–651, 1982.

[35] R. Klein: *Semi-implicit extension of a Godunov-type scheme based on low Mach number asymptotics i: One-dimensional flow.* Journal of Computational Physics, 121(2):213–237, 1995.

[36] R. Klein, N. Botta, T. Schneider, C. D. Munz, S. Roller, A. Meister, L. Hoffmann, and T. Sonar: *Asymptotic adaptive methods for multi-scale problems in fluid mechanics.* Journal of Engineering Mathematics, 39(1):261–343, 2001.

[37] R. F. Kunz, D. A. Boger, D. R. Stinebring, T. S. Chyczewski, J. W. Lindau, H. J. Gibeling, S. Venkateswaran, and T. R. Govindan: *A preconditioned Navier-Stokes method for two-phase flows with application to cavitation prediction.* Computers & Fluids, 29(8):849–875, 2000.

[38] S. Langer: *Accuracy investigations of a second order finite volume code towards the incompressible limit.* Report, 2016.

[39] O. Le Métayer and R. Saurel: *The Noble-Abel stiffened-gas equation of state.* Physics of Fluids, 28(4):046102, 2016.

[40] B. van Leer, W. T. Lee, and P. Roe: *Characteristic time-stepping or local preconditioning of the Euler equations.* In *10th Computational Fluid Dynamics Conference*, page 1552, 1991.

[41] M. S. Liou: *A sequel to AUSM: AUSM+.* Journal of Computational Physics, 129(2):364–382, 1996.

[42] M. S. Liou: *A sequel to AUSM, part II: AUSM+-up for all speeds.* Journal of Computational Physics, 214(1):137–170, 2006.

[43] M. S. Liou and C. J. Steffen Jr: *A new flux splitting scheme.* Journal of Computational Physics, 107(1):23–39, 1993.

[44] A. Mack and V. Hannemann: *Validation of the unstructured DLR-TAU-code for hypersonic flows.* In *32nd AIAA Fluid dynamics conference and exhibit*, page 3111, 2002.

[45] S. J. Malham: *An introduction to asymptotic analysis.* University Lectures, 2005.

[46] A. Meister: *Asymptotic single and multiple scale expansions in the low Mach number limit.* SIAM Journal on Applied Mathematics, 60(1):256–271, 1999.

[47] A. Meister: *Analyse und Anwendung Asymptotik-basierter numerischer Verfahren zur Simulation reibungsbehafteter Strömungen in allen Mach-Zahlbereichen.* 2001.

[48] A. Meister: *Asymptotic based preconditioning technique for low Mach number flows.* ZAMM-Journal of Applied Mathematics and Mechanics/Zeitschrift für Angewandte Mathematik und Mechanik: Applied Mathematics and Mechanics, 83(1):3–25, 2003.

[49] A. Meister: *Viscous fluid flow at all speeds: analysis and numerical simulation.* Zeitschrift für angewandte Mathematik und Physik ZAMP, 54(6):1010–1049, 2003.

[50] C. L. Merkle: *Computational modelling of the dynamics of sheet cavitation.* In *Proc. of the 3rd Int. Symp. on Cavitation, Grenoble, France, 1998*, 1998.

[51] C. L. Merkle and Y. H. Choi: *Computation of low-speed compressible flows with time-marching procedures.* International Journal for Numerical Methods in Engineering, 25(2):293–311, 1988.

[52] A. Murrone and H. Guillard: *Behavior of upwind scheme in the low Mach number limit: III. Preconditioned dissipation for a five equation two phase model.* Computers & Fluids, 37(10):1209–1224, 2008.

[53] S. Noelle, G. Bispen, K. R. Arun, M. Lukacova-Medvidova, and C. D. Munz: *A weakly asymptotic preserving low Mach number scheme for the Euler equations of gas dynamics.* SIAM Journal on Scientific Computing, 36(6):B989–B1024, 2014.

[54] D. Y. Peng and D. B. Robinson: *A new two-constant equation of state.* Industrial & Engineering Chemistry Fundamentals, 15(1):59–64, 1976.

[55] A. Pfennig: *Thermodynamik der Gemische.* Springer-Verlag, 2013.

[56] O. Redlich and J. N. Kwong: *On the thermodynamics of solutions. V. An equation of state. Fugacities of gaseous solutions.* Chemical Reviews, 44(1):233–244, 1949.

[57] G. E. Reisman, Y. C. Wang, and C. E. Brennen: *Observations of shock waves in cloud cavitation.* Journal of Fluid Mechanics, 355:255–283, 1998.

[58] F. Rieper: *A low-Mach number fix for Roe's approximate Riemann solver.* Journal of Computational Physics, 230(13):5263–5287, 2011.

[59] P. L. Roe: *Approximate Riemann solvers, parameter vectors, and difference schemes.* Journal of Computational Physics, 43(2):357–372, 1981.

[60] C. C. Rossow: *A flux-splitting scheme for compressible and incompressible flows.* Journal of Computational Physics, 164(1):104–122, 2000.

[61] J. Sachdev, A. Hosangadi, and V. Sankaran: *Improved flux formulations for unsteady low Mach number flows.* In *42nd AIAA Fluid Dynamics Conference and Exhibit*, page 3067, 2012.

[62] T. Schneider, N. Botta, K. J. Geratz, and R. Klein: *Extension of finite volume compressible flow solvers to multi-dimensional, variable density zero Mach number flows.* Journal of Computational Physics, 155(2):248–286, 1999.

[63] W. Schneider: *Mathematische Methoden der Strömungsmechanik*. Springer, 1978.

[64] D. Schwamborn, T. Gerhold, and R. Heinrich: *The DLR TAU-code: recent applications in research and industry*. 2006.

[65] G. Soave: *Equilibrium constants from a modified Redlich-Kwong equation of state*. Chemical Engineering Science, 27(6):1197–1203, 1972.

[66] E. Turkel: *Preconditioned methods for solving the incompressible and low speed compressible equations*. Journal of Computational Physics, 72(2):277–298, 1987.

[67] E. Turkel: *Review of preconditioning methods for fluid dynamics*. Applied Numerical Mathematics, 12(1-3):257–284, 1993.

[68] E. Turkel: *Preconditioning techniques in computational fluid dynamics*. Annual Review of Fluid Mechanics, 31(1):385–416, 1999.

[69] E. Turkel, R. Radespiel, and N. Kroll: *Assessment of preconditioning methods for multidimensional aerodynamics*. Computers & Fluids, 26(6):613–634, 1997.

[70] S. Ukai: *The incompressible limit and the initial layer of the compressible Euler equation*. Journal of Mathematics of Kyoto University, 26(2):323–331, 1986.

[71] S. Venkateswaran, M. Deshpande, and C. Merkle: *The application of preconditioning to reacting flow computations*. In *12th Computational Fluid Dynamics Conference*, page 1673, 1995.

[72] S. Venkateswaran, J. W. Lindau, R. F. Kunz, and C. L. Merkle: *Computation of multiphase mixture flows with compressibility effects*. Journal of Computational Physics, 180(1):54–77, 2002.

[73] W. G. Vincenti and C. H. Kruger: *Introduction to physical gas dynamics 1967*. Robert Krieger Publ., New York.

[74] G. Volpe: *Performance of compressible flow codes at low Mach numbers*. AIAA Journal, 31(1):49–56, 1993.

[75] J. D. Van der Waals: *Over de Continuiteit van den Gas-en Vloeistoftoestand*, volume 1. Sijthoff, 1873.

[76] B. Weigand, J. Köhler, and J. Von Wolfersdorf: *Thermodynamik kompakt*. Springer, 2010.

[77] J. M. Weiss and W. A. Smith: *Preconditioning applied to variable and constant density flows.* AIAA Journal, 33(11):2050–2057, 1995.

[78] D. Whitfield: *Three-dimensional unsteady Euler equations solution using flux vector splitting.* In *17th Fluid Dynamics, Plasma Dynamics, and Lasers Conference*, page 1552, 1984.

[79] N. Zong and V. Yang: *An efficient preconditioning scheme for real-fluid mixtures using primitive pressure-temperature variables.* International Journal of Computational Fluid Dynamics, 21(5-6):217–230, 2007.